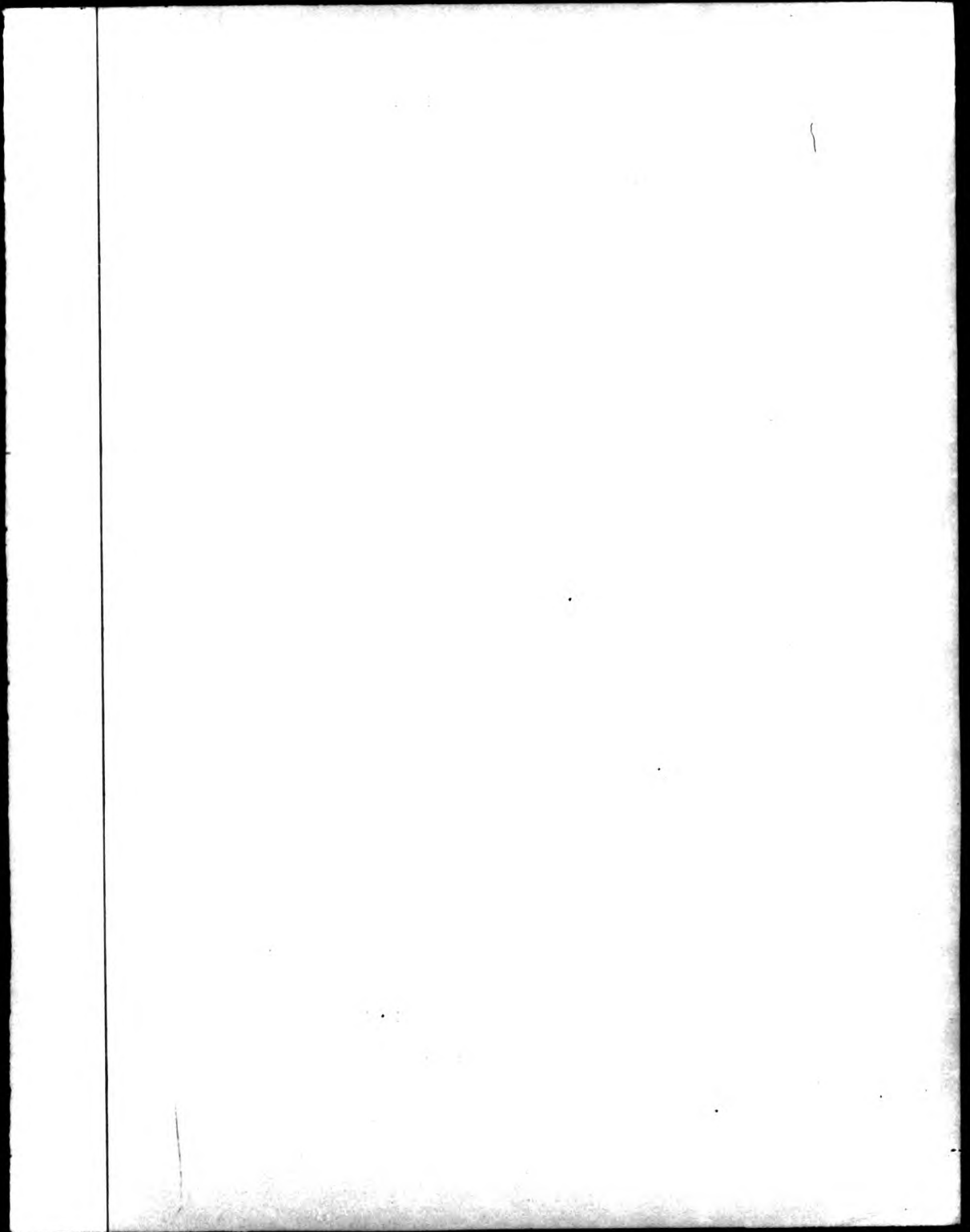
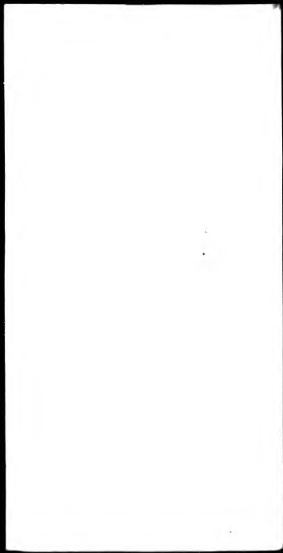


This PDF was created from the British Library's microfilm copy of the original thesis. As such the images are greyscale and no colour was captured.

Due to the scanning process, an area greater than the page area is recorded and extraneous details can be captured.

This is the best available copy

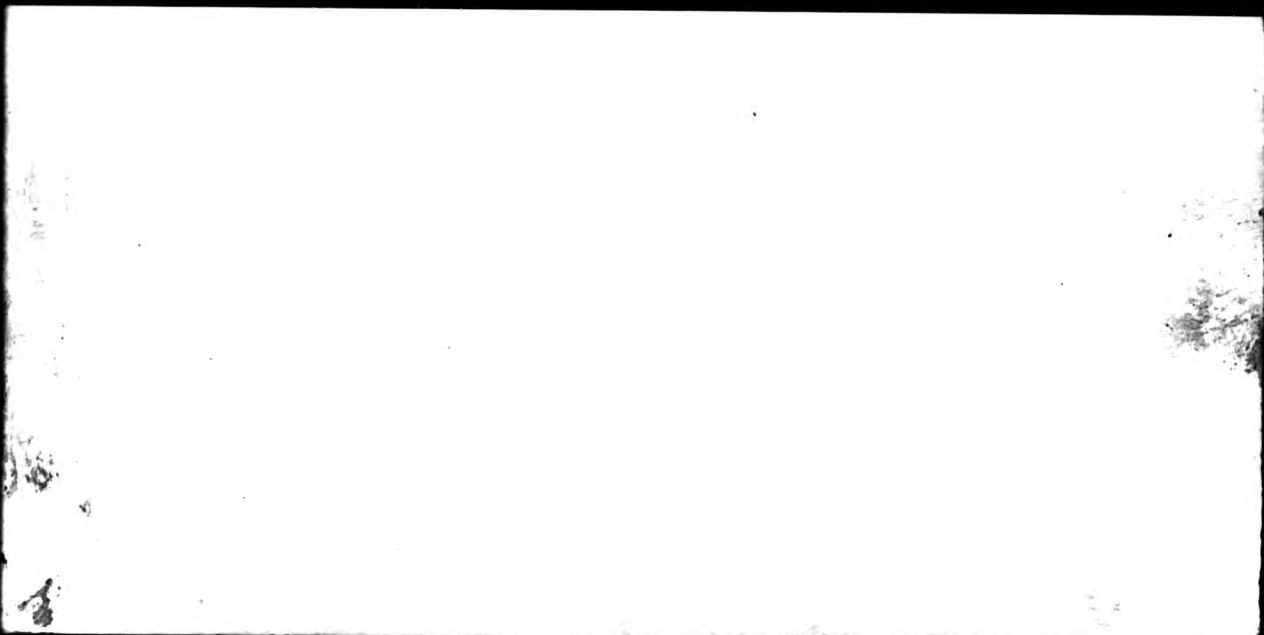


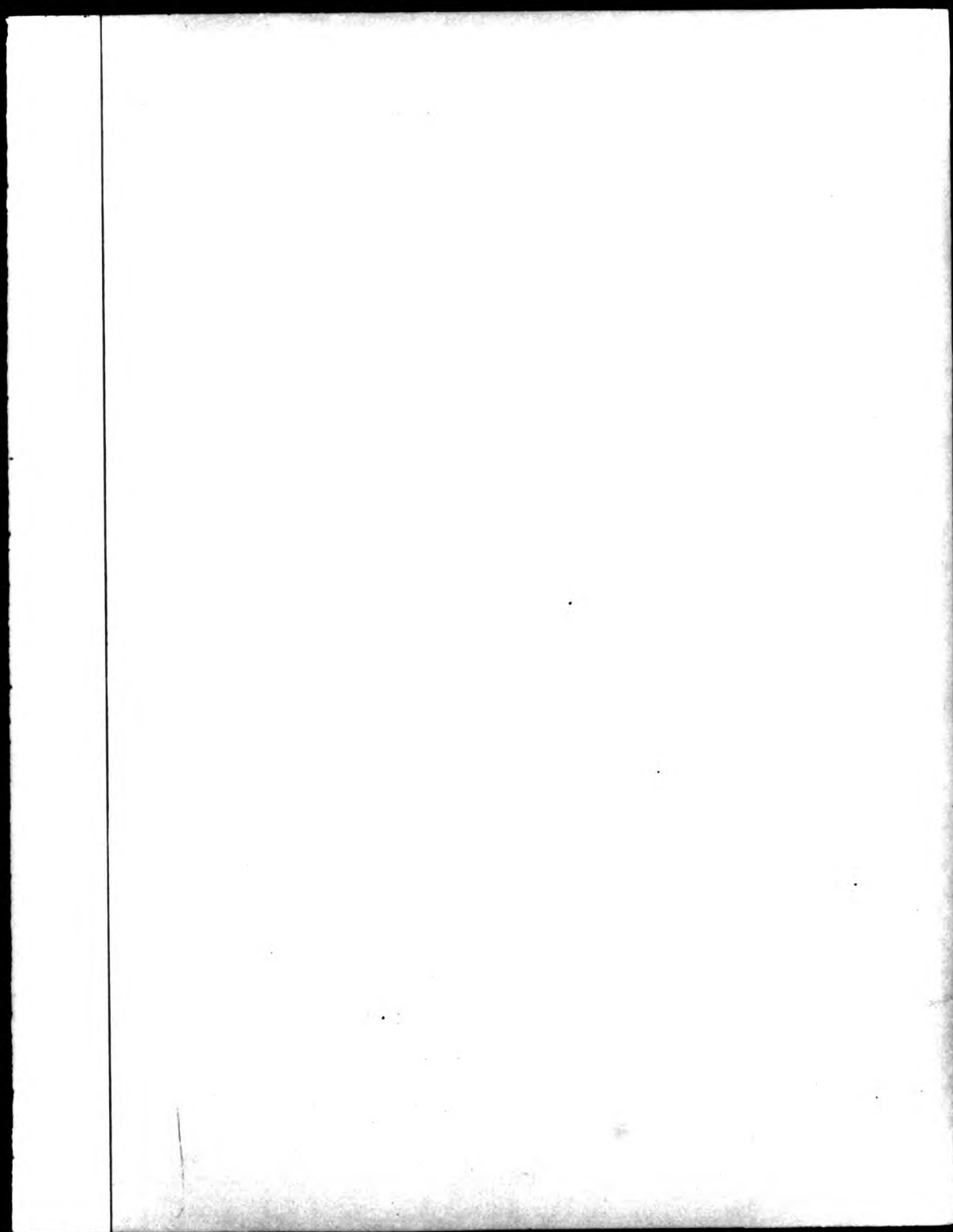
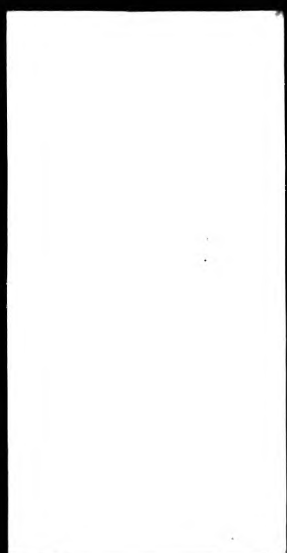


DX



85359





THE BRITISH LIBRARY DOCUMENT SUPPLY CENTRE

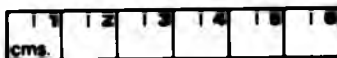
TITLE A study of spectral line intensities
and excited Atom Populations in a
Hollow cathode Discharge.

AUTHOR C. E. Light

INSTITUTION
and DATE North London Polytechnic
1988

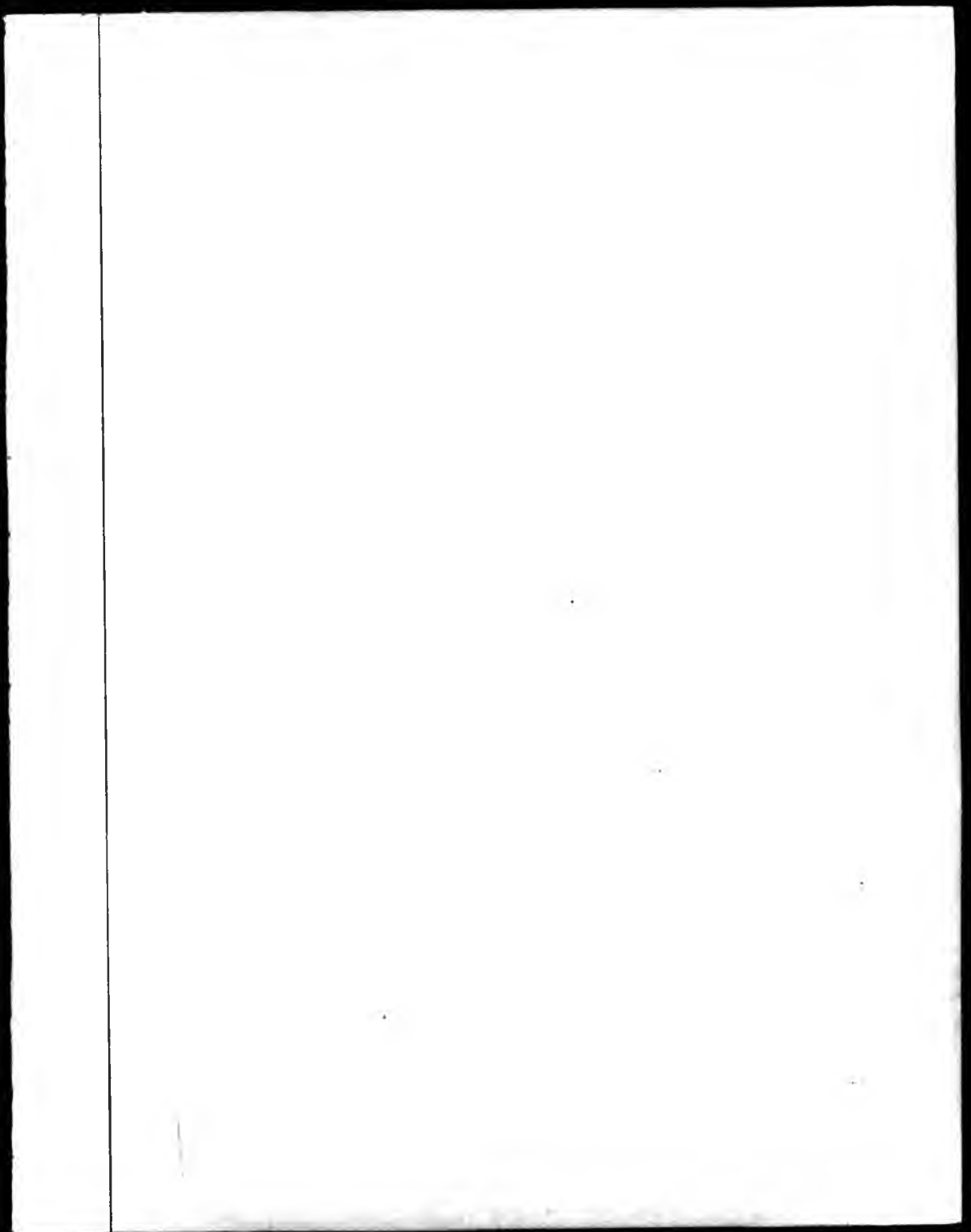
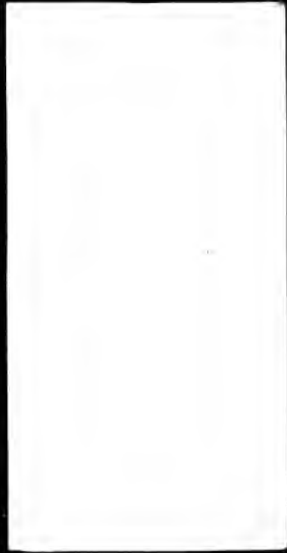
Attention is drawn to the fact that the copyright of
this thesis rests with its author.

This copy of the thesis has been supplied on condition
that anyone who consults it is understood to recognise
that its copyright rests with its author and that no
information derived from it may be published without
the author's prior written consent.



THE BRITISH LIBRARY
DOCUMENT SUPPLY CENTRE
Boston Spa, Wetherby
West Yorkshire
United Kingdom

REDUCTION X: 20



**A STUDY OF SPECTRAL LINE INTENSITIES AND EXCITED ATOM
POPULATIONS IN A HOLLOW CATHODE DISCHARGE**

by C.E.LIGHT, B.Sc, P.G.C.E.

**A Thesis submitted for the degree of Doctor Of Philosophy
of the Council for National Academic Awards.
The work was carried out at the Polytechnic of North London.
Collaborating Establishment: Cathodeon Ltd., Cambridge.
September 1988**

ABSTRACT

Discharge processes within hollow cathode lamps with cylindrical mild steel cathodes and neon carrier gas were investigated for a range of discharge currents and different neon pressures. Experimental methods used were :-

- (a) Visual inspection of the cathode glow.
- (b) Photographic recording of spectra.
- (c) Measurement of the intensity / current (I/i) relationship of selected Ne I spectral lines.
- (d) Recording of emission spectral line profiles using a pressure scanning Fabry - Perot interferometer.
- (e) Measurement of voltage / current characteristics.
- (f) Absorption measurements of the number density of excited neon atoms in the 3s, 3s' group of states.

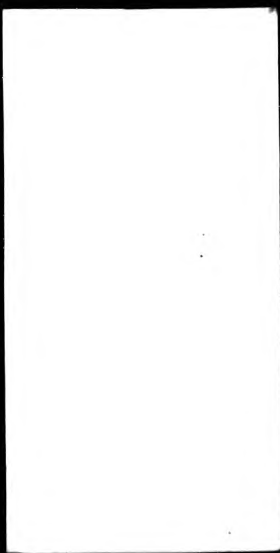
Self - reversal of spectral lines terminating in the $3s [^3/2]_2^o$ metastable state was detected. Number densities of atoms in the $3s [^3/2]_2^o$ state were $\sim 2 \times 10^{17} \text{ m}^{-3}$ and marked saturation of the density with current noted. Densities of atoms in other states of the 3s, 3s' group were $\sim 10^{16} - 10^{17} \text{ m}^{-3}$. A model equation of the I/i relationship was developed of the form

$$I = \frac{A i (1 + B \sum_j N_j(i)) + D}{(1 + C i)}$$

where $N_j(i)$, $j = 1, \dots, 4$ are the number densities of atoms in the 3s, 3s' group of states and A, B, C and D parameters independent of current. The I/i results were fitted to this equation. Evidence of the breakdown of proportionality between electron density and current at low current values was obtained and related to observed discharge properties. A method for correcting recorded spectral line profiles for instrumental broadening was developed.

STATEMENT

The author attended a postgraduate course at Southampton University in theoretical physics, and attended specialist short courses on analytical atomic absorption and optical emission spectroscopy and final year honours courses, at the Polytechnic of North London. Part of the work was presented by the author in a lecture at the **Second Biennial National Atomic Spectroscopy Symposium, Leeds, July 1984** (subsequently published in the *Analyst* [73]) and a further lecture was given at **Gas Discharges and Their Applications, Oxford, September 1985** [74]. A poster including part of the work was presented by Dr. E.B.M. Steers at the **21st Colloquium Spectroscopium Internationale, Garmish - Partenkirchen, September 1985**. Copies of the abstracts and *Analyst* paper are included at the end of this thesis.



ACKNOWLEDGEMENTS

The author would like to thank Dr. E.B.M. Steers for his supervision and advice and Mr. D.W. Ward of Cathodeon Ltd. Cambridge for helpful discussion and the vacuum furnace processing of lamp components by Cathodeon Ltd.

CONTENTS

p 1	LIST OF DIAGRAMS
p 7	LIST OF TABLES
p 8	CHAPTER 1
	INTRODUCTION
p 8	1/A HOLLOW CATHODE DISCHARGES
p 8	1/B REVIEW OF PREVIOUS INVESTIGATIONS
p 8	1/B.1 Discharges Investigated
p 9	1/B.2 Electrical Properties
p 10	1/B.3 Electron Densities and Distributions
p 11	1/B.4 Ion Densities and Sputtering
p 12	1/B.5 Visual Observations
p 12	1/C ORIGIN OF THE WORK
p 15	CHAPTER 2
	HOLLOW CATHODE LAMP SYSTEMS
p 15	2/A POWER SUPPLY
p 15	2/B EXPERIMENTAL H.C.L. SYSTEM
p 15	2/B.1 Outline of System
p 15	2/B.2 Vacuum / Fill Gas Supply System
p 19	2/B.3 Vacuum System Control
p 19	2/B.4 Leak Testing
p 22	2/B.5 Degassing of U.H.V. Section of the System
p 22	2/B.6 Impurity Products of Outgassing
p 23	2/B.7 Vacuum Performance
p 23	2/B.8 Experimental Lamp
p 23	2/B.8(a) Outline
p 26	2/B.8(b) Lamp Configuration A
p 26	2/B.8(c) Lamp Configuration B
p 27	2/C SEALED H.C.L.'S
	CHAPTER 3
p 28	EXPERIMENTAL METHODS
p 28	3/A OUTLINE OF EXPERIMENTAL METHODS
p 28	3/B PHOTOMETRIC MEASUREMENTS (GENERAL DESCRIPTION)

p 28	3/B.1	Introduction
p 29	3/B.2	The Microcircuit
p 32	3/B.3	Photodetector and Recording System
p 36	3/B.4	Basic Arrangement of Optical System
p 38	3/B.5	Pressure Scanning Fabry - Perot Interferometer
p 38	3/B.5 (a)	The Interferometer
p 39	3/B.5 (b)	Adjustment and Finesse
p 40	3/C	PHOTOMETRIC MEASUREMENTS (PARTICULAR EXPERIMENT DETAILS)
p 40	3/C.1	Emission Experiments
p 40	3/C.1 (a)	Interferometer Scans of Emission Line Profiles
p 40	3/C.1 (b)	I/I Measurements
p 41	3/C.2	Absorption Experiments
p 41	3/C.2 (a)	Absorption Measurements by Fabry - Perot Scans of Probe Beam Spectral Line Profiles
p 43	3/C.2 (b)	Measurements of Total Transmitted Intensity of Probe Beam Spectral Line
p 46	3/D	RECORDING OF V/I CHARACTERISTICS
p 46	3/E	VISUAL INSPECTION OF GLOW
p 48		CHAPTER 4
		RESULTS
p 48	4/A	PHOTOMETRIC MEASUREMENTS
p 48	4/A.1	Spectral Lines Studied
p 52	4/A.2	Photometric Results
p 52	4/A.2. (a)	Fabry - Perot Scans of Emission Lines
p 55	4/A.2. (b)	I/I Measurements
p 64	4/A.2. (c)	Fabry - Perot Scanning Absorption Measurements
p 64	4/A.2. (d)	Total Absorption Measurements
p 65	4/B	V/I CHARACTERISTICS
p 70	4/C	SPECTROGRAPHIC EXPERIMENTS
p 70	4/D	VISUAL INSPECTION OF GLOW
p 73		CHAPTER 5
		THE INSTRUMENT FUNCTION OF THE FABRY - PEROT INTERFEROMETER
p 73	5/A	INTRODUCTION

p 73	5/B	THEORY
p 73	5/B.1	<u>Instrument Function Definition</u>
p 74	5/B.2	<u>Theory of the Fabry - Perot Interferometer Instrument Function</u>
p 74	5/B.2. (a)	History of Theory
p 74	5/B.2. (b)	Ideal Case
p 76	5/B.2. (c)	Practical Case
p 77	5/C	<u>Empirical Investigation</u>
p 82	5/D	Comparison of Empirical I.F. Results with Theory
p 85	5/E	Choice of Instrument Parameters Used
p 90		CHAPTER 6
		ANALYSIS
p 90	6/A	FABRY - PEROT ABSORPTION MEASUREMENTS OF EXCITED STATE NUMBER DENSITIES
p 90	6/A.1	Theory of Method
p 91	6/A.2	Graphical Analysis
p 94	6/A.3	Computer Aided Analysis (Method)
p 94	6/A.3. (a)	Methods Review
p 95	6/A.3. (b)	The Iterative Procedure
p 96	6/A.3. (c)	Data Fit
p 99	6/A.3. (d)	Source Profile Synthesis Procedure
p 100	6/A.3. (e)	Source Profile Synthesis Program
p 106	6/A.3. (f)	Absorption Profile Synthesis Procedure
p 107	6/A.3. (g)	Absorption Profile Synthesis Program
p 110	6/A.4	Computer Aided Analysis (Output)
p 110	6/A.4. (a)	Correction of Recorded Profiles for Effect of Instrument Function
p 112	6/A.4. (b)	Synthesized Source Profiles
p 118	6/A.4. (c)	Synthesized Absorption Profiles
p 120	6/A.4. (d)	Excited Atom Number Densities
p 120	6/A.4. (e)	Estimation and Errors
p 127	6/B	TOTAL ABSORPTION MEASUREMENTS
p 127	6/C	I/I MEASUREMENTS
p 127	6/C.1	Fitting Procedure and Computer Program
p 132	6/C.2	Physical Models of I/I Curves
p 135	6/C.3	Fitting of I/I Curves

p 144	6/C.4	Parameter Values
p 147		CHAPTER 7
		DISCUSSION AND CONCLUSIONS
p 147	7/A	SELF - REVERSAL OF SPECTRAL LINE PROFILES
p 147	7/B	NUMBER DENSITIES OF EXCITED ATOMS IN THE 3s, 3s' STATES
p 147	7/B.1	General Features of Number Density Results
p 149	7/B.2	Comparison with Results of Other Workers
p 150	7/B.3	Saturation of Metastable Atom Population
p 153	7/B.4	Quasi - metastable Atom Population
p 156	7/C	INTENSITY/CURRENT CURVES
p 156	7/C.1	Comparison with Howard's Results
p 156	7/C.2	Summary of I/I Fitting
p 158	7/D	V/I CHARACTERISTICS AND VISUAL OBSERVATIONS
p 159	7/E	EFFECTS OF FILL GAS IMPURITY
p 160	7/F	CORRECTION OF SPECTRAL PROFILES FOR INSTRUMENTAL BROADENING
p 160	7/G	SUMMARY OF CONCLUSIONS
p 163	7/H	SUGGESTIONS FOR FURTHER STUDY
p 164		LIST OF REFERENCES
APPENDIX A.		ABSTRACTS AND PAPER
APPENDIX B.		COMPUTER CODE

LIST OF DIAGRAMS

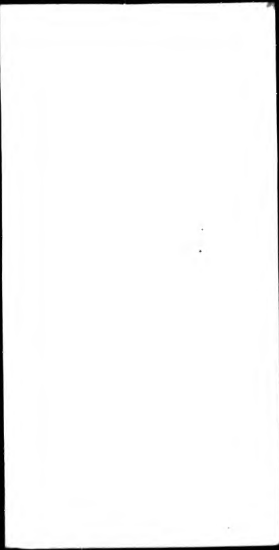
- | | | |
|------|---------|-------------------------------------------------------------------------------|
| p 16 | FIG. 1 | H.C.L. POWER SUPPLY & V/I MEASUREMENT
CIRCUIT |
| p 17 | FIG. 2 | SCHEMATIC DIAGRAM OF VACUUM SYSTEM |
| p 20 | FIG. 3 | U.H.V. SECTION OF VACUUM SYSTEM |
| p 21 | FIG. 4 | VACUUM SYSTEM CONTROL CIRCUIT |
| p 24 | FIG. 5 | EXPERIMENTAL H.C.L. IN CONFIGURATION A |
| p 25 | FIG. 6 | EXPERIMENTAL H.C.L. IN CONFIGURATION B |
| p 30 | FIG. 7 | EAGLE MONOCHROMATOR |
| p 31 | FIG. 8 | SCHEMATIC DIAGRAMS OF MONOCHROMATOR |
| p 33 | FIG. 9 | SCHEMATIC DIAGRAM OF I/I MEASUREMENT
SYSTEM FOR SEALED H.C.L.'S |
| p 34 | FIG. 10 | FABRY - PEROT SYSTEM USED TO RECORD
EMISSION LINE PROFILES |
| p 35 | FIG. 11 | SCHEMATIC DIAGRAM OF FABRY - PEROT
ABSORPTION MEASUREMENT SYSTEM |
| p 37 | FIG. 12 | LOG PLOT OF P.M.T. RESPONSE/POTENTIAL |
| p 45 | FIG. 13 | EXAGGERATED SCHEMATIC DIAGRAMS OF RAY
PATHS THROUGH HOLLOW CATHODE |
| p 50 | FIG. 14 | Ne I ENERGY LEVEL DIAGRAM |
| p 53 | FIG. 15 | Ne I EMISSION LINE PROFILES, EXPERIMENTAL
LAMP (CONFIG. A) (1 & 2 TORR) |
| p 54 | FIG. 16 | Ne I 640.2 nm EMISSION LINE PROFILES AT
THREE LAMP CURRENTS, SEALED H.C.L. |
| p 54 | FIG. 17 | Ne I EMISSION LINE PROFILES AFFECTED BY
CONTAMINATION OF FILL GAS |
| p 56 | FIG. 18 | I/I CURVES OF Ne I LINES, EXPERIMENTAL LAMP
(CONFIG. A) (1 TORR) |

p 57	FIG. 19	I/I CURVES OF Ne I LINES, EXPERIMENTAL LAMP (CONFIG. A) (2 TORR)
p 58	FIG. 20	I/I CURVES OF Ne I LINES, EXPERIMENTAL LAMP (CONFIG. A) (3 TORR)
p 59	FIG. 21	I/I CURVES OF Ne I LINES, EXPERIMENTAL LAMP (CONFIG. A) (5 TORR)
p 60	FIG. 22	I/I CURVES OF Ne I AND Fe I LINES, SEALED H.C.L.
p 61	FIG. 23	Ne I LINE PROFILES RECORDED IN FABRY - PEROT ABSORPTION EXPERIMENTS (1 TORR)
p 62	FIG. 24	Ne I LINE PROFILES RECORDED IN FABRY - PEROT ABSORPTION EXPERIMENTS (1 TORR)
p 63	FIG. 25	Ne I LINE PROFILES RECORDED IN FABRY - PEROT ABSORPTION EXPERIMENTS (2 TORR)
p 66	FIG. 26	VARIATION OF PROBE BEAM SPECTRAL INTENSITY WITH EXPERIMENTAL LAMP CURRENT (1 AND 5 TORR)
p 67	FIG. 27	V/I CHARACTERISTICS OF EXPERIMENTAL LAMP (CONFIG. A) (1 AND 2 TORR)
p 68	FIG. 28	V/I CHARACTERISTICS OF EXPERIMENTAL LAMP (CONFIG. A) (3 AND 5 TORR)
p 69	FIG. 29	V/I CHARACTERISTICS OF SEALED H.C.L. SHOWING HYSTERESIS EFFECT
p 69	FIG. 30	I/I CURVE OF Ne I LINE AFFECTED BY CONTAMINATION OF FILL GAS
p 71	FIG. 31	MEDIUM QUARTZ AND GLASS SPECTROGRAMS OF CONTAMINATED H.C.L. EMISSION

p 72	FIG. 32	MEDIUM QUARTZ SPECTROGRAMS OF CONTAMINATED H.C.L. EMISSION
p 79	FIG.33	VARIATION OF FABRY - PEROT I.F. WITH CHANGING ETALON APARALLELISM
p 79	FIG.34	VARIATION OF FABRY - PEROT I.F. WITH CHANGING ETALON ORIENTATION
p 80	FIG.35	VARIATION OF FABRY - PEROT I.F. WITH ETALON DIAMETER A_1 , POOR PARALLELISM
p 80	FIG.36	VARIATION OF FABRY - PEROT I.F. WITH DIFFERENT DIAMETERS OF APERTURE A_2
p 81	FIG.37	VARIATION OF FABRY - PEROT I.F. WITH ETALON DIAMETER A_1 , OPTIMIZED PARALLELISM
p 81	FIG. 38	CHANGE IN FABRY - PEROT I.F. ON LOCKING ORIENTATION ADJUST. SCREW
p 88	FIG. 39	FABRY - PEROT I.F. OVER TWO ORDERS OF INTERFERENCE, OPTIMIZED ETALON ADJUSTMENT
p 89	FIG. 40	FABRY - PEROT I.F. EXHIBITING RESIDUAL ASYMMETRY AFTER LIMITED OPTIMIZATION OF ETALON PARALLELISM
p 92	FIG. 41	PLOT OF APPARENT ABSORPTION COEFFICIENT AGAINST WAVENUMBER
p 92	FIG. 42	PLOT OF NUMBER DENSITY OF METASTABLE STATE $3s [^3/2]_2^0$ AGAINST LAMP CURRENT
p 97	FIG. 43	FLOWCHART OF DIGITIZATION AND CUBIC SPLINE FITTING OF DATA

p 101	FIG. 44	FLOWCHART OF SOURCE PROFILE SYNTHESIS
p 108	FIG. 45	FLOWCHART OF ABSORPTION LINE PROFILE SYNTHESIS
p 111	FIGS. 46 (a), (b) AND (c)	TYPICAL FORMS OF SOURCE PROFILE AND INSTRUMENT FUNCTION
p 113	FIGS. 47 (a), (b) AND (c)	SCHEMATIC DIAGRAMS SHOWING CONVOLUTION OF TYPICAL LF. AND SOURCE PROFILES
p 114	FIGS. 48 (a), (b) AND (c)	SCHEMATIC DIAGRAMS SHOWING CORRECTION OF TYPICAL OBSERVED SPECTRAL LINE PROFILES FOR EFFECT OF LF.
p 115	FIG. 49	SYNTHESIZED SOURCE & RECORDED EMISSION PROFILES & RESIDUAL VALUES
p 116	FIG. 50	SYNTHESIZED TRANSMITTED SOURCE PROFILE & RECORDED TRANSMITTED PROFILE, & RESIDUAL VALUES
p 117	FIG. 51	SYNTHESIZED SOURCE & RECORDED PROFILES, & RESIDUAL VALUES
p 119	FIG. 52	SYNTHESIZED ABSORPTION PROFILE & RESIDUAL VALUES
p 121	FIGS. 53 (a) AND (b)	PLOTS AGAINST LAMP CURRENT OF Ne I EXCITED STATE NUMBER DENSITIES AT 1 TORR

p 122	FIGS. 54 (a) AND (b)	PLOTS AGAINST LAMP CURRENT OF Ne I EXCITED STATE NUMBER DENSITIES AT 2 TORR
p 123	FIGS. 55 (a) AND (b)	PLOTS AGAINST LAMP CURRENT OF Ne I EXCITED STATE NUMBER DENSITIES AT 5 TORR
p 124	FIGS. 56 (a) AND (b)	PLOTS AGAINST LAMP CURRENT OF Ne I EXCITED STATE NUMBER DENSITIES SUMMED OVER 3s, 3s' LEVELS (1 AND 2 TORR)
p 125	FIG. 57	PLOTS AGAINST LAMP CURRENT OF Ne I EXCITED STATE NUMBER DENSITIES SUMMED OVER 3s, 3s' LEVELS (5 TORR)
p 128	FIGS. 58 (a) AND (b)	PLOTS AGAINST LAMP CURRENT OF SPECTRAL ABSORBANCE AT 1 AND 5 TORR FOR Ne I 640.2 nm
p 130	FIG. 59	FLOWCHART OF I/λ FITTING PROGRAM
p 133	FIG. 60	EXCITATION AND DE - POPULATION PROCESSES OF Ne I EXCITED STATE
p 136	FIG. 61	I/λ FITTED CURVE, DATA AND RESIDUALS FOR Ne I 630.5 nm, 1 TORR
p 137	FIG. 62	I/λ FITTED CURVE, DATA AND RESIDUALS FOR Ne I 630.5 nm, 1 TORR
p 138	FIG. 63	I/λ FITTED CURVE, DATA AND RESIDUALS FOR Ne I 630.5 nm, 2 TORR
p 139	FIG. 64	I/λ FITTED CURVE, DATA AND RESIDUALS FOR Ne I 360.0 nm, 1 TORR
p 140	FIG. 65	I/λ FITTED CURVE, DATA AND RESIDUALS FOR



- Ne I 585.2 nm, 1 TORR
- p 141 FIG. 66 I/I FITTED CURVE, DATA AND RESIDUALS FOR Ne I
630.5 nm, 5 TORR
- p 151 FIGS. 67 (a) AND (b)
SCHEMATIC PLOTS OF METASTABLE ATOM
NUMBER DENSITY AGAINST CURRENT
- p 154 FIG. 68 ENLARGED Ne I ENERGY LEVEL DIAGRAM OF
3s, 3s' STATES
- p 161 FIG. 69 POTENTIAL ENERGY CURVES FOR CO AND CO⁺

LIST OF TABLES

- p 49 TABLE 1
SPECTRAL LINES STUDIED IN EXPERIMENTS
- p 51 TABLE 2
SOME Ne I SPECTRAL LINES AND ENERGY LEVELS
- p 93 TABLE 3
NUMBER DENSITY OF ATOMS IN $3s [^3/2]_2^o$ AT 20 mA AND THREE
PRESSURES, GRAPHICAL ANALYSIS ($\pm \sim 15\%$)
- p 93 TABLE 4
NUMBER DENSITY OF ATOMS IN STATES OF $3s, 3s'$ GROUP AT
2 TORR AND 20 mA, GRAPHICAL ANALYSIS ($\pm \sim 15\%$)
- p 142 TABLE 5
VALUES OF PARAMETERS OBTAINED FITTING MODEL
EQUATIONS B6 & B7 TO OBSERVED I/I_0 CURVES
- p 143 TABLE 6
VALUES OF PARAMETERS OBTAINED FITTING
MODEL EQUATIONS (OTHER THAN B6 & B7) TO OBSERVED
 I/I_0 CURVES
-
-
- p 131 LIST OF I/I_0 MODEL EQUATIONS

CHAPTER 1 INTRODUCTION

1/A HOLLOW CATHODE DISCHARGES

The work described was part of an extensive study of the discharge processes within hollow cathode lamps (H.C.L.'s) carried out at the Polytechnic of North London. Since its first use by Paschen [1] over seventy years ago the hollow cathode discharge (H.C.D.) has been employed as a source of intense spectral line emission with currents that may rise up to 1A. However H.C.L.'s are most commonly used as sources of narrow line emission of analytic elements in modern atomic absorption spectroscopy. A typical commercial lamp consists of a cathode, made wholly or partly of the element in question, which has a cylindrical hollow ~ 10 mm deep and ~ 3 mm bore. In front of this is a small, often ring-shaped anode made of an chemically stable metal. The electrodes are enclosed in an envelope with a quartz window, filled with an inert carrier gas, usually neon or argon, to a pressure between ~ 0.1 and ~ 20 torr. Typically, discharge currents used are ~ 10 to 20 mA. The spectrum of the emission is rich in spectral lines of both cathode material and carrier gas.

In the early 1970's it was shown by a number of workers (eg. Scheubel [2], Piper and Webb [3]) that the negative glow region of a H.C. discharge is especially favourable one for the excitation of upper laser levels of metal ions in helium - metal vapour mixtures. In 1974 Callag et al [4] demonstrated laser oscillation of spectral emission by sputtered cathode material and a number of H.C. laser systems have been developed [5]. The open-ended cathodes used in laser applications are of similar bore to those used in spectroscopy but are usually considerably longer > 10 cm and are operated at higher current densities > 100 mA/cm², with cooling of the cathode, Helium or neon carrier gas is usually used at somewhat higher pressure ~ 10 - 50 torr.

1/B REVIEW OF PREVIOUS INVESTIGATIONS

1/B.1 Discharges Investigated

Since the introduction of the H.C.L. the nature of the discharge has received considerable attention and a number of its characteristics have been elucidated. The facts have been summarized in detailed reviews by Pillow [6] and by Caroli [7]. Lamps with H.C.'s made with a number of materials of various geometries have been studied and the shape of the cavities in cathodes in the different studies have varied. Cathodes consisting of two parallel plates, cathodes with cylindrical cavities both open-ended and closed at one end, and cup-shaped cavities have been studied. The essential feature is cathode geometry in which a region of space is partially enclosed so increasing the surface area

of the cathode in relation to the negative glow. The smaller dimension of the cathode cavity is usually $\sim 0.2 - 4$ cm; research studies have tended to be carried out with larger cathode hollows ~ 10 mm than the smaller commercial spectroscopic sources. The cathode inner surface area is usually in the range $\sim 1 - 50$ cm². The anode is often positioned so as to allow little or no positive column. At suitable carrier gas pressure the discharge consists almost entirely of negative glow within the cathode cavity. A number of pure gases and gas mixtures have been studied, mostly inert gases in the pressure range $\sim 0.1 - 100$ torr. Current ranges in most studies [eg. 11, 20] have not exceeded ~ 200 mA with current densities usually < 10 mA/cm². However more recent investigations by workers interested in laser applications [25, 5] have been for higher current densities in the range $\sim 10 - 200$ mA/cm² with water cooled cathodes.

1/B.2 Electrical Properties

A distinctive electrical property of the H.C.D. soon recognised was the pronounced current enhancement relative to a similar plane cathode discharge, with increased current for a given maintenance voltage and reduced voltage for a given current. Guntherschulze [8], who used a cathode consisting of two parallel water cooled blocks about 1 cm apart, showed that when both blocks were connected to act as one cathode the dark space was reduced compared to the case of one cathode and the depth of dark space was essentially independent of pressure. The current for a given voltage was increased by an amount that depended on gas pressure. Little and Von Engel [9] obtained similar results and showed that almost the entire applied voltage fall occurred across this narrow dark space. Clobotaru [10] showed that the 'amplification factor', i.e. the ratio of the current for a given voltage compared to a plane cathode, was a function of the product of gas pressure p and plate separation a and varied approximately as $(p a)^{-2.5}$. The dependence on the product of p and a is consistent with the similarity principle known for plane cathode discharges in which properties depend on the product of pressure and a characteristic linear dimension.

The distribution of current density over the inner surface of lamps with cylindrical H.C.'s has been investigated by Lompe, Seeliger and Wolter [11] and also by Howorka and Pahl [12], who found that current density was quite evenly distributed at lower current (~ 100 mA) for a range of gas pressures, at higher currents (~ 250 mA) and lower pressures, current density tended to be concentrated deeper inside the cavity. Other workers [12, 13] have found evidence of marked variation of current density over the cathode surface.

The maintenance voltage/total current (V/A) characteristics of H.C.L.'s of varying cathode depth were also studied by Lompe et al [11] who plotted results in terms of

mean current density j . The V/j characteristics became progressively flatter for deeper cathode cavities until the voltage is relatively insensitive to changes in current and equal to about 200V. Similar behaviour has been observed by numerous workers eg. Dopel [14], Masha [15, 16] and White [17], who also noted a 'bump' at low current. Typical maintenance voltages observed have been in the range ~ 50 - 500V depending on the pressure and type of gas and cathode size. The reduced cathode fall and enhanced current of the H.C.D. relative to a planar discharge have been a subject of considerable discussion by Little and Von Engel [9], and by Warren [18], and have been attributed to

- (a) enhanced electron emission from the cathode arising from bombardment by photons and metastables more effectively retained by the concave geometry of the H.C.D.
- (b) an increased ionization efficiency due to the oscillatory motion of high energy electrons.

1/B.3 Electron Densities and Distributions

The number density and energy distribution of electrons within H.C.D.'s have been studied at lower energies by means of small probes, notably by Kagan and different co-workers [19 - 23], and Howorka and Pahl [12], and higher energies have been studied by Okhmatovski [24] using an electrostatic analyser. These measurements have been made at current densities $< \sim 10 \text{ mA/cm}^2$. More recently van Veldhuizen and de Hoog [25] have used Stark broadening of line profiles recorded with saturated absorption spectroscopy to derive electron number densities at higher current densities ~ 10 - 100 mA/cm². Kagan et al [20] found electron densities to be in the range $\sim 1 - 5 \times 10^{17} \text{ m}^{-3}$, about five times those of the positive column and markedly different in energy distribution. The electron energy distribution in the positive column was very nearly Maxwellian and peaked at about 6 eV. This distribution may reasonably be ascribed an electron temperature. In contrast the electron energy distribution in the H.C.D. is markedly non-Maxwellian with a sharp peak at about ~ 0.5 eV but a greater proportion of high energy ($> 20 \text{ eV}$) electrons than the positive column, with an appreciable population having nearly the full cathode fall energy. Such a distribution cannot be ascribed a unique temperature and has been described by Howorka and Pahl [12] in terms of three groups of electrons of differing mean energy, a group of thermalized electrons at low energy ~ 0.5 eV, a group of intermediate energy electrons with mean energy ~ 4 eV but wide energy range, which have suffered few collisions, and a group of high energy electrons which have suffered no collisions since leaving the cathode. A similar argument, involving three groups of electrons of different average energy, has been used by Pringle and Farvis [26] to explain the energy distribution of electrons in the

planar cathode negative glow. The difference in electron energy distribution compared to the positive column is seen as a consequence of the proximity of negative glow to the cathode so that electrons emitted from the cathode are accelerated by the cathode fall and injected at high energy into the negative glow region.

Electron number densities reported by van Veldhuizen and de Hoog at higher current density (10 - 100 mA/cm²) are in the range $\sim 1 - 9 \times 10^{19} \text{ m}^{-3}$.

The radial distribution of electron number density in cylindrical H.C.D.'s have been studied with probes by Howorka and Pahl [12] and Kagan et al [23] and marked variations in radial electron density distribution with gas pressure have been found. At low pressures the electron density is concentrated in the centre of the cavity, is more uniform at intermediate pressure and is concentrated in an annular region near the cathode at high pressure. The electron density in the cathode dark space remains very low.

Electric field strengths within the H.C. glow have been found in probe measurements [19, 12] to be small compared to those in the negative dark space and rarely exceed 400 V/m. This indicates that the plasma is near macroscopic neutrality.

1/B.4 Ion Densities and Sputtering

The species and energy distribution of ions impinging on the cathode have been investigated with mass spectrometers for the planar and H.C. discharges, usually for argon carrier gas. For a planar cathode normal glow discharge both A^+ and A^{++} have been detected, though predominantly A^+ . The majority of A^+ ions had less than half the voltage fall energy though a small proportion had up to the maximum (eg. Chandri and Oliphant [27], and Bodarenko [29]). Similar results have been obtained by Bodarenko for the abnormal planar cathode glow. However Bodarenko [29] found the energy distribution of ions striking the cathode in an H.C.D. markedly different from that in the planar case with a large proportion of ions with nearly the full fall energy. A^+ was still found to be the dominant argon ion species.

Howorka, Lindinger and Pahl [30] measured the number density and radial distribution of argon ions in an H.C.D. at low current ($\sim 2 - 4 \text{ mA}$) using a mass spectrometer and obtained densities $\sim 2 \times 10^{16} \text{ m}^{-3}$ and detected an annular radial density distribution varying with pressure and current.

Spectral emission by atoms of cathode material in the negative glow arises because ion bombardment of the cathode, ejects atoms which are excited in the negative glow. The removal of surface atoms by bombardment by ions and accelerated atoms is known as sputtering and results in significant cathode erosion. The process has been studied by Wehner et al [31, 32, 35] and others and reviewed by Gusherschalzo [33], and by

Weston [34]. The sputtering efficiency of ions has been found to rise rapidly above 30 eV and approaches a constant at higher energy ~ 200 eV [35]. The large proportion of ions with high energy striking the cathode in the H.C.D. ensures a high sputtering rate.

Cathode sputtering can lead to significant number densities of cathode atoms in the H.C.D. which have been measured by de Hoog, McNeil, Collins and Persson [5] in a high current density Ne - Cu H.C. laser discharge and found to be $\sim 2 \times 10^{19} \text{ m}^{-3}$ with strong dependence on current.

1/B.5 Visual Observations

The changes in the radial distribution of electron density are accompanied by changes in visible glow distribution and the intensity of spectral emission. Lompe et al [11] reported the results of detailed visual observation of a H.C.D. in an inert gas - metal vapour mixture. They noted outward movement of the orange and brick red glow, spreading at higher currents. Measurements of the radial distribution of intensity of spectral lines were made photographically by Lompe et al and showed variations in radial distribution which depended on the spectral line. Kagan et al [21, 22] also report similar results and Gill and Webb [36] found comparable behaviour for Zn^+ emission in laser investigations; recently Howard [37] at the Polytechnic carried out a more systematic investigation consistent with earlier work.

1/C ORIGIN OF THE WORK

Masha [15] studied the relationship between the intensity (I) of some neon lines and discharge current (i) for an H.C.L. with a molybdenum cathode consisting of two parallel plates and published his results in the form of log - log plots, assuming an intensity / current (I/i) relationship of the form $I \propto i^p$. He obtained very approximately straight lines of differing gradients ~ 1, some considerably less than 1, but suggested no physical reasons for a fractional power law relationships between intensity and current.

(Unless otherwise stated, all H.C.L.'s referred to subsequently had mild steel cathodes and were filled with neon as the carrier gas).

Howard [37,38] investigated the I/i relationship of selected Ne I spectral lines emitted by a demountable H.C.L. with cylindrical cathodes of three different sizes (3×10 , 6×20 and $15 \times 50 \text{ mm}^2$) at various neon pressures. These measurements were for 6 or 7 data points in the current range 3 to 20 mA. The results were fitted to an equation, proposed in a paper by Howard, Pillow, Steers and Ward [38], derived from a model in which the population of the upper state of the atomic transition, and so the intensity of the spectral line, was determined by the balanced rates of single - step excitation by electron collision from the ground state, two - step excitation by electron collision via an

intermediate state and depopulation of the state by radiation and electron collision. The equation had the form

$$I = \frac{A'i(1+B'i)}{(1+Ci)} \quad (1.1)$$

where the magnitude of A' depended on the rate of single - step excitation and intensity scaling, B' depended on the relative importance of two - step compared to single - step excitation and C the relative importance of depopulation by electron collision and radiation. It was assumed that both electron number density and the density of neon atoms in the intermediate state, were proportional to discharge current.

Howard's results fitted reasonably well to the proposed equation, but the lack of measurements below 3 mA and above 20 mA and limited number of data points, did not allow a rigorous test of the model. Also there was some evidence of self - absorption effects. The nature of the intermediate state in the proposed model was not elucidated.

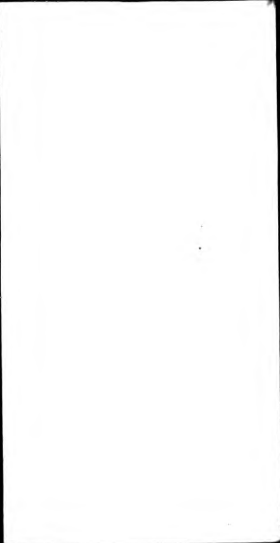
In the light of this work, a programme of research was undertaken by the author intended to develop the experimental methods and the proposed model. The initial aims of this programme were :-

- (i) To investigate the possibility of self - absorption of Ne I spectral lines by recording line profiles.
- (ii) To confirm Howard's I/i results for the demountable lamp with large cathode and sealed lamps, with a different monochromator and experimental set - up.
- (iii) To extend the measurements to allow a more rigorous test of the balance model proposed.
- (iv) To investigate how different observable properties of H.C. discharge such as V/i characteristics, I/i curves and spectral line profiles could be related.

In order to achieve these aims various experimental methods were employed, namely :-

- (a) Visual inspection of the H.C. glow.
- (b) Photographic records of spectra.
- (c) Recording of emission spectral line profiles with a pressure scanning Fabry - Perot interferometer.
- (d) Measurement of the I/i relationship of selected Ne I spectral lines.
- (e) Measurement of V/i characteristics (d) and (e) to be carried out with continuous recording of results using an X - Y recorder and over a wider range of current values.

In the course of this programme of research, evidence was gathered from the line profile measurements of high population densities of excited atoms in the metastable state $3s [^3/2]_2^o$, suggesting that this was the intermediate state proposed in the model. The



demountable lamp was modified to allow absorption measurements to be carried out and the number densities of neon atoms in the four excited states of the 3s, 3s' group, measured for a number of current values and neon pressures.

As a result of these measurements the assumption of proportionality between the number density of the intermediate state(s) and current was found to be incorrect and a new model equation of the I/i relationship was developed and fitted to the results obtained.

CHAPTER 2 HOLLOW CATHODE LAMP SYSTEM

2/A POWER SUPPLY

A controlled current D.C. supply (KSM, HVI 2200) was used to power the H.C.L.'s - Fig.1 shows a diagram of the H.C.L. supply and V/I measuring circuit - The current was controlled rather than supply voltage, as the V/I characteristic of H.C.L.'s are typically very flat and the lamp voltage is almost constant for a wide range of lamp current - E.g. see the V/I characteristic shown in Fig 25 - The P.S.U. could provide a maximum current of 200 mA and maximum voltage of 1.5 kV. The minimum controlled current that the unit could stably supply was ~ 0.1 mA depending on load conditions. A load resistance (R_L), 10 or 20 k Ω depending on maximum current, was included in the circuit to improve stability at low currents. The current control knob could be driven by an electric motor fitted by the author to provide a steadily increasing or decreasing current when required.

The cathode was earthed and the anode potential measured with a calibrated digital multimeter (Keithley, 169). The lamp current was measured with an Avometer positioned in the circuit at near earth potential for reasons of safety, as extreme caution is necessary when dealing with an up to 1.5 kV controlled current source - see Fig. 1 -.

The current flowing to earth through R_1 and R_2 and the D.M.M., causing a small difference between the Avometer reading and the true lamp current, was very small and less than the error in reading the meter.

2/B EXPERIMENTAL H.C.L. SYSTEM

2B. 1 Outline of System

An experimental H.C.L. system built by a previous worker in the group C. Howard [37], which allowed the fill gas pressure and electrode configuration to be altered, was developed and modified by the author for use in the work. In this H.C.L. system, demountable lamp electrodes were enclosed in an experimental chamber - see Fig. 5 - which was connected to a vacuum/gas supply system, so that after evacuation the chamber could be filled with gas to the desired pressure.

2/B.2 Vacuum/Fill Gas Supply System.

This system vacuum pump was a diffusion/rotary pump combination (Edwards, DIFFSTAK 63/150 diff. pump with Santovac 5 pump oil, Edwards 2S20 rotary pump) with a liquid nitrogen cold trap (Edwards, NCT 63) on the diffusion pump and a molecular sieve foreline trap (Zeolite in a VG, RT 3 trap) between pumping stages.

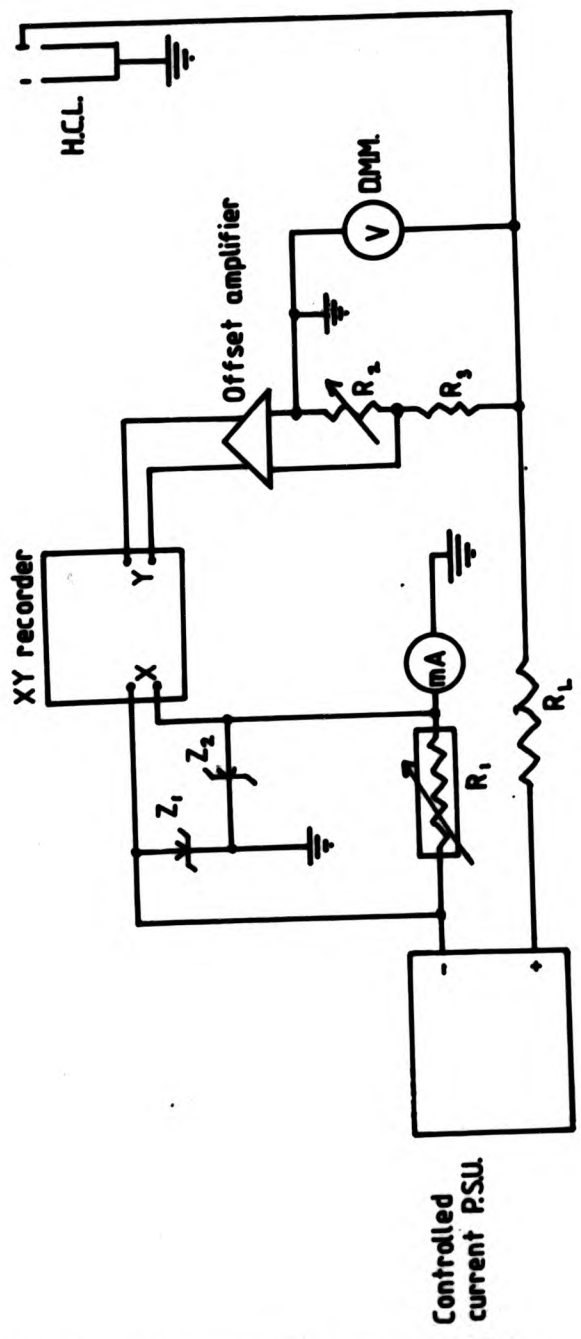


FIG.1 HCL. POWER SUPPLY & V/i MEASUREMENT CIRCUIT

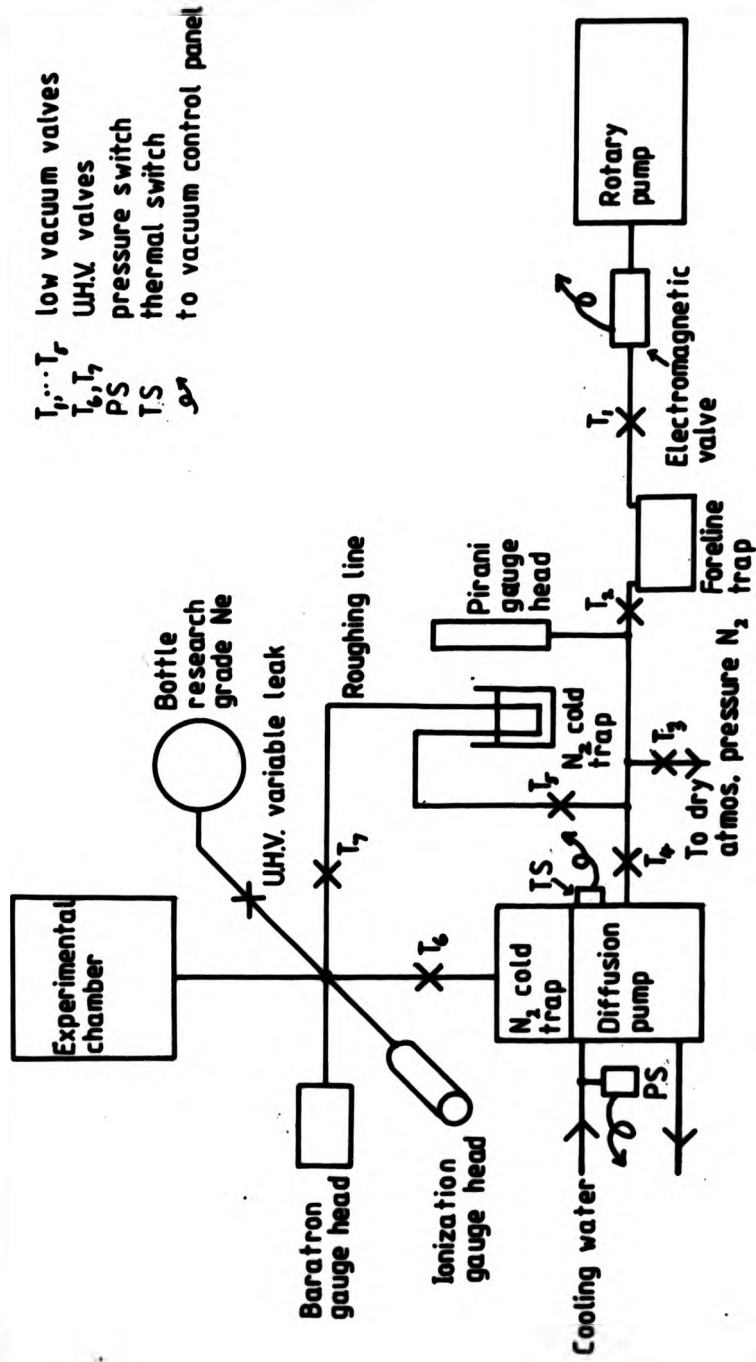


FIG. 2. SCHEMATIC DIAGRAM OF VACUUM SYSTEM

Fig. 2 shows a schematic diagram of the system, and Fig. 3 a detailed diagram of the high vacuum section of the system with the experimental chamber and lamp electrodes in the first of the lamp configurations (A) studied. U.H.V. stainless steel vacuum components were used in the high vacuum section of the system and 15 mm copper tubing with brazed joints for the low vacuum section.

A 64mm I.D. 4-way cross (VG, XF 64) formed the main walls of the experimental chamber and this was connected to the diffusion pump cold trap via a 34mm I.D. 6-way cross (VG, XXF 38) to which fill gas supply, roughing line and two pressure gauge heads were also connected - see Fig. 3. A Pirani gauge (Edwards, M9, range 10^{-2} torr - atmospheric) monitored the pressure in the low vacuum section of the system, an ionization gauge (VG, VIG 21 and TCS 6 control panel, range 10^{-11} - 10^{-2} torr) the high vacuum pressure and a diaphragm capacitance gauge (Baratron, 221 AHS - D - 10, range 0 - 10 torr) the pressure of the fill gas. Connections between components in the high vacuum section were of conflat flange type with copper gaskets (VG), except those to the Baratron gauge head and gas fill supply which were Klein flange type with aluminium gaskets (Leybold - Heraeus, 8815 1 015). Bellows sealed U.H.V. valves with viton seating (VG, VRD 38A) were used in the high vacuum section.

Fill gas was supplied from a glass bottle of research grade neon via a glass to metal graded seal and variable leak valve. When the system was first built, a needle valve (Balzer, EVN 010 H1) with a viton 'O' ring seal to atmosphere had been used, however this was found to have unsatisfactory vacuum performance and was replaced by the author, with an all-metal variable leak valve (VG, MD 6). Maintenance of gas purity in the experimental chamber was assisted with a getter (SAES 171/H1/16 - 10/300) of zirconium/aluminum powder sintered into one piece around an activation heater.

In addition to replacement of the needle valve, other modifications were made by the author to improve the vacuum performance of the system. Modifications made to the system were: -

- (i) Reorientation of valve T_7 - see Fig. 3 - so that the bellows were not enclosed in the experimental section when the valve was closed.
- (ii) Improved bake-out heating and the addition of thermocouples in order to monitor all temperature limited vacuum components and ensure uniform baking so that no "cool spots" existed on which impurities could condense.
- (iii) Replacement of a viton seal between the cold trap and pump with an indium wire seal.
- (iv) Replacement of the needle valve with the all-metal variable leak valve as described above.
- (v) Changes to vacuum system control circuit to provide improved protection in

the event of power failure.

When the system was first used by the author the ultimate pressure after bake - out was $\sim 10^{-7}$ torr, the sealed pressure rise rate was $\sim 10^{-7}$ torr/s and impurity effects were detected in the emission spectrum of the filled lamp - see 2/B.6 and 4/C - . After the modifications the ultimate pressure was reduced to $< 10^{-8}$ torr and the sealed pressure rise rate to $\sim 10^{-9}$ torr/s and the impurity effects were eliminated.

2/B.3 Vacuum Control System

The vacuum control system was controlled from a central panel circuit which incorporated a number of safety features - see Fig. 4 for circuit diagram -. The control circuit was designed to protect the system against :-

- (i) Loss of mains power.
- (ii) Return of mains power after system shut down - undesirable because of the burst of gas, which occurs when a magnetic air release valve opens.
- (iii) Loss of cooling water for the diffusion pump.
- (iv) Overheating of the diffusion pump.
- (v) The low vacuum backing pressure rising above 10^{-2} torr.

The relay logic circuit included a thermal switch to monitor the diffusion pump temperature, a water pressure switch and a set of contacts in the Pirani gauge control panel - See Figs. 2 and 4 - .

2/B.4 Leak testing

Leak testing was carried out to check the overall U.H.V. seal of the system to atmosphere and was vitally necessary when the seal of the aluminium gasket Klein flange connecting the Baratron gauge head to the 6 - way cross failed during cooling after bake - out - see Fig. 3 - . This type of flange was found to be prone to failure if not cooled very slowly and care was subsequently taken to ensure very slow cooling of the overall system and Klein flanges in particular, after bake - out.

Probe gas leak testing was employed [39]. Probe gas from a regulated supply was allowed to escape through a fine drawn glass nozzle and the jet produced, moved slowly over the vicinity of suspected leaks, while the ionization gauge reading was monitored and the chamber pumped. When the jet covered a leak, probe gas entered the system and was registered on the ionization gauge by either an increase or decrease in reading depending on the probe gas used. Two probe gases were tried, butane and helium, the former registering as an increase in ionization gauge reading and the latter as a decrease. The ionization gauge was found to be less sensitive to helium, but helium was preferred on grounds of safety as it is not inflammable.

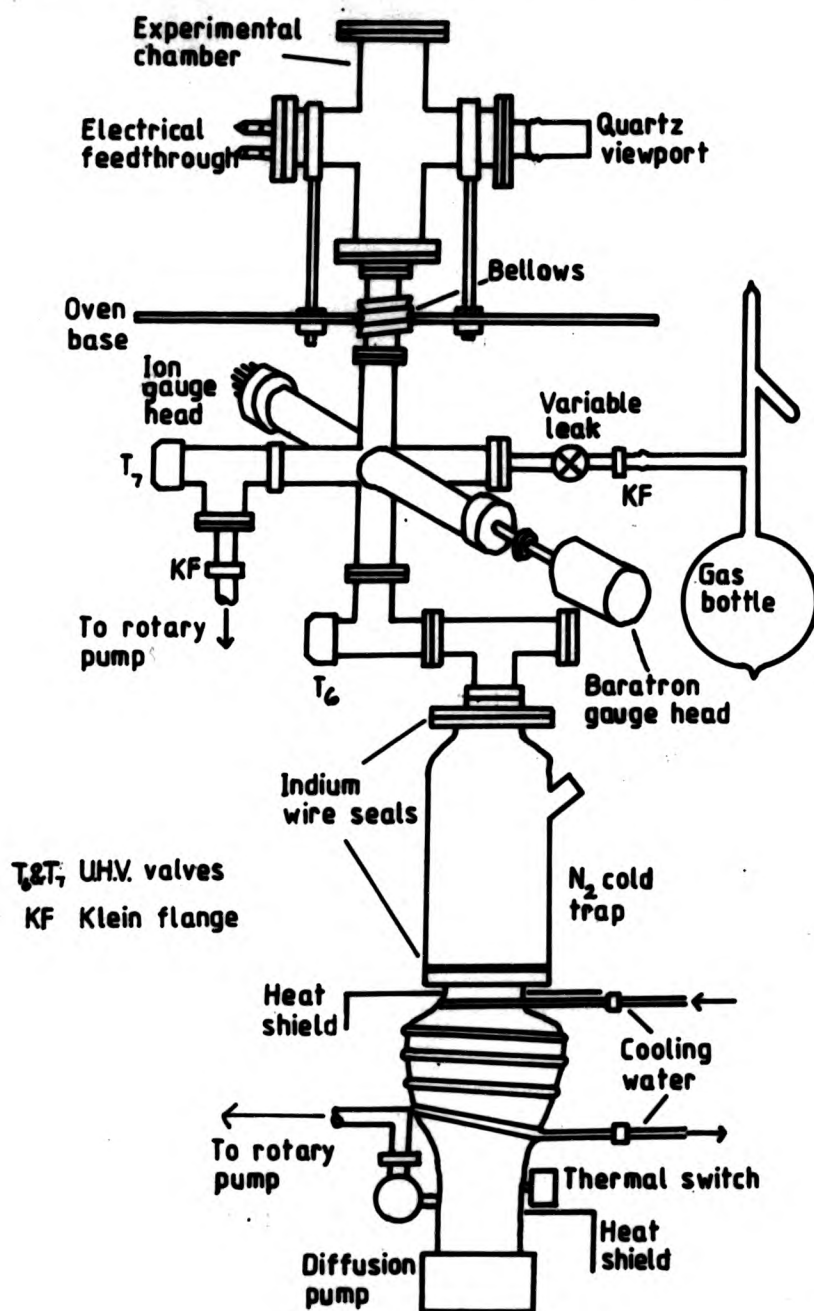


FIG. 3 UHV. SECTION OF VACUUM SYSTEM

2/B.5 Degassing of U.H.V. Section of the System

The U.H.V. section of the system needed to be baked extensively while pumping in order to degas the system before fill gas was introduced. To do this the experimental chamber could be enclosed in an oven and other parts heated with electrical tape. When first encountered, the lowest ultimate pressure, after baking, achievable was $\sim 2 \times 10^{-7}$ torr although the diffusion pump was rated as achieving $< 2 \times 10^{-8}$ torr [40], furthermore impurity effects in lamp emission were detected - see 2/B.6 and 6/C -. It was realized that the heating arrangements of the parts of the system outside the oven were inadequate.

More heating tape and cord (Electrothermal) were added and carefully wrapped around all the parts of the U.H.V. section of the system not within the oven. The oven heater and individual heating tapes and cords were provided with separate variable power supplies and thermocouples placed on all critical components. Chromel - alumel thermocouples were used and thermo - e.m.f.'s measured with a digital multimeter (D.M.M.) to within ± 0.1 mV, allowing temperature to be determined to within $\pm 2.5^\circ\text{C}$. The thermocouples were insulated electrically from the metal of the system with thin mica sheets and good thermal contact was ensured with zinc oxide grease. Temperature limited components were the Baratron gauge head, bakeable to 150°C (with lead removed), and the viton seating U.H.V. valves bakeable to 140°C . The needle valve initially used was only bakeable to 120°C but the all metal, variable leak valve used subsequently was bakeable to 200°C .

These changes to the bake - out heating and the introduction of temperature monitoring on limited components, allowed the whole U.H.V. section of the system to be uniformly heated to 140°C . A bakeable lead was made for the ionization gauge head to allow the high vacuum pressure to be monitored during baking of the system.

The fact that the liquid nitrogen cold trap on the diffusion pump needed refilling at least every 12 hours, proved inconvenient during baking, which required several days if the system had been returned to atmospheric pressure. Dry nitrogen was used instead of air to fill the system when bringing it up to atmospheric pressure in order to reduce contamination.

The getter was activated at 900°C for 10 min, by supplying current to its internal heater, while cooling of the system after bake - out. The getter was replaced after about 8 activations.

2/B.6 Impurity Products of Outgassing

As has been already stated, the effects of impurities - see 2/B.5 - were initially detected in the emission spectra of the experimental lamp by the author. These impurities were the products of outgassing, identified from their spectra as principally CO and to a

much lesser extent OH and H [41]. Spectra of the lamp emission under impure gas conditions, photographed with medium quartz and glass spectrographs (Hilger), - see Fig. 32 - exhibit prominent molecular bands due to CO and CO⁺ [41]. The modifications to the vacuum system carried out by the author removed these impurity effects.

2/B.7 Vacuum Performance.

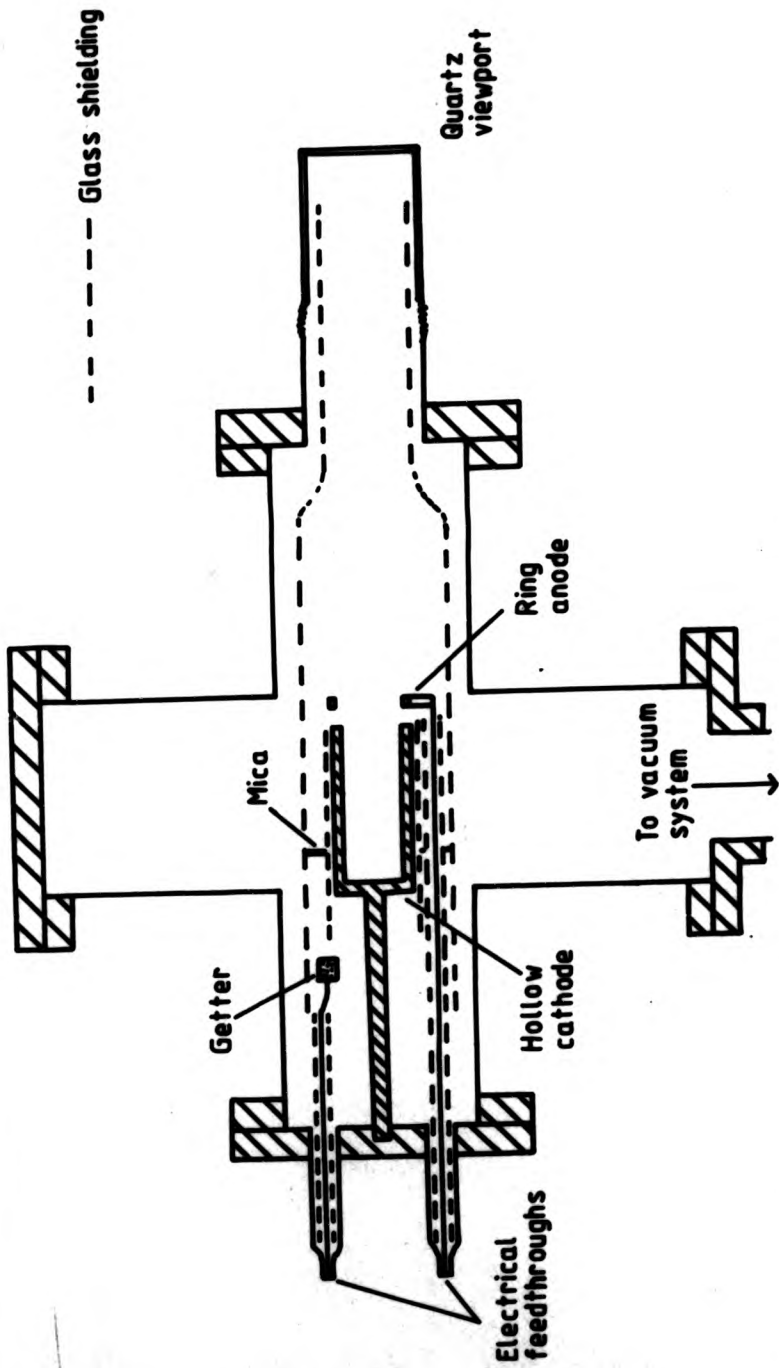
The rotary pump easily maintained the low vacuum backing pressure below 10^{-2} torr, as required for the diffusion pump, but the lowest ultimate pressure of U.H.V. section achievable with the system as initially built was only $\sim 10^{-7}$ torr. The diffusion pump was quoted by the manufacturer [40] as being capable of 2×10^{-8} torr with a viton seal between cold trap and pump and 2×10^{-9} torr with an indium wire seal. The pump air speed was quoted as 90 l/s when used with the liquid nitrogen cold trap.

The reorientation of valve T₇ and improved system bake - out as described above, reduced the ultimate pressure after bake - out to 2.5×10^{-8} torr. The change from viton seal to indium wire seal between cold trap and diffusion pump, at first only reduced the ultimate pressure to 1.5×10^{-8} torr but after replacement of the needle valve with the all - metal variable leak valve - see Fig. 3 - the lowest ultimate pressure achieved was $\sim 2 \times 10^{-9}$ torr. The scaled pressure rise rate was also reduced by two decades from 10^{-7} to 10^{-9} torr/s and with U.H.V. $< 10^{-8}$ torr, between lamp refills with neon, routinely obtainable, all impurity effects in lamp emission were eliminated.

2/B.8 Experimental Lamp

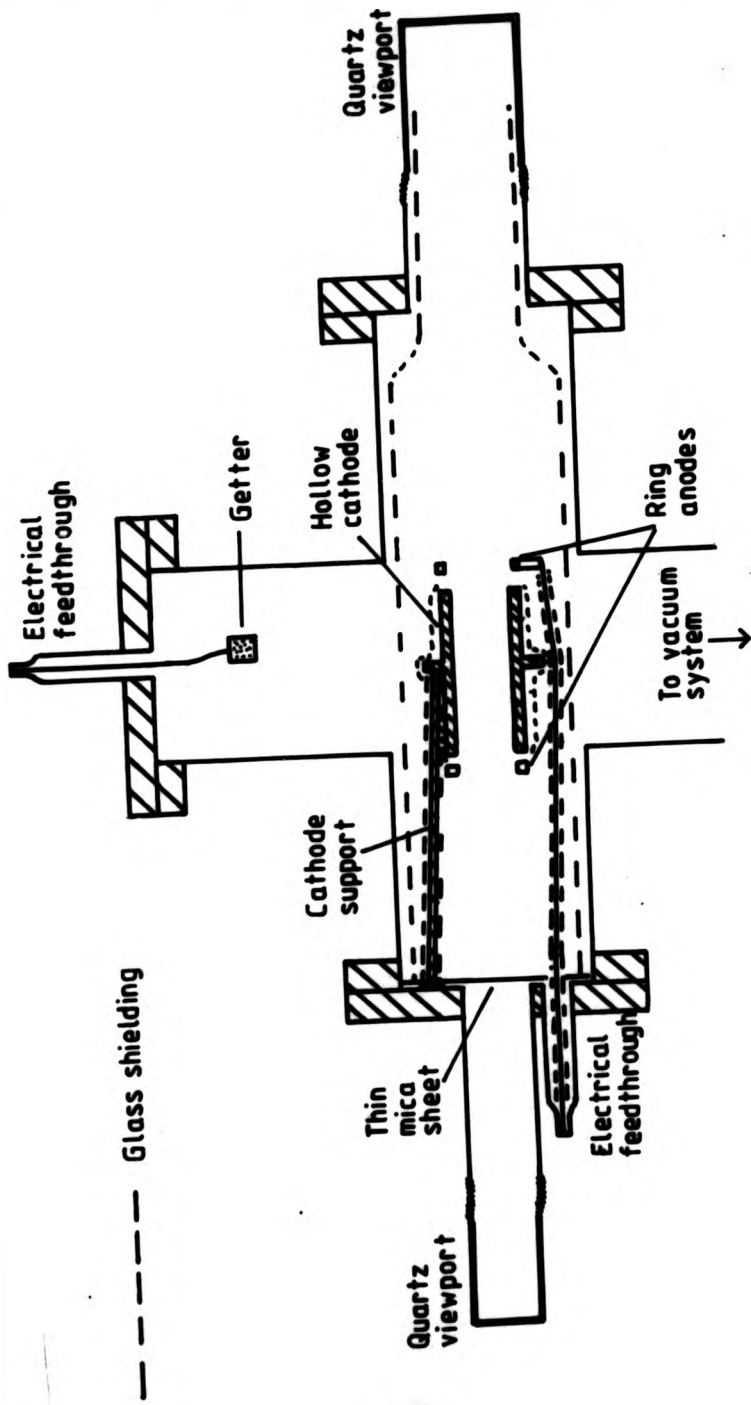
2/B.8 (a) Outline

Two configurations of experimental H.C.L. were studied and will be referred to as configurations A and B - diagrams shown in Figs. 5 and 6 respectively -. In both configurations a cylindrical mild steel hollow cathode of 15 mm bore and 50 mm deep was used, mounted in a 4 - way cross experimental chamber. The cathode and experimental chamber walls were connected and maintained at earth potential and lamp voltage supplied to a 17 mm diameter stainless steel ring anode. Glass and mica shielding was necessary to prevent stray discharges between the anode and the cathode exterior, mounting or chamber walls. The lamp electrodes were vacuum furnace by Cathodean Ltd. before mounting in the chamber in order to remove absorbed gas. All parts of the mounting structures which might trap gas were provided with gas release holes. Lamp configuration A, the first studied in the work, was designed by Howard [37] for emission measurements only, configuration B was designed by the author to allow absorption measurements to be carried out as well.



24

FIG.5 EXPERIMENTAL HCL. IN CONFIGURATION A



25

FIG. 6 EXPERIMENTAL HCL. IN CONFIGURATION B

2/B.8 (b) Lamp configuration A.

In lamp configuration A - see Fig. 5 - the hollow cathode, closed at one end, was mounted horizontally, supported at the closed end by a steel rod which screwed into the centre of a plain flange covering one side port of the chamber 4 - way cross. This flange also admitted the electrical supply for anode and getter via ceramic insulated feedthroughs in the flange. The light weight anode was supported by a thin stainless steel rod, shielded with glass tube, joined directly to one of the electrical feedthroughs in the flange. The anode ring was coaxial with the cylindrical hollow cathode and separated from it by ~ 5 mm. A 63 mm diameter quartz viewport, connected to the opposite side port of the 4 - way cross allowed light emitted by the hollow cathode glow and having passed through the anode ring, to leave the chamber. An outer glass sleeve and annular mica discs prevented stray discharges between anode and chamber walls; the other surface of the hollow cathode was glass shielded.

2/B.8 (c) Lamp configuration B

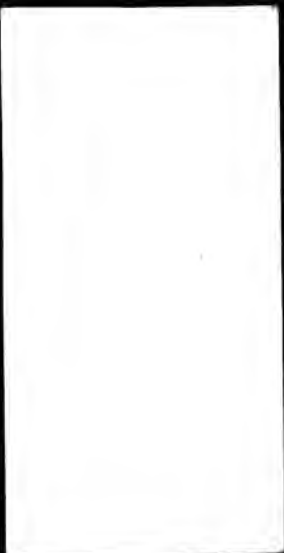
In lamp configuration B - see Fig. 6 - the hollow cathode, this time open at both ends, was mounted horizontally supported by three steel rods connected to a non - standard flange (made to order by VG) on the chamber side port. The lamp configuration and flange were designed so that the flange could:-

- (i) Support the cathode mounting.
- (ii) Admit electrical supply separately to two anodes, one at either end of the hollow cathode.
- (iii) Allow a beam of light to enter the experimental chamber through a 19 mm quartz viewport mounted on the central axis of the flange, pass through the open ended hollow cathode and out of the main viewport, for absorption measurements.
- (iv) Allow an H.C.L. with variable hollow cathode depth to be studied by replacing the 19 mm viewport with a linear motion feedthrough joined to a clearance fit disc "plunger" in the cathode cylinder.

Electrical supply to the getter was via a feedthrough in the flange covering the top port of the chamber.

The electrode structure and mounting were built in the Polytechnic physics workshop. In this structure the three steel rods screwed into an annulus which supported the cathode from a shoulder on the cathode cylinder midway between the ends. This arrangement allowed the cathode to be changed without affecting the rest of the structure. The anode rings at each end of the cathode were joined with short lengths of platinum wire to thin steel rods connected to the electrical feedthroughs in the support flange.

An outer glass sleeve and glass shielding on the cathode structure and mounting



was used to prevent stray discharges and a thin mica disc with holes for mounting rods shielded the support flange. A mica sheet only covering the annular, vertical flange surface was not found to be adequate, as the stainless steel tube supporting the 19 mm second viewport tended to act as an extension of the hollow cathode and contain cathode glow if not shielded. A very thin, uniform sheet of mica was used so that the probe beam of light, which had to pass through it, suffered little attenuation.

2/C SEALED H.C.L.'S

Two sealed H.C.L.'s (Cathodeon, 3QNY/Fe), of the type manufactured for use in commercial atomic absorption spectrometers, were studied. The two similar lamps, coded C12 and 22639 by the manufacturer, were filled with neon at different pressures, C12 at 10 ± 1 torr and 22639 at 15 ± 1 torr. Both had cylindrical mild steel hollow cathodes of 3 mm bore and 10 mm depth, however the anodes differed; 22639 had a ring anode coaxial with the cathode and C12 an anode which was a curved rectangular plate. The anode connections were shielded with ceramic and annular mica sheets prevented stray discharge to the cathode exterior.

CHAPTER 3 EXPERIMENTAL METHODS

3/A OUTLINE OF EXPERIMENTAL METHODS

Spectral sources were studied with a number of experimental methods.

(i) Photometric

Photometric study of H.C.L. Ne I spectral lines, to which the greater part of the work was devoted. Emission and absorption measurements were made in experiments of four types.

Emission -

- (a) Fabry - Perot interferometer scans of spectral lines.
- (b) Measurement of the variation of spectral line intensity with lamp current (I/I measurements).

Absorption -

- (c) Fabry - Perot interferometer scans of probe beam spectral line profiles.
- (d) Measurement of total transmitted intensity of spectral lines of the probe beam.

(ii) Electrical

Recording of V/I characteristics.

(iii) Spectrographic

Photographic recording of emission spectra with prism spectrograph to identify gaseous impurities (see 2/B.6)

(iv) Visual

Visual inspection of discharge glow both directly and through direct vision spectroscope.

3/B PHOTOMETRIC MEASUREMENTS (GENERAL DESCRIPTION)

3/B.1 Introduction

In all the photometric experiments the same monochromator and photomultiplier tube (P.M.T.) were used to isolate and detect spectral lines and optical bench used to support components, additional smaller optical benches being used, as necessary in each experimental arrangement. Results of experiments were recorded on an X - Y chart recorder, with the P.M.T. output controlling the Y - deflection of the recorder and either interferometer housing pressure or lamp current controlling the X - deflection.



3/B.2 The Monochromator

The monochromator used to isolate spectral lines for study was a concave grating spectrometer with Eagle mounting and in - plane configuration, built previously in the Polytechnic - see Fig. 7 -. The 1m radius grating was ruled with 600 lines/mm over an area 90 mm x 50 mm and blazed for use in first order. The P.M.T. mounted in a housing behind the exit slit could be changed and a tube of suitable spectral response chosen. The right angled prism was made of high quality fused silica to ensure the monochromator could be used in the ultraviolet spectral region. With a critical slit width of 15 μm the wavelength passband was ~ 0.05 nm, however except in those cases in which close lying spectral lines occurred, a slit width of 50 μm with passband ~ 0.15 nm was used, as this provided sufficient wavelength isolation and allowed greater light transmission.

The grating table was free to rotate about a vertical axis (AX) - see Fig. 8 - for wavelength selection and to travel on a track towards and away from the exit slit for focussing. These motions were controlled via mechanical linkages, and care was necessary to avoid "backlash". Focussing was controlled manually and table rotation driven electrically or set by hand. The rotation setting and focus setting indicated by counter and wheel markings, were wavelength calibrated with a set of Phillips lamps of different elements (Hg, Zn, Cd, and Ne). The correct focus was obtained by repeated rescanning of chosen spectral lines and the best focus setting was that which gave maximum peak height on a chart recorder.

The monochromator required modification and adjustment when first encountered. These were greatly facilitated by the employment of a low power He - Ne laser to define the optical axis, as the narrow high intensity beam was easy to follow through the instrument. The monochromator had three principal faults which required rectification:

- (i) The right - angled prism was too small, so the grating could not be fully illuminated (a smaller grating had been replaced previously). This reduced the light through - put and prevented the full resolving power being realised.
- (ii) As the grating was rotated the point at which light fell on the exit slit moved up or down.
- (iii) Light leakage from outside the monochromator and stray light within it, were unacceptably high.

The existing prism was replaced with a larger one (Spectrosil) of entrance face 25.4 mm x 25.4 mm, which transmitted about two and a half times as much light and allowed the full number of grating lines to be illuminated. A new prism mounting was designed by the author and built in the Physics workshop. The mounting was designed for maximum ease of adjustment combined with rigid positive location.

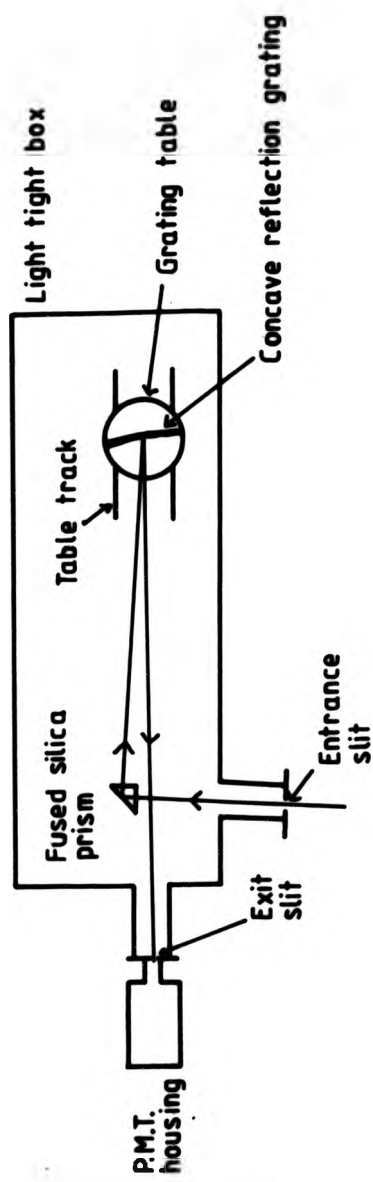
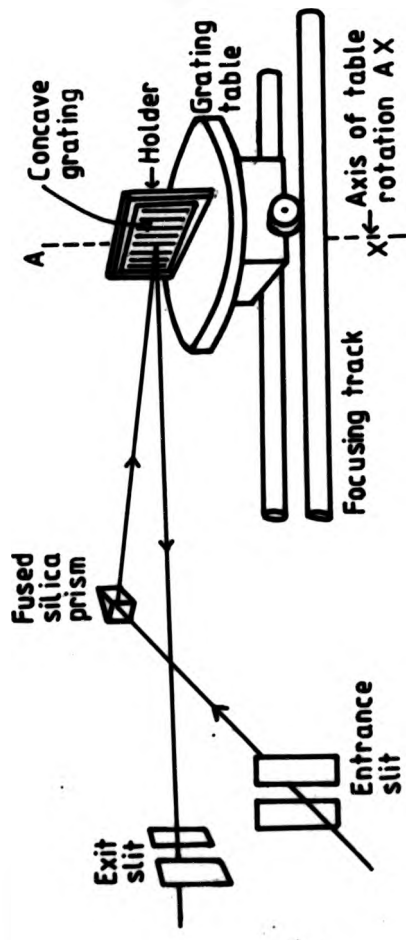


FIG. 7 EAGLE MONOCHROMATOR



PERSPECTIVE DIAGRAM OF EAGLE MONOCHROMATOR

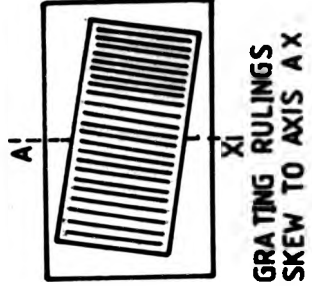
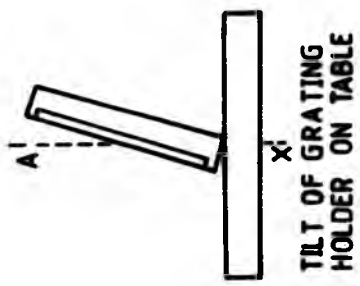
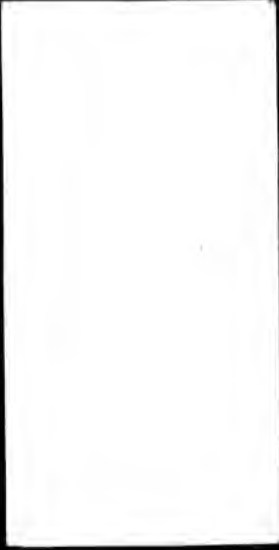


FIG. 8 SCHEMATIC DIAGRAMS OF MONOCHROMATOR



Careful observation of the path of a laser beam through the instrument showed that the movement of the optical axis relative to the exit slit was caused by misorientation of the grating on the grating table - see Fig. 8 -. The grating face was not normal to the grating table and the rulings were skew to the axis of table rotation AX. Metal shims, chosen by trial and error, placed under one edge of the grating holding before it was clamped to the table, corrected the tilt of the grating face and rotation of the grating in the plane of the holder corrected the skew error of the rulings. With these adjustments made the optical axis remained at the centre of the exit slit as the table was rotated.

The monochromator box and join to the P.M.T. housing were light sealed with matt black tape and cloth, and internal stray light reduced by suitably positioned matt black baffles. With these modifications the instrument functioned satisfactorily as a spectral line isolator.

3/B.3 Photodetector and Recording Systems

Spectral lines studied lay in the wavelength range 330 - 750 nm. The photomultiplier tube chosen (EMI, 9558B) had peak quantum efficiency of ~ 20 % at 400 nm falling to ~15% at 330 nm and ~ 2% at 750 nm [42], and allowed the full wavelength range of interest to be studied. The P.M.T. was powered by a stabilized high voltage D.C. supply, (Thorn - EMI, PM28B) and tube potential monitored with a calibrated digital multimeter. Tube volts used were in the range ~ 300 - 1100V.

The P.M.T. output signal current passing through a high resistance (R) developed a potential difference which, when amplified, controlled the Y - deflection of a RIKADENKI model BN-133A X - Y chart recorder. The X - deflection of the recorder was controlled by H.C.L. current (i) when making I/I measurements and the Fabry - Perot interferometer housing pressure when recording spectral line profiles.

Two different systems were used to amplify the P.M.T. signal - see Figs. 10 and 11 -. When recording the profiles of spectral lines emitted by lamps and the variation of spectral line intensities with discharge conditions, a D.C. coupled valve amplifier was used - see Fig. 10 -. The amplifier which had been built previously in the Physics laboratory specifically for photometric work, incorporated a choice of 6 values of R (1 to 110 M Ω), in parallel with a choice of 7 values of smoothing capacitor C (- 0, 0.01 to 0.5 μ F). The value of R selected determined the amplifier gain. The choice of values of C and R, which fixed the time constant RC, depended on the signal to noise ratio encountered.

The second amplifier system - Fig 11 - was used when making absorption measurements of excited atom number densities in H.C. discharges. In order to discriminate between the intensity of the probe beam and the light emitted by the discharge itself, the probe beam was modulated at 33.33 Hz by a rotating mechanical

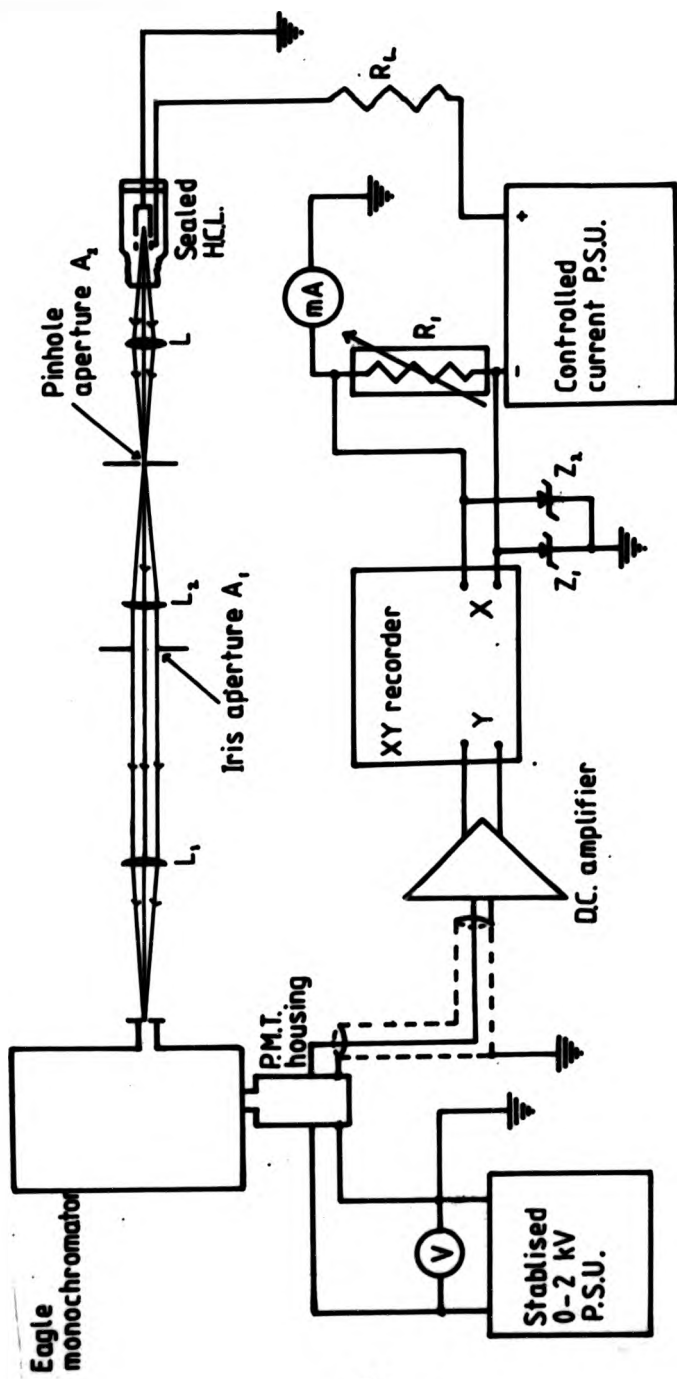


FIG. 9 SCHEMATIC DIAGRAM OF I/i MEASUREMENT SYSTEM FOR SEALED HCL'S

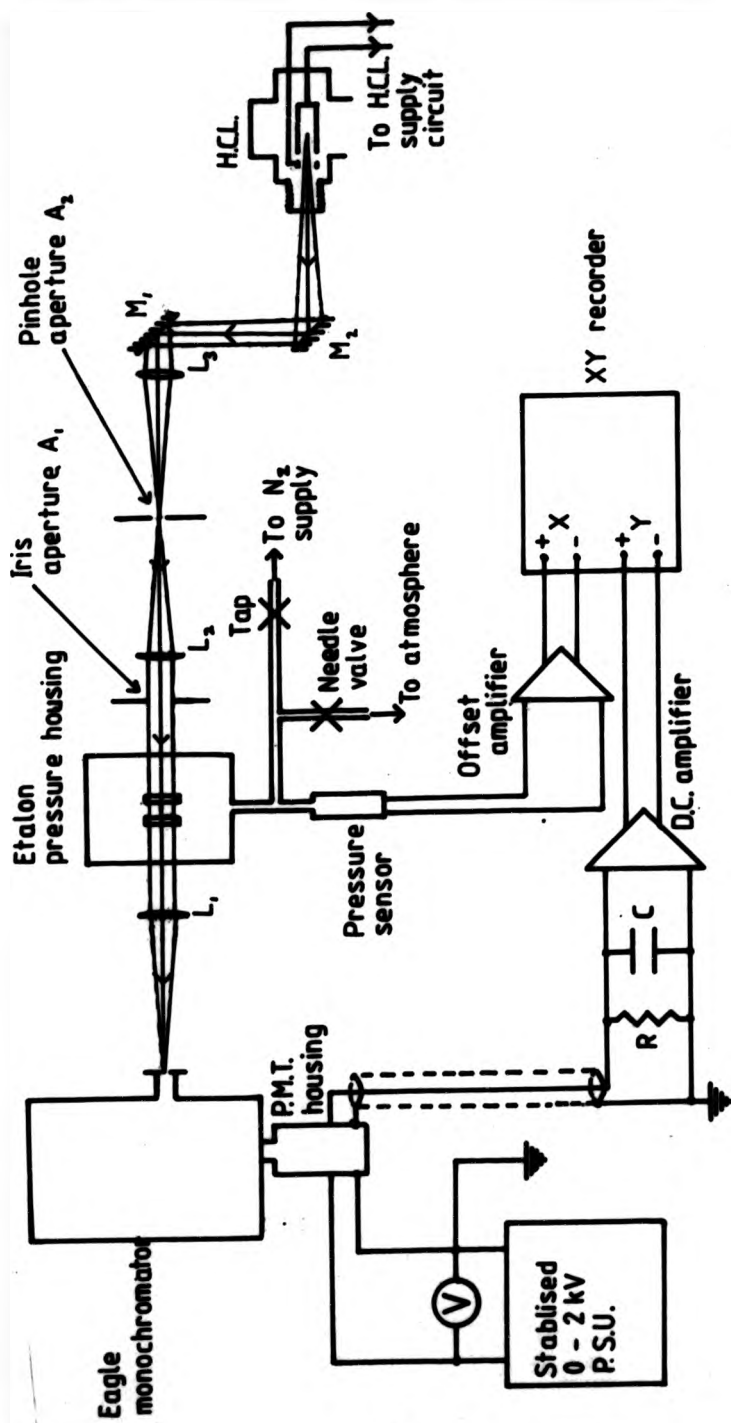


FIG.10 FABRY-PEROT SYSTEM USED TO RECORD EMISSION LINE PROFILES

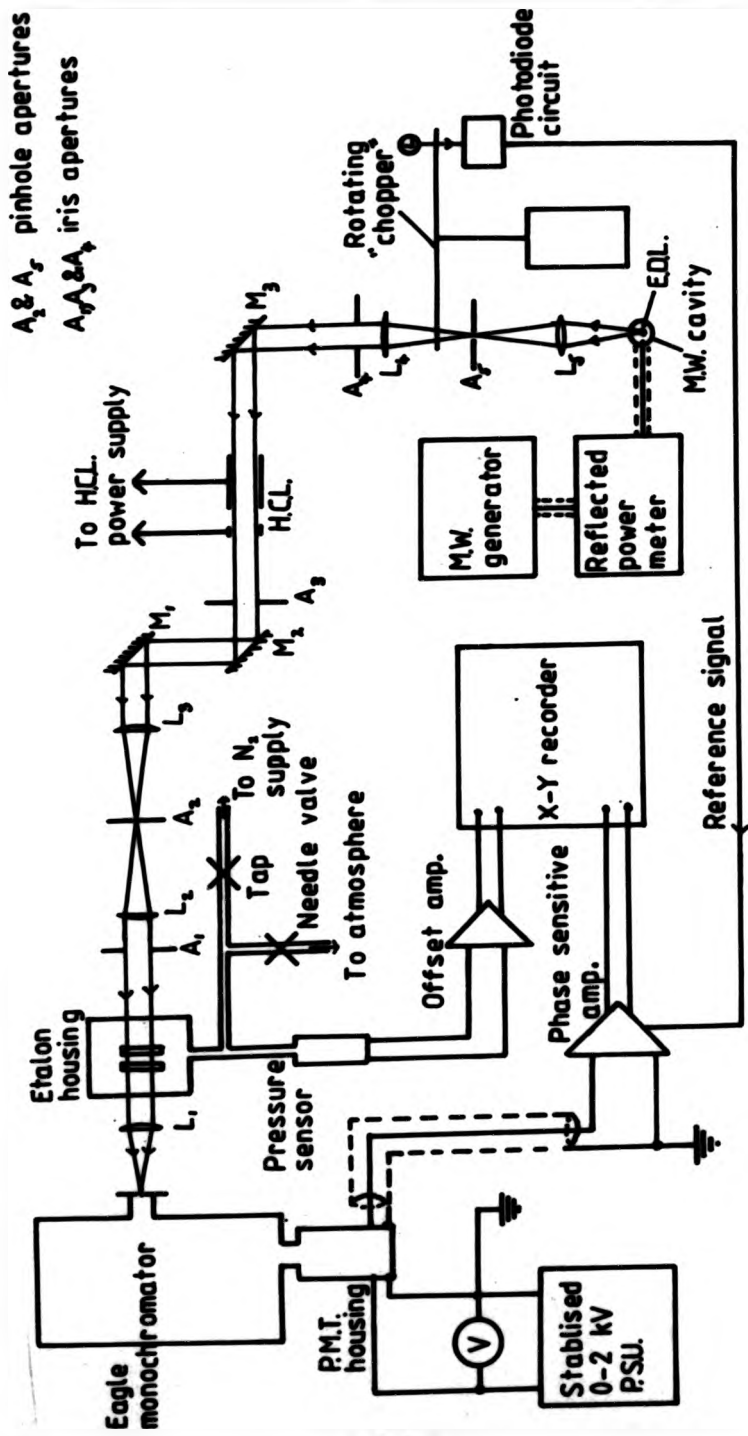


FIG. 11 SCHEMATIC DIAGRAM FABRY-PEROT ABSORPTION MEASUREMENT SYSTEM

chopper, and a phase sensitive amplifier (Brookdeal, 401) used in place of the D.C. coupled valve amplifier. The chopper also interrupted light falling on a photodiode illuminated by a small light bulb, providing a reference signal to the phase sensitive amplifier which only amplified that component of the P.M.T. signal which had a fixed phase relative to the reference signal. The phase angle could be varied with a control on the amplifier. Resistor R was external to the amplifier and value fixed at 2 M Ω , and gain was varied by turning the sensitivity control. The time constant was also controlled at the amplifier with no capacitor in parallel with resistor R. Both amplifiers used were subject to baseline drift and provided balance controls to adjust baseline offset.

By varying the P.M.T. potential V and amplifier gain, a suitable output level could be obtained for a wide range of intensities. The variation of P.M.T. response with tube potential V was measured in a series of steps. Starting with a high light flux and low tube potential, the light intensity was reduced until the signal level was halved, then V increased until the output was restored to the original level. By repeating this process the full range of the P.M.T. could be covered. A log/log plot of the response curve is shown in Fig. 12, which is well represented, within experimental error, by a straight line of gradient ~ 9.5 , which indicated that the response was proportional to V^n with $n \sim 9.5$. This is typical of P.M.T.'s, with the value of n increasing with the number of dynodes. The 9558B has eleven dynodes.

3/B.4 Basic Arrangement of Optical System

Setting up of the optical system was facilitated by the use of a low power He - Ne laser to define the optical axis. The monochromator and 1.5 m main optical bench (P.T.I.) were supported by separate heavy oak tables resting on a concrete floor and after initial setting - up of the bench, remained in the same position throughout the photometric experiments.

Placing suitable shims under it, the 1.5 m optical bench was made parallel to the optical axis defined by the laser beam, to within 1 mm in its entire length. Components, supported by bench saddles, were positioned with their centres on the optical axis and orientated normal to the axis by ensuring that light from the laser reflected at component faces, returned down the axis.

Lens L_1 and L_2 , and pinhole aperture A_2 - see Fig. 10 - remained in the same position on the main optical bench, in the different arrangements used in the photometric experiments. L_1 and L_2 were identical plano - convex, fused silica lens, of 350 mm focal length and 45 mm diameter. The two lenses, convex surfaces facing each other, were 0.6 m apart with pinhole aperture A_2 at the focal point of L_1 and L_2 with its focal point at the centre of the monochromator entrance slit.

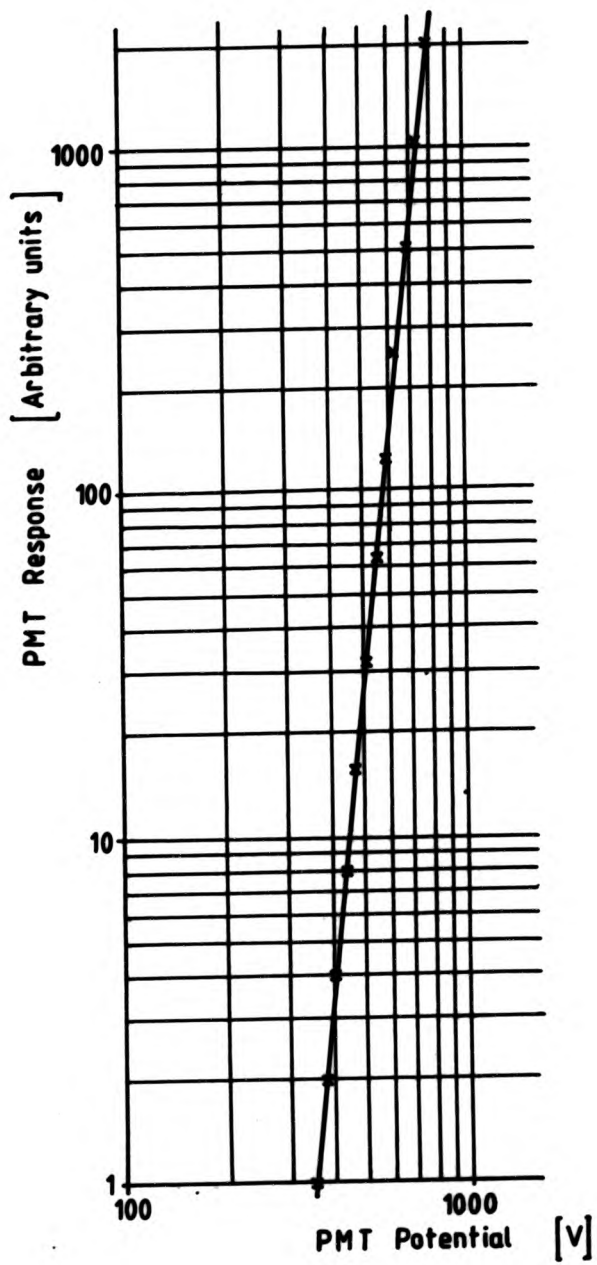
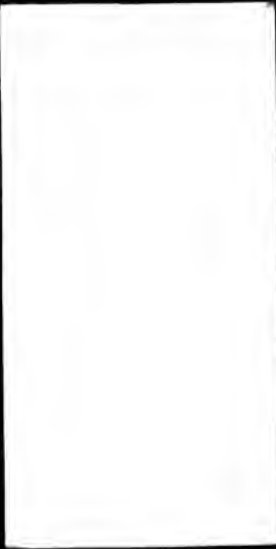


FIG.12 LOG PLOT OF PMT RESPONSE/POTENTIAL



An image of the light source to be analysed was formed on the pinhole aperture A_2 which acted as a near point source at the focal point of lens L_2 . Rays passing through aperture A_2 and intercepted by lens L_2 , travelled parallel to the optical axis between L_2 and L_1 and were converged to an image at the centre of the monochromator entrance slit. An iris aperture A_1 between L_1 and L_2 limited the diameter of the parallel beam between the lenses.

The interferometer housing, containing the Fabry - Perot etalon, was placed between L_1 and L_2 for interferometric experiments and removed when not required. Filters, when used, were also positioned between L_1 and L_2 .

3/B.5 Pressure Scanning Fabry - Perot Interferometer

3/B.5 (a) The Interferometer

A pressure scanning Fabry - Perot interferometer developed by a previous worker in the group A.Reed [43] was adapted to record Ne I spectral line profiles in this work. A schematic diagram of the interferometer system used is shown in Fig. 10. The Fabry - Perot etalon (constructed at Pye Unicam Cambridge) was mounted in an air tight housing, the internal pressure of which could be raised by allowing nitrogen from a regulated high pressure cylinder to enter the housing and reduced again controllably by allowing the gas to escape to atmosphere through a needle valve. The pressure within the housing was sensed by a Schaevitz P744-002 pressure transducer, the output of which controlled the X - deflection of an X - Y chart recorder via an offset amplifier. The offset amplifier subtracted that portion of the transducer output corresponding to atmospheric pressure. The Y - deflection of the X - Y recorder was controlled by the amplified P.M.T. output. By raising the pressure in the housing by about one atmosphere and then allowing it to fall, the refractive index of the gas between the etalon plates could be varied and the etalon passband be made to scan a spectral line isolated by the monochromator and the line profile plotted on the X - Y recorder. Direct recording of the housing pressure removed the need for an accurately controlled rate of change of pressure. A slow rate of change of pressure was necessary to ensure equal temperature and pressure at all points within the etalon housing and to prevent possible scanning error due to the X - Y recorder response time and the P.M.T. amplifier time constant. Typical spectral line scans took several minutes, and slower scanning rates were necessary with weak spectral lines requiring long P.M.T. time constants to smooth signal noise.

The etalon, plates supported by a steel sleeve, were pressed together against a

quartz spacer by two sets of three ball bearings, one set fixed, the other forced inwards via lever arms by three leaf springs. The tension in the leaf springs could be adjusted from outside the pressure housing in which the etalon was mounted. By varying the tension in the leaf springs the degree of parallelism of the coated faces of the plates could be adjusted. The etalon housing was supported on the 1.5 m optical bench by a mounting on two bench saddles which provided positive location but allowed the orientation and position of the etalon to be altered.

The plates, of quoted flatness $\lambda/150$, had a multilayer coating of diameter 35 mm with a peak reflectivity of 93% at 700 nm with 140 nm bandwidth [43]. The plates were of average thickness 10 mm with opposite faces slightly sparallel to ensure that unwanted light reflected at the uncoated faces "walked off" the optical axis. The quartz plate spacer used was 6 mm thick corresponding to a free spectral range of 83.3 m^{-1} .

3/B.5 (b) Adjustment and Finesse

The centres of the optical components were aligned on the optical axis defined by the laser beam and orientated so that the images of aperture A_2 , formed on the back of the aperture diaphragm because of reflection, were coincident with the aperture and hence the component surfaces were normal to the axis.

The Fabry - Perot interferometer instrument function and its width (usually expressed in terms of finesse $F = \frac{\Delta \sigma}{\sigma}$) are particularly sensitive to errors in the orientation and parallelism of the etalon. The orientation of the etalon obtained with the above method served as a first approximation before further optimisation. Initial etalon parallelism before optimisation was obtained by removing lens L_1 , replacing aperture A_2 with a Hg single isotope lamp and viewing the circular interference fringes produced by the etalon. The position of the observer's eye was moved over the surface of the etalon and the tension in the leaf springs adjusted until the diameter of the fringe circles remained constant independent of eye position.

The methods of optimisation employed were:-

- (i) The profile of a spectral line exhibiting isotope or hyperfine splitting (Eg. Hg 546.1 nm or Li 670.8 nm) was recorded repeatedly and etalon orientation and parallelism adjusted for maximum resolution of the spectral structure.
- (ii) A mode - stabilised He - Ne laser obtained temporarily from the National Physical Laboratory was used as a source of near ideally monochromatic light, allowing the instrument function of the interferometer at a wavelength of 632.8 nm to be recorded. The laser beam was diffused with a ground glass screen and the light focussed on aperture A_2 , ensuring that the full etalon area

was illuminated. The laser emission profile was repeatedly recorded and etalon orientation and parallelism adjusted for minimum width and maximum peak height of the profile.

With this latter optimisation technique a finesse of > 35 could be obtained after very careful adjustment however due to limited time for adjustment and temperature drift of etalon parallelism, routinely measurements were made with a finesse of ~ 30 (aperture A_2 diameter of 1.1 mm and A_1 diameter of 30 mm). The instrument function and finesse, and their dependence on interferometer parameters are discussed fully in Chapter 5.

3/C PHOTOMETRIC MEASUREMENTS (PARTICULAR EXPERIMENT DETAILS)

3/C.1 Emission Experiments

3/C.1 (a) Interferometer Scans of Emission Line Profiles.

The optical systems in the different photometric experiments included the same P.M.T., monochromator and arrangement of lens L_1 and L_2 and aperture A_2 . The systems differed in whether the interferometer housing was in position between L_1 and L_2 , for scanning spectral lines or not, and the systems used to form the image of the analytical source.

The system used for interferometric recording of the profile of spectral lines emitted by the experimental H.C.L. in configuration A is shown in Fig. 10. The image of the cathode glow, reduced by magnification of $1/2$, formed at pinhole aperture A_2 was produced by a bi-convex fused silica lens L_3 via two plane mirrors M_1 and M_2 arranged as a periscope. By adjusting the orientation of mirror M_1 , the position of the cathode image could be varied in order to isolate light from different regions of the glow.

When smaller, sealed lamps were analysed plane mirrors M_1 and M_2 were not used. The image of the source was formed directly with magnification of 1 by a shorter focal length condenser lens. The arrangement was the same as that shown in Fig. 9 for I/I measurements but with the interferometer housing in place between L_1 and L_2 .

3/C.1 (b) I/I Measurements

The system used to measure the variation of emission, spectral line intensity with lamp current, was similar to that used for Fabry - Perot scans of emission lines but with the etalon pressure housing removed and lamp current controlling the X - deflection of

the X - Y recorder, instead of etalon housing pressure. As in the case of the Fabry - Perot scans slightly different optical arrangements were used for measurements on sealed lamps and the experimental lamp. A diagram of the system used for sealed lamps is shown in Fig. 9, a separate diagram of the arrangement used for the experimental lamp is not provided, as the periscope arrangement was the same as that shown in Fig. 10 for Fabry - Perot scans.

Once the monochromator had been set to isolate the spectral line of interest and suitable gain and time constant chosen, the lamp current was slowly ramped and a curve of spectral intensity against lamp current plotted by the X - Y recorder. Currents were in the range $\sim 0 - 20$ mA and $\sim 0 - 50$ mA for sealed lamps and experimental lamp respectively, and were ramped in both increasing and decreasing current directions. Measurements could not be made from true zero current but from a small minimum current, that the controlled current P.S.U. could stably supply. This minimum current, indicated above by ~ 0 , was in fact ~ 0.1 mA depending on load conditions, and is discussed further in section 2/A on the lamp power supply.

Typical signal to noise ratios were more favourable than those encountered during Fabry - Perot scans, as, at high resolution only a very limited wavelength region is detected at any one time.

3/C.2 Absorption Experiments

3/C.2 (a) Absorption Measurements by Fabry - Perot Scans of Probe Beam Spectral Line Profiles

A diagram of the system is shown in Fig. 11; the experimental lamp, in configuration B, had an open - ended hollow cathode mounted in a chamber between two viewports, which allowed a probe beam to pass axially through the H.C. discharge. The experimental lamp is described fully in 2/B.8 and a diagram of lamp configuration B shown in Fig. 6.

A neon, microwave excited, electrodeless discharge lamp (E.D.L.) was used as the source of the probe beam. This type of primary source was chosen as it was the most intense neon source available and high primary source intensity was important because of the low level of P.M.T. signal in these experiments. This was because only a small fraction of the total source emission passed through the optical system due to its small solid angle and because of the high resolution of the Fabry - Perot interferometer only a small wavelength range was detected by the P.M.T. The E.D.L. consisted of a fused silica envelope, containing neon at ~ 1 torr, one end of which was inserted in an Evenson type microwave cavity, which had been designed at the Polytechnic (EMS, 215L). The tunable cavity was water cooled and driven by a 2.45 GHz microwave generator (EMS, MICROTRON 200 MK 2), via a reflected power meter and coaxial

cable interconnections. After initiation of the discharge with a Tesla coil, the microwave excited E.D.L. was run for at least half an hour before use, to allow conditions to stabilize. Microwave generator power was set at 50 W and the cavity tuning screws adjusted for minimum reflected power (~ 13 W).

In the optical arrangement used - see Fig 11 -, an image of the E.D.L. was formed by lens L_3 on pinhole aperture A_4 , which was at the focal point of lens L_4 . The parallel probe beam so produced, reflected by plane mirrors M_1 , M_2 and M_3 passed axially through the experimental hollow cathode discharge to be converged to an image on pinhole aperture A_2 . Probe beam width was controlled by iris apertures A_3 and A_4 .

The Fabry - Perot system was the same as that used for emission line profile measurements, except that the P.M.T. output was amplified by a phase sensitive amplifier instead of a D.C. coupled amplifier - see 3/B.3 for further details -. The probe beam was modulated at 33.33 Hz by a rotating "chopper" which also interrupted light illuminating a photodiode providing a reference signal for the phase sensitive amplifier (P.S.A). The P.S.A. only amplified that part of the P.M.T. output signal changing with fixed phase relative to the probe beam, hence the steady experimental H.C.L. emission was not amplified and only the probe beam spectral line profiles recorded. A modulating frequency of 33.33 Hz was used, to avoid spurious amplification of the 50 Hz mains frequency or its harmonics.

Spectral lines terminating in the Ne I levels of interest were chosen and the profiles of these spectral lines of the probe beam were recorded, initially with the experimental lamp off, then with the discharge running.

In this way the source spectral line profiles, with no absorption by the H.C. discharge, could be compared with the profile of these spectral lines after passage of the same source emission through the H.C. discharge, so that the absorption coefficients could be calculated and hence the number density of the Ne I lower levels deduced. - Details of the theory and method of the analysis are described in section 6/A -. Absorption measurements were carried out at 1, 2 and 5 torr H.C.L. fill gas pressures and lamp currents of 1, 2, 5, 10, 20 and 50 mA.

The probe beam filled the full diameter of the hollow cathode so that average absorption was observed and any spatial variation lost. Spatially resolved measurements scanning a narrow probe beam were not found possible as the small apertures required, resulted in an unacceptably poor signal to noise ratio. Measurements of total line absorption, without Fabry - Perot scanning, intended to observe spatial variation were carried out and are described in the next subsection.

A measurement "run" on a number of spectral lines was preceded and followed by a recording of the interferometer instrument function (I.F.), by scanning Ne I 632.8 nm

laser emission - see 3/B.5 (b) - to detect any variation. This was done as the calculation of absorbing atom number density required that the I.F. be known so that spectral lines, corrected for the effect of the interferometer, could be synthesised.

Measurements for a given spectral line and H.C.L. fill gas pressure started with a recording of the probe beam spectral profile with the H.C.L. switched - off. Then with the lamp running at current values of 0.6, 1.0, 2.0, 5.0, 10.0, 20.0 and 50.0 mA then decreasing through the same current values and finally with the H.C.L. switched - off again. In this way reproducibility of the results could be checked, and any showing excessive drift repeated. Usually the profiles were reproducible within a few percent.

Intermittent pulses of external interference badly degraded some profile measurements which had to be repeated with extra scans. The phase sensitive amplifier system, used in the Fabry - Perot absorption experiments, was found to be much more susceptible to this type of interference than the D.C. coupled amplifier system used in the I/I measurements. The interference could not be eliminated with simple mains filters and considerable time was wasted with the extra measurements.

3/C.2 (b) Measurements of Total Transmitted Intensity of Probe Beam Spectral Line

In order to measure the total spectral line intensity transmitted by the H.C.L. the system described above for Fabry - Perot scanning absorption measurements - see Fig. 11 - was modified. The etalon pressure housing was removed and H.C.L. lamp current controlled the X - deflection of the X - Y recorder instead of etalon housing pressure. The intensity of the spectral line isolated by the monochromator was recorded with the H.C.L. switched off, then the lamp was switched on and the lamp current ramped slowly from ~ 0 to 50 mA in the same way that H.C.L. I/I emission measurements were made - see 3/C.1 (b) -.

Measurements were made with a probe beam which fully filled the H.C. diameter for comparison with results from the Fabry - Perot scanning absorption experiments described in the previous subsection (3/C.2 (a)) and with a narrow probe beam for spatially resolved measurements of absorption. Spatially resolved measurements of total spectral absorption were possible, whereas spatial resolution could not be achieved in Fabry - Perot scanning absorption measurements, because, as the total intensity of a spectral line was detected, instead of the narrow wavelength range transmitted by the etalon, the P.M.T. signal level was much greater without the etalon. Consequently signal to noise ratios were much more favourable without the high dispersion of the etalon and allowed measurements to be made with the small apertures necessary to produce a narrow parallel beam (~ 3 mm diameter); a very small pinhole (< 1 mm diameter) was



used for aperture A_3 to ensure a high degree of probe beam parallelism and iris aperture A_4 (3 mm diameter) limited beam width - see Fig. 11.

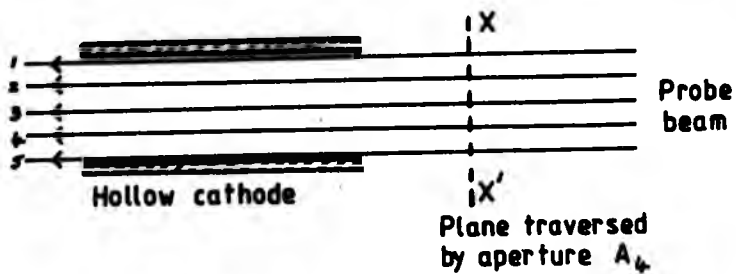
The total absorption experiments were carried out when little time remained of the period allowed for experimental work, consequently measurements were restricted to Ne I 640.2 nm from the number of spectral lines studied in the scanning absorption experiments. Furthermore an error was made in the design of the spatially resolved absorption experiments and by the time the error was recognised the measurements could not be repeated with the error in experimental method corrected.

When measuring the spatial variation of total absorption across a diameter of the hollow cathode, either the probe beam or the cathode can in principle be moved. The author chose to move the probe beam because the experimental arrangement could be set up more quickly for structural reasons. In the experimental method used, aperture A_4 was placed at different positions across the full probe beam width to confine the beam to different regions of H.C. glow.

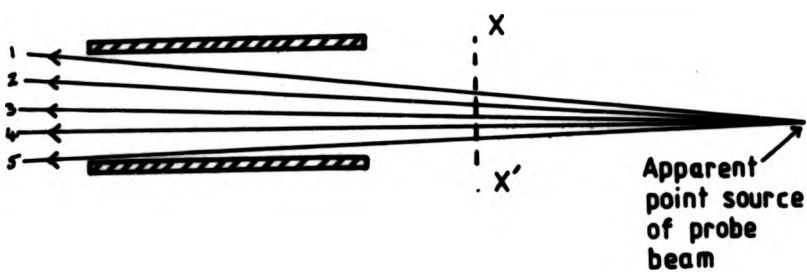
It would have been much better to move the cathode and keep aperture A_4 fixed, and so keep constant the angles at which rays of the probe beam passed through the optical system. The heavy experimental lamp apparatus could have been jacked up and down or traversed laterally on a sturdy carriage. Schematic ray diagrams which illustrate the problem with the method used are shown in Fig. 13, the idealized case of parallel rays, parallel to the cathode axis is shown in Fig. 13 (a). Although different rays (1 to 5 in diagram) take different paths through the subsequent optics, this may be corrected for by adjusting the P.M.T. potential so that the deflection on the X - Y recorder, with the H.C.I. switched off, was the same for each position of aperture A_4 . However, if one includes a degree of beam divergence (with solid angle determined by the focal length of L_4 and diameter of aperture A_3) and apertures of probe beam and cathode axis due to setting - up error, the problem is apparent - see Fig 13 (b) -. Pencils of rays isolated by A_4 in different positions of plane XX' do not take similar, parallel paths through the H.C. producing asymmetric results.

Fig. 13 (c) shows the situation if the cathode is traversed laterally relative to a single narrow pencil of rays. The effect of beam divergence will be small, and assuming the cathode travel is accurate, ray paths relative to the cathode will be strictly self parallel.

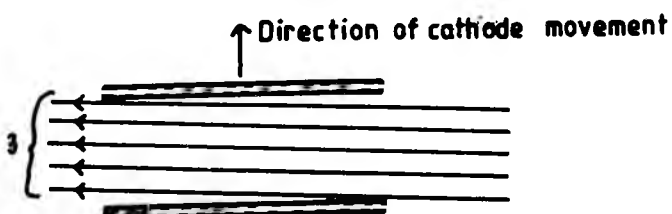
With the method used, the asymmetry of ray paths made it difficult to analyse the results and deduce information about the radial variation of the density of the metastable excited atoms.



- (a) Ideal case - no probe beam divergence or aparrallem of probe beam and hollow cathode axis



- (b) Situation with probe beam divergence and aparrallem of beam and cathode axis



- (c) Positions of ray 3 relative to cathode as the cathode is traversed - same aparrallem of beam and cathode axis as (b)

FIG.13 EXAGGERATED SCHEMATIC DIAGRAMS OF RAY PATHS THROUGH HOLLOW CATHODE

3/D RECORDING OF V/I CHARACTERISTICS

V/I characteristics of the H.C.L.'s were recorded for the following reasons:-

- (a) at low currents there are changes in the I/I curves and other observed parameters; there were linked changes in V/I characteristics.
- (b) the V/I characteristic is sensitive to gas purity, which was particularly important in early stages of the work.
- (c) subsequently the maintenance voltage was routinely monitored.

A system for measuring the variation of H.C.L. maintenance voltage with lamp current (V/I characteristic) was incorporated into the power supply circuit - Fig. 1 shows a diagram of the circuit used -. The design and performance of the H.C.L. power supply is described in subsection 2/A. When recording V/I characteristics the lamp current was slowly ramped and the V/I characteristic recorded on the X - Y chart recorder. The lamp current was made to control the X - deflection of the X - Y recorder by passing the current through a resistance box (R_1) which provided a suitable potential difference ($\sim 1V$) to drive the recorder's X - axis input.

The anode voltage controlled the Y - deflection of the recorder via a potential divider (R_2 and R_3) and an offset amplifier. The potential divider reduced the voltage to a level ($\sim 1V$) suitable to drive the recorder's Y - axis input. The offset amplifier was used, because of the very flat nature of H.C.L. V/I characteristics, to subtract a portion of the voltage signal corresponding to 150 V of anode potential.

The V/I scales, voltage 150 to 250 V and current (0 to 20 or 50 mA), were calibrated against the D.M.M. and Avometer, adjusting the values of R_1 , R_2 and amplifier offset, with the H.C.L. replaced by a 20 k Ω resistor. The X - axis input terminals were provided with Zener diodes connected to earth to protect the recorder input amplifier in the event of an accidental open circuit in which case the P.S.U. would deliver the full 1.5 kV.

3/E VISUAL INSPECTION OF GLOW

The H.C. glow of the 15 mm bore experimental lamp in both configurations used, were inspected visually and viewed through a direct vision spectroscope. Visual inspection of the glow provided useful information as the sudden changes in glow brightness at low currents could be detected. Further, the development of an annular glow structure at higher pressure and current could be observed - see section 4/D. Visual inspection was also very useful when eliminating stray discharges in the experimental lamp in configuration B (see 2/B.8 (c)). Positive column, stray discharges could be observed visually but also could be detected by their effect on the V/I characteristic. The

H.C. stray discharge described in 2/B.8 (c) however, could only be detected by visual inspection as it did not affect the V/I characteristic significantly.

Observation via the spectroscope was used as a quick check for the presence of impurity bands.

CHAPTER 4 RESULTS

4/A PHOTOMETRIC MEASUREMENTS

4/A.1 Spectral Lines Studied

The work was primarily concerned with Ne I spectral lines although some results were obtained for Ne II spectral lines and one Fe I spectral line. A complete list of the spectral lines studied is provided in Table 1, showing which spectral lines were included for study in each of the four types of photometric experiment :-

<u>Emission</u>	(a) Fabry - Perot scans
	(b) I/λ measurements
<u>Absorption</u>	(c) Fabry - Perot scans of probe beam
	(d) Measurements of total transmitted probe beam intensity

An Ne I energy level diagram and table of levels [44, 45] are provided in Fig 14 and Table 2.

The choice of spectral lines studied was restricted in both wavelength and intensity by the range of the P.M.T. spectral response, the P.M.T. dark current and the level of noise. When the Fabry - Perot etalon was used, its high dispersion reduced the detected intensity and so further restricted the choice of spectral lines which could be usefully studied.

Interference by close lying spectral lines of sputtered cathode material and, to a lesser extent, Ne II, also eliminated some Ne I spectral lines from possible study.

The prominent Ne I spectral lines in the 'red' region of the spectrum, accounting for a large majority of spectral energy emitted, arise from atomic transitions between the 3p, 3p' group of energy levels and the 3s, 3s' group of levels. Consequently all the results obtained from Fabry - Perot scanning experiments and the majority of those from I/λ measurements were for spectral lines with transitions between these groups of energy levels.

The 3s, 3s' group of four energy levels includes the two metastable states $3s [^3/2]_2^0$ and $3s' [^1/2]_0^0$; the former is the lowest energy Ne I excited state. Spectral lines with transitions terminating in both metastable and non - metastable energy levels were studied.

Within the constraints described above, the basis on which Ne I spectral lines were chosen for study were :-

Emission experiments

- (a) Fabry - Perot scans - a wide selection of spectral lines with atomic transitions between the 3s, 3s' and 3p, 3p' groups of energy levels.

Spectrum	λ [nm]	Emission		Absorption	
		I/i	Fabry-Perot	Fabry-Perot	Total
Fe I	363.4	✓			
NeII	371.3	✓			
NeII	337.8	✓			
Ne I	360.0	✓			
"	363.4	✓			
"	470.4	✓			
"	534.3	✓			
	540.1	✓			
	585.2	✓	✓	✓	
	588.2	✓	✓	✓	
	614.3	✓	✓	✓	
	630.5	✓	✓	✓	
	640.2	✓	✓	✓	✓
	659.9	✓	✓		
	667.8	✓			
	671.7	✓			
	692.9	✓			
	703.2	✓	✓	✓	
	724.5	✓			
	743.8	✓			
	748.9	✓			
	626.6	✓	✓	✓	
	594.5		✓		
	633.4		✓		
	665.2		✓		
	616.4		✓		
	618.2		✓		
	705.9		✓		
	621.7		✓		

TABLE 1 SPECTRAL LINES STUDIED IN EXPTS.

λ [nm]	Paschen	Level	Energy [eV]	Paschen	Level	Energy [eV]
360.0	3p _o	4p[3P] ₁	20.29	1s ₂	3s[3P] ₁	16.85
363.4	3p _o	4p[3P] ₂	20.26	1s ₂	3s[3P] ₂	16.85
470.4	5d _o	5d[3D] ₁	21.02	2p _o	3p[3P] ₁	18.38
534.3	4d _o	4d[3D] ₁	20.70	2p _o	3p[3P] ₁	18.38
540.1	2p _o	3p'[3P] ₁	18.97	1s _o	3s[3P] ₁	16.67
585.2	2p _o	3p'[3P] ₂	18.97	1s _o	3s[3P] ₂	16.85
588.2	2p _o	3p[3P] ₁	18.73	1s _o	3s[3P] ₁	16.62
614.3	2p _o	3p[3P] ₂	18.64	1s _o	3s[3P] ₂	16.62
630.5	2p _o	3p[3P] ₂	18.64	1s _o	3s[3P] ₂	16.67
640.2	2p _o	3p[3P] ₁	18.56	1s _o	3s[3P] ₁	16.62
659.9	2p _o	3p[3P] ₁	18.73	1s _o	3s[3P] ₁	16.85
667.8	2p _o	3p[3P] ₂	18.70	1s _o	3s[3P] ₂	16.85
671.7	2p _o	3p[3P] ₁	18.67	1s _o	3s[3P] ₁	16.85
692.9	2p _o	3p[3P] ₂	18.64	1s _o	3s[3P] ₂	16.85
703.2	2p _o	3p[3P] ₁	18.38	1s _o	3s[3P] ₁	16.62
724.5	2p _o	3p[3P] ₁	18.38	1s _o	3s[3P] ₁	16.67
743.8	2p _o	3p[3P] ₁	18.38	1s _o	3s[3P] ₁	16.72
748.9	3d _o	3d[3D] ₁	20.04	2p _o	3p[3P] ₁	18.38
626.6	2p _o	3p'[3P] ₁	18.69	1s	3s[3P] ₁	16.72

TABLE 2
SOME NeI SPECTRAL LINES & ENERGY LEVELS

- (b) I/A measurements - wide selection of the spectral lines with $3p, 3p' - 3s, 3s'$ transitions and transitions from higher energy levels.

Absorption Experiments

- (c) Fabry - Perot scans of probe beam - two spectral lines with transitions from the $3p, 3p'$ group of energy levels to each of the metastable $3s, 3s'$ energy levels and one each for the two non - metastable levels.
- (d) Total absorption experiments - confined, because of lack of time to Ne I 640.2nm with a transition from a level of the $3p, 3p'$ group ($3p [^3/2]_3$) to $3s [^3/2]_2^o$.

4/A.2 Photometric Results

4/A.2 (a) Fabry - Perot Scans of Emission Lines

Recording of the profiles of Ne I spectral lines emitted by H.C. discharges proved interesting as it revealed self - reversal of spectral lines with transitions terminating in the metastable state $3s [^3/2]_2^o$. This self - reversal was first observed with a sealed H.C.L. manufactured by Cathodeon and subsequently with the experimental lamp at different fill gas pressures (1, 2, 3, and 5 torr) and in the two lamp configurations studied.

The self - reversal first noted in Ne I 614.3 nm, was observed in all spectral lines with transitions terminating in $3s [^3/2]_2^o$, with the exception of Ne I 588.2 nm. No spectral lines with transitions to other energy levels were observed to show this effect.

An example of this effect is shown in Fig 15 (a) containing Fabry - Perot scans of Ne I 640.2 nm and Ne I 585.2 nm emitted by the experimental lamps (config. A) at 1 torr; the former with a transition terminating in $3s [^3/2]_2^o$ shows marked self - reversal whereas the latter with transition terminating in $3s' [^1/2]_1^o$ shows no sign of reversal. Ne I 640.2 nm was found to have the greatest degree of self - reversal of all the spectral lines studied.

Fabry - Perot scans of Ne I 640.2 nm emitted by a sealed H.C.L. at different values of lamp current are shown in Fig 16 with system gain adjusted to make the profiles of approximately the same height. As the lamp current is increased the degree of self - reversal and overall line width increases also. This is consistent with the behaviour observed in the better known self - reversal and self - absorption of resonance radiation of sputtered cathode atoms [43, 46].

Self - reversal of Ne I spectral lines was found to be very sensitive to the presence of impurities produced by outgassing and thorough degassing of the experimental lamps was necessary before reproducible results could be obtained - see

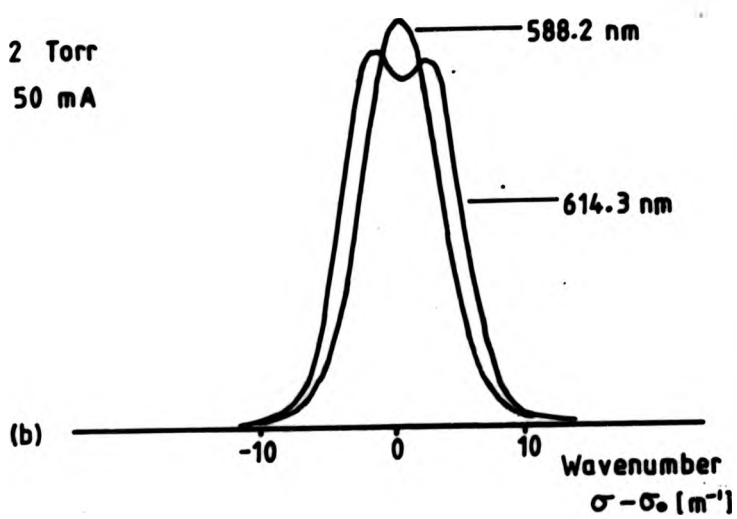
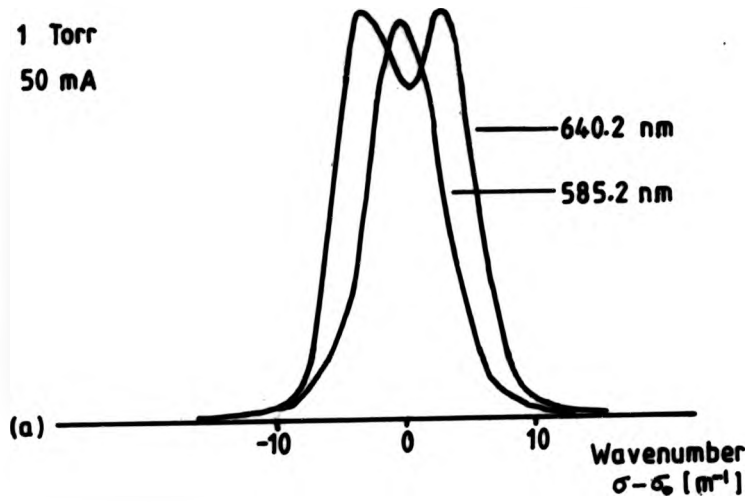


FIG.15 NeI EMISSION LINE PROFILES
EXPERIMENTAL LAMP (CONFIG. A)

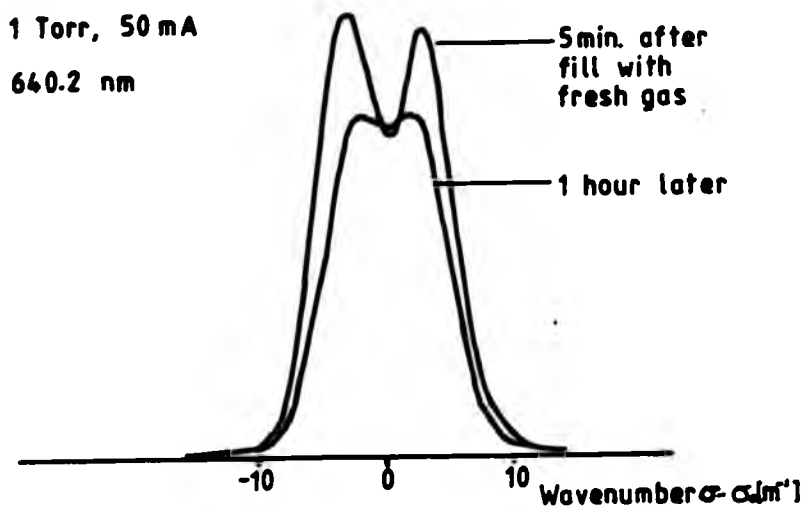


FIG.17 NeI EMISSION LINE PROFILES AFFECTED BY CONTAMINATION OF FILL GAS

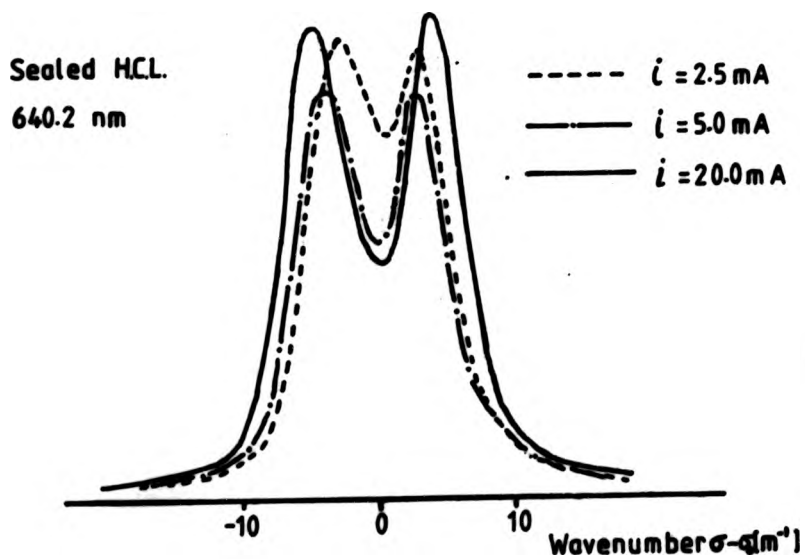


FIG.16 NeI 640.2 nm EMISSION LINE PROFILES AT THREE LAMP CURRENTS, SEALED HCL.

Fig. 17 - . In fact, the degree of self - reversal was later used as a check of fill - gas purity.

The effect of impurities on Ne I spectral line profiles is described in the section on impurities 7/E .

4/A.2 (b) I/I measurements

Examples of typical results obtained from measurements of the variation of Ne I spectral intensity with lamp current are shown in Figs. 18 to 21. Results presented are for the experimental H.C.L. in configuration A and fill gas pressures of 1, 2, 3 and 5 torr and a sealed H.C.L.; examples of results for Ne II and Fe I spectral lines are provided in Fig. 22 for comparison. Results obtained for the experimental H.C.L. in configuration A and B were very similar and only those for lamp configuration A are presented.

A slight hysteresis effect was observed when measurements were made with the lamp current ramped in both increasing and decreasing current directions. This effect disappeared after prolonged running of discharge and results presented are for increasing current, after running the lamp to establish steady condition.

The form of the I/I curves was found to depend on fill gas purity and results presented here are for conditions of maximum neon purity. The effect on I/I curves of gas impurities, due to contamination initially encountered with the experimental lamps (see section 2/B.6), is discussed in section 7/E on impurity effects.

The principal features of the Ne I I/I curves obtained under high purity condition, may be summarized:

- (i) The intensity I shows a generally increasing trend with increasing lamp current i.
- (ii) The I/I curves of spectral lines with atomic transitions from high energy levels (i.e. 3d and above) curve over tending to saturate with increasing current - Eg. Ne I 360.0 nm, Fig. 18.
- (iii) I/I curves of spectral lines corresponding to atomic transitions between the 3s, 3s' and the 3p, 3p' groups of energy levels, with the exception of $3p' [^1/2]_0$, are approximately linear with an upward curvature - Eg. Ne I 588.2 nm, Fig. 18.
- (iv) I/I curves of spectral lines with transitions from $3p' [^1/2]_0$ (which is of significantly higher energy than the rest of the 3p, 3p' group) are similar to those for the rest of the group but offset at low current - Eg. Ne I 585.2 nm, Fig. 19.
- (v) At high fill gas pressure I/I curves for spectral lines with transitions between the

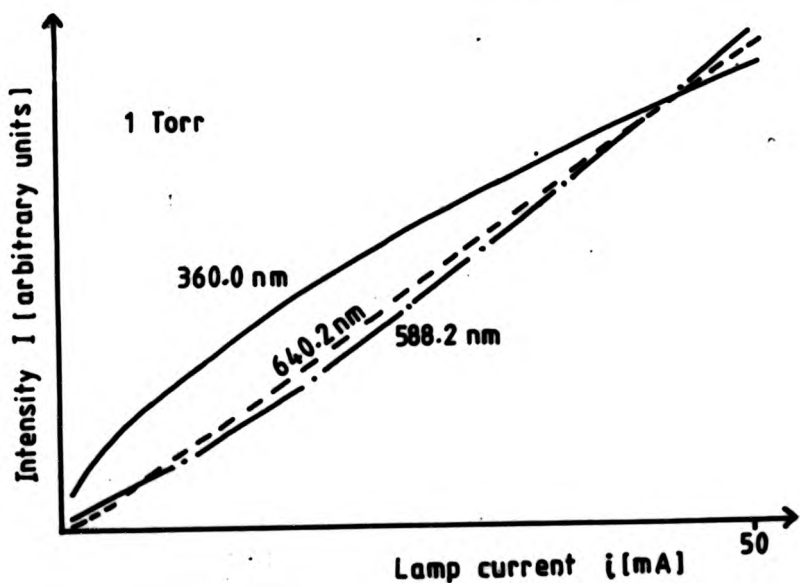
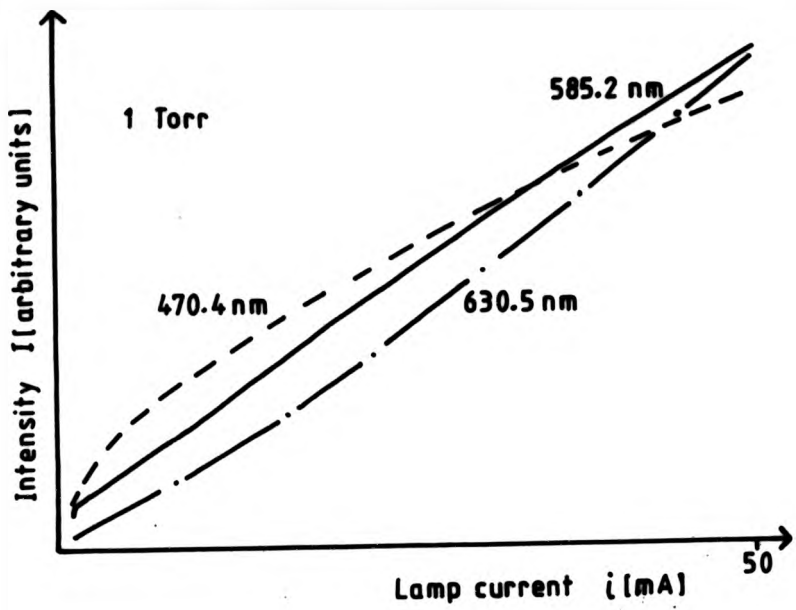


FIG.18 I/i CURVES OF NeI LINES
EXPERIMENTAL LAMP (CONFIG. A)

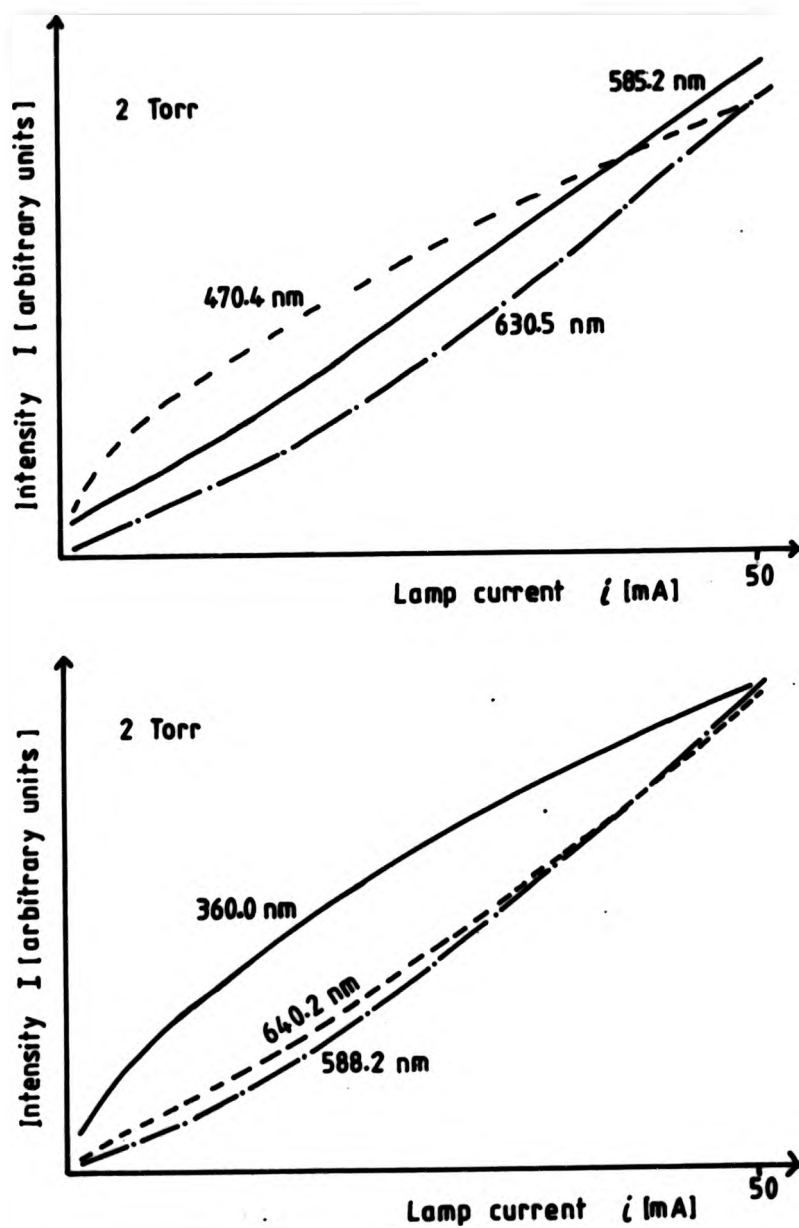


FIG.19 I/i CURVES OF Ne I LINES
EXPERIMENTAL LAMP (CONFIG. A)

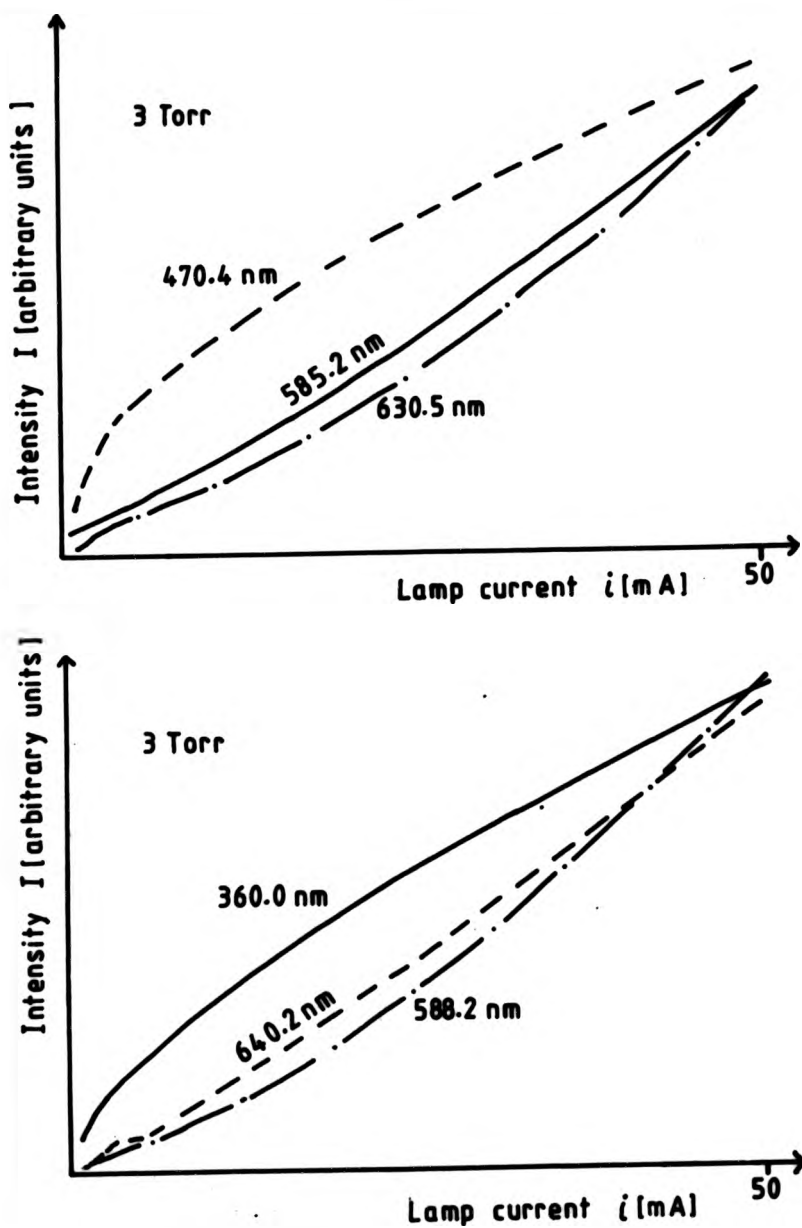


FIG.20 I/i CURVES OF Ne I LINES
EXPERIMENTAL LAMP (CONFIG. A)

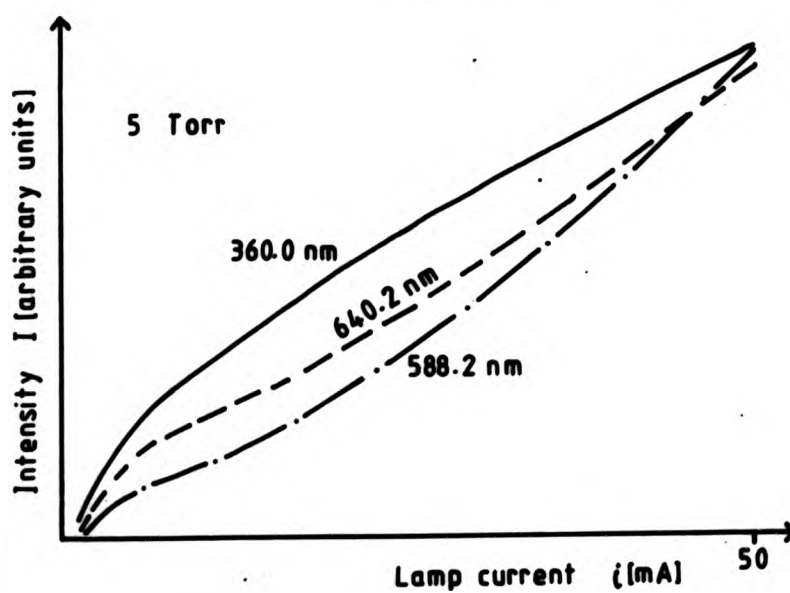
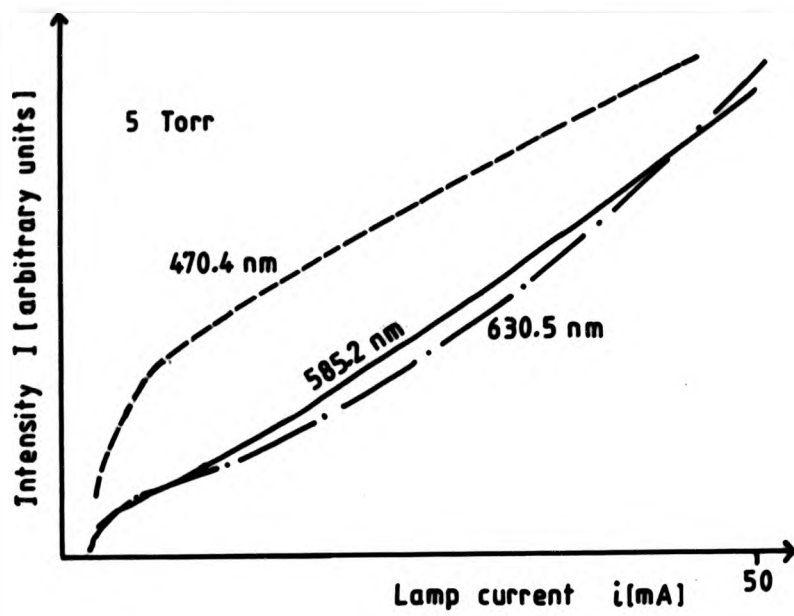


FIG. 21 I/i CURVES OF Ne I LINES
EXPERIMENTAL LAMP (CONFIG. A)

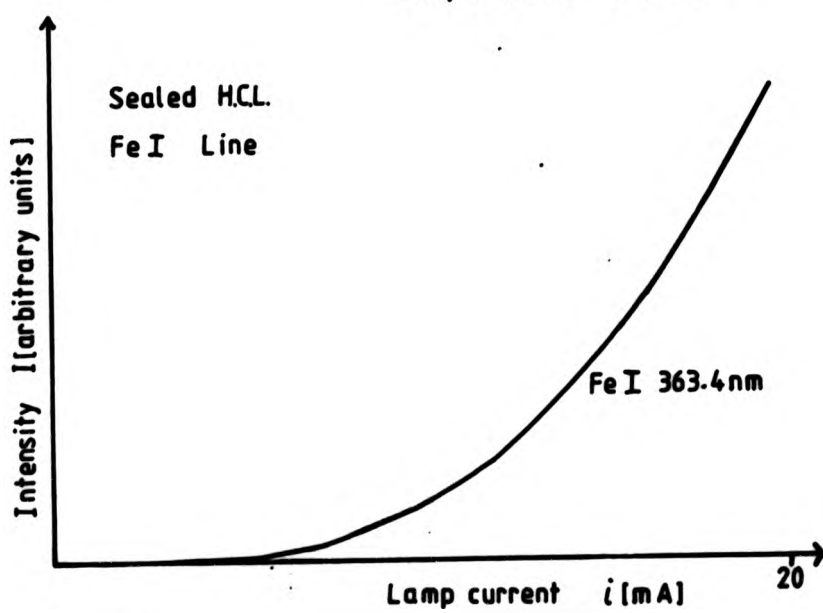
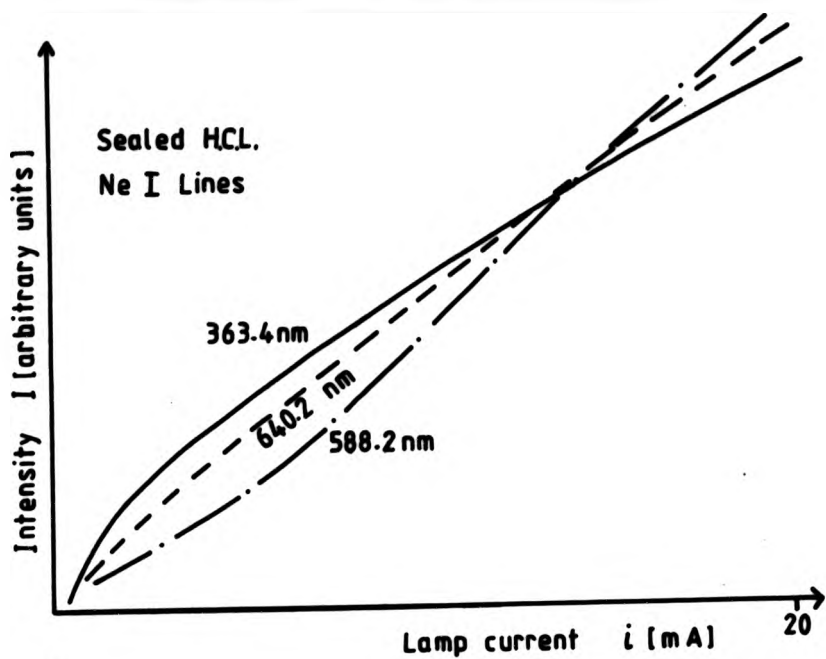
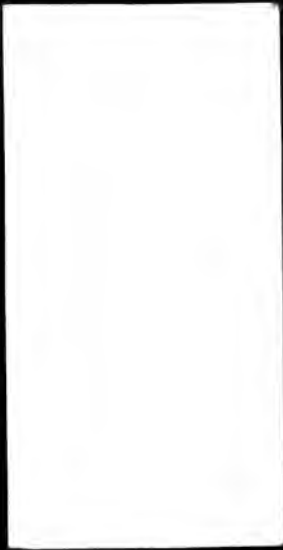
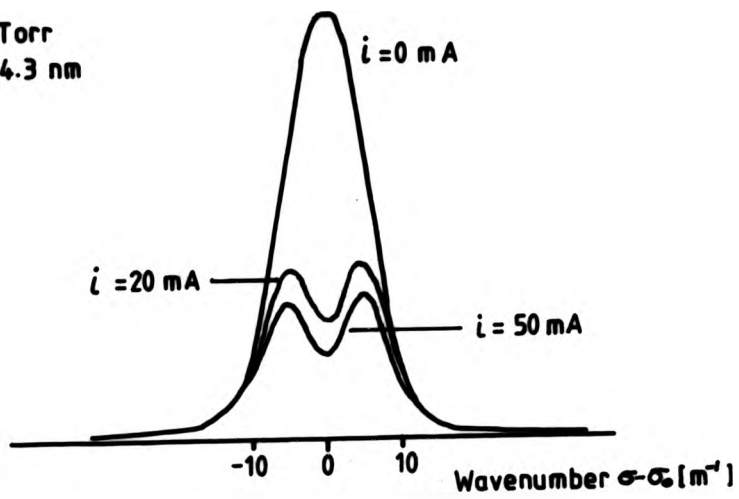


FIG.22 I/i CURVES OF NeI & Fe I LINES
SEALED HCL.



1 Torr
614.3 nm



1 Torr
585.2 nm

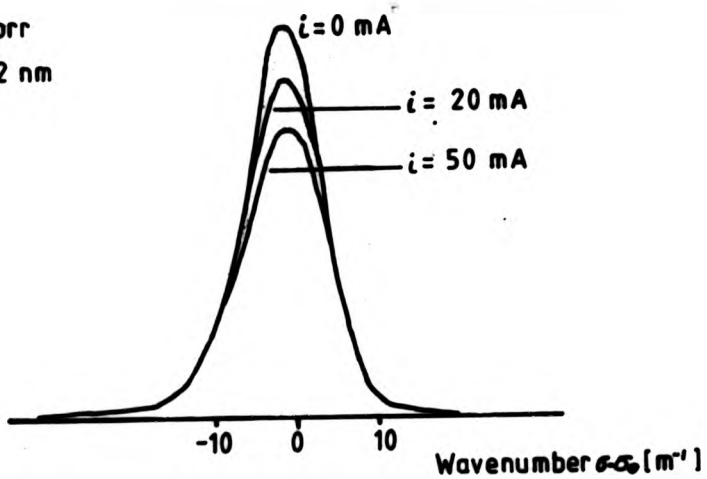


FIG.23 NeI LINE PROFILES RECORDED IN
FABRY-PEROT ABSORPTION EXPERIMENTS

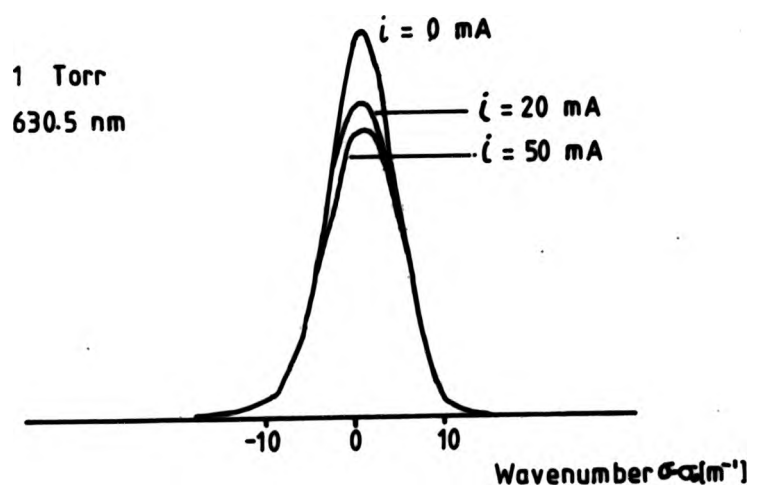
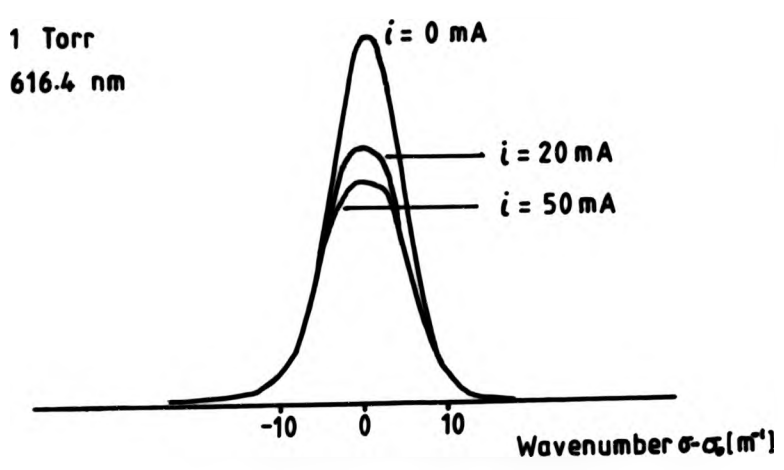
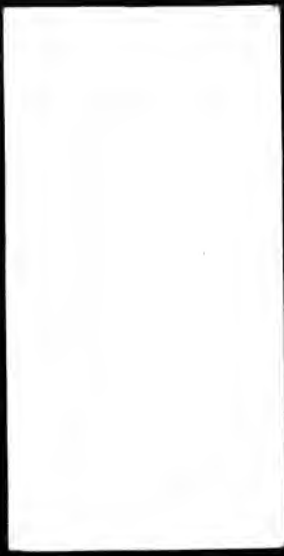


FIG.24 Ne I LINE PROFILES RECORDED IN FABRY-PEROT ABSORPTION EXPERIMENTS
62

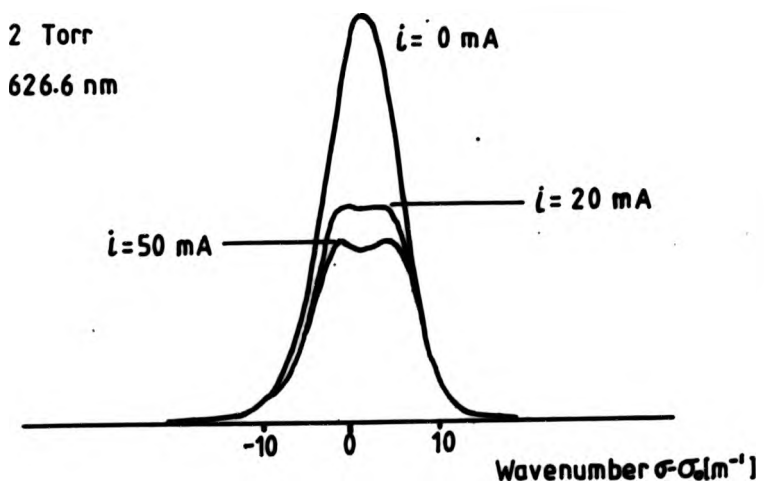
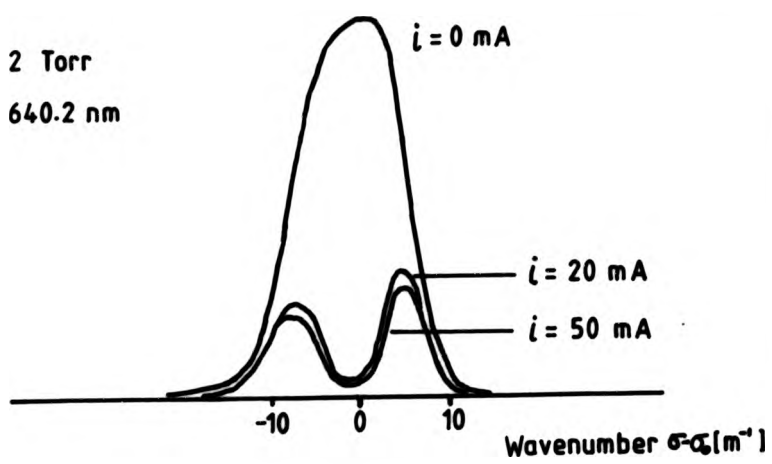


FIG.25 Ne I LINE PROFILES RECORDED IN
FABRY-PEROT ABSORPTION EXPERIMENTS

3s, 3s' and 3p, 3p' groups of levels develop a "hump" at about 6 mA - see Fig. 21.

In contrast to results for Ne I spectral lines, I/I_0 curves for Ne II spectral lines are in general straight lines passing through the origin. I/I_0 curves for Fe I spectral lines of sputtered cathode material however exhibit strong curvature. They are tangential to the current axis near the origin and rise steeply at higher currents - see Fig. 22.

4/A.2 (c) Fabry - Perot Scanning Absorption Measurements

Typical probe beam, spectral line profiles, recorded with the H.C.L. switched off and with it running are shown in Figs. 23 to 25.

Some general features of these results are: -

- (i) The profiles of Ne I 640.2 and 614.3 nm spectral lines with transitions terminating in the metastable state $3s [^3/2]_2^o$ show evidence of strong absorption by the H.C. discharge - see Figs. 23 and 25.
- (ii) Spectral lines with transitions terminating in other energy levels of the 3s, 3s' group exhibit (eg. Ne I 585.2 nm) less pronounced absorption - see Fig. 23.
- (iii) The spectral profiles for H.C.L. fill gas pressures of 1, 2 and 5 torr are similar, indicating that the degree of absorption (and hence the population of absorbing atoms) varies little with fill gas pressure.
- (iv) Profiles recorded exhibit a pronounced saturation of the degree of absorption with increasing H.C.L. current.
- (v) The profile of the Ne I 640.2 nm spectral line emitted by the primary source was broadened and has a slight dip near the peak indicating that some self-absorption by $3s [^3/2]_2^o$ metastable excited neon atoms occurred within the microwave excited E.D.L. - see Fig. 25 -.

4/A.2 (d) Total Absorption Measurements

The measurements of probe beam total absorption of Ne I 640.2 nm, carried out were of two types

- (a) full aperture
- (b) limited aperture measurements intended to achieve spatial resolution.

For reasons described in the experimental section 3/C. 2(b) the latter measurements were unreliable and will not be presented.

The former measurements of total absorption were made with the same optical arrangement as the Fabry - Perot scanning absorption measurements and are useful for comparison with these results.

Spectral absorbance (given by $\log \frac{I(i=0)}{I(i)}$ where $I(i)$ is the total line intensity),

is usually assumed to be proportional to the number density of absorbing atoms. Measurements of spectral absorbance are much easier to both record experimentally and analyse, than measurements of absorption coefficient. Consequently, investigations of the variation of excited atom number densities are often made via measurements of spectral absorbance, though absolute number densities cannot readily be calculated from absorbance.

Typical results of the total absorption experiments are provided in Fig. 26. In these figures the detected intensity of the probe beam Ne I 640.2 nm spectral line is shown as the experimental lamp current was increased from the minimum value that would sustain a stable discharge to 50 mA. The detected intensity with experimental lamp switched off, which provided the reference ($i = 0$) intensity level with no absorption, is indicated.

Notable features of these results are :-

- (a) Slow change in transmitted probe beam spectral intensity with lamp current.
- (b) Local minimum in transmitted spectral intensity in low current region at 5 torr.

4/B V/i CHARACTERISTICS

The voltage/current characteristics of the experimental H.C.L. in configuration A with fill gas pressures of 1, 2, 3 and 5 torr are shown in Figs. 27 and 28 and that of a sealed lamp in Fig. 29 (Note that these graphs have an expanded voltage scale with the origin not shown). The V/i characteristics of the experimental H.C.L. in configurations A and B were very similar and only those for configuration A are presented.

Hysteresis effects were noted as in the I/i measurements and results were not reproducible until the lamp had warmed - up and stabilized.

Principal features of the results are :-

- (a) The pronounced flatness of the V/i characteristics. The maintenance voltage typically changes by no more than a few percent over the main zone of the characteristic (i.e. current above ~ 5 mA), while the lamp current increases many times.
- (b) The maintenance voltage and V/i characteristic form vary little with different fill gas pressures.
- (c) However the V/i characteristics develop a small 'bump' in the low current region as fill gas pressure is increased - see Fig. 28.

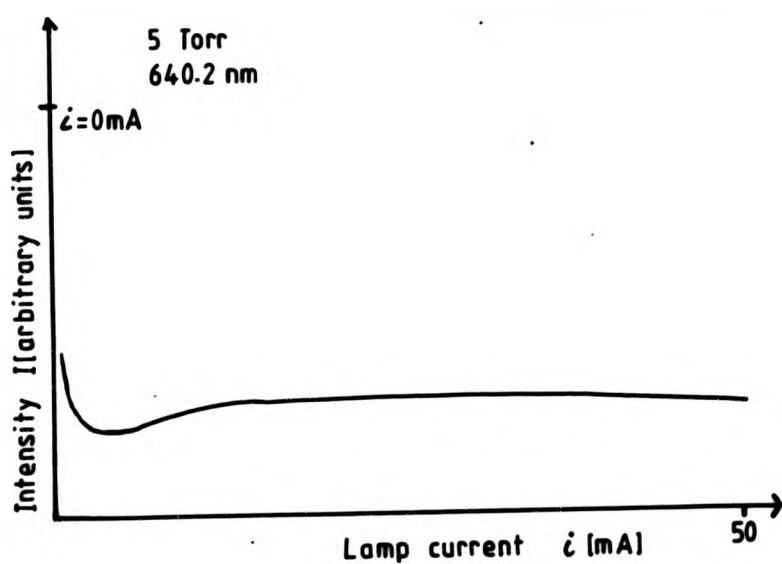
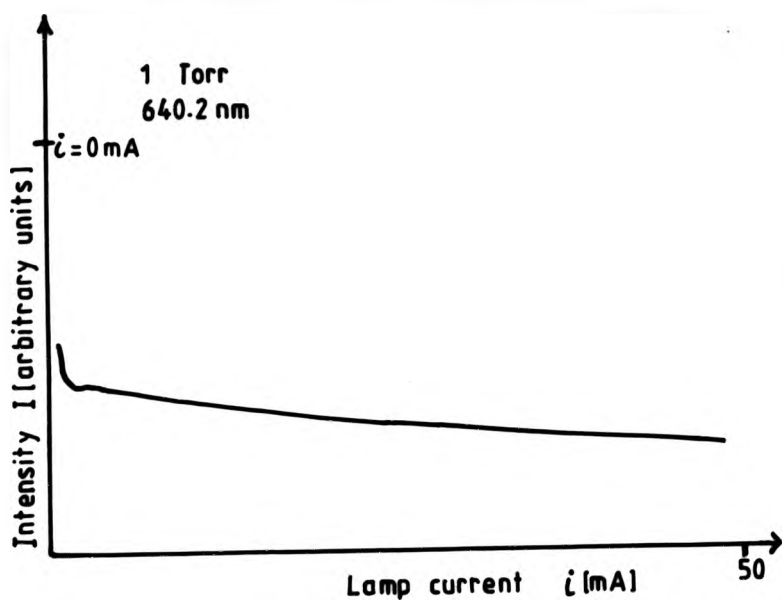


FIG.26 VARIATION OF PROBE BEAM SPECTRAL INTENSITY WITH EXPERIMENTAL LAMP CURRENT

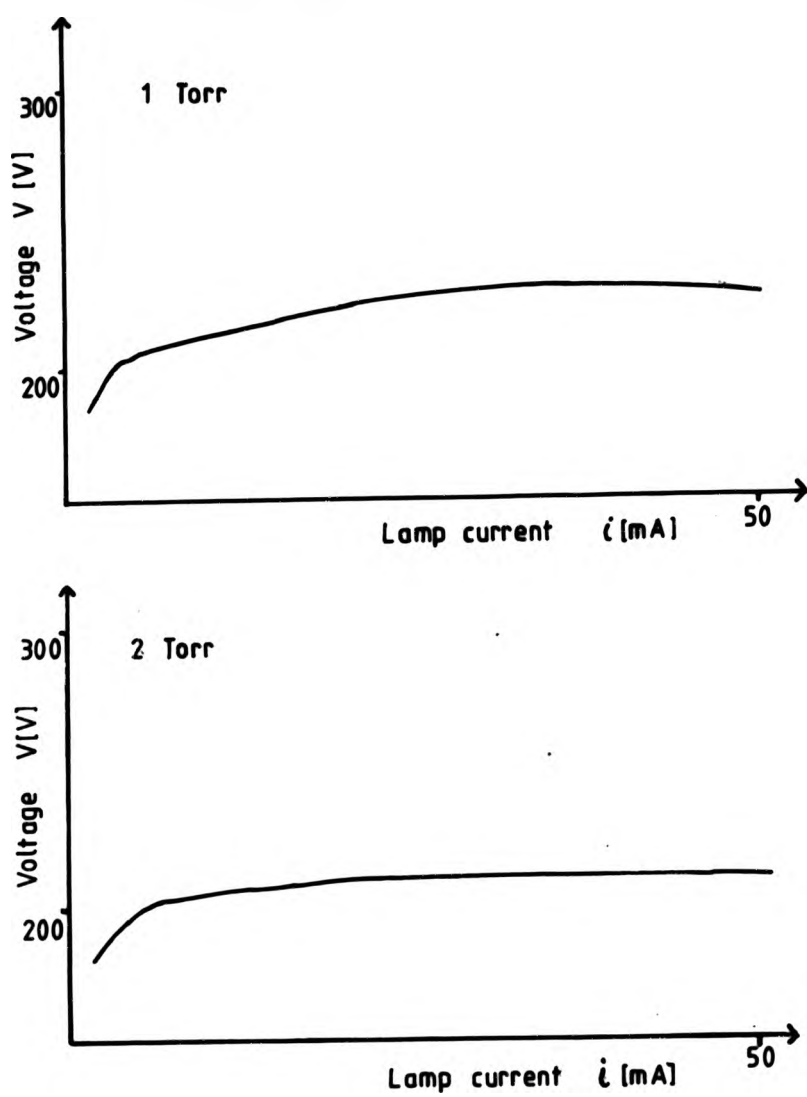


FIG.27 V/i CHARACTERISTICS OF EXPERIMENTAL LAMP (CONFIG. A)

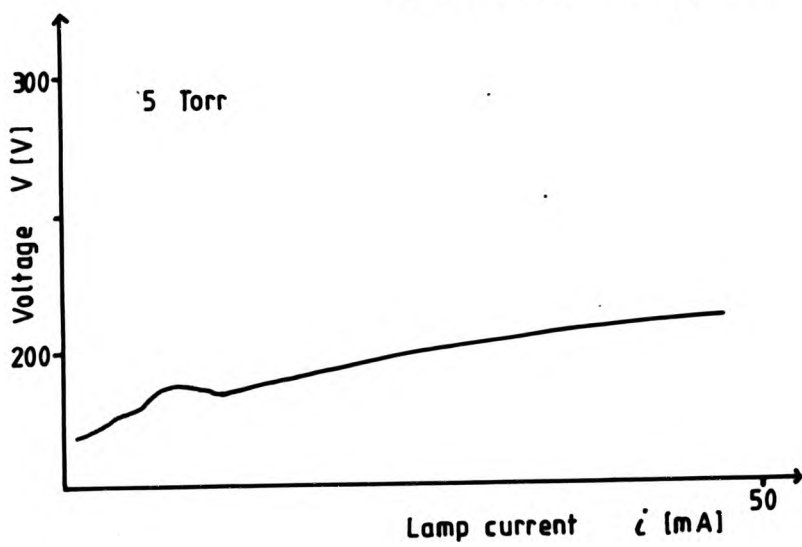
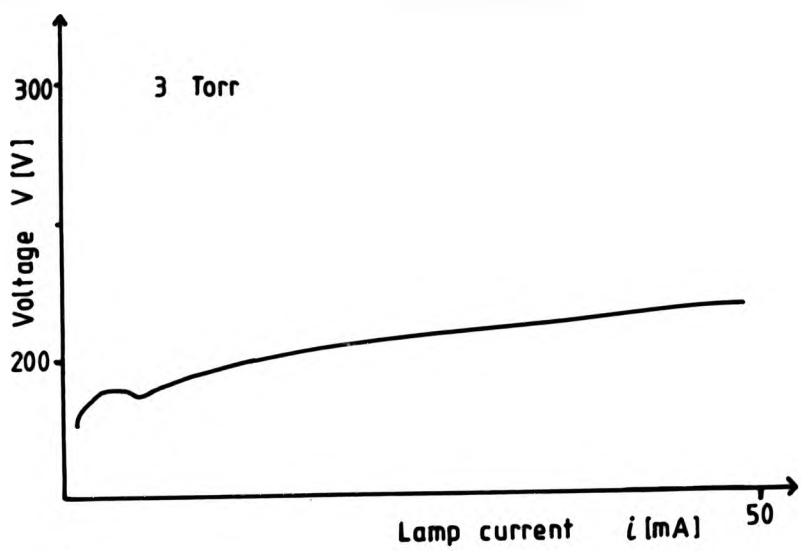


FIG.28 V/i CHARACTERISTICS OF EXPERIMENTAL LAMP (CONFIG. A)

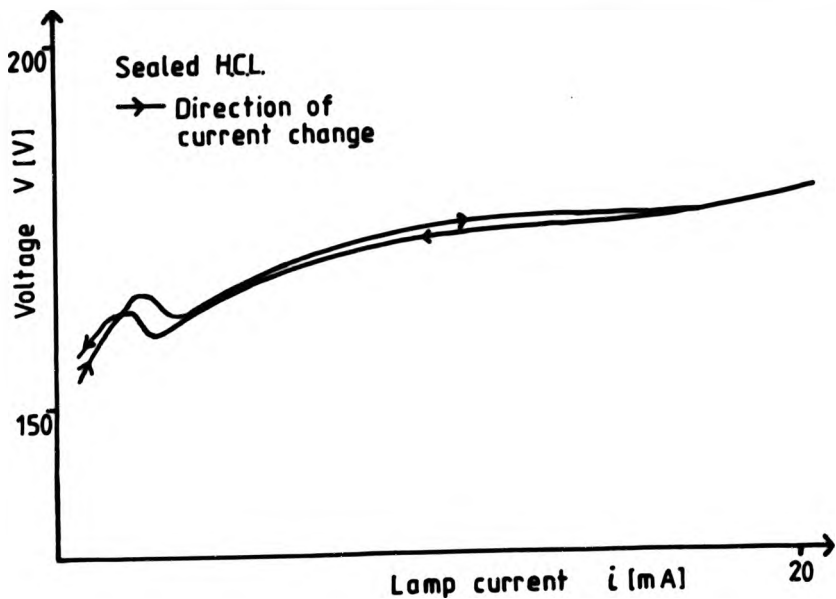


FIG.29 V/i CHARACTERISTICS OF SEALED HCL. SHOWING HYSTERESIS EFFECT

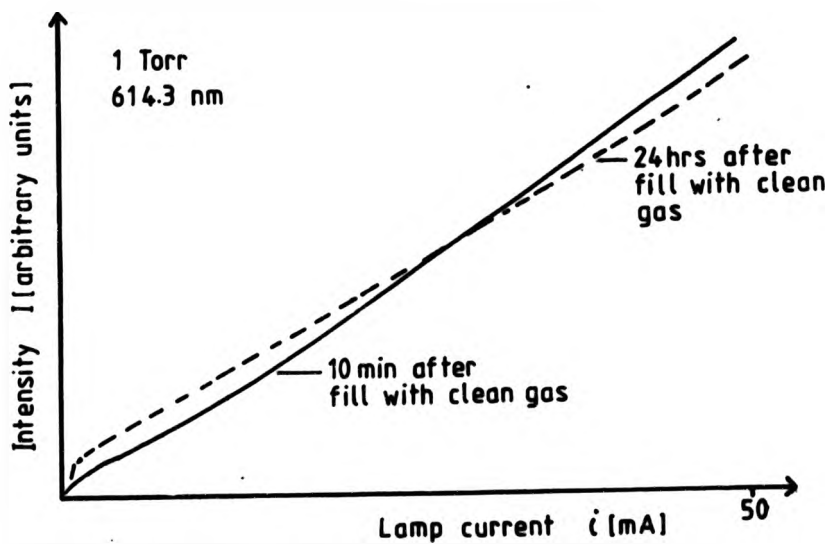


FIG.30 I/i CURVE OF Ne I LINE AFFECTED BY CONTAMINATION OF FILL GAS

4/C SPECTROGRAPHIC EXPERIMENTS

Copies of spectrograms of the experimental H.C.L. emission made with quartz and glass prism spectrographs are shown in Figs. 31 and 32. Spectrographs shown in Fig. 31 were recorded when the H.C.L. fill gas was contaminated and Fig. 32 under conditions of maximum gas purity.

Molecular bands may be seen in the spectrogram of the contaminated lamp. By comparison with standard molecular spectra [41] the bands were identified as being predominantly due CO and CO⁺ and to a lesser extent OH and H. No O₂ or N₂ bands were detected, indicating that the contamination was due to outgassing and not a real leak.

An additional notable difference between the medium quartz spectrograms recorded under 'clean' high purity conditions and contaminated gas conditions is the strong quenching of Fe spectral lines of sputtered cathode atoms, most noticeably in the ultraviolet spectral region, by gas impurities. The effects of fill gas impurities is discussed further in section 7/E.

4/D VISUAL INSPECTION OF GLOW

The H.C. glow in the experimental lamp was visually inspected over the full current range (0 - 50 mA) and with fill gas pressures of 1, 2, 3 and 5 torr. Some general features of the glow appearance and its variation with discharge conditions were noted :-

- (a) In the low current range of a few mA the colour, brightness and distribution of the glow changed rapidly as lamp current was increased.
- (b) In the higher current range above about 5 mA the appearance of the glow was very stable, showing little change as lamp current was increased.
- (c) At low current the glow was confined to a central cylinder of reddish colour, which suddenly brightened in colour and intensity as current was increased, and grew to fill the cathode hollow except for a narrow dark space near the cathode wall.
- (d) This rapid change was accompanied by a jump in the I/i curve and a 'bump' in the V/i characteristic - see Fig 28.
- (e) With the H.C.L. filled to low neon pressures of 1 and 2 torr, the glow in the stable current range was uniform up to the dark space.
- (f) At fill gas pressures of 3 and 5 torr the glow had an annular bright region near the cathode and the central region was less bright and reddened in colour. This was more noticeable at 5 torr than at 3 torr.



7

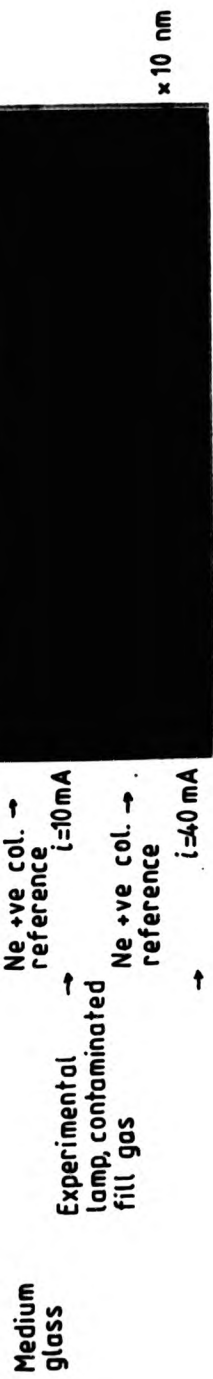


FIG.31 MEDIUM QUARTZ & GLASS SPECTROGRAMS OF CONTAMINATED H.C.L. EMISSION

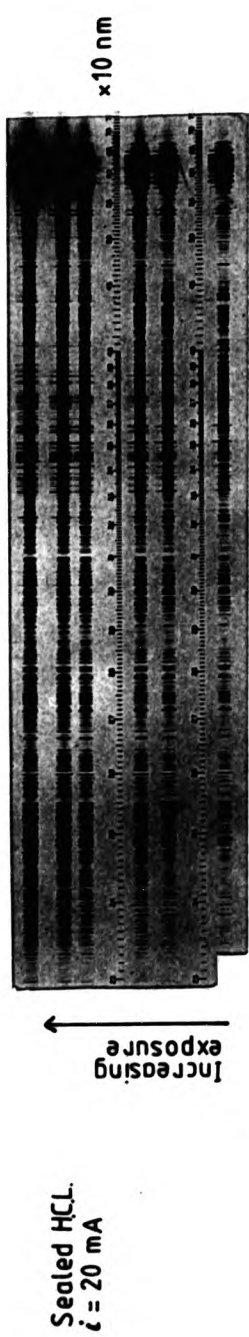


FIG.32 MEDIUM QUARTZ SPECTROGRAMS OF 'CLEAN' HCL. EMISSION

CHAPTER 5
THE INSTRUMENT FUNCTION OF THE FABRY - PEROT
INTERFEROMETER

5/A INTRODUCTION

Recording of the instrument function (I.F.) of the Fabry - Perot interferometer was necessary for optimization of the etalon adjustment (see 3/B.5 (b)) and was required for the synthesis of spectral profiles corrected for instrumental broadening (see 6/A).

The I.F. of a Fabry - Perot interferometer depends sensitively on a number of parameters and is subject to considerable variation with even quite small changes in some of them. A study was made of the interferometer I.F. and its dependence on the different parameters investigated.

5/B THEORY

5/B. 1 Instrument Function Definition

Any spectrometer may be analysed into three main elements: -

- (i) A dispersing element, combining wavefronts of differing phase retarded by optical depth Δ which may be varied by means of a control parameter ν .
- (ii) An optical imaging system of overall transmittance (including the dispersing element) $\mathcal{T}(\sigma)$.
- (iii) A detector of sensitivity $D(\sigma)$
 (where σ represents wavenumber in m^{-1})

The recorded spectral profile is a graph of the variation of detector output with changing values of the control parameters over some interval.

If the spectrometer is illuminated with radiation, with a distribution of intensity with wavenumber $I(\sigma)$, then the recorded profile value $Y(\nu)$ is given by

$$Y(\nu) = \int I(\sigma) \mathcal{T}(\sigma) D(\sigma) G(\sigma, \nu) d\sigma \quad - (5.1)$$

where $G(\sigma, \nu)$ is the Green's Function describing the relationship between the dispersion and the control parameter space.

If the optical retardation varies linearly with changing control parameter and the Green's function is invariant over the range of the spectral distribution and ν is suitably scaled in wavenumber units then eq. 5.1 may be expressed as the convolution integral

$$Y(\sigma') = \int I(\sigma) g(\sigma' - \sigma) d\sigma \quad - (5.2)$$

where $g(\sigma' - \sigma) = \mathcal{T}(\sigma) D(\sigma) G(\sigma, \nu)$
 is the instrument function of the spectrometer, and σ' is the scaled control parameter.

If the source illumination is monochromatic radiation of wavenumber σ_0 , then $I(\sigma)$ is an impulsive distribution

$$I(\sigma) = \alpha \delta(\sigma - \sigma_0)$$

where $\alpha = \int I(\sigma) d\sigma$, is the source luminance and $\delta(\sigma - \sigma_0)$ is the Dirac δ -function.

$$\text{Then } Y(\sigma') |_{\sigma = \sigma_0} = g(\sigma' - \sigma_0)$$

and hence the instrument function $g(\sigma' - \sigma_0)$ is the profile recorded with unit source luminance.

5/B. 2 Theory of the Fabry - Perot Instrument Function

5/B. 2(a) History of theory

The theory of the Fabry - Perot I.F. has received considerable attention from a number of workers [see 47], notably by Jacquinot and various co-workers [48]. The salient features of the theory of the I.F. of the ideal and practical case may be outlined as follows.

5/B.2 (b) Ideal Case

In the ideal Fabry - Perot the dispersing element is an etalon consisting of two plane parallel partially reflecting surfaces of infinite extent. If one surface of the etalon is illuminated by a parallel beam of monochromatic radiation of wavenumber σ and intensity I , incident at angle of incidence i .

Then the intensity of light transmitted by the etalon $I(\sigma)$ given by the Airy function

$$I(\psi) = \frac{I}{(1 + A/T)^2 (1 + f \sin^2 \psi / 2)} \quad - (5.3)$$

$$\text{where } f = \frac{4R}{(1-R)^2}$$

$$\psi = 2\pi\sigma\Delta, \quad \text{the phase change due to optical path retardation}$$

$$\Delta = 2t n \cos i$$

and R , A and T are the surface intensity reflectance, absorptance and transmittance respectively, t is the separation of the etalon surfaces and n is the refractive index of the intersurface medium.

If the surface reflectance is high, the Airy function is a "comb" of evenly spaced sharp peaks which occur when $\sigma\Delta$ assumes integer values N and $\psi = 2\pi N$,

where N is the order of interference. The width of the peaks at half maximum value, is most conveniently expressed in terms of the finesse F defined as the ratio between the inter-order spacing $\Delta\psi = 2\pi$ and the width $\delta\psi$:

$$F = \frac{\Delta\psi}{\delta\psi} \quad \text{where} \quad F = \frac{\pi\sqrt{R}}{2(1-R)} \quad (5.4)$$

It should be noted that in this ideal case, the finesse depends only on the surface reflectance, and may be more correctly termed the reflectance finesse and denoted by F_R .

If the optical retardation is fixed, the etalon transmits radiation of narrow ranges of wavenumber centred about successive, evenly spaced values

$$\sigma_1, \sigma_2, \dots, \sigma_j, \dots \quad \text{where} \quad j = 1, 2, \dots \quad (5.5)$$

satisfying $\sigma\Delta = N$

The difference in wavenumber between successive orders of interference $\sigma_{j+1} - \sigma_j$ is termed the free spectral range, and conventionally denoted (somewhat confusingly) by $\Delta\sigma$. From eq. 5.5 it follows that $\Delta\sigma$ is given by

$$\Delta\sigma = \frac{1}{\Delta} \quad (5.6)$$

Conversely, for a fixed wavenumber of monochromatic illumination, if the optical retardation is varied the etalon will transmit radiation for narrow ranges of optical retardation centred on successive, evenly spaced values $\Delta_1, \Delta_2, \dots, \Delta_j, \dots$ where $j = 1, 2, 3, \dots$ satisfying eq (5.3), with

$$\Delta_{j+1} - \Delta_j = \frac{1}{\sigma} \quad (5.7)$$

When the etalon is used as the dispersing element of an interferometer, the radiation to be spectrum analysed is limited to a wavenumber range less than $\Delta\sigma$, and the optical retardation is varied via a suitable control parameter. The optical path retardation $\Delta = 2tn \cos i$ may be varied by changing any of the three variables t , n or i , and in the pressure scanning interferometer the refractive index n of the gaseous intersurface medium is varied by changing the gas pressure which is the control parameter.

If the control parameter ψ , is scaled so that the difference in value of the scaled parameter σ' , between successive orders of interference is $\Delta\sigma'$, then the I.F. is an Airy function

$$g(\sigma') = \frac{A(\sigma')}{(1 + A/T)^2 (1 + f \sin^2(\pi\sigma'\Delta))} \quad (5.8)$$

of width $w = \frac{\Delta \sigma}{F_R}$

and maximum value $= \frac{1}{(1+A/T)^2}$

5/B. 2(c) Practical Case

In a practical Fabry - Perot interferometer the situation is complicated by a number of additional factors so that the instrument function departs significantly from the Airy function of the ideal case and the finesse achieved in practice is less than that calculated from the reflectance of the etalon surface.

In the simplest and commonly used practical arrangement (also that employed in the work), a pinhole aperture at the focal point of a collimating lens on the optical axis, normal to the etalon, limits angles of incidence to a small range around zero (an annular aperture is possible in principle, but rarely used in practice). Consequently the radiation falling on the etalon is not incident at a fixed angle ($i = 0$) but a small range of angles determined by the diameter of the aperture and the focal length of the lens.

Also the etalon surfaces are not perfectly flat or parallel, hence the surface separation is not fixed but varies slightly over different regions of the etalon. Furthermore the surfaces are not of infinite extent but limited to a finite area, either by the size of etalon or more usually by a circular aperture placed on axis, near it.

If the situation is considered in which the finesse is limited to a value, the aperture finesse F_A , much less than that calculated from the reflectance, only by the range of angles of incidence. Then the I.F. $TF(\sigma')$ is rectangular and the aperture finesse given by $F_A = \frac{2\pi}{\Omega N}$ - (5.10)

where Ω is the solid angle subtended at the centre of the collimating lens by the pinhole aperture.

Considering the case where the finesse is limited to a value F_D much less than the calculated reflectance finesse, only by the range of values of etalon surface separation. Then, if the range of values of surface separation and t is δt , the finesse F_D is given by $F_D = \frac{m}{2}$, where $m = \frac{\lambda}{\delta t}$ - (5.11).

The form of the I.F. $D(\sigma')$ depends on the nature of the source of variation of surface separation. Three sources of variation can be identified.

- (i) local departures of the etalon surfaces from plane, due to small, randomly

- (ii) Non - local departures of the etalon surfaces from plane due to figuring error, e.g. a slight curvature of the surfaces.
- (iii) Aparallelism of the etalon surfaces due to initial setting error or temperature variations.

Consider each source of variation of surface separation in turn, assuming it to be the only source of variation present. Randomly distributed defects can be expected to give rise to a Gaussian form for $\mathcal{D}(\sigma')$, figuring error a form depending on the nature of the figuring error and aparallelism a non - symmetrical form corresponding to the I.F. of a circular section of a wedge of small angle of inclination.

If comparable contributions to the variation of the surface separation are made by the three sources, then $\mathcal{D}(\sigma')$ will be the convolution of functions representing the effect of each separate source.

Similarly, in a practical interferometer all of the above effects will contribute to the observed I.F. which will be the convolution of functions representing each of them, so that

$$g(\sigma') = \mathcal{A}(\sigma') * \mathcal{F}(\sigma') * \mathcal{D}(\sigma')$$

and the observed finesse F will depend on the finesse factors F_R , F_A and F_D in a manner dependant on the form of $\mathcal{F}(\sigma')$ and $\mathcal{D}(\sigma')$. This is excluding the possible effects of aperture diffraction and finite etalon area.

To evaluate such a convolution for the general case is very difficult, though calculations relating the observed finesse F to F_R , F_A and F_D have been carried out by various workers for some simple cases [see 47 and 48]. The author feels that all that can be stated with a measure of certainty about the general case is: -

- (i) F is less than the smallest of F_R , F_A and F_D
- (ii) F is probably greater than that calculated from

$$\frac{1}{F} = \frac{1}{F_R} + \frac{1}{F_A} + \frac{1}{F_D}$$

- (iii) if one of the three separate finesse parameters F_D (say) is much less than the other two then

$$F \approx F_D$$

$$\text{and } g(\sigma') \approx \mathcal{D}(\sigma')$$

5/C Empirical Investigation

Because of the involved nature of a full theoretical description of the I.F. of the Fabry - Perot interferometer it is not possible to calculate what the I.F. of a given device will be, except in some limiting cases. The I.F. of the interferometer used in the work was measured experimentally, and its dependence on some variable parameters of the

was measured experimentally, and its dependence on some variable parameters of the instrument investigated.

The Fabry - Perot etalon, used with a 6mm spacer, had quoted flatness of $\lambda/150$ with reflective coatings over regions of 35 mm diameter and measured reflectance of 93% [43] at a wavelength of 700 nm with 140 nm bandwidth. The I.F. was recorded at a wavelength of 632.8 nm by scanning diffused emission of a mode - stabilized He - Ne laser which acted as a near ideal monochromatic source. Details of the practical interferometer arrangement and how the I.F. was recorded may be found in Section 3/B.5; Fig. 10 shows a schematic diagram of the interferometer.

The free spectral range $\Delta \sigma$, reflectance finesse F_R and "limiting" finesse due to surface defects F_D , calculated for the instrument from the above values, were:

$$\Delta \sigma = 83.3 \text{ m}^{-1}$$

$$F_R = 43.3$$

$$\text{and } F_D = 70$$

The finesse measured in practice, could vary widely, from as little as 10 to as much as 40, depending on the values of several variable instruments parameters, namely:

- (i) The diameter of the pinhole aperture A_2 .
- (ii) The diameter of the iris aperture A_1 limiting the effective etalon area.
- (iii) The orientation of the etalon, relative to the optical axis of the imaging system
- (iv) The degree of parallelism of the etalon surfaces

The values of these parameters had to be set empirically when adjusting the interferometer for use, and the effect of varying them was examined in order to assist the setting of optimal values. Examples of experimental recordings of the I.F. showing the effect on the observed function of varying each of instrument parameters in turn, are provided in Figs. 33 to 37.

An immediately noticeable feature of these I.F. recordings is the sensitivity of the observed I.F. to small change in etalon orientation and degree of parallelism. Fig. 34 shows the effect of changing etalon orientation and Fig. 33 changing degree of parallelism. The marked change in the profile shown in the figures correspond to small changes of position of the adjustment screws controlling the two instrument parameters. The sensitivity to changes in etalon orientation is further illustrated in Fig. 38 where merely tightening the nut locking the adjustment screw can be seen to have a significant effect on the I.F., and allowance had to be made for this.

In addition, it is evident that as the etalon orientation or degree of parallelism



Mode-stable
He-Ne laser
632.8 nm

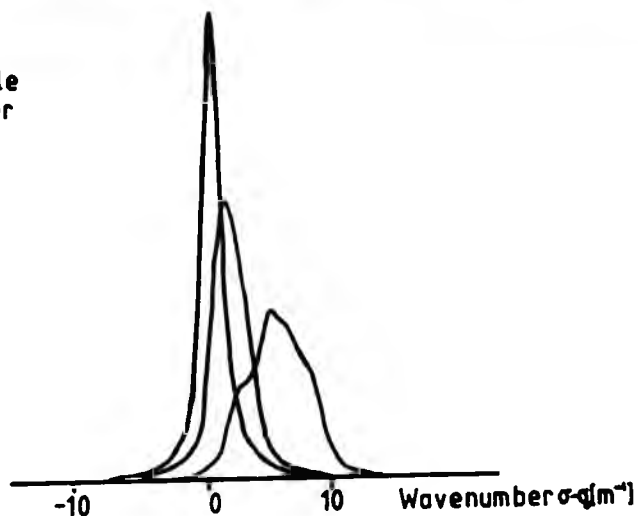


FIG.34 VARIATION OF FABRY-PEROT I.F. WITH
CHANGING ETALON ORIENTATION

Mode-stable
He-Ne laser
632.8 nm

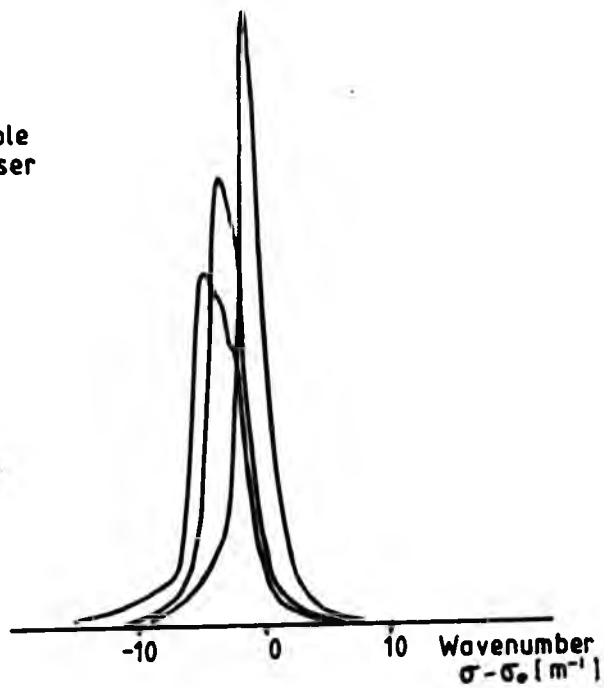
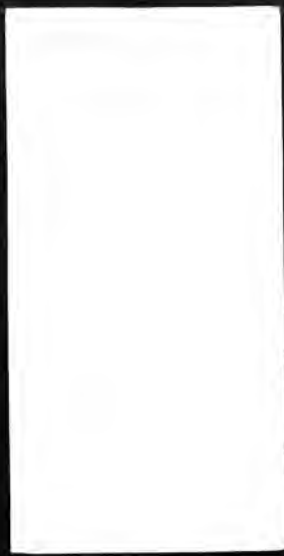


FIG.33 VARIATION OF FABRY-PEROT I.F. WITH
CHANGING ETALON APARALLELISM



Mode-stable
He-Ne laser
632.8 nm

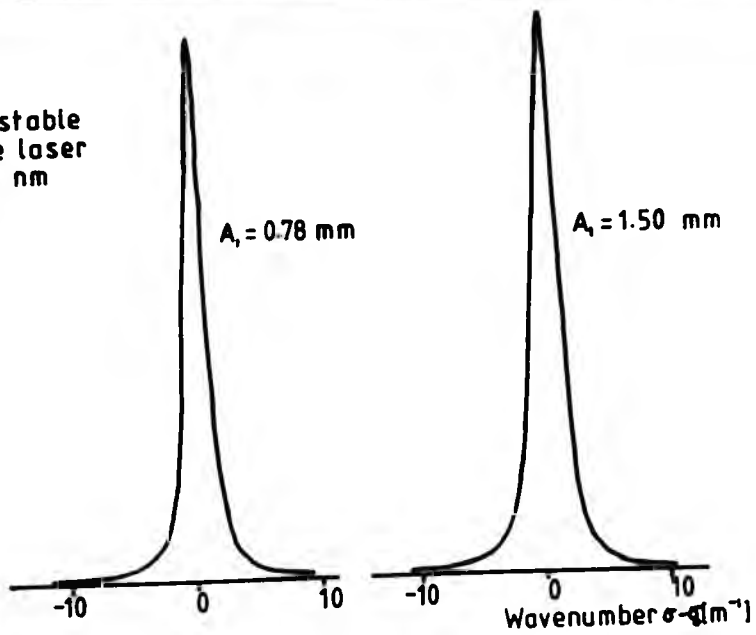


FIG.36 VARIATION OF FABRY-PEROT I.F. WITH DIFFERENT DIAMETERS OF APERTURE A_1

Mode-stable
He-Ne laser
632.8 nm

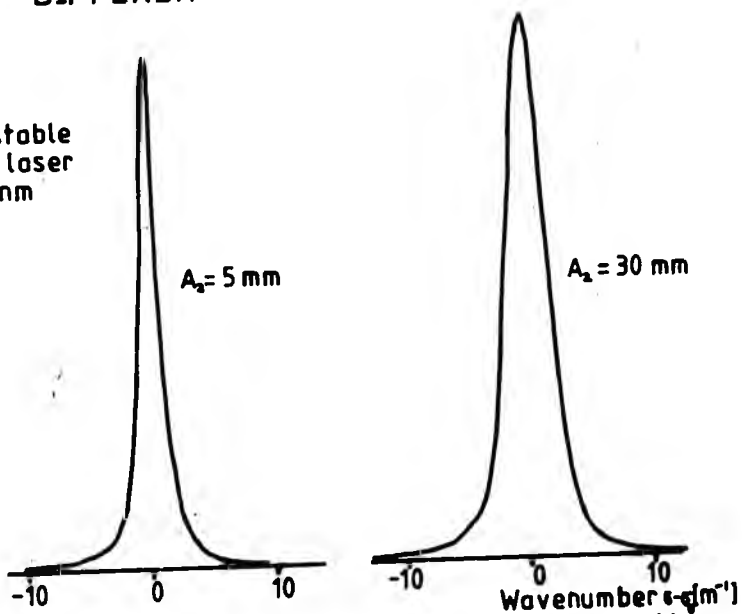


FIG.35 VARIATION OF FABRY-PEROT I.F. WITH ETALON DIAMETER A_2 , POOR PARALLELISM

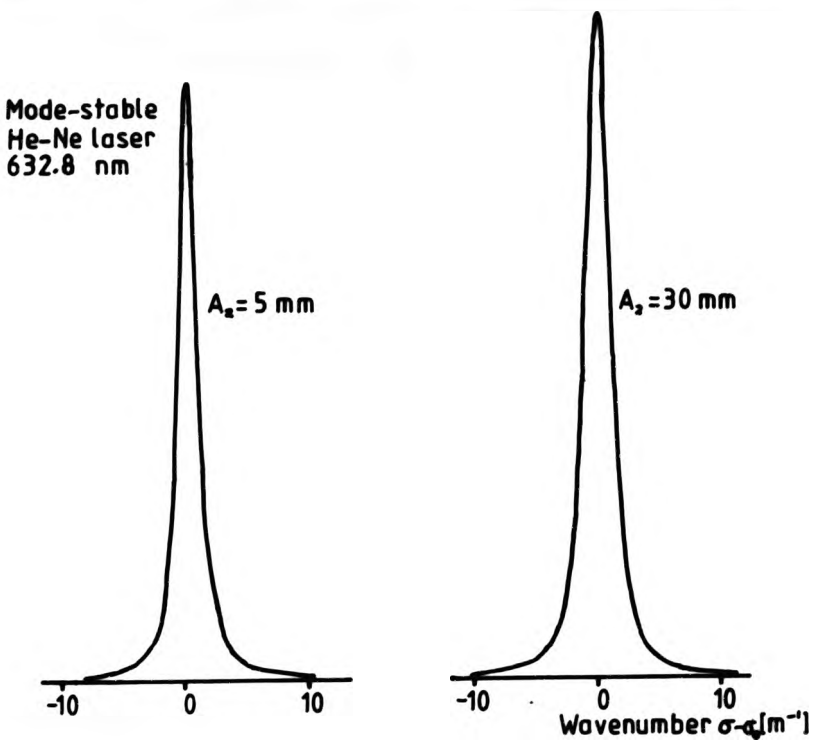
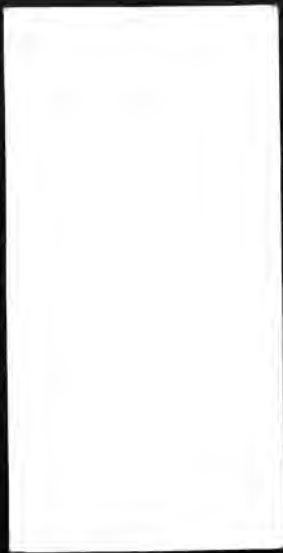


FIG.37 VARIATION OF FABRY-PEROT I.F. WITH ETALON DIAMETER A_2 , OPTIMIZED PARALLELISM

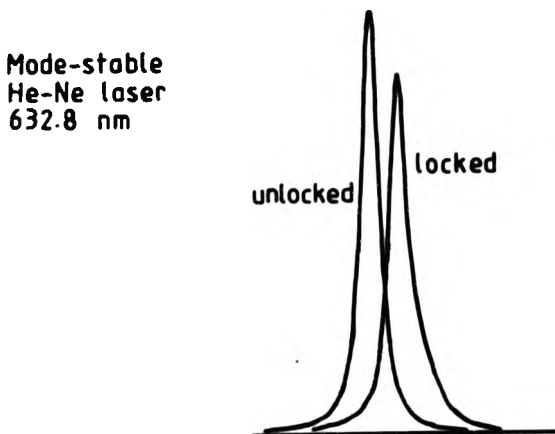


FIG.38 CHANGE IN FABRY-PEROT I.F. ON LOCKING ORIENTATION ADJUST. SCREW



departs further from optimum adjustment, the I. F. not only reduces in peak height and increases in width, but also becomes progressively more asymmetric.

The I.F. is however, much less sensitive to changes in the diameter of the pinhole aperture A_2 , and the diameter of the iris aperture A_1 limiting the effective etalon area. Increasing the diameter of either aperture clearly increased the light flux transmitted and consequently the peak height of the I.F.; however the width and shape of the I.F. changed much less significantly.

When a series of pinhole apertures were used, the diameter increasing by about 0.1 mm between each aperture, the instrumental width was unchanged until apertures larger than about ~ 1.2 mm, whereafter the I.F. slowly broadened with the profile remaining symmetrical. Fig. 36 shows two recordings of the I.F. with diameter of aperture A_2 of 0.78 and 1.50 mm, detector gain having been adjusted to give similar peak heights. The etalon adjustment was near optimal and the effective etalon diameter limited to 10 mm.

The effect on the observed I.F. of increasing the effective etalon area by varying the diameter of aperture A_1 , depended on the degree of aparrallelism of the etalon surfaces. Increasing the aperture diameters generally increased the width of the I.F., however the rate of increase was greater the more aparrallel the etalon surfaces. The profile also tended to become asymmetric with large apertures if the degree of parallelism was poor.

This dependence may be seen by comparing Fig. 33 and 37. Fig. 37 shows recordings of the I.F. with aperture A_1 diameters of 5 mm and 30 mm with near optimum adjustment of parallelism and Fig. 35 shows similar recordings but with poorer parallelism adjustment (detector gain adjusted).

5/D Comparison of Empirical I.F. Results With Theory

The first question to consider is how well the measured values of finesse calculated from $F = \frac{\Delta\sigma}{\delta\sigma}$ - (5.12)

can be explained in terms of the finesse factors related to reflectance, flatness and aperture, given by

$$F_R = \frac{\pi\sqrt{R}}{1-R} \quad - (5.13)$$

$$F_D = \frac{m}{2} \quad - (5.11)$$

$$F_A = \frac{2\pi}{\Omega N} \quad - (5.10)$$

In order to do this an estimate of the likely errors in values of finesse must be made.

The measured values of finesse given by eq. 5.12 will be considered first. The free spectral range $\Delta \sigma$ could be determined, by measuring the spacer thickness, much more accurately than the width of the recorded I.F. $\delta \sigma$, hence the error in the observed finesse was dominated by errors in measuring the instrumental width. The width $\delta \sigma$ could be determined to $\sim \pm 8\%$, so that the finesse could also be determined to about $\sim \pm 8\%$, equivalent to $\sim \pm 3$ in value.

The likely errors in the values calculated for F_R , F_D and F_A , given by eqs. 5.13, 5.11 & 5.10 will be considered next. It should be noted that the expression $\frac{\pi \sqrt{R}}{1-R}$, giving the value of F_R , is very sensitive to small errors in R if the value of R is close to unity, as it is in a Fabry - Perot etalon. If $R = 0.93$, then a change of $\pm 1\%$ in the value of R results in a change of $\sim \pm 15\%$ in the calculated value of F_R corresponding to a change in value of $\sim \pm 6$.

Accurate determinations of reflectance are difficult to achieve; the reflectance of the etalon surfaces used in the work had been measured on specialized commercial equipment, some time before, by a previous worker [43] and could not be readily repeated. Any small error in these measurements or changes due to ageing, would cause a considerable error in the calculated reflectance finesse. Hence the value of reflectance finesse of 43.3, calculated for the etalon, should be considered an estimate of uncertain accuracy.

The likely error in the value calculated for the aperture finesse F_A given by eq. 5.10 depended on the error in the value of solid angle Ω subtended by the pinhole aperture. The distance between the aperture and collimating lens could be measured to $\sim \pm 1\%$ and the mean aperture diameter to $\sim \pm 2\%$, giving an error estimate for F_A of $\sim \pm 5\%$ or $\sim \pm 2$ in value.

As the finesse $F_D (= 70)$ calculated from the manufacturers quoted value of flatness ($\lambda / 150$) was much greater than the reflectance finesse, errors in its value had little significant effect.

To directly compare measured values of finesse with calculated values, configurations of the instrument must be considered where the finesse is dominated by one parameter only and is hence approximately equal to the finesse factor corresponding to that parameter. With well optimized etalon orientation and parallelism, and small effective etalon area limiting the effects of any residual aparallelism, the finesse will be determined by the relative magnitude of F_A and F_R . Flatness finesse F_D is much larger

than F_R and has little effect.

The diameter of pinhole aperture A_2 which gives a value of aperture finesse $F_A = 43$, equal to the calculated reflective finesse, is 1.1 mm. If a pinhole diameter less than 1 mm is used, then the finesse can be expected to be approximately equal to F_R . The observed finesse in these circumstances was ~ 45 , in remarkably good agreement with calculated value of reflectance finesse of 43, given the uncertainty in the calculated value.

If aperture diameters larger than ~ 1.1 mm are used then the finesse may be expected to be approximately equal to F_R . This is in reasonable agreement with that which was observed in practice, where broadening of the I.F. was noted if apertures larger than ~ 1.2 mm were used. However the finesse measured, when pinhole diameters larger than 1.2 mm were used, tended to be larger than the calculated value of F_A by an amount more than would be expected from the estimated errors. For example, the recording of I.F. shown in Fig. 36 for a diameter of 1.50 mm has a corresponding measured finesse of $\sim 33 \pm 3$, but the calculated aperture finesse was $\sim 23 \pm 1$. As theory indicates that the overall finesse is always less than the smallest separate finesse factor, this observation was initially puzzling.

Detailed analysis of ray paths however, suggests a possible explanation. Aperture limitation after the etalon, causes a greater proportion of rays with large angles of incidence at the etalon not to reach the detector than with small angles of incidence make a greater contribution to the detected intensity. As a result, the finesse is not degraded as much as would have occurred with no aperture limitation after the etalon.

The dependence of the observed I.F. on the degree of etalon aparaallelism is fully consistent with theory, and the fact that the variation of the I.F. with effective etalon aperture also depended on the degree of etalon aparaallelism may be readily explained. The range of values of etalon surface separation, caused by aparaallelism of the surfaces, increases with increasing effective etalon diameter. As a result, the width and shape of the I.F. is more influenced by aparaallelism the larger the effective etalon aperture.

The sensitivity of the shape and width of the observed I.F. to small errors in etalon orientation has not been addressed in the theoretical treatment (outlined above), as far as the author is aware. Analysis of ray paths however again suggests a possible explanation. When the plane of the etalon is inclined at some angle to the optical axis, rays suffering successive reflection between the etalon surfaces will be progressively displaced further from the axis, and finally make no contribution to the detected intensity, because of the limited effective aperture. The loss of these higher order terms

I.F. of errors in etalon orientation and parallelism, producing both broadening and asymmetry, would seem to confirm this.

5/E Choice of Instrument Parameters Used

The choice of instrument parameters used in practice, depends in part on the performance desired in a given application. The resolving power, light transmittance and wavenumber invariance of the I.F. are interdependent factors, the relative importance of which can vary considerably. As the finesse, which determines resolving power for a given free spectral range, is very sensitive to the orientation and degree of parallelism of the etalon, the adjustment of the parameters have to be well optimized to achieve high resolution. However increases in finesse gained by reducing either aperture A_1 or A_2 must necessarily entail loss of light transmission, a serious problem when dealing with low levels of intensity.

Invariance of the I.F. over a range of wavenumber values was a desirable feature because the I.F. could only be measured at one wavelength, that of the mode stable He-Ne laser available, but knowledge of the I.F. was required over a range of wavelength values, in order to correct observed spectral profiles for instrumental broadening. If the finesse was dominated by reflectance, then because F_R is very sensitive to small change in R , any slight variation of reflectance with wavelength (a small "ripple" for example) would cause the I.F. to vary rapidly with changing wavelength making profile corrections impossible. Finesse contributions corresponding to other parameters can be expected to vary more slowly with changing wavelengths.

The diameter of pinhole aperture A_2 was set at 1.16 mm for routine measurements. This value was chosen from the sequence of apertures, as it was slightly less than the value at which broadening of the I.F. was observed so that light transmitted was the maximum possible with no loss of finesse. In addition the aperture was sufficiently small so that the light accepted by the instrument was limited to a small region of the source image.

The maximum diameter of the effective etalon aperture A_1 was limited by the diameter of the coated regions of the etalon plates to 35 mm. The value used for routine measurements was 30 mm, set by the diameter of the iris aperture A_1 . The best choice of value of diameter A_1 was not straight-forward however. The desirable features of high resolution and high light transmission are naturally conflicting but the situation was further complicated by the effect of small errors in the adjustment of etalon parallelism.

Optimization of etalon adjustment by the methods of scanning laser emission was

further complicated by the effect of small errors in the adjustment of etalon parallelism.

Optimization of etalon adjustment by the methods of scanning laser emission was very time consuming and optimization of parallelism particularly so. Once etalon orientation had been set, the adjustment was stable; this was not the case however, with the adjustment of etalon parallelism. Because of the extreme sensitivity of the I.F. to small changes in the degree of parallelism of the etalon surfaces and the limitations of the linkages, via which the tension of the leaf springs and so the parallelism of the etalon surfaces [see section 3/B.5 for details] were controlled, the optimization of parallelism adjustment was a slow process. In addition, the adjustment of parallelism once set, was not stable but tended to drift out of optimal adjustment with time, particularly when fluctuations in ambient temperature occurred. The most likely reason for this drift in parallelism adjustment, was differences in the temperature coefficients of the stiffness of the three leaf springs causing uneven changes in the tensions of the springs. But whatever the true source of this drift, it was a serious problem, as reoptimization of parallelism took a long time and the mode - stable laser was available for a limited period. Reducing the effective aperture of the etalon, reduced the effect of small errors in parallelism, so increasing the period for which interferometer could be used before the etalon parallelism had to be reoptimized.

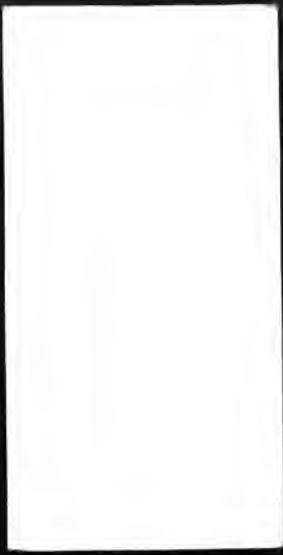
An additional consequence of the tendency of the parallelism adjustment to drift was that the I.F. had to be recorded before and after a run of measurements to ensure that it had not changed appreciably due to parallelism drift. This was important when carrying out the Fabry - Perot scanning absorption experiments where correction of spectral profiles for instrumental broadening was required.

Use of the maximum possible effective aperture diameter of 35 mm was found to produce unacceptable sensitivity of the I.F. to parallelism drift and use of apertures of diameter less than ~ 25 mm caused problems of insufficient light transmission with weaker spectral lines. The effective aperture diameter of 30 mm was chosen as an uneasy compromise between the factors.

Fig. 39 shows a typical recording of the I.F., over two orders of interference, with the above aperture diameters and optimized etalon adjustment. The measured finesse for this recording is ~ 30 typical of values obtained during routine experiments. Fig. 40 shows a typical recording of the I.F. over one order of interference exhibiting residual asymmetry due to a small error of etalon adjustment. The finesse for this recording is however ~ 30 . If the measured finesse fell below ~ 25 , parallelism adjustment of the etalon was reoptimized.

As the value of finesse for routine measurements was significantly less than the calculated reflectance finesse and so dominated by setting errors, small changes of

reflectance with wavelength would not cause large changes in the I.F.



Mode-stable
He-Ne laser
632.8 nm

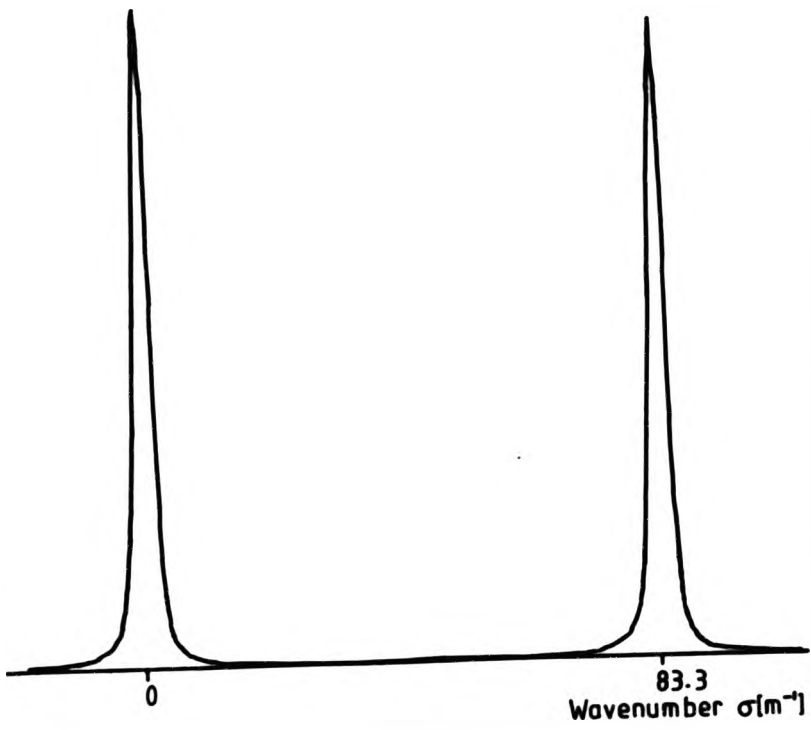
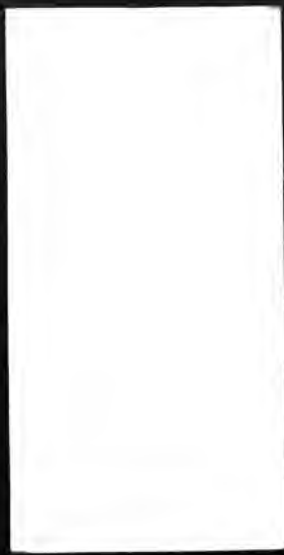


FIG. 39 FABRY-PEROT I.F. OVER TWO ORDERS OF INTERFERENCE, OPTIMIZED ETALON ADJUSTMENT



Mode-stable
He-Ne laser
632.8 nm

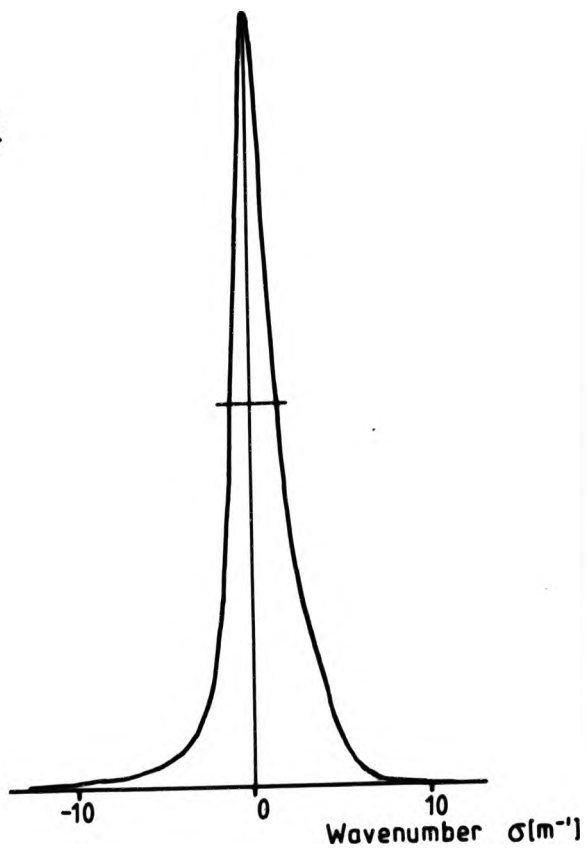


FIG. 40 FABRY-PEROT I.F. EXHIBITING RESIDUAL
ASYMMETRY AFTER LIMITED
OPTIMIZATION OF ETALON PARALLELISM

**CHAPTER 6
ANALYSIS**

**6/A FABRY - PEROT ABSORPTION MEASUREMENTS OF
EXCITED STATE NUMBER DENSITIES**

6/A.1 Theory of Method

Methods usually used [5, 49] to determine number densities of excited atoms are based on one of the methods described by Mitchell and Zemansky. All of these methods contain various assumptions as to the form and stability of spectral line profiles and are prone to systematic error. The method used in this work, developed from that employed by Jarrett and Frankin, and Gibbs and Hull [51, 52] to measure atomic number densities in alkali metal vapours, avoids these uncertainties by determining number densities of absorbing atoms from measurements of the absorption profiles. The absorption line profiles are calculated from Fabry - Perot interferometric measurements of primary source and transmitted spectral line profiles.

The observed primary source and transmitted line profiles ($I_o(\sigma)$ and $I_o'(\sigma)$ respectively) are given by :

$$I_o(\sigma) = \int f(\sigma') g(\sigma - \sigma') d\sigma' \quad (6.1)$$

$$I_o'(\sigma) = \int f(\sigma') \exp[-k(\sigma')l] g(\sigma - \sigma') d\sigma' \quad (6.2)$$

and the apparent absorption coefficient ($k_o(\sigma)$) by

$$k_o(\sigma) = l^{-1} \ln [I_o(\sigma) / I_o'(\sigma)] \quad (6.3)$$

where $f(\sigma')$ is the primary source line profile

$g(\sigma')$ the interferometer instrument function

$k(\sigma')$ the true absorption coefficient

$k_o(\sigma')$ the apparent absorption coefficient

l the absorption path length

and σ the wavenumber.

The number density of absorbing atoms (N) is given by :

$$N = \frac{8 \pi g_2 c}{g_1 A_{12}} \int k(\sigma) d\sigma \quad (6.4)$$

where g_1 is the statistical weight of the upper energy level

g_2 the statistical weight of the lower energy level

λ the central wavelength of the spectral line

A_{12} the transition probability

and c the speed of light.

In order to substitute in this expression to determine N , the true absorption profile, $k(\sigma)$ must be obtained from the observed profiles, corrected for the effect of the interferometer instrument function. This requires solutions of integral equations 6.1 and 6.2 which can only be obtained after considerable data processing.

A preliminary graphical analysis was carried out on some of the results in which effect of the instrument function was ignored, and the absorbing atom number density calculated using the apparent absorption coefficient given by eq. 6.3 in eq. 6.4. This is justified as the instrument function is narrow compared to the observed profiles and hence the true and apparent absorption coefficients are approximately the same.

6/A.2 Graphical Analysis

Denoting the estimate of N , calculated from data uncorrected for the interferometer instrument function, by N_0 , then

$$N_0 = \alpha \int k_0(\sigma) d\sigma \quad (6.5)$$

where
$$\alpha = \frac{8 \pi g_2 c}{g_1 A_{12}}$$

The apparent absorption coefficient was calculated from raw intensity values at about fifteen evenly spaced points across the spectral profile and a graph of these values plotted against wavenumber. It was found that points near the "wings" of the spectral lines, where intensity values were small, gave rise to divergences and were not plotted. (divergences are discussed in detail in section 6/A.3 (a))

The area under the curve was found by counting squares of graph paper and N_0 calculated using this graphical estimate of $\int k_0(\sigma) d\sigma$ and values of atomic transition probability obtained from data published by the National Bureau of Standards [53]. This was a laborious process and was only carried out on a limited number of the results.

Fig 41 shows a typical graph of apparent absorption coefficient against wavenumber plotted for Ne I 640.2 nm (2 torr neon pressure) and Fig 42 a graph of the estimated number density of neon atoms in metastable excited state $3s [^3/2]_2^o$, against lamp current (calculated from Ne I 640.2 nm, 1 torr neon pressure). Table 3 gives the estimated number density ($\sim \pm 15\%$) of atoms in metastable state $3s [^3/2]_2^o$ (calculated from Ne I 640.2 nm results) at a fixed lamp current of 20 mA, for 1, 2 and 5 torr neon pressure.

The strong saturation of the metastable atom population with increasing lamp

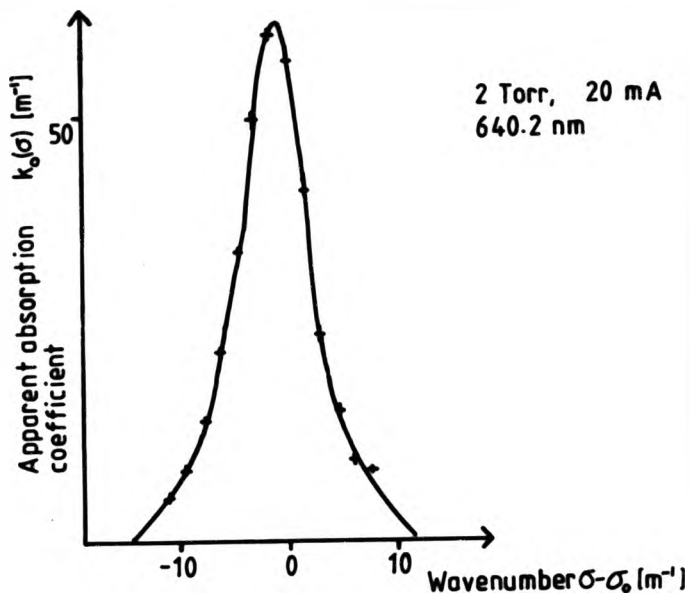
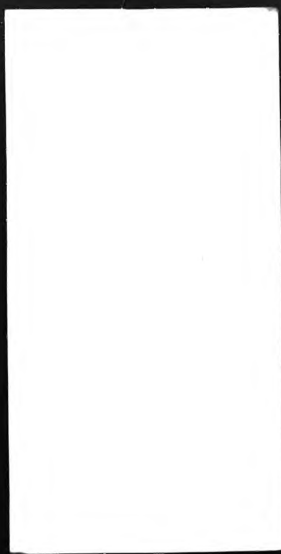


FIG.41 PLOT OF APPARENT ABSORPTION COEFFICIENT AGAINST WAVENUMBER

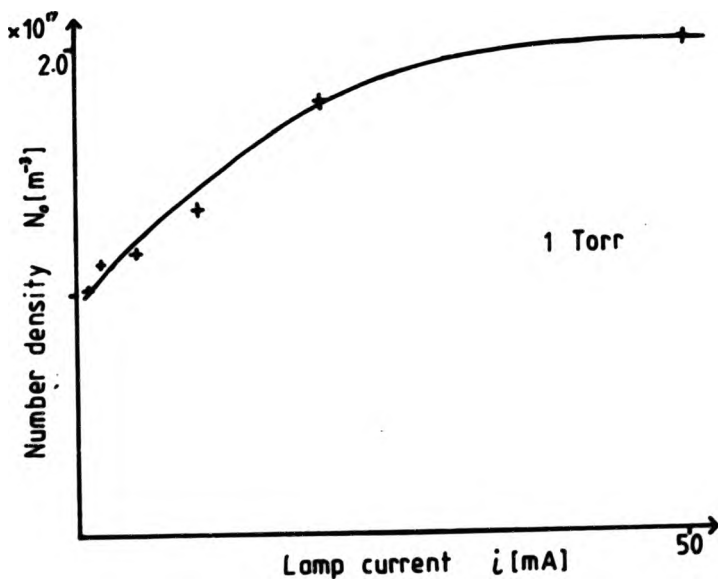


FIG.42 PLOT OF NUMBER DENSITY OF METASTABLE STATE $3s[3/2]_0$ AGAINST LAMP CURRENT

Pressure [Torr]	Number density [m ⁻³]
1	1.7 × 10 ¹⁷
2	1.6 × 10 ¹⁷
5	1.65 × 10 ¹⁷

TABLE 3
NUMBER DENSITY OF ATOMS IN 3s[$\frac{3}{2}$]₂^o AT
20 mA & THREE PRESSURES, GRAPHICAL
ANALYSIS (± ~15%)

Level	Number density [m ⁻³]
3s[$\frac{3}{2}$] ₂ ^o	2.0 × 10 ¹⁷
3s[$\frac{3}{2}$] ₁ ^o	1.0 × 10 ¹⁷
3s'[$\frac{1}{2}$] ₀ ^o	4.3 × 10 ¹⁶
3s'[$\frac{1}{2}$] ₁ ^o	1.8 × 10 ¹⁶

TABLE 4
NUMBER DENSITY OF ATOMS IN STATES OF
3s, 3s' GROUP AT 2 TORR & 20 mA,
GRAPHICAL ANALYSIS (± ~15%)

current and its lack of sensitivity to fill gas pressure is apparent. The graphically estimated number density of atoms in state $3s [^3/2]_2^o$ calculated from Ne I 640.2 nm is $\sim 2 \times 10^{17} \text{ m}^{-3}$ for a wide range of discharge conditions.

When the number density (at 20 mA) of atoms in this state is estimated from results for Ne I 614.3 nm, a value of $\sim 4 \times 10^{17} \text{ m}^{-3}$ is obtained, which is reasonable agreement bearing in mind the poor accuracy to which atomic transition probabilities are known and the rough and ready nature of this graphical treatment of the analysis.

The number density of neon atoms in the three other excited states in the $3s, 3s'$ group were also graphically estimated and the values obtained (20 mA, 2 torr neon pressure) shown in Table 4. The estimated number densities are of the same order of magnitude as that of $3s [^3/2]_2^o$ but smaller by factors between 2 and 10.

6/A.3 Computer Aided Analysis (Method)

6/A.3 (a) Methods Review

An analysis of the results, taking into account the effects of the instrument function, was carried out with the aid of a digital computer (DEC, DEC - 10). In order to do this it was necessary to devise algorithms which would provide approximate solutions to integral equations

$$I_o(\sigma) = \int f(\sigma') g(\sigma - \sigma') d\sigma' \quad (6.1)$$

$$\text{and } I_o'(\sigma) = \int f(\sigma') \exp[-k(\sigma')l] g(\sigma - \sigma') d\sigma' \quad (6.2)$$

from data experimentally determined and inevitably containing errors. Direct methods of obtaining solutions generally encounter difficulty as they are numerically unstable and produce spurious value divergences in the presence of experimental errors in the input data.

Both equations 6.1 and 6.2 involve convolution integrals and two direct methods of obtaining solution to this type of integral equation were examined :

- (a) Fourier Transform method. [54] Denoting the Fourier transform of $I_o(\sigma')$, $f(\sigma)$ and $g(\sigma)$ by $T(s)$, $F(s)$ and $G(s)$ where s is a generalised complex frequency and the transform is defined as :

$$F(s) = \int f(\sigma) \exp(-j 2 \pi s \sigma) ds \quad (6.6)$$

$$\text{if } I_o(\sigma) = \int f(\sigma') g(\sigma - \sigma') d\sigma'$$

$$\text{then by the convolution theorem } T = F G \text{ and hence } F = T / G \quad (6.7)$$

Fourier Transforms $F(s)$ and $G(s)$ can be obtained by using a Fast Fourier Transform (F.F.T.) algorithm on the measured values of $I_o(\sigma)$ and $g(\sigma)$, and values of $f(\sigma)$ found by applying the transform to the value of $F(s)$

calculated from equation (6.7).

(b) Serial product inversion

If the functions $f(\sigma)$ and $g(\sigma)$ are represented by sequences of discrete values $\{f\}$ and $\{g\}$

$$\{f\} = \{f_i\}, i = 0, 1, \dots, m$$

$$\{g\} = \{g_j\}, j = 0, 1, \dots, n$$

corresponding to samples of the function taken at even closely spaced intervals of width w .

Then the convolution of $f(\sigma)$ and $g(\sigma)$, $\int f(\sigma') g(\sigma - \sigma') d\sigma'$, is approximated by sequence of discrete values

$\{h\} = \{h_k\}, k = 0, 1, \dots, m + n$ where

$$h_k = w \sum_i f_i g_{k-i} \quad (6.8)$$

which is termed the serial product of sequence $\{f\}$ and $\{g\}$ and may be written in the shorthand form $\{h\} = \{f\} * \{g\}$ (6.9).

Obtaining a solution to eq. 6.1 corresponds in this discrete representation to calculating the sequence $\{f\}$ given values of the sequences $\{h\}$ and $\{g\}$. This may be achieved by a stepwise process, first calculating $f_0 (= h_0/g_0)$ then the next term f_1 and so on through the sequence [55].

Both of these solution methods are numerically unstable because they involve evaluation of expressions of the form x/y , where x and y may assume small values. When x and y do assume small values, in the presence of data errors, then the value of x/y is dominated by the effect of the errors and divergences may occur. The same type of problem was encountered in the graphical analysis, where divergent points in the wings of the spectral lines were simply ignored (- see section 6/A.2)

To overcome these divergence difficulties, a procedure was developed which provided approximate solutions to the equations by iterative refinement. Use was made of numerical analysis subroutines from NAG library wherever possible, with GINO and GINOGRAPH library subroutines used for graphical output. All source coding was written in FORTRAN 77. Code listings of those program sections marked by $x \quad x$ on the flowcharts (Figs. 44, 45, and 59) are included in Appendix B of the thesis

6/A.3 (b) The Iterative Procedure

The procedure breaks naturally into two separate parts; first obtain an adequate approximation to $f(\sigma)$ from equation 6.1, then use this to generate an approximation to $k(\sigma)$ from equation 6.2. The strategy adopted in developing the procedure, suggested

by D. Stacey [56], may be outlined as follows:

Part 1

- (1) Find a function, with sufficient parameters, that can represent $f(\sigma)$ to a good degree of approximation when suitable values of the parameters are chosen.
- (2) Guess an initial set of parameters, convolve the function with the instrument function $g(\sigma)$ then compare the result with the observed profile $I_o(\sigma)$.
- (3) Vary the parameters until the two profiles agree as closely as possible.

Part 2

- (4) Find a function with sufficient parameters which can represent $k(\sigma)$ to a good degree of approximation when suitable values of the parameters are chosen.
- (5) Take approximation to $f(\sigma)$ found from the first part, guess initial parameters of the absorption coefficient and apply the absorption feature to the approximation to $f(\sigma)$.
- (6) Convolve with the instrument function $g(\sigma)$ and compare result with the observed transmitted profile $I_o(\sigma)$.
- (7) Vary the parameters of the absorption coefficient until the profiles agree as closely as possible.

6/A.3 (c) Data Fit

Before any manipulation of the data could be carried out it was first necessary to translate the raw graphical line profiles into numerical form stored in the computer memory. To do this a peripheral digitizer (Hypad) was used which could determine the (x, y) co-ordinates of chosen points to an accuracy of ± 0.1 mm and transmit them to the computer for storage, from a V.D.U. terminal. A program was written which opened a memory file of user chosen name and directed data into it. The program allowed the first line for the file to contain information typed in by the user and was used to hold a specification of the raw experimental data, wavelength profile type etc.

With the graph paper temporarily fixed to the digitization surface, two points defining the chosen origin and baseline were digitized and then a large number of points across the line profile. For reasons discussed below more points were digitized, where the profiles changed rapidly such as near peaks, and near the ends of the interval digitized.

Fig. 43 shows a flowchart of the first stages of data processing carried out after digitization of a spectral line profile. The processing was broken into relatively small steps with data stored in files between execution of separate programs. Although this required extra file storage space and execution time reading and writing files it allowed

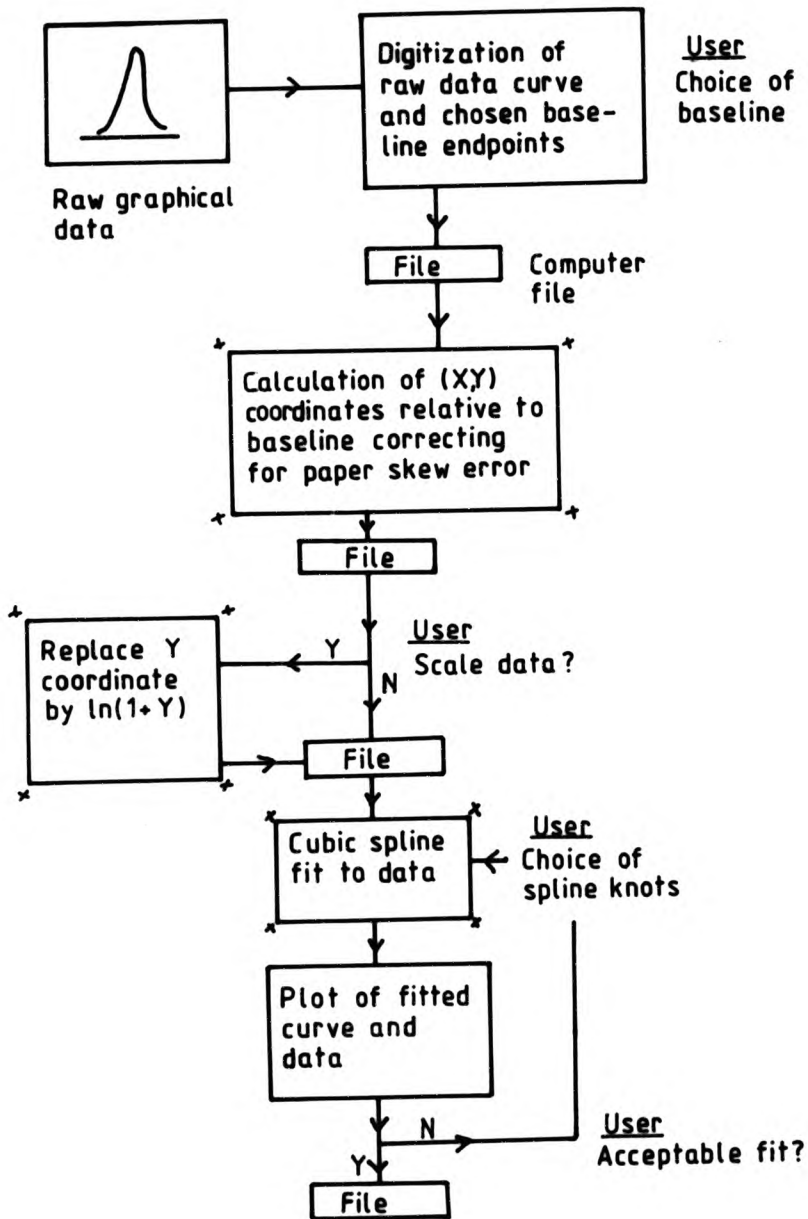


FIG. 43 FLOWCHART OF DIGITIZATION AND CUBIC SPLINE FITTING OF DATA

greater control of the process and made testing and debugging easier.

After initial digitization of a line profile, the coordinates of points relative to the chosen origin and baseline were calculated. The program corrected for the slight aparaallelism of the graph and digitizer axes due to positioning error and allowed for manual correction of baseline drift if desired. Also any points of the corrected set with x - ordinate not in strictly non - decreasing order were eliminated, as such points were unacceptable to the cubic spline fitting subroutine E02BAF described below and could easily be generated by mistake, particularly when digitizing rapidly changing curves such as the interferometer I.F.

Curve fitting to the profile data, carried out next, was often easier if the data was scaled, with the y - coordinate replaced by $\ln(1 + y)$. This is generally true of sharply peaked curves such as the instrument function [see 57] and usually a scaled and an unscaled version of the data were stored.

Curve fitting to the data points was necessary so that arrays of exactly evenly spaced sample values could be obtained, and digitization errors smoothed. Least squares fits to Chebichef polynomial series and cubic splines were tried, and cubic splines found to give better results.

The fitting program called the NAG subroutine E02BAF [59] which computed a weighted least - squares approximation to the data points with spline knots chosen by the user. After return from E02BAF the cubic spline was evaluated with NAG subroutine E02BBF [60] and the fitted curve and data points plotted on line with a graphics V.D.U., or a plot file created for subsequent output on a Benson plotter. The plot was examined by the user and new knots chosen as necessary. The process was repeated until a satisfactory fit was obtained and the knot position and the spline coefficients stored in a file. The cubic splines were represented in the form of normalized B - splines of degree 3 [see 62, 63]. The data points had equal absolute error probabilities and hence equal weights of 1 were used for unscaled data, however scaling of the data by $y \rightarrow \ln(1+y)$ required the weights to be adjusted to $1/(1+y)$ [see 61, 57].

Algorithms which least squares fit polynomials to data can generate unwanted oscillations of value, particularly towards the ends of the x - interval digitized [61, 57]. To reduce this tendency to oscillation, extra data points, near the ends of the x - interval and in regions of abrupt change, were digitized. The scaling of the data referred to above also helped reduce unwanted oscillations when fitting rapidly changing functions. The number and position of the knots are also important factors and knots were chosen so that the underlying function being represented was separated into sections of different curvature [57].

6/A.3 (d) Source Profile Synthesis Procedure

The generation, by iterative refinement, of an approximate solution of equation 6.1 for the source profile $f(\sigma)$, given the observed emission profile $I_o(\sigma)$ and the I.F. $g(\sigma)$, will be referred to as source profile synthesis and the approximate solution profile so generated referred to as the synthesized source profile. The convolution of the synthesized source profile with the I.F. will be referred to as the synthesized emission profile.

Once an acceptable representation of the experimentally observed emission profiles had been found, the next step in obtaining an approximate solution to equation 6.1 was to choose the functional form used to represent the source profile. A function derived from a model of the primary source discharge could be used or a more generalized representation such as the polynomial splines used to represent the observed profiles.

A function derived from a model has the disadvantage that an adequate model of the primary source discharge is required to start with. The source profile depends on spectral broadening and radiative transfer processes within the discharge, about which, it is difficult to have adequate information. The effect of self - absorption in regions of inhomogeneous temperature creates particular uncertainty.

A further disadvantage is the loss of generality implied by model dependence. Solutions of integral equations of the convolution type similar to equation (6.1) are often required in a number of important applications and it was desirable to develop a method which could be applied generally to equations of this type.

The main advantage of a model derived function is that unwanted oscillations, which can occur with more generalized functions such as polynomials, can more easily be avoided.

The most straight forward approach, and the one adopted, was to use the same type of generalized representation of the source profile as that used when curve fitting the observed emission profile. In fact cubic spline fitting of the observed line profile was chosen in preference to a single Chebyshev polynomial fit, because a cubic spline representation of the profile was found to be less prone to unwanted oscillation in the source profile synthesis.

The other important choice which had to be made before the source profile synthesis algorithm could be designed was the method of approximating the convolution integral. Three possible methods were considered

- (a) Fast Fourier Transform (F.F.T.)
- (b) Serial product
- (c) Other integral approximation

The F.F.T. method is somewhat complicated, requiring three Fourier transforms for each evaluation of the convolution integral. The principal advantage of the method is that it is potentially the fastest for sequences with large numbers of elements. If a sequence has N elements, then the number of calculations required to obtain its discrete Fourier transform by F.F.T. is $\sim N \log_2 N$ [55], hence the time taken to obtain an approximation to the convolution of two functions, represented by sequences of N elements, is roughly proportional to $N \log_2 N$. The number of calculations required to form the serial product of these sequences is $\sim N^2$ and other methods of approximating the integral will, at least, require numbers of calculations proportional to N^2 . $N \log_2 N$ grows more slowly than N^2 with increasing N , and the F.F.T. method is the only computational feasible method if N is very large.

The main advantage of the serial product method is that it is straight forward and an algorithm forming the serial product of two arbitrary sequences of numbers given by eq. 6.8 can easily be constructed.

The serial product method approximates the convolution integral by a summation and some other type of integral approximation could be used. However a separate approximation of the integral would be necessary for each point at which the value of the convolution integral was desired. It would probably require more calculations, and consequently computation time, and would be more complicated to implement.

The serial product method was chosen and execution of the source profile synthesis program not found to be excessively slow as long as it involved sequences not larger than about 150 elements.

6/A.3 (c) Source Profile Synthesis Program

The flowchart of the program which synthesized a source profile as an approximate solution to equation 6.1 is shown in Fig. 44. The main program segment in particular has been simplified for reasons of clarity, and details, such as user control over the choice of the files opened and minimization parameters, have been omitted.

The program used the NAG subroutine E04FCF, a comprehensive algorithm for finding an unconstrained minimum of a sum of squares of M residual functions in N variables ($M \geq N$), with no derivatives required [58]. E04FCF calls two subroutines supplied by the user, LSQFUN which calculates the values of the residual functions $f_i(\mathbf{X})$, $i = 1, 2, \dots, M$ at a given point \mathbf{X} in the space of N variables, and LSQMON which monitors the minimization process. After an initial starting point $\mathbf{X}^{(1)}$ is supplied, the routine generates a sequence of points $\mathbf{X}^{(2)}$, $\mathbf{X}^{(3)}$, ... intended to converge to the

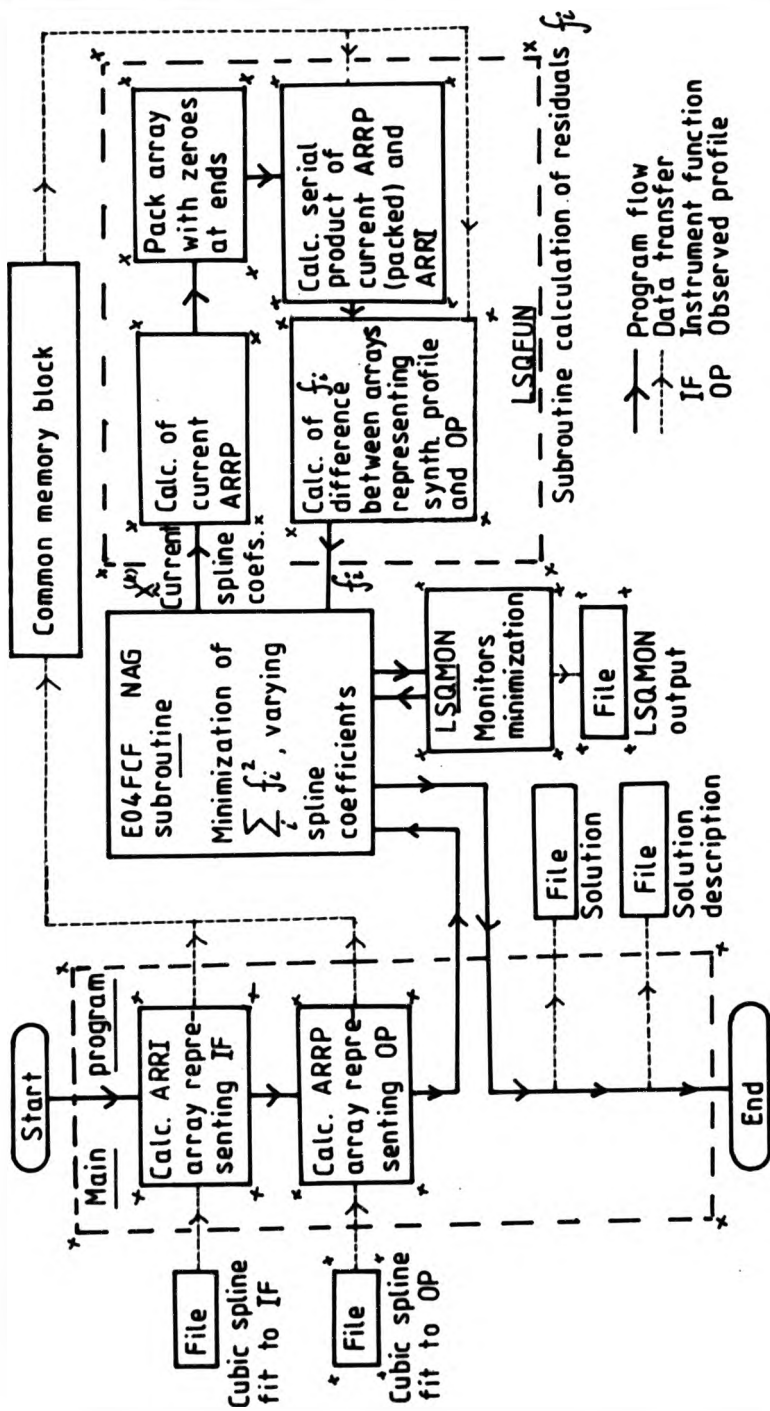


FIG. 44 FLOWCHART OF SOURCE PROFILE SYNTHESIS

local minimum of $F(\mathbf{X}) = \sum (f_i)^2$, $i = 1, 2, \dots, M$.

In this application a point \mathbf{X} was a given set of cubic spline coefficients and the residual functions f_i , the difference between elements of an array representing the observed emission profile and elements of an array representing the synthesized emission profile. The knot positions were not included in the variable set as this would have imposed constraints on the values of this subset of the variables, precluding the use of an unconstrained minimization algorithm such as E04FCF, greatly complicating the problem. Constraint on the knot positions arises because the NAG routine E02BBF, used to evaluate the cubic spline, requires that the knots be in strictly non-decreasing order and be confined to the base interval. Failure to satisfy this condition causes immediate termination of program execution.

After initiating execution of the program, the user supplied the names of the two files holding the knot positions and spline coefficients derived from fitting of the I.F. and observed emission profile. The user also supplied the number of points to be evaluated across the observed profile and a factor controlling the accuracy to which a solution was required.

The main segment then calculated arrays ARRI and ARRP, representing the I.F. and the observed profile respectively, from the cubic spline fits as sequences of discrete values of equal sample width. A small calibration correction was necessary for the difference in wavelength of the laser spectral line (632.8 nm) and the spectral line in question. The values of the elements of array ARRI were normalized so that their sum was always equal to unity, and the array ARRP packed with strings of leading and trailing zeroes at each end. The two arrays were held in a common memory block so that values could be transferred to the subroutine LSQFUN, called by E04FCF, which calculated the residual functions f_i .

The routine E04FCF requires values to be assigned to number of parameters which control the minimization process, in addition to the number of residuals and acceptable solution accuracy [see 58]. These parameters were set to suitable values within the main program segment, however it was found convenient to have residual number and solution accuracy under user control for reasons discussed below.

After a file, of user supplied name, had been opened to hold the monitor output of subroutine LSQMON, control was transferred to NAG routine E04FCF with the spline coefficients of the observed line profile as the starting point of the minimization.

E04FCF in turn called subroutine LSQFUN to calculate the residual function for different sets of spline coefficients. LSQFUN calculated an array of profile values with the current set of spline coefficients, packed the array with strings of leading and trailing

zeroes, formed the serial product with the array ARRI, representing the I.F., obtained from the common block and calculated the difference between resulting array and the array ARRP representing the observed profile, also obtained from common.

The serial product of two sequences of numbers, is a sequence containing one element less than the sum of the numbers of elements in the initial sequence [55]. Consequently the serial product of ARRI and the current ARRP, calculated from the spline coefficients supplied by E04FCF, contains more elements than the array ARRP representing the observed profile. Hence when calculating the difference between the array values representing the observed profile, and serial product of ARRI and the current ARRP, a large number of elements had to be ignored. The packing of the current and observed ARRP with strings of zeroes at the array ends was done to prevent possible loss of significant residual contributions from the sequence ends. Fifteen zeroes at each end were found to be sufficient to ensure that the residual were very small near the ends of the sequence of residuals, hence lost elements of small value.

The sum of the elements of the serial product of two sequences of numbers, is the product of the sums of the elements in the two initial sequences. The normalization of the elements of ARRI so that they summed to unity, ensured that the sum of elements of the array representing the current profile, and hence the area under the profile it represented, remained unchanged by the formation of the serial product with ARRI.

During the process of minimizing $\sum (f_i)^2$, E04FCF provided useful information on its progress and this information was handled by monitor subroutines LSQMON. The frequency with which LSQMON was called was determined by the value of an interger parameter on entry to E04FCF, and as the monitor information was found very useful this parameter was set so that LSQMON was called once every iteration.

The information available was extensive and some compaction was necessary to save space and make the information more easily intelligible. The information available from E04FCF and that file stored by LSQMON was :

- (a) co-ordinates of the current point X (i.e. the current set of spline coefficients)
- file stored with no reduction.
- (b) the current values of the residuals f_i - $F = \sum (f_i)^2$ stored
- (c) an approximation to the Jacobian Matrix $\frac{\partial f_i}{\partial X_j}$ - gradient vector $g_i = \frac{\partial F}{\partial X_i}$
and $g^T g$ - stored
- (d) singular values of the current approximation to the Jacobian matrix - stored
- (e) the grade of the Jacobian Matrix - stored
- (f) number of iterations performed by E04FCF so far - stored

(g) The number of times LSQFUN has been called - stored

On exit from E04FCF, returning to the main segment it was important to check the value of the interger parameter IFAIL which indicated the exit status. On successful exit IFAIL = 0, however if IFAIL \neq 0 some form of failure had occurred [see 58]. The most common non - zero exit value of IFAIL was 3, indicating that no acceptable solution had to be found. This could happen if the parameter XTOL, which specifies the accuracy to which the solution was sought, was set too small.

If an exit with IFAIL = 3 occurred, then control was returned to the point in the main segment at which the user determined the accuracy of acceptable solutions and E04FCF re - entered. It was found convenient to fix the value of XTOL by the user specifying the value of a scale factor XTOLS F, so that $XTOL = XTOLS F \sqrt{\xi}$, where ξ is the smallest positive real number such that $1.0 + \xi > 1.0$. The value of ξ is machine dependent and was obtained with NAG routine X02AAF. Values of XTOLS F were ~ 10 .

Exit from E04FCF with a non - zero value of IFAIL other than 3, resulted in termination of program execution. The program was restarted after suitable changes in the light of the exit value of IFAIL and the other routine parameters.

On exit from E04FCF with IFAIL = 0, indicating that an acceptable local minimum of $\sum (f_i)^2$ had been found, subroutine parameters provided the solution point $X^{(k)}$ (i.e. the set of spline coefficients of the synthesized source profile) and information describing the nature of the solution. The user supplied the names for two files; the solution set of spline coefficients and associated knots were stored in one file and the solution description stored in the other.

The solution description, complementing the information provided by the last call of LSQMON by E04FCF before exit, included a complete list of the residuals f_i for the solution obtained.

A plot of the synthesized source profile and observed emission profile data points could be produced if desired. In addition the user could return execution to the point in the main segment at which the number of residuals and acceptable solution accuracy were determined, or restart the program altogether. Fig 49 shows an example of a typical plot of a synthesised source profile and observed emission profile with a plot of the residual values below.

The quality of solution fit could be judged from the magnitudes of the residual values (i.e. the differences between the synthesized emission profile and the observed emission profile) in comparison to the estimated experimental error ($\sim \pm 1.5$ mm deflection). These residual values showed an oscillatory pattern and this is a general feature of any polynomial representation. The magnitude of these oscillations, and hence

the quality of fit, was found to depend on a number of factors.

In particular :

- (a) the number of residuals calculated
- (b) whether scaled data was used or not
- (c) the accuracy of acceptable solutions determined by the value of XTOLSF
- (d) the number and positions of the knots of the cubic spline representation.

Optimum values of these parameters were determined by trial and error. Choice of the optimum number of residuals calculated was a compromise between the quality of fit obtained and program execution time. The number of residuals calculated had to be sufficiently high so that the serial product of discrete array representation of the profiles was a good approximation to their convolution. The execution time of the program was dominated by the time taken to calculate the serial product of the sequences of discrete values, including the total of 30 extra zeroes added to the beginning and end of the sequences to improve numerical stability. It was found that the number of unpacked residuals had to be greater than about 50 and less than about 12, and 80 residuals was chosen as a reasonable value.

Scaling of the profiles had a relatively small effect on the values of residuals obtained, usually moving the position of value oscillations without greatly changing the maximum values. As a result unscaled representations of the recorded and synthesised source profiles were used; scaling in the representation of the I.F. was always used as described in section 6/A.3 (c).

The accuracy of acceptable solutions determined by the value of XTOLSF also had a relatively small effect on the residual values obtained. Setting of this parameter to too small a value (found to be about ~ 20) resulted in an exit from NAG routine with IFAIL = 3 indicating that an acceptable solution had not been found. However, the synthesized source profiles in these cases were found to be similar to the acceptable solutions obtained by increasing of this scale factor and in practice it was set at 20 and IFAIL = 3 solutions accepted.

With suitable choices of (a), (b) and (c), which once determined usually did not have to be changed, the most important factor was (d), the knot set used. If an acceptable fit could not be obtained with the initially chosen set of knots, then a new set was chosen, and the observed profile fitted again and the synthesis program rerun. This process was repeated until an acceptable fit was obtained. Facility at choosing knot sets increased with practice and an appropriate set could usually be obtained on the first or second attempt.

6/A.3 (f) Absorption Profile Synthesis Procedure

Once a source profile has been synthesized, with acceptably small residuals, as an approximate solution to equation 6.1, it is possible to progress to the synthesis of an absorption profile as an approximate solution to equation 6.2.

As in the synthesis of the source profile, the functional form of the profile to be synthesized has to be decided. As before, an initial choice has to be made between a generalized representation, such as the cubic splines used in the case of the source profile, and a function derived from a model.

The advantages and disadvantages of the two approaches are similar to those already described for the source profile case (see 6/A.3 (d)), however a model derived function was chosen to represent the absorption profile. There were several reasons for this different choice of functional form,

- (a) Absorption profiles can be more readily modelled than emission line profiles. Unaffected by self - absorption, they can generally be well represented by Gaussian or Voigt profiles.
- (b) Solutions to integral equations of the form of eq. 6.2 are not required as often as solutions to convolution integral equations like eq. 6.1, hence the desirability of a general method of approximate solution was not as great.
- (c) Polynomial spline functions had been used to represent the synthesized source profile and some oscillations of value had inevitably occurred. As the synthesis of the absorption profile depended on the source profile, these value oscillations could "seed" large oscillations in the absorption profile synthesized if represented in a similar manner.
- (d) The ease with which x and y shifts of the profile, corresponding to amplifier drift effects and shift of the absorption profile relative to the emission line profile, could be incorporated in a model derived function.

Having decide to use a model function representation of the absorption profile, the exact function form must be determined. A Gaussian profile has the great advantage over a Voigt profile that an explicit analytic function is available for its calculation. A Voigt profile can only be obtained from an approximation to the convolution integral of Gaussian and Lorentzian functions.

A Gaussian function representation would clearly be easier to implement, and importantly, Gaussian function values could be obtained much faster during program execution than Voigt profile values generated by an approximation algorithm. Such an algorithm would have to approximate the convolution integral each time a profile was required or interpolated from an extensive pre - calculated table of values. In either case it

would require substantial numbers of calculations. As the subroutine which calculate the residuals is called many times by E04FCF during the minimization, slow evaluation of the absorption profile would entail a substantial increase in overall execution time.

A heuristic approach was taken based on the size of the residual values obtained, starting with a Gaussian type function and modifying its form if necessary to obtain a satisfactory set of residuals. It should be noted that a true theoretical expression is not required, merely one that with suitable values of its parameter can approximate the profile closely enough to obtain residual values of the order of experimental error.

6/A.3 (g) Absorption Profile Synthesis Program

The flowchart of the program which synthesized an absorption profile as an approximate solution to eq. 6.2 is shown in Fig. 45. The program structure is similar to that used in the program to synthesize the source profile (compare Fig. 44) and as before the main segment flowchart has been simplified, and control details omitted, for clarity.

The user provided the names of three files in which were stored the cubic spline coefficients and associated knots representing the instrument function, synthesized emission profile and observed transmitted profile, respectively. When the user had specified the number of points to calculated across the synthesized profile, three arrays of numbers representing these profiles were computed and held in a common memory block.

The program main segment set suitable values for most of the parameters of E04FCF and when the user had specified the scale factor controlling the accuracy of acceptable solutions and the name of a file to opened to hold the minimization monitor output of LSQMON, program control was transferred to E04FCF.

The coordinate of the point $X^{(k)}$, in the space of variables, in this case correspond to parameters specifying the Gaussian absorption profile and three x - y shifts, i.e. :

- (a) the absorption profile peak height
- (b) the profile width
- (c) relative shift of absorption and emission spectral lines.
- (d) shift in x - direction due to amplifier drift
- (e) shift in y - direction due to amplifier drift

The values at the starting point of the minimization, for the absorption profile peak height and width were estimates derived from the preliminary graphical analysis (see 6/A.2) and the three shift components set to zero.

After entry, NAG routine E04FCF sought to minimize $F(X) = \sum (f_i)^2$, where the residual functions f_i were the differences between corresponding elements of two arrays, one representing the observed transmitted profile and the other the synthesized

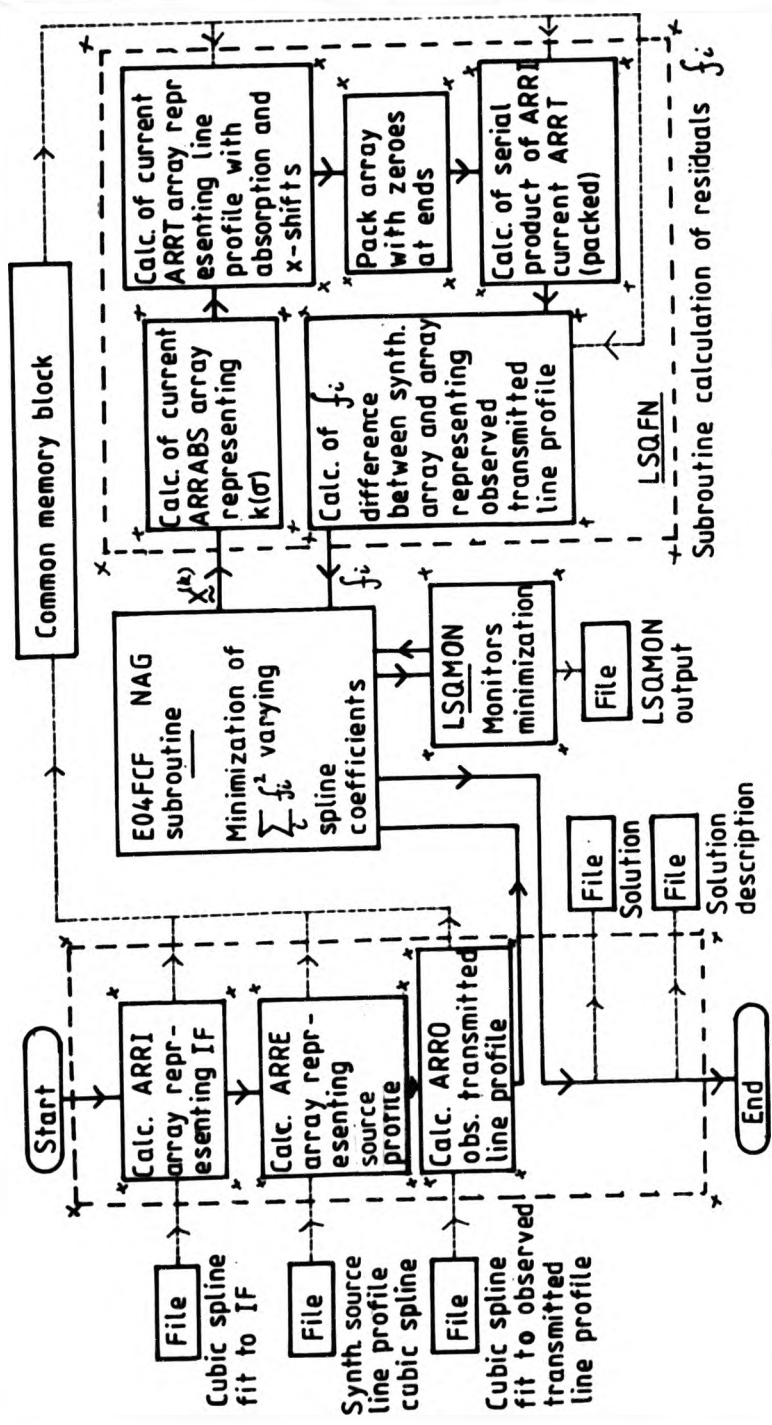


FIG.45 FLOWCHART OF ABSORPTION LINE PROFILE SYNTHESIS

transmitted profile. The values of f_i were calculated by calls to subroutine LSQFN and the progress of minimization monitored with calls to subroutine LSQMON. This was the same subroutine used to monitor the minimization process in the source profile synthesis described in 6/A.3 (e).

On entry to subroutine LSQFN from E04FCF at a given variable point $X^{(k)}$ an array ARRABS was computed representing the term $\exp[-k(\sigma)l]$, $l = 0.05$ m, where $k(\sigma)$, the absorption coefficient was a Gaussian function depending on the first three components of $X^{(k)}$ corresponding to peak height, width and wavenumber shift. The ranges of function arguments had to be limited to prevent floating point underflow errors. The number of elements of ARRABS was the same as the number of elements as the array ARRE representing the synthesized source profile, held in the common memory block.

The component by component product of the two arrays ARRT, was formed representing the transmitted profile $f(\sigma) \exp[-k(\sigma)l]$, and array ARRT packed with leading and trailing zeroes (see 6/A.3 (e)).

The serial product of ARRT (packed with zeroes) was formed with the array ARRI representing the instrument function, the values of which were obtained from the common memory block. As in the synthesis of the source profile the elements of ARRI had to be normalized so that they summed to unity.

Shifts in the x and y directions, controlled by the 4th and 5th component of $X^{(k)}$ corresponding to amplifier drift, were introduced, and the difference in element values computed, between the resulting array and ARRO representing the observed transmitted profile obtained from the common memory block. These residual values f_i were then transferred and control returned to E04FCF.

On exit from E04FCF, returning to the main program segment, the value of the integer parameter IFAIL, indicating the exit status, was examined in the same manner as in the synthesis of the source profile and the program restarted if necessary at a suitable point in the execution.

Exit from E04FCF with IFAIL = 0, indicated that an acceptable local minimum of $\sum (f_i)^2$ had been found and the coordinates of the final point $X^{(k)}$ (i.e. the optimal absorption and shift parameters) and solution description stored in files, named by the user as in the source profile synthesis.

Residual values of the order of the experimental error ~ 1.5 mm (deflection) could be obtained and Fig. 52 shows a plot of a typical set of residuals at an acceptable solution point.

The integration of the synthesized absorption coefficient required in Eq. 6.4 in

order to calculate the absorbing atom number density was approximated by means of the trapezium rule applied to a large number of points over the base interval (200 points was found to be sufficient). This numerical method was used in preference to one based on analytic integration, as no modification was necessary if the assumed functional form of the absorption coefficient was changed, and the method did not depend on the feasibility of analytical integration.

The dependence of the calculated values of number density on the qualities of fit at the two stages of solution synthesis and parameters such as the number of residuals is discussed in sections 6/A.4 (c) and (d) describing the characteristics of the analysis output.

6/A.4 Computer Aided Analysis (Output)

6/A.4 (a) Correction of Recorded Profiles for Effect of LF.

Before discussing the emission profiles, corrected for instrumental broadening, obtained by the synthesis method described above, it is worth enquiring what may be expected from general considerations.

Eq. 6.1 relating the observed emission profile $h(\sigma)$ (denoted by $I(\sigma)$ on p 90), the true source profile $f(\sigma)$ and the instrument function $g(\sigma)$,

$$h(\sigma) = \int f(\sigma') g(\sigma - \sigma') d\sigma' \quad (6.1)$$

may be written more compactly as

$$h = f * g \quad (6.10)$$

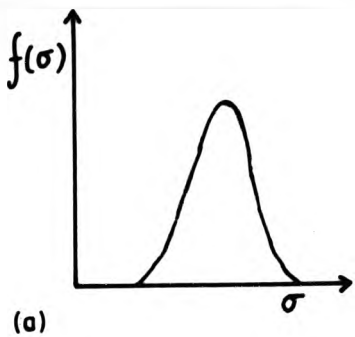
with h , f and g representing the complete functions $h(\sigma)$, $f(\sigma)$ and $g(\sigma)$ respectively, and $*$ convolution. How may we expect the form of h , f and g to be related?

These questions may be divided into two components :

- (a) What shapes of function are likely for f and g ?
- (b) How is the shape of the function h likely to be related to functions f and g of these shapes?

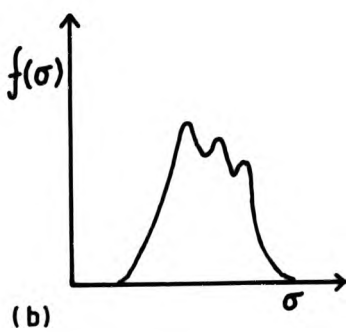
Clearly, as f represents the physical intensity distribution of a spectral emission line, its values are strictly non - negative, finite, and have a finite integral so that, $f(\sigma) \geq 0$ for all σ and $\int f(\sigma) d\sigma$ is well defined. Furthermore f is localized so that an interval $[a, b]$ may be defined outside which, values of $f(\sigma)$ are negligible, i.e. $f(\sigma) = 0$ if $\sigma < a$ or $\sigma > b$.

The simplest form that f can have is that of a single peaked function with "wings" decreasing asymptotically to zero such as that shown in Fig. 46 (a), or it may have a more complex structure, with a number of peaks separated by troughs, such as that shown in Fig. 46 (b).



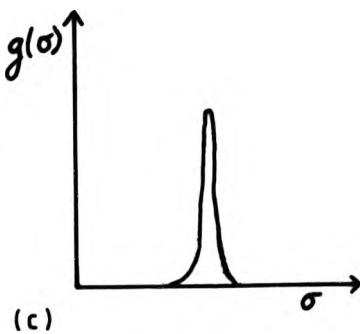
(a)

f
TYPICAL SOURCE PROFILE
WITH SINGLE PEAK



(b)

f
TYPICAL SOURCE PROFILE
WITH THREE PEAKS AND
TWO TROUGHS



(c)

g
TYPICAL INSTRUMENT FUNCTION
WITH SINGLE PEAK NARROW
RELATIVE TO SOURCE
PROFILE

FIGS. 46 (a),(b) & (c) TYPICAL FORMS OF
SOURCE PROFILE AND
INSTRUMENT FUNCTION

Functions g and h however, represent distributions of values of deflection on an instrument output device, in this case an instrument output device, in this case an X - Y recorder, and are only strictly non - negative if the baseline is correctly adjusted to compensate for any amplifier drift, and this will be assumed.

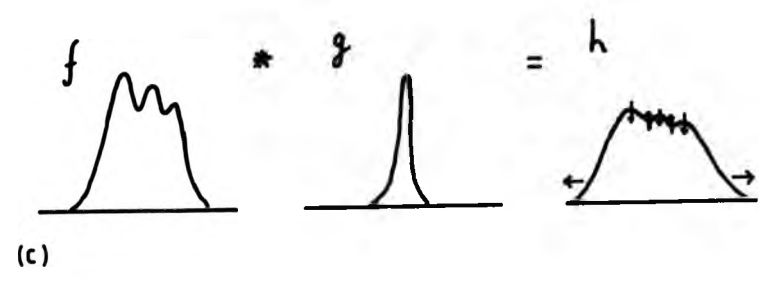
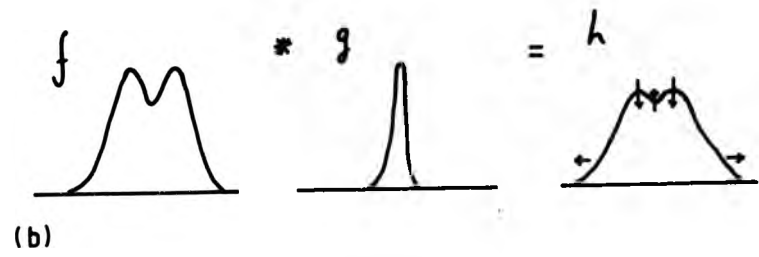
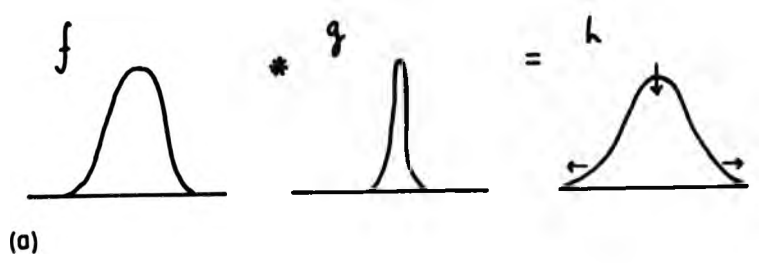
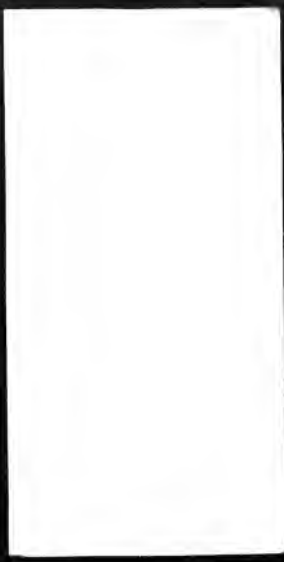
The instrument function of a reasonably well adjusted Fabry - Perot interferometer is a "comb" of impulse - like peaks of constant separation $\Delta \sigma$, the free spectral range (see section 5/B.2). If the free spectral range is much greater than the width of the spectral line, i.e. $\Delta \sigma \gg b - a$, then no overlap between different orders will occur and we may confine our attention to a single order. Further, if much useful information is to be obtained about the spectral line of interest the instrument function must be significantly narrower than this spectral line, in which case g is a localized, narrow function with a single peak, such as that shown in Fig. 46 (c). Significant values of $g(\sigma)$ are limited to an interval and the integral of g is well defined. As the units of intensity measurement are arbitrary, depending on overall gain, the shape of the I.F., rather than the magnitude of values, is of interest, and it will be assumed that g has been normalized to unity so that $\int g(\sigma) d\sigma = 1$.

Having established the possible shapes of the functions f and g , it must now be considered what shape of function will result from their convolution.

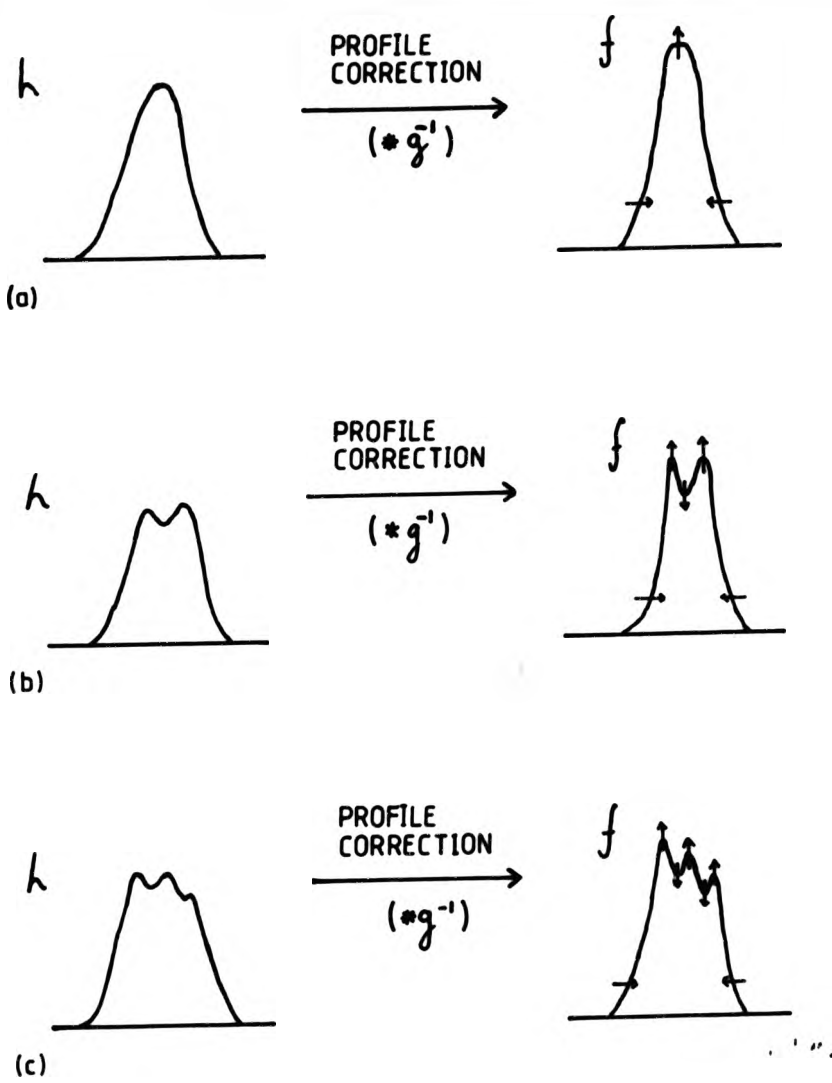
The convolution of one profile function with another will in general have a "smoothing" effect, leading to a profile which is broader and less rapidly varying than either of the initial functions. In a case such as that under discussion, where one of the functions (g) has a rapidly varying "impulse - like" profile and the other function (f) varies relatively slowly, the result of their convolution will be a "smoother" version of the relatively slowly varying function (f). Consequently peaks of the source profile will be reduced, troughs "filled - in" and the wings moved further outward, while keeping the area under the profile constant, as shown schematically with arrows in Figs. 47 (a), (b) and (c). Hence a procedure which corrects observed emission profiles for the effect of instrumental broadening, should raise peaks of the profile, deepen troughs and move the wings inward, while keeping the area under the profile constant, as shown in Figs 48 (a), (b) and (c).

6/A.4 (b) Synthesized Source Profiles

Some typical synthesized source profiles, along with observed profiles and plots of the residual between the latter and the synthesized emission profiles, are shown in Figs. 49, 50 and 51. As the source profile synthesis procedure was developed as part of the synthesis procedure of absorption profiles, it was mainly applied to profile recordings obtained in the absorption measurements. The primary source, emission line profiles in



FIGS.47 (a),(b) & (c) SCHEMATIC DIAGRAMS SHOWING CONVOLUTION OF TYPICAL I.F. AND SOURCE PROFILES



FIGS. 48 (a),(b)&(c) SCHEMATIC DIAGRAMS SHOWING CORRECTION OF TYPICAL OBSERVED SPECTRAL LINE PROFILES FOR EFFECT OF I.F.

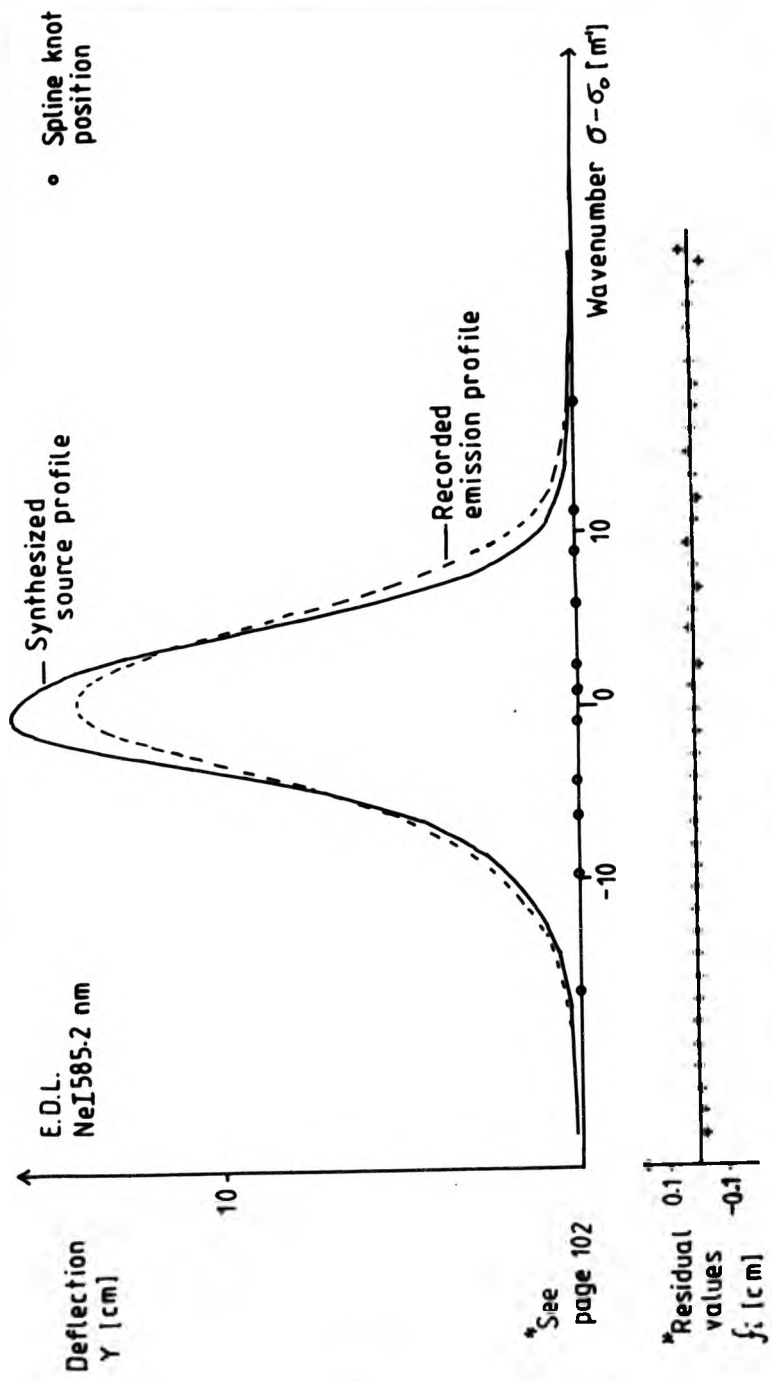


FIG. 49 SYNTHESIZED SOURCE & RECORDED EMISSION PROFILES, & RESIDUAL VALUES

* See page 102

* Residual values f_i [cm]

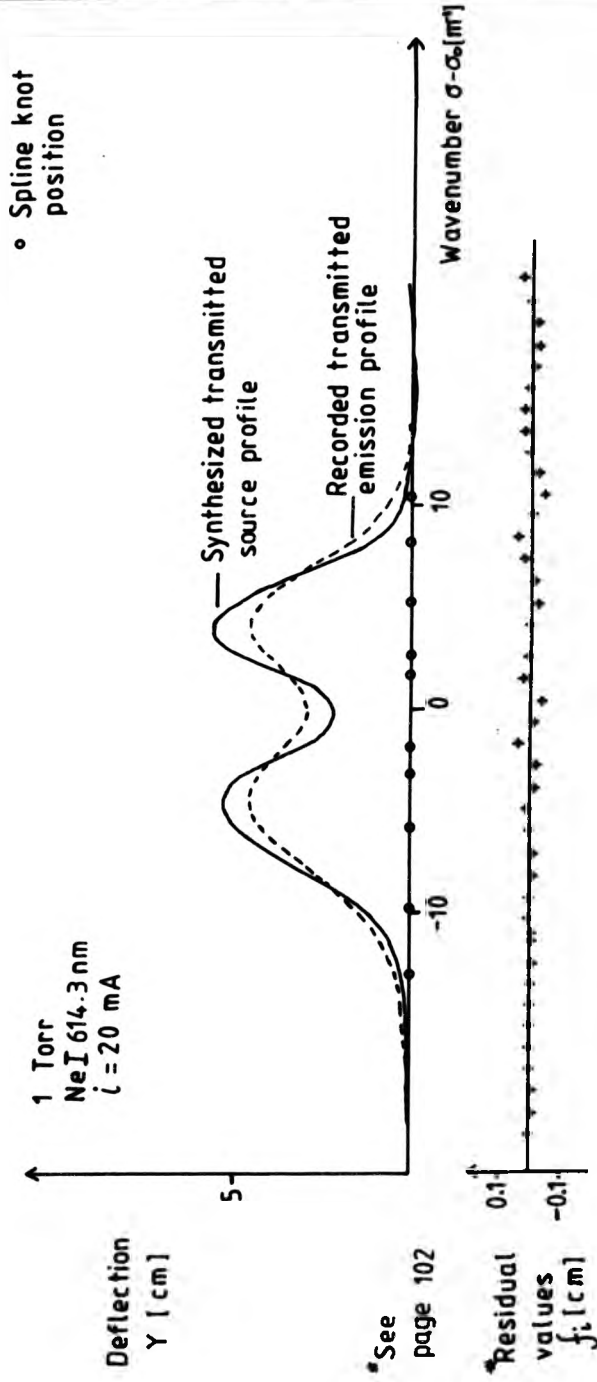


FIG. 50 SYNTHESIZED TRANSMITTED SOURCE PROFILE & RECORDED TRANSMITTED PROFILE, & RESIDUAL VALUES

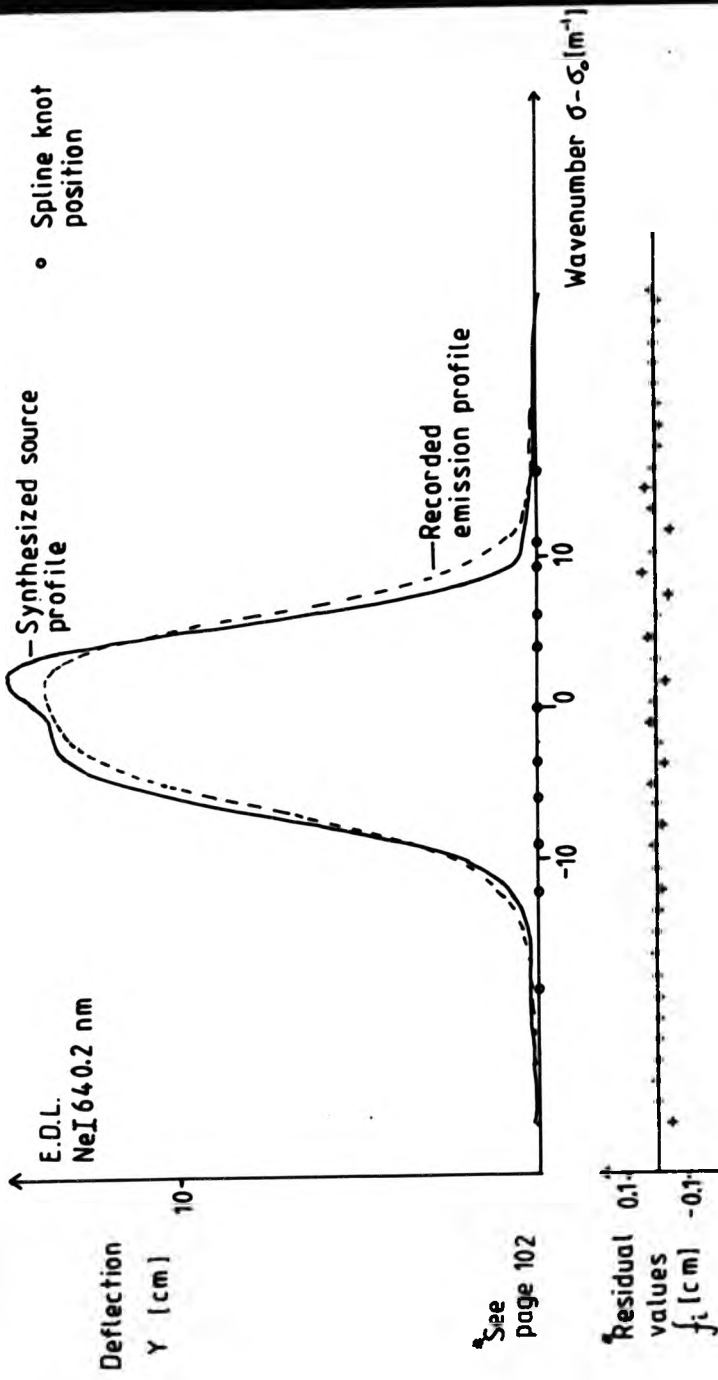


FIG. 51 SYNTHESIZED SOURCE & RECORDED EMISSION PROFILES, & RESIDUAL VALUES

these experiments had for the most part single symmetrical peaks, as shown in Fig. 49, the exception was Ne I 640.2 nm which had a single peak but with a noticeably asymmetric top, shown in Fig. 51. The synthesis procedure was also applied to some spectral line recordings having more complex profiles with two peaks and a trough as shown in Fig. 50. This example is not a pure emission profile but a transmitted probe beam spectral profile.

As can be seen from these examples, the synthesized profiles obtained conformed well with that expected of spectral profiles corrected for the effect of instrumental broadening as described in section 6/A.4 (a) above. If one compares the synthesized profiles with the recorded spectral profiles the principle effects of the correction procedure may be summarized as :

- (a) Peaks of the recorded profiles were raised
- (b) Troughs of the recorded profiles were deepened
- (c) Wings of the recorded profiles were moved inward
- (d) The width of profile (at half peak height) was reduced slightly but not by very much.
- (e) The flattened peak of a recorded profile, deepened into a trough (see Fig.51)

As discussed in section 6/A.3 (g), the quality of fit obtained depended on the values chosen for parameters of the synthesis procedure. The synthesized source profiles shown in the examples were generated with suitable values of these parameters to obtain good fits over the regions containing the most significant spectral information, though oscillations of value about zero can be detected.

6/A.4 (c) Synthesized Absorption Profiles

A typical synthesized absorption profile obtained and plot of the corresponding residual values is shown in Fig. 52. Naturally the quality of fit obtained for the synthesized absorption profile depended on the quality of fit obtained for the synthesized source profile and the final residual values were usually about double those at the source profile stage. The residual values obtained in the absorption profile synthesis, also depended on the number of residuals calculated, the value of the solution accuracy scale factor XTOSF and whether scaled data was used, in a manner similar to that discussed in 6/A.3 (e) for the source profile synthesis. The number of residuals in the absorption profile synthesis was fixed at 80, the same number as in the source profile synthesis, not because they had to be the same but because 80 was close to the optimum value in both cases. A value of XTOLSF of 20 and unscaled data was used, the same as in the source profile synthesis.

The Gaussian functional form assumed for the absorption profile was found to be

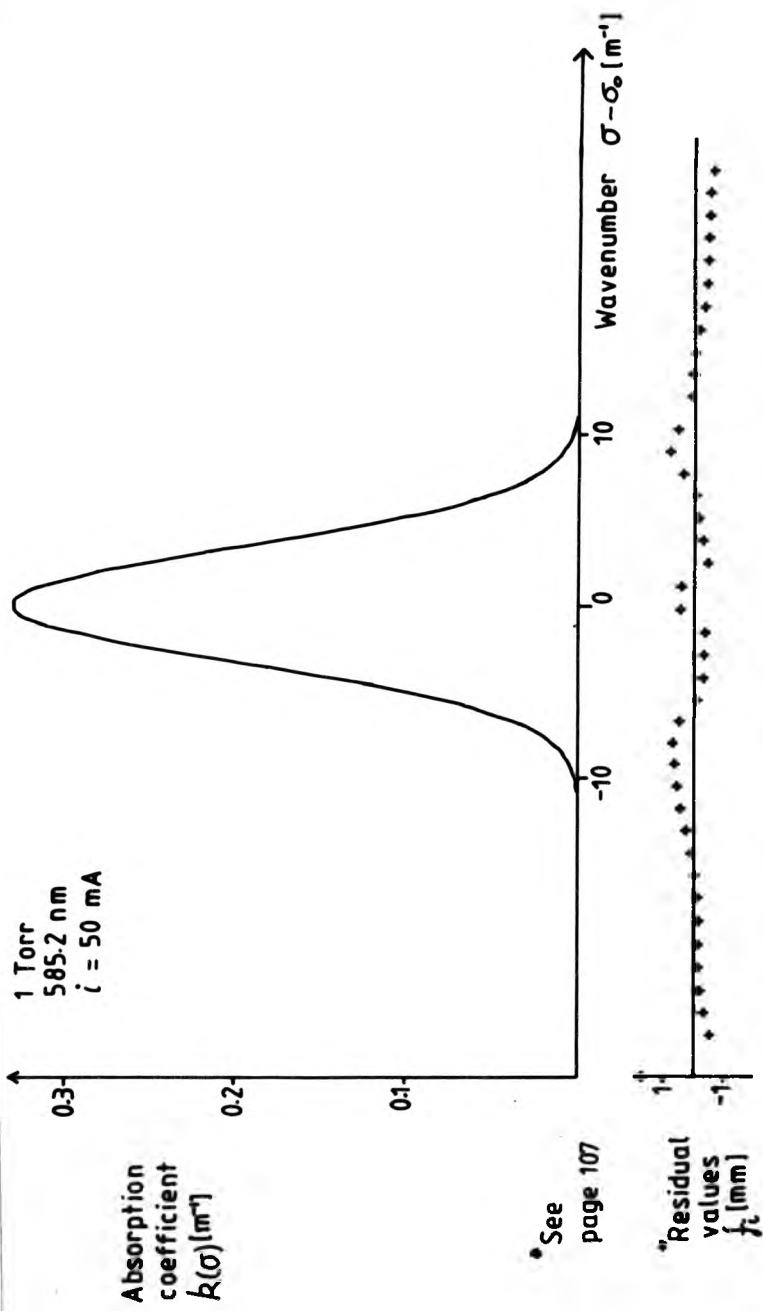


FIG.52 SYNTHESIZED ABSORPTION PROFILE & RESIDUAL VALUES

sufficient to obtain a reasonable quality of fit relative to the underlying experimental error ($\pm \sim 1.5$ nm) and approximation to the area under the profile needed to calculate the number density of absorbing atoms. The general pattern of residuals obtained, with greater values in the wings and centre of the profile did suggest a small Lorentzian component which would however have made little difference to the area under the curve, and a Lorentzian component was not introduced into the functional representation of the absorption profile.

6/A.4 (d) Excited Atom Number Densities

Plots of the number densities of neon atoms in the four 3s, 3s' excited states, obtained by the synthesis method, against discharge current, at pressures of 1, 2 and 5 torr are shown in Figs. 53, 54 and 55. Values of number density obtained by this method, which were in the range $\sim 10^{16} - 10^{17} \text{ m}^{-3}$, were of the same order of magnitude as those obtained from the graphical method (see 6/A.2), differing by factors ranging from $\sim 1 - 2$.

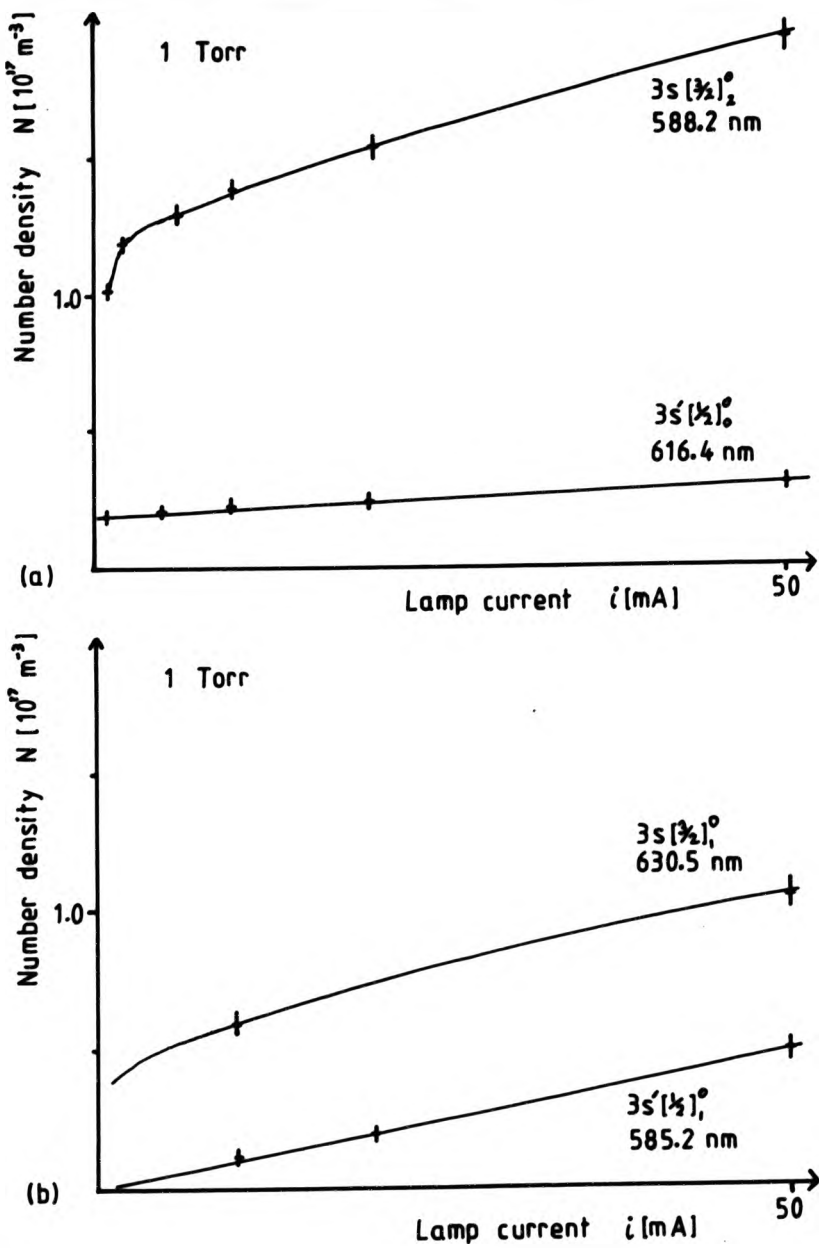
Values of number density for the same excited state obtained from different spectral lines with the same lower level, were in agreement to within $\sim 10 - 25$ %, consistent with the uncertainties in the values of individual transition probabilities stated by NBS as being in this range [53]. For example, Figs. 54.(a) and (b) show plots of number density against current for $3s [^3/2]_2^o$ at 2 torr, obtained from two different spectral lines Ne I 588.2 and 640.2 nm. The two plots are very similar to each other and that obtained for 614.3 nm (not shown) also terminating in $3s [^3/2]_2^o$. The error bars shown in all these plots represent estimates of error excluding that due to uncertainty in the value of transition probabilities.

Plots against lamp current of the sum of the number densities of excited atoms in the 3s, 3s' group of states are shown in Figs. 56 (a) and (b) and 57 for pressures of 1, 2 and 5 torr.

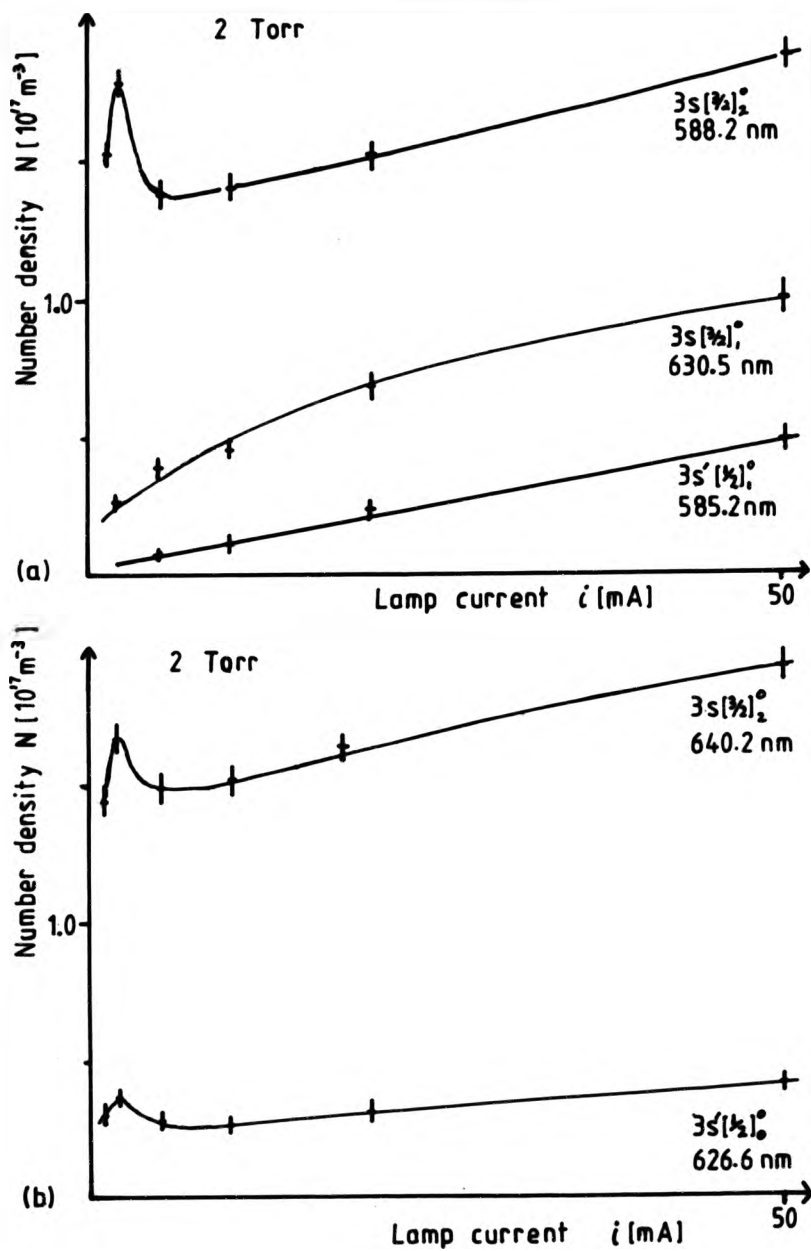
6/A.4 (e) Estimation of Errors

A number of factors contributed to the uncertainty in the values of number density obtained and these were, in descending order of importance :

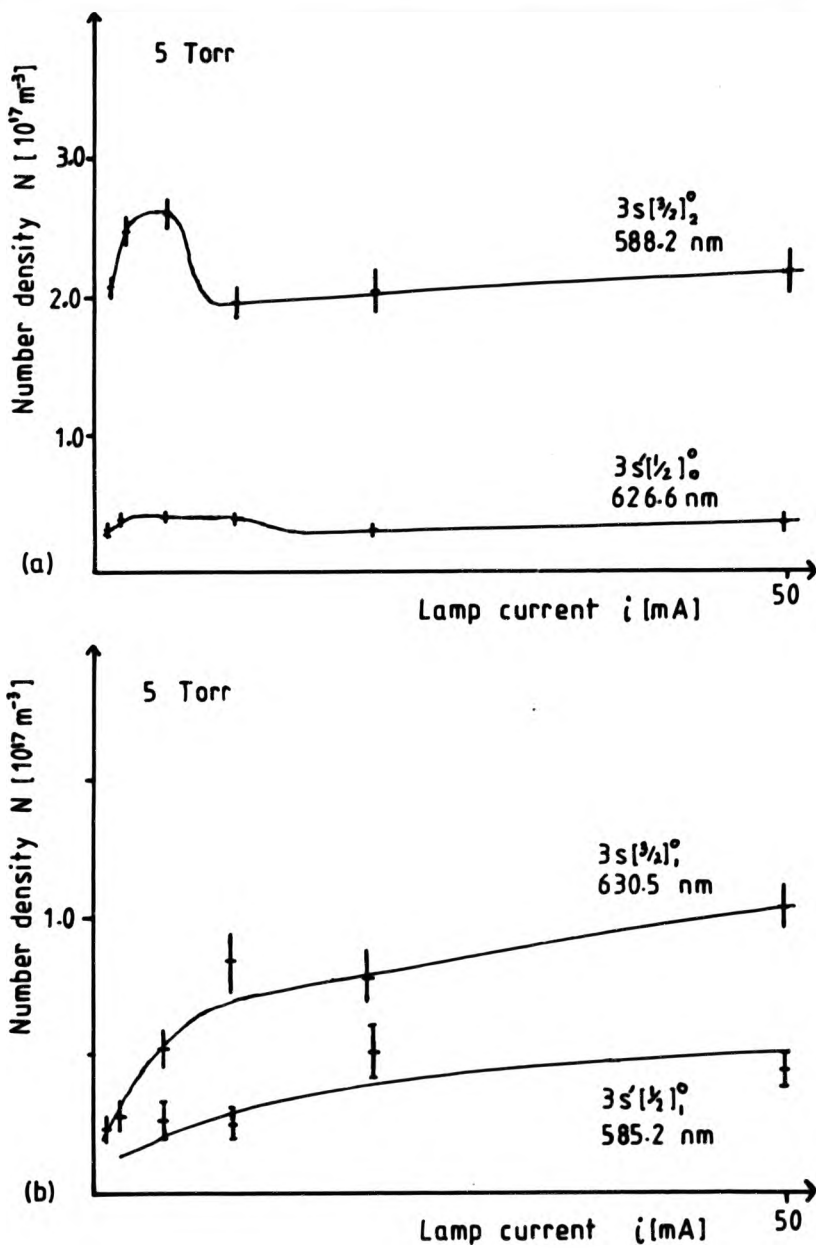
- (a) Uncertainty in the values of transition probability
- (b) Variations in recorded profiles due either to amplifier drift or variations in primary source intensity
- (c) Poor quality of fit in the two stages of the synthesis procedure
- (d) Error due to the purely Gaussian form assumed for the absorption profile.
- (e) Errors due to numerical approximation such as the serial product approximation



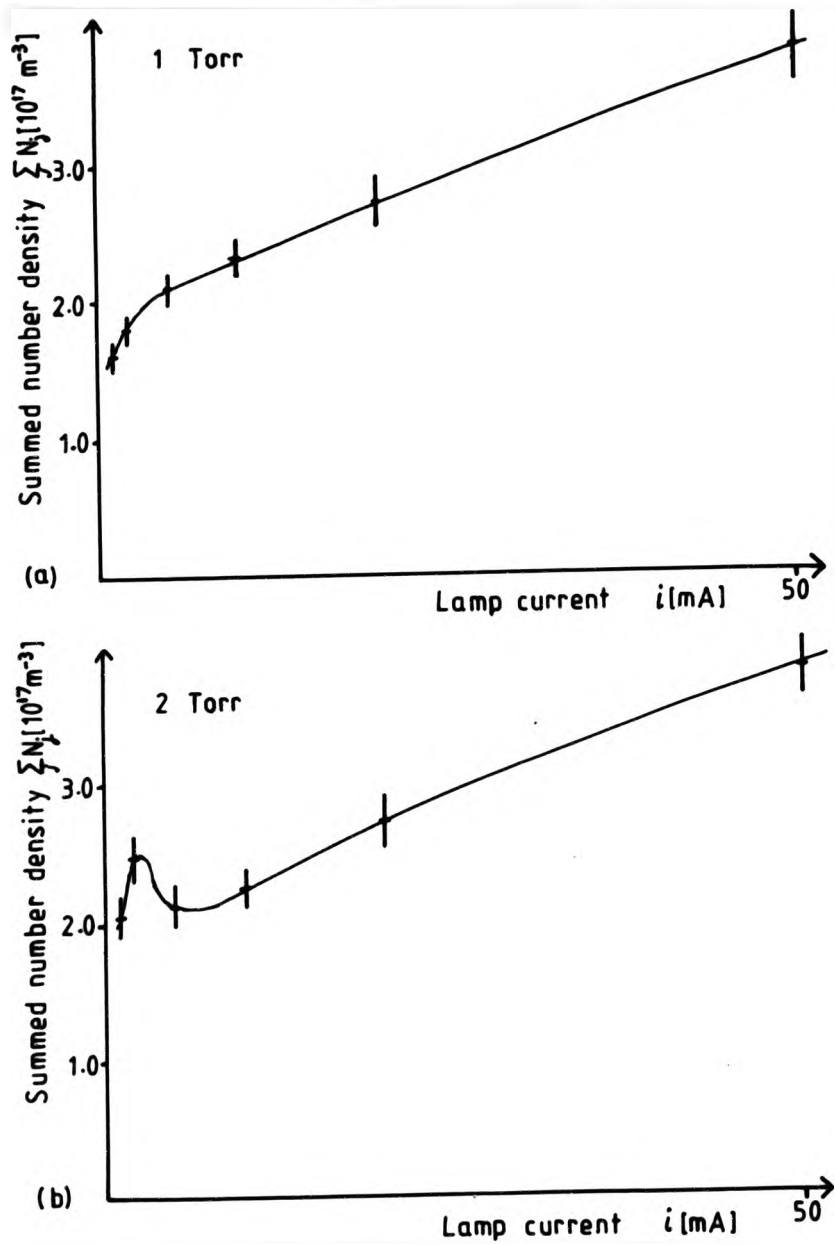
FIGS.53 (a)&(b) PLOTS AGAINST LAMP CURRENT OF NeI EXCITED STATE NUMBER DENSITIES AT 1 TORR



FIGS.54 (a) &(b) PLOTS AGAINST LAMP CURRENT OF NeI EXCITED STATE NUMBER DENSITIES AT 2 TORR



FIGS.55 (a)&(b) PLOTS AGAINST LAMP CURRENT OF NeI EXCITED STATE NUMBER DENSITIES AT 5 TORR



FIGS.56 (a)&(b) PLOTS AGAINST LAMP CURRENT OF NeI EXCITED STATE NUMBER DENSITIES SUMMED OVER $3s, 3s'$ LEVELS

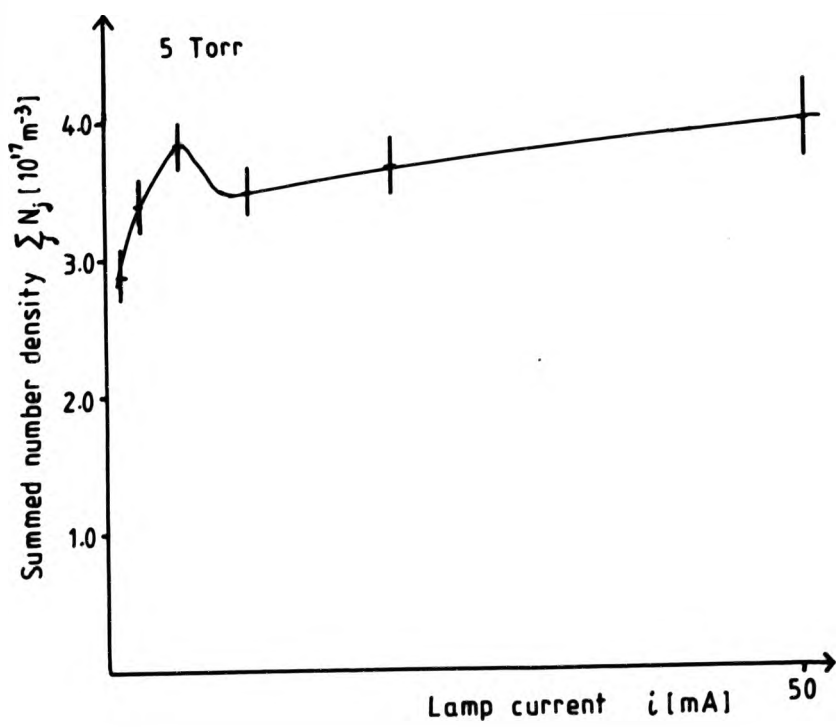


FIG. 57 PLOT AGAINST LAMP CURRENT OF
NeI EXCITED STATE NUMBER DENSITIES
SUMMED OVER $3s, 3s'$ LEVELS

to the convolution integral and the use of the trapezoidal rule to evaluate the area under the absorption profile.

The values of transition probability used, were classified by NBS [53] with an arbitrary notation AA, B, C, D and E indicating the uncertainty limits of the value provided. The values for the spectral lines used in the absorption measurements were classified as B⁻ or B, with uncertainty of B stated as being within 10% and of C within 25%. Hence uncertainty in the values of transition probability introduced an uncertainty of about $\pm \sim 15\%$ in the values of absolute number density calculated; so that number densities calculated for the same atomic state with different spectral lines should agree within $\sim 30\%$, consistent with that obtained - see Figs 54 (a) and (b) -. This uncertainty of $\sim 15\%$ due to the uncertainty in values of transition probability was the dominant source in error the absolute values of number density.

For a given spectral line and value of transition probability, uncertainty in the relative variation of the values of number density with current and pressure, depended on the other error contributions. Uncertainty in the values of number density due to drift in the recorded profiles and poor filling during the synthesis procedure were estimated by noting the change caused in the final calculated value, by changing these factors.

Uncertainty due to drift of the recorded profile intensities (a) was estimated by calculating a number of values using the emission profiles ($i = 0$) recorded before and after a set of transmitted intensity profiles recorded at different H.C. discharge currents. The two values differed by up to $\sim 5\%$ and $\pm 5\%$ was taken as an estimate of the uncertainty in the value of number density due to drift of recorded intensity.

Poor fitting during the synthesis procedure (c) was found to have considerably less effect on the final number density values. For results recorded at lamp pressures of 1 and 2 torr the values obtained when considerable care had been taken to ensure good fitting, with residual values much less than experimental error in deflection (± 0.15 cm), differed by only $\sim 1 - 2\%$, from those obtained for the same recorded profiles where the fitting had been poor, with maximum residual values several times the experimental error. Hence the uncertainty in the values of number density obtained, due to variations in the quality of fit was estimated as $\sim \pm 1.5\%$ for 1 and 2 torr results, increasing to about $\pm 4\%$ for results recorded at 5 torr lamp pressure or very low degrees of absorption.

The uncertainty in values due to error contributions (d) and (e), a small Lorentzian component in the absorption profile and errors in numerical approximation respectively, were estimated to be not greater than 1% and were neglected as relatively insignificant.

The combined effect of contributions (b) and (c) to the uncertainty in relative number density values obtained (as indicated by the error bars in Figs. 53 to 55) was

estimated about $\pm 5\%$ at 1 and 2 torr and about $\pm 8 - 10\%$ at 5 torr.

6/B TOTAL ABSORPTION MEASUREMENTS

Spectral absorbances, defined as the logarithm of the ratio of the probe beam spectral intensity with and without absorption,

$$A = \log \frac{I(i=0)}{I(i)}$$

were calculated for the Ne I 640.2 nm total absorption results shown in Fig. 26. Plots of absorbance (A) against lamp current (i) for the 1 and 5 torr results are shown in Figs. 58 (a) and (b).

The error bars shown in the A/i plots, corresponding to relative errors of $\sim \pm 4\%$, were obtained by recalculating absorbance at a typical point with values of intensity deflection differing by the estimated error in deflection of ~ 1.5 mm.

Principal features of these A/i curves are :

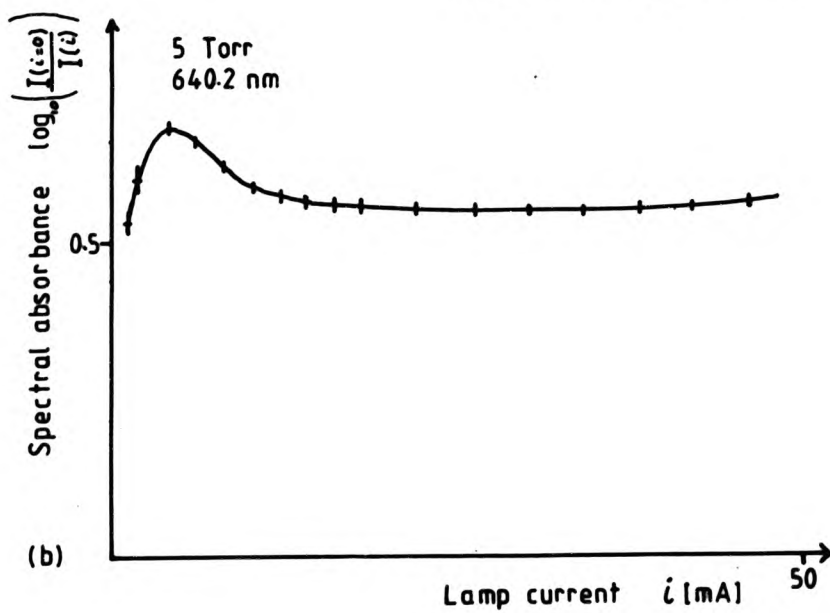
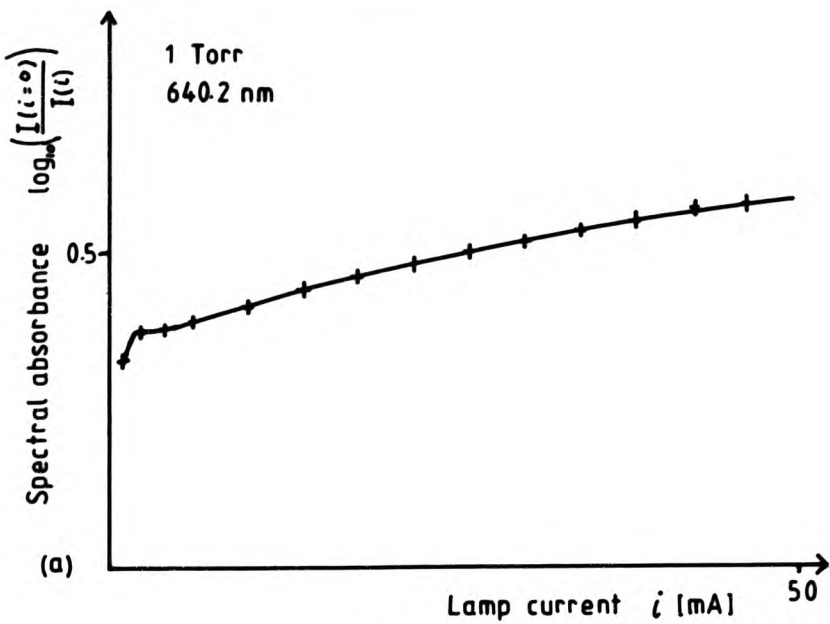
- (i) Sudden increase in absorbance to within $\sim 30\%$ of maximum value as soon as H.C. discharge is initiated at the lowest current at which a discharge could be maintained (~ 0.5 mA)
- (ii) Slow variation of absorbance with lamp current with value changing by no more than $\sim 30\%$ over a range of current of 0.5 - 50 mA.
- (iii) Smooth increase of absorbance with current for 1 torr results.
- (iv) A peak in absorbance at ~ 5 mA for the 5 torr results with very slow change with current thereafter.

Comparing these plots of absorbance against lamp current with plots of the values of number density of $3s [^3/2]_2^2$ obtained by the Fabry - Perot scanning method shown in Figs. 5.3 (a) and 5.5 (a), there is close similarity between the forms of the curves obtained by the two methods.

6/C I/I MEASUREMENTS

6/C.1 Fitting Procedure and Computer Program

The procedure used to fit the I/i curve data to various possible model functions, employed the same NAG subroutine E04FCF as was used in the profile syntheses [see 6/A.3 (e) and (g)] to minimize the sum of square of residuals by varying the components of a vector X. I/i data curves to be fitted were digitized at 2 mA intervals and then the values corrected for the orientation of the graph on the digitizer pad and the scaling of the current axis and the data stored in a file. The summed number density/current ($\sum N_j(i)/i$) curves for 1, 2 and 5 torr were processed in a similar manner but with points digitized more densely, and the values representing the curves then



FIGS.58 (a)&(b) PLOTS AGAINST LAMP CURRENT OF SPECTRAL ABSORBANCE AT 1 & 5 TORR FOR NeI 640.2 nm

fitted to cubic spline representations with a program using NAG subroutine E02BAF and the spline coefficients and knots stored in files. This cubic spline fitting procedure was similar to that used when fitting the spectral profiles in the synthesis procedure (see 6/A.3 (c) for further details).

The flow chart of the main fitting program is shown in Fig. 59. After initiating program execution the user provided the name of the file containing the I/λ data to be fitted and chose the model to be used in the fit. The choice of model fixed the value of an integer identifier which controlled program execution appropriately for each type of model, and determined how the residual values depended on the components of \mathbf{X} .

When the name of the I/λ data file had been provided, the file of this name was opened and intensity and current values read, along with the pressure at which the results had been obtained, wavelength and experimental run information. If the fitting model required $\sum N_j(i)/\lambda$ values, then a file containing the cubic spline fit of the curve at the correct pressure (1, 2 or 5 torr) was opened and read. An array of $\sum N_j(i)$ values at the current values obtained from the file containing the I/λ data were calculated from the spline knots and coefficients.

The arrays of intensity and current values from the data file, array containing values of summed excited state number density ($\sum N_j(i)$) at these current values, and the model identifier were stored in a common memory block (blank common) so that the values could be accessed by RESI2, the subroutine which evaluated the residuals f_i , without having to be transferred through the NAG routine E04FCF. The value of a given residual was the difference between the observed intensity deflection and the deflection calculated from the model function at the observed value of current.

For the starting point of the minimization process the first component of \mathbf{X} was set to 0.5 and all other components set to zero. The number (N) of components of \mathbf{X} depended on the model that was chosen and the number of residuals fixed by the number of I/λ points stored in the file. The choice of the other input parameters required by E04FCF was similar to that used in the synthesis procedure (6/A.3 (g)) and will not be discussed further.

On entry to E04FCF the subroutine sought to minimize the sum of residuals $\sum (f_i)^2$ by varying the components of \mathbf{X} , as it did so information about the minimization process was provided by E04FCF and handled by monitor subroutine LSQMON and compressed information stored in a file (see 6/A.3 (g) for further details).

The subroutine RESI2 was called by E04FCF in order to calculate the array of residual values for a given set of components of \mathbf{X} and model identifier. The physical models assumed the components of \mathbf{X} to be positive, however E04FCF sought

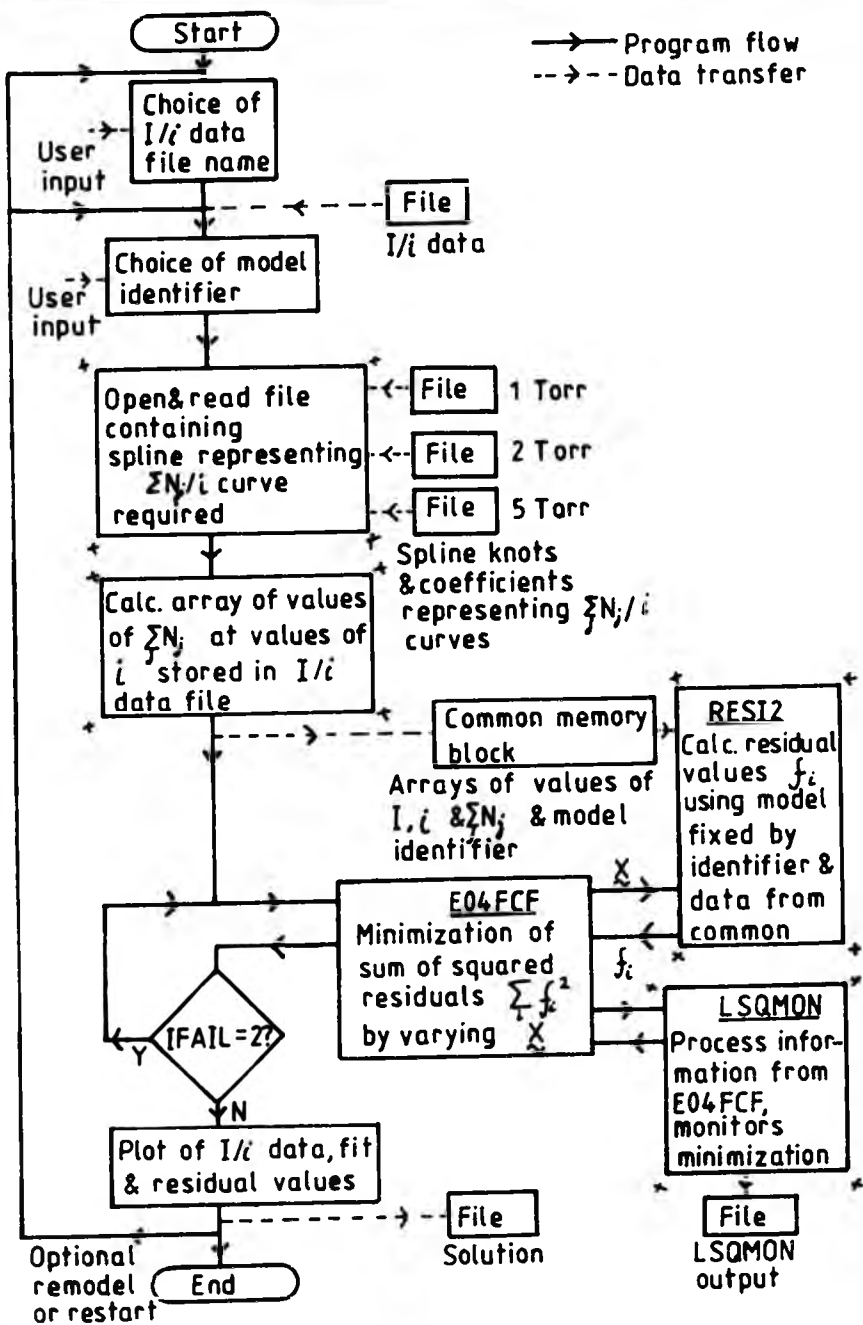


FIG. 59 FLOWCHART OF I/i FITTING PROGRAM

unconstrained minima and would generate negative values of the components if allowed to do so. To ensure that only positive values of the components of X were examined in the minimization process. RESI2 replaced the components of X by their absolute value immediately after entry irrespective of the model identifier value. RESI2 then calculated the set residual values for the current X , using the arrays transferred from common and the given model.

The model functions used in the fitting, fell into two groups denoted by A and B with each model group containing several versions. The physical bases of the model functions are discussed separately below (see 6/C.). The models in group A did not use data derived from the measured number densities, those in group B did. The only difference between B2 and B5 is the order in which the terms are evaluated.

Group A

$$\begin{aligned}
 \text{A1} \quad I &= A'i(1+B'i) \\
 \text{A2} \quad I &= \frac{A'i(1+B'i)}{(1+Ci)} \\
 \text{A3} \quad I &= A'i(1+B'i)(1-Hi) \\
 \text{A4} \quad I &= \frac{A'i(1+B'i)(1-Hi)}{(1+Ci)}
 \end{aligned}$$

Group B

$$\begin{aligned}
 \text{B1} \quad I &= Ai(1+B \sum N(i)) \\
 \text{B2} \quad I &= \frac{Ai(1+B \sum N(i))}{(1+Ci)} \\
 \text{B3} \quad I &= Ai(1+B \sum N(i))(1-G \sum N(i)) \\
 \text{B4} \quad I &= \frac{Ai(1+B \sum N(i))(1-G \sum N(i))}{(1+Ci)} \\
 \text{B5} \quad I &= \frac{iA+iE \sum N(i)}{(1+Ci)} \\
 \text{B6} \quad I &= Ai(1+B \sum N(i))+D \\
 \text{B7} \quad I &= \frac{Ai(1+B \sum N(i))+D}{(1+Ci)} \\
 \text{B8} \quad I &= (Ai(1+B \sum N(i))+D)(1-Hi)
 \end{aligned}$$

The program was structured so that additional model functions could be introduced with little difficulty into the software in the light of the fits obtained with the model functions tried initially. Model functions A2 and B2 were the first to be tried and the others listed, introduced later.

The integer parameter IFAIL (see 6/A.3 (f)) set to 1 before entry to E0FCF was

examined on exit, with IFAIL = 0 or 3 accepted as a solution. In the event of an IFAIL = 3 exit from E04FCF the minimization could be rerun with a greater scale factor XTOLSF (see 6/A.3 (f)) but this was not found to be necessary as it made little difference to the minimum point obtained. On exit with IFAIL = 2, indicating a minimum had not been reached within the prescribed number of iterations (400 x M), an option was provided to re - enter E04FCF using the final point of the minimization just obtained, as a starting point. Exit with IFAIL = 0 or 3 was usually obtained after one rerun of this type after an exit with IFAIL = 2.

After an acceptable minimum had been obtained (IFAIL = 0 or 3) the fitting function and the I/i data points to be fitted were plotted, with the residual values shown beneath (see Fig. 61). A plot was created on the VDU screen and a hard copy plot created on a Benson plotter as an on - line plotter (eg. an HP plotter) was not available.

The components of χ at the solution point, model function used, and the name of the I/i data file and monitor output file, were finally stored in a solution file.

The user then had the option to rerun the fitting of the I/i data with a different model function or to rerun the program with a different set of I/i data.

6/C.2 Physical Models of I/i Curves

A model function for H.C.L. Ne I I/i curves was proposed by Howard et al [38] and had the form :-

$$I = \frac{A_i(1+B_i)}{(1+C_i)} \quad (1.1)$$

In the physical model from which this function was derived, the population of atoms in the upper level of the transition, and hence the intensity of corresponding spectral emission was determined by the relative magnitudes of four rates - represented schematically in Fig. 60 - :-

- (a) the rate of single - step excitation by electron collision from neon ground state.
- (b) the rate of two - step excitation by electron collision via an intermediate state.
- (c) the rate of de - population by electron collision (further excitation, de - excitation or ionization)
- (d) the rate of radiative de - excitation.

If the drift velocity of electrons within the discharge is independent of discharge current, then the electron number density and hence the rate of electron collisions with neon atoms will be proportional to current. Consequently the rate of single - step excitation by electron collision will be proportional to current, giving rise to linear term A_i , with the magnitude of A depending on the single - step excitation rate and intensity scaling. Similarly the rate of de - population by electron collision will also be

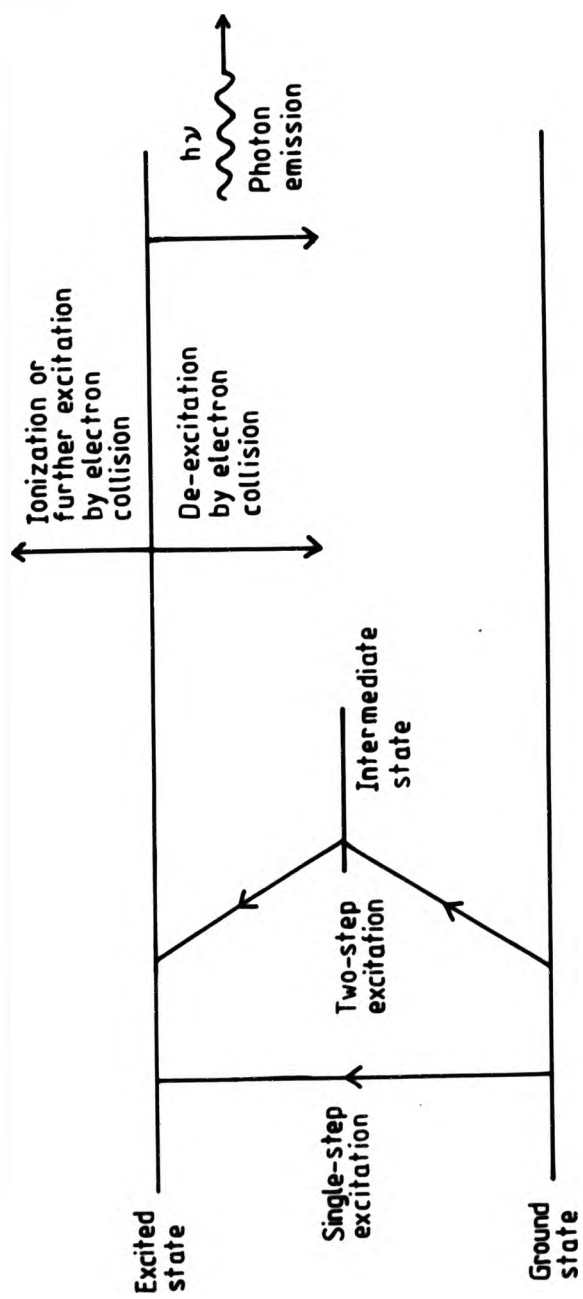


FIG. 60 EXCITATION & DE-POPULATION PROCESSES OF Ne I EXCITED STATE

proportional to the discharge current giving rise to the term $1/(1 + Ci)$ with the magnitude of C depending on the relative magnitudes of the rates of de - population by electron collision and radiation.

The rate of two - step excitation by electron collision via an intermediate state will depend on the rate of electron collision with neon atoms in the intermediate state. If it is assumed that the number density of atoms in the intermediate state is proportional to discharge current then the rate of two - step excitation will be proportional to the square of the current, giving rise to the term $(1 + Bi)$ with the magnitude of B depending on the relative magnitudes of the rates of single and two - step excitation.

For such two - step excitation to be probable the number density of atoms in the intermediate state would have to be relatively high, suggesting that the intermediate state was metastable or quasi - metastable. A suitable candidate for this intermediate level was metastable state $3s [^3/2]_2^o$.

The detection of self - reversal in the profiles of a number of the Ne I emission lines terminating in $3s [^3/2]_2^o$, recorded by means of Fabry - Perot interferometry by the author - see 4/A.2 (a) -, confirmed that this state was indeed highly populated. However direct measurements of the number densities of neon atoms in all four of the $3s, 3s'$ group of excited states, carried out subsequently by the author - see 6/A.4 (d) -, show that the number density of neon atoms in excited state $3s [^3/2]_2^o$ is not proportional to discharge current. Furthermore the number densities of atoms in the other three states of the group (one metastable, two non - metastable) were shown to be significant with number densities down by factors between 1 and 10 from that of the $3s [^3/2]_2^o$ state, the most highly populated of the group.

With direct information about the number densities of excited neon atoms in the $3s, 3s'$ group of state within the discharge available, the I/i model function had to be modified, as the assumption of the proportionality between the number density of the intermediate state and discharge current had been proved incorrect.

If the number density of excited neon atoms in the four states in $3s, 3s'$ group are denoted, at a given current i , by $N_j(i)$, $j = 1, 2, 3$ or 4 , with the j index indicating the level in order of increasing energy, then the rate of excitation of the upper level of a spectral line by two - step excitation via any of their levels will be proportional to $i \sum_j w_j N_j(i)$ where w_j are weighting factors depending on the cross sections for excitation, by electron collision, from each of the four levels to the upper level of the transition corresponding to the spectral line. If it is assumed that the cross sections are equal then the rate is proportional to $i \sum N_j(i)$, the four states of the group acting as

one 'super - state' intermediate level of summed number density $\sum N_j(i)$.

The I/i function resulting from this model is

$$I = \frac{A i (1 + B \sum N_j(i))}{(1 + C i)} \quad (6.11)$$

with the magnitude of A depending on the rate of single - step excitation by electron collision and intensity scaling, the magnitude of B , the relative importance of two - step and single - step excitation and the magnitude of C , the relative importance of de - population by electron collision and radiation. It should be noted that if $\sum N_j(i) = a + bi$ then eq. 6.11 takes the same form as eq. 6.1 with $A' = A (1 + B a)$ and $B' = B b / (1 + B a)$. Plots of $\sum N_j(i)$ against i , calculated from the Fabry - Perot scanning number density measurements at 1, 2 and 5 torr neon pressure, are shown in Figs. 56 (a), 56 (b) and 57.

Self - absorption within the H.C. may also have an effect on the shape of the I/i curve of spectral lines corresponding to transition terminating in the highly populated states of the $3s, 3s'$ group. The amount of self - absorption of photons of a given spectral line will be proportional to the number density of excited neon atoms in the lower energy state of the transition $N_j(i)$, giving rise to a term of the form $(1 - G N_j(i))$, with magnitude of G depending on the importance of self - absorption. The effect of a self - absorption term of this form was not investigated as cubic spline fitting of the $N_j(i)/i$ curves of individual states in the $3s, 3s'$ group and the resulting modification of the I/i fitting program was not attempted due to lack of time remaining at the end of the work. However the effect of terms of the form $(1 - H i)$ and $(1 - G \sum N_j(i))$, not requiring further fitting of the $N_j(i)/i$ curves, were examined.

A number of different model functions based on equations 1.1 and 6.11, including and excluding various terms described above, were tried and are listed in subsection 6/C.1 divided into two groups A and B, model functions A1 to A4 derived from eq. 6.1 and B1 to B8 derived from eq. 6.11.

6/C.3 Fitting I/i Curves

Examples of plots of the fitted I/i curves obtained with different model functions and I/i data are shown in Figs. 61 to 66, with corresponding residual values plotted beneath. The model function number and the fitted values of the parameters (A, B, C etc) in the function are also shown. Table 5 shows the values of the parameters obtained by fitting model equations B6 and B7 to all the 1 & 2 torr experimental results analysed. Parameter values obtained fitting the other model functions are given in Table 6.

Model function

$$I = \frac{A i (1 + B i)}{1 + C i}$$

$A = 0.276$ (arbitrary/mA)

$B = 0.0057$ (mA)⁻¹

$C = 0.000$ (mA)⁻¹

[arbitrary units = cm,

estimated deflection expt.

error ± 0.15 cm]

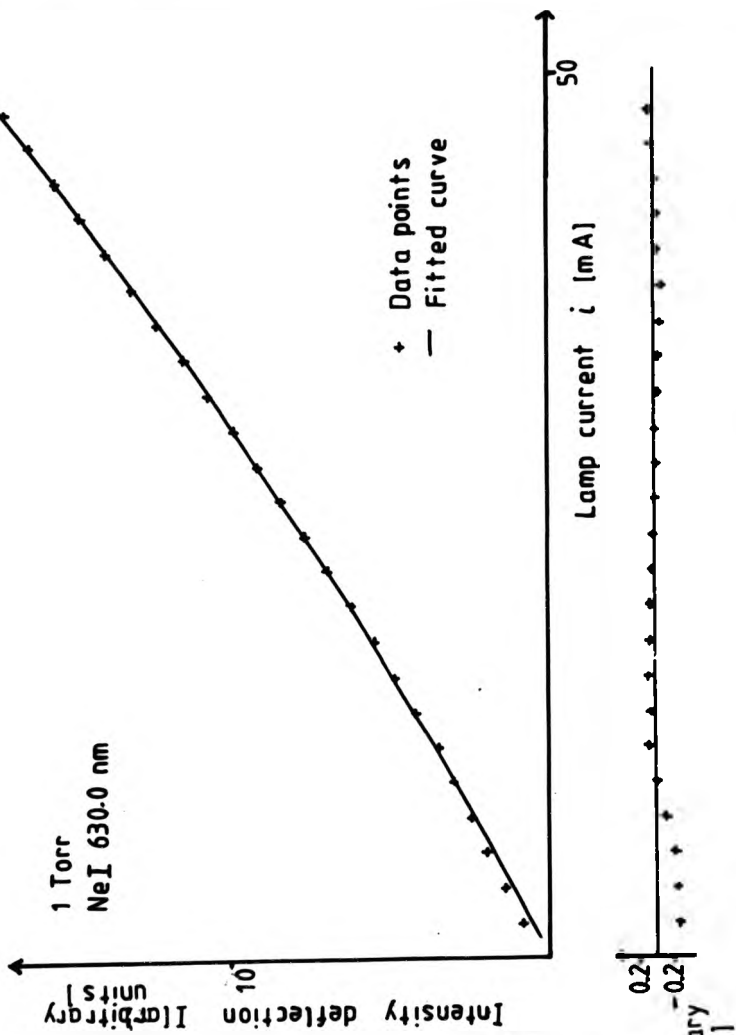


FIG.61 I/i FITTED CURVE, DATA & RESIDUALS FOR NeI 630.5 nm, 1 TORR

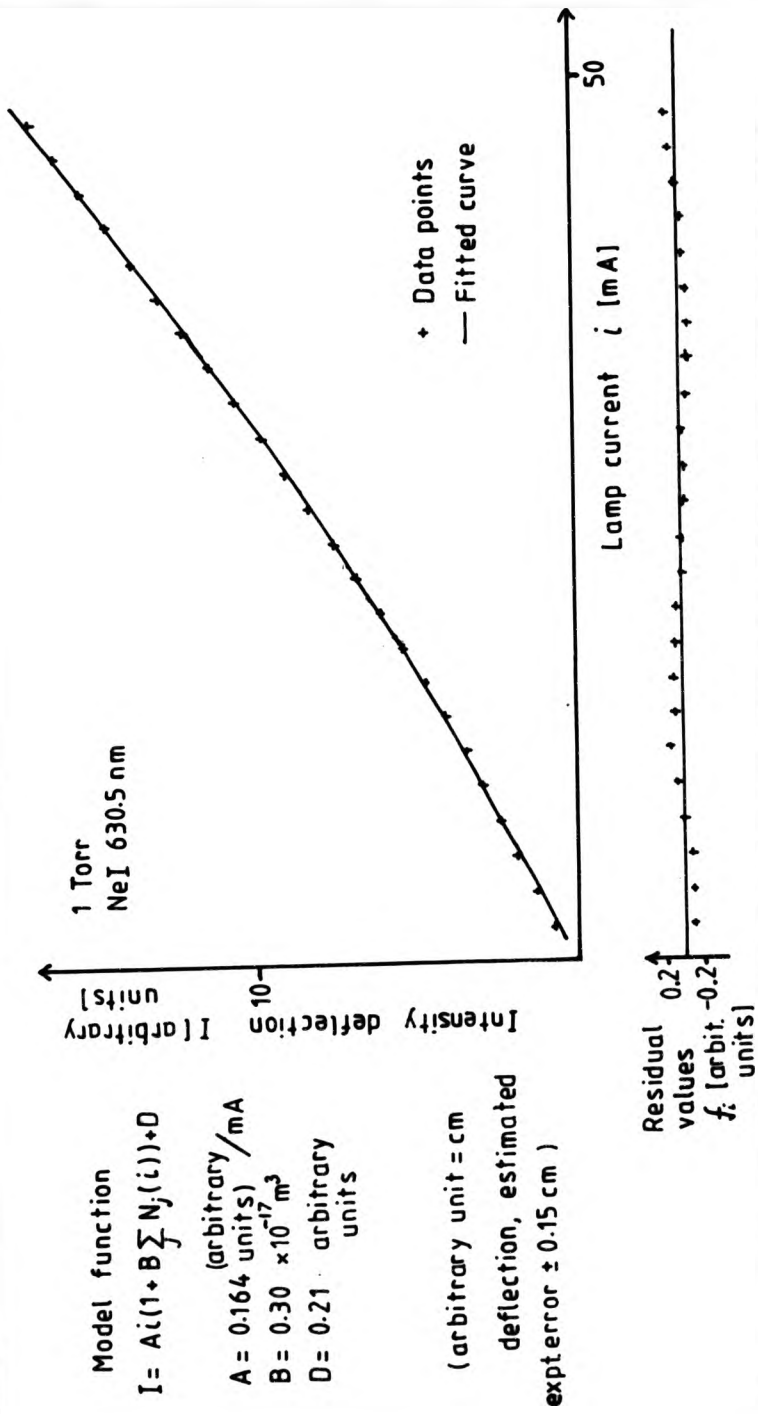


FIG. 62 I/i FITTED CURVE, DATA & RESIDUALS FOR Ne I 630.5 nm, 1 TORR

Model function

$$I = A i (1 + B \sum_j N_j(i)) + D$$

$$A = 0.0407 \text{ (arbitrary/mA)}$$

$$B = 1.8 \cdot 10^{-17} \text{ m}^2$$

$$D = 0.24 \text{ arbitrary units}$$

(arbitrary unit = cm deflection, estimated exp. error ± 0.15 cm)

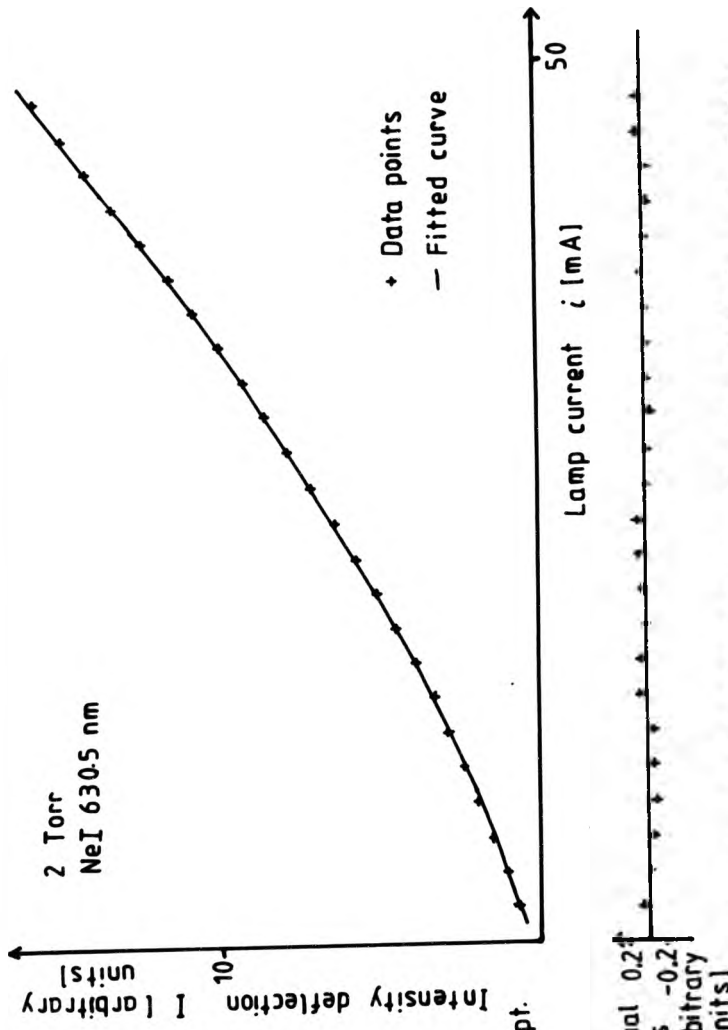
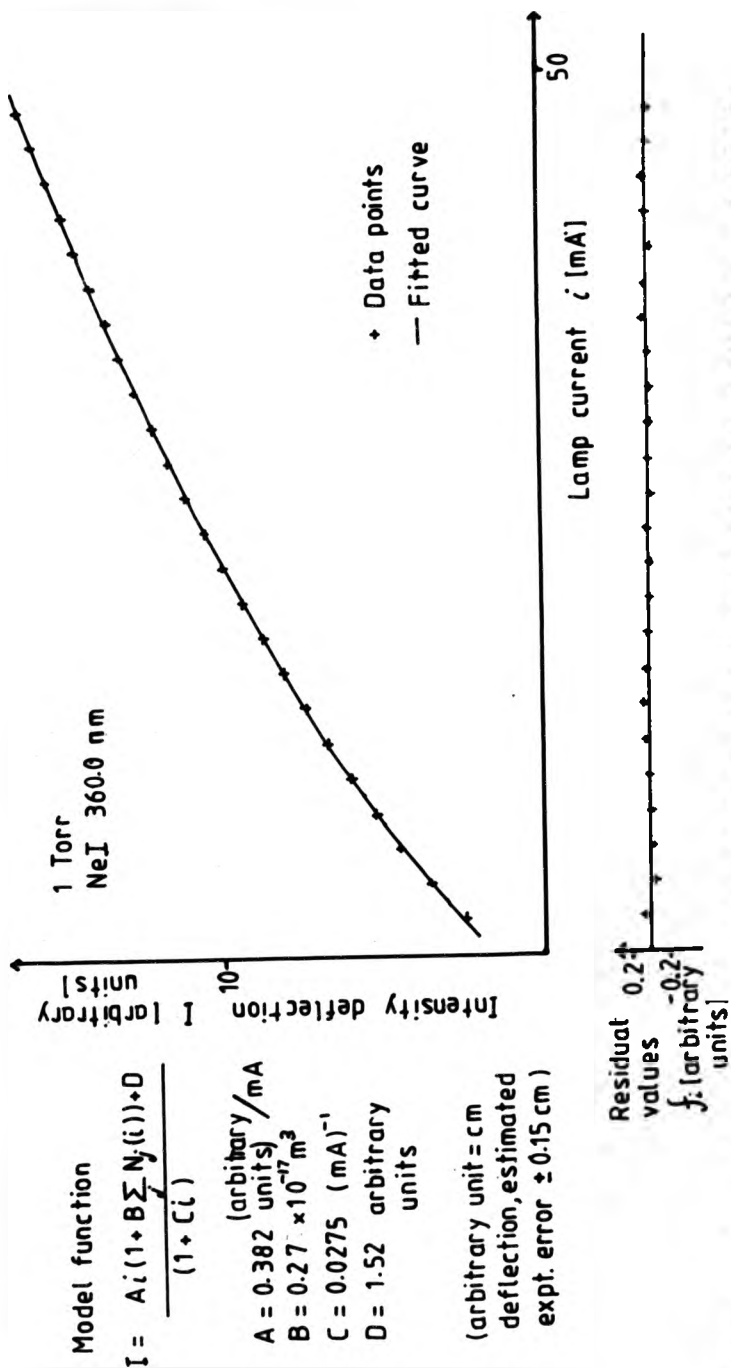


FIG. 63 I/i FITTED CURVE, DATA & RESIDUALS FOR NeI 630.5 nm, 2 TORR



Model function

$$I = \frac{A_i(1 + B \sum_j N_j(i)) + D}{(1 + C i)}$$

- A = 0.382 (arbitrary units) / mA
- B = $0.27 \times 10^{-17} \text{ m}^3$
- C = 0.0275 (mA)⁻¹
- D = 1.52 arbitrary units

(arbitrary unit = cm deflection, estimated expt. error $\pm 0.15 \text{ cm}$)

FIG.64 I/i FITTED CURVE, DATA & RESIDUALS FOR NeI 360.0 nm, 1 TORR

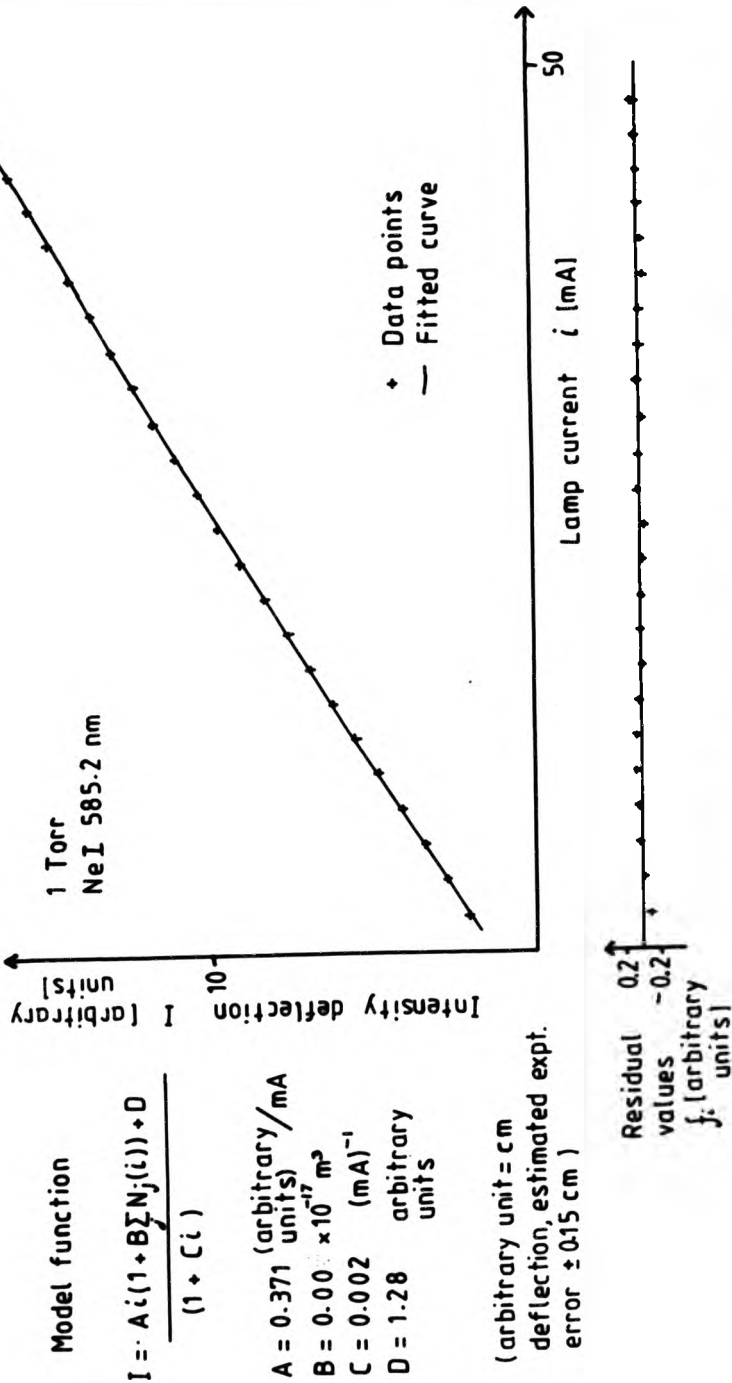


FIG. 65 I/i FITTED CURVE, DATA & RESIDUALS FOR Ne I 585.2 nm, 1 TORR

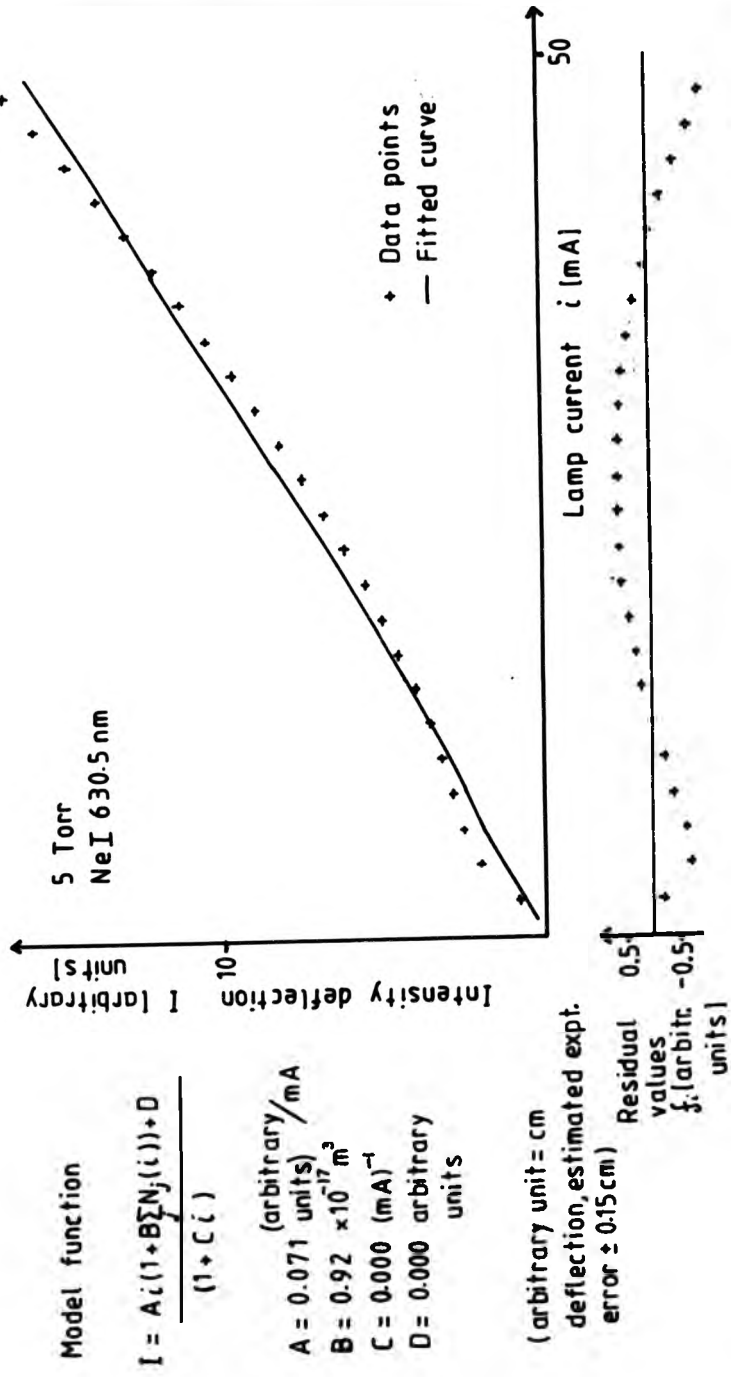


FIG.66 I/i FITTED CURVE, DATA & RESIDUALS FOR Ne I 6305 nm, 5 TORR

wave-length nm	1 Torr					2 Torr				
	fit	A a.u./mA	B 10^{-17} m^3	C mA^{-1}	D a.u.	fit	A a.u./mA	B 10^{-17} m^3	C mA^{-1}	D a.u.
748.9	α^+	0.301	0.035	0.000	0.53	α^+	0.216	0.16	0.000	0.55
743.8	α^+	0.154	0.36	0.000	0.00	α^+	0.0767	0.99	0.000	0.02
724.5	α	0.256	0.085	0.000	0.05	α^+	0.129	0.47	0.000	0.16
703.2	α^-	0.254	0.094	0.000	0.00	α	0.139	0.37	0.000	0.00
692.9	α	0.311	0.025	0.000	0.19	α^+	0.239	0.13	0.000	0.08
671.7	α^-	0.206	0.176	0.000	0.17	α^+	0.0984	0.70	0.000	0.02
667.8	α^-	0.311	0.044	0.000	0.05	α	0.207	0.20	0.000	0.00
659.9	α^-	0.239	0.12	0.000	0.14	α^+	0.148	0.37	0.000	0.01
† 640.2	α^-	0.306	0.038	0.000	0.00	α^+	0.123	0.45	0.000	0.31
630.5	α	0.164	0.31	0.000	0.21	α	0.0407	1.8	0.000	0.25
* 630.5	β^+	0.182	0.25	0.000	0.10					
614.3	α	0.251	0.080	0.000	0.04	α	0.102	0.61	0.000	0.00
588.2	α^-	0.167	0.31	0.000	0.09	α^+	0.0284	3.0	0.000	0.00
* 585.2	α^+	0.37	0.00	0.002	1.28	α^+	0.0731	1.5	0.0088	1.00
585.2	α^-	0.339	0.00	0.000	1.45					
* 363.4	α^+	0.172	0.98	0.0323	1.22	α	0.481	0.00	0.0086	1.21
* 360.0	α^+	0.382	0.27	0.028	1.52	α	0.166	2.4	0.0747	0.80

(1) arbitrary units (a.u.) = cm deflection of XY recorder

(2) * Indicates a fit to model equation

$$I = \frac{A i (1 + B \sum N_j(i)) + D}{(1 + C i)} \quad (B7)$$

unmarked a fit to B6 (i.e. C clamped to value C = 0)

(3) † parameter values obtained with fits to model equations including absorption terms are provided in Table 6

(4) α = good fit, all residuals less than experimental error ($\pm 1.5\text{a.u.}$)

β = fair fit, most residuals of the order of experimental error

TABLE 5. VALUES OF PARAMETERS OBTAINED FITTING MODEL EQUATIONS B6 & B7 TO OBSERVED I/i CURVES

wave-length [nm]	pressure [torr]	model #	fit	A' [a.u./mA]	B' [mA ⁻¹]	A [a.u./mA]	B [10 ⁻¹⁷ m ³]	C [mA ⁻¹]	G [10 ⁻¹⁷ m ³]	H [mA ⁻¹]
640.2	1	B1	α ⁻			0.296	0.049			
640.2	2	A1	β	0.258	0.0064					
640.2	2	B3	β			0.17	0.26		0.000	
640.2	1	B2	α ⁻			0.0171	9.2	0.0148		
640.2	1	B3	α ⁺			0.137	0.98		0.122	
640.2	1	B1	β			0.197	0.21			
630.5	1	A1	β	0.276	0.0057					
630.5	1	A2	β	0.276	0.0062			0.00034		
630.6	1	A3	β	0.275	0.0064					0.00046
630.5	1	A2	β ⁻	2.75	0.163			1.35		
588.2	1	A2	β	0.259	0.186			0.00777		
588.2	1	A1	β ⁻	0.272	0.00663					
588.2	2	A1	β	0.191	0.0167					0.00394
588.2	1	A3	β	0.258	0.0147					0.00467
588.2	2	A3	α	0.166	0.0343					
588.2	1	B1	β ⁺			0.181	0.27			
588.2	2	B1	α ⁺			0.0237	3.61			
.360.0	1	A2	β	1.29	0.031			0.172		

(1) arbitrary units (a.u.) = cm deflection of XY recorder

(2) # see p 131 for list of model equations

(3) α = good fit, all residuals less than experimental error (± 1.5 a.u.)

β = fair fit, most residuals of the order of experimental error

TABLE 6. VALUES OF PARAMETERS OBTAINED FITTING MODEL EQUATIONS (OTHER THAN B6 & B7) TO OBSERVED I/I CURVES

For I/i results at neon pressures of 1 and 2 torr, model functions A2 and B2 provided acceptable fit, with residual values of the order of experimental error ($\sim \pm 1.5$ mm), except in the low current region. The term $1/(1 + Ci)$ was not found necessary except in the case of spectral lines, such as Ne I 360.0 nm, with transitions from high lying energy levels. The inclusion of this term in cases of spectral lines with transitions from lower lying energy levels, such as Ne I 630.5 nm, which do not "turn-over" with increasing current, did not improve the fit but merely changed the values of A and B, with C small, because of the effect of "trade-off". Model functions A1 and B1 were adequate in these cases. The only exception to this was the I/i curve of 585.2 nm which corresponds to a transition from the highest energy state of the 3p, 3p' groups. The I/i curve of this spectral line had slight downward curvature and a significant but small value for parameter C was required in order to obtain a good fit. Acceptable fits for the 5 torr results could not be obtained. The main difference between the fits obtained for 1 and 2 torr I/i results corresponding to transitions between the 3s, 3s' and the 3p, 3p' group of states, was that B was always greater for the 2 torr than the 1 torr results. This reflects that fact the I/i curves corresponding to these transitions show greater departure from linearity at 1 torr than at 2 torr and curve upward more rapidly - See Figs. 18 and 19 and Figs. 62 and 63.

Inclusion of terms corresponding to the effect of self-absorption in model functions A3 and A4 and B3, B4 and B8 did not improve the fit in cases where an acceptable fit had been obtained without such terms and did not provide an acceptable fit for results at 5 torr where acceptable fits had not been obtained with A1, A2, B1 and B2, the only exception to this being Ne I 640.2 nm for which model function B3 provided an improved fit.

In an attempt to improve the fit obtained with model functions B1 and B2 in the low current region of the 1 and 2 torr results, a factor (D) independent of current was introduced in model function B6 lacking the $1/(1 + Ci)$ term and B7 including this term. With these two model functions B6 and B7, good fits over the whole current range could be obtained for all 1 and 2 torr results; model function A7 including the $1/(1 + Ci)$ term was only necessary for spectral lines with transitions from high lying levels.

6/C.4 Parameter Values

If one considers different spectral lines with transitions from the same upper energy level, it may be expected that the values of the parameters B and C obtained will be the same for the different spectral lines, because the values of these parameters depend only on the ratios of excitation or de-excitation rates of the energy level. The values of

parameters A and D however will depend on the arbitrary intensity scaling.

However the value of parameter B obtained fitting experimental data to eq. 7.5 is subject to considerable uncertainty because of the effect of trade - off, particularly trade - off with respect to parameter A. (Trade - off is the complementary variation of parameters so that the value of $F(\underline{X}) = \sum (f_i)^2$ is not significantly changed.) The large degree of trade - off in this case arises because of the relatively slow variation of $\sum N_j(i)$ with increasing current. If one considers the extreme case in which $\sum N_j(i)$ is a constant, then the expression $A(1 + B \sum N_j(i))$ can be replaced by a single parameter (P say) independent of current and all values of A and B giving the same value P will give the same residual contributions. A family of solutions will exist with small values of A matched with suitably large values of B with parameter ranges $0 \leq A \leq P$ and $0 \leq B \leq \infty$.

In fact $\sum N_j(i)$ is not constant but increases slowly with increasing current so that the trade - off effect between A and B will only be partial but will still allow considerable complementary variation of the parameters without significantly changing the value of $F(\underline{X})$. The value of B in particular will be subject to most uncertainty. The presence of parameters D and C will further increase the scope for trade - off uncertainty.

The effect of trade - off may be seen in parameter values obtained fitting the 1 torr 630.5 nm I/i curve data to the model equation (B6) with C clamped to $C = 0$, and with C free to vary (B7) - see Table 5 -. The value of C obtained when C was free to vary was not zero but very small ($\sim 2 \times 10^{-8} \text{ mA}^{-1}$). The value of D changed by an amount approximately equal to the experimental error in deflection ($\pm 0.15 \text{ cm}$). The value of A obtained increased by $\sim 10\%$ and the value of B reduced by $\sim 25\%$. Even with numerically identical input data substantial trade - off occurred. Sets of data affected by different random experimental errors will be subject to greater trade -off. Thus the values of B obtained fitting the I/i curves of spectral lines with the same upper level may differ considerably (although they should be of similar order of magnitude).

The variances of solution parameter values $X_{i, \text{sol}}$ are measures of the uncertainty of the solutions obtained from least squares fitting. If the matrix H is the inverse of the Hessian matrix $G = \frac{\partial^2 F(\underline{X})}{\partial X_i \partial X_j}$ and $S = F(\underline{X}_{\text{sol}})$ then the best unbiased estimate of

the variance of $X_{i, \text{sol}}$ is approximately

$$\text{var } X_i = \frac{2S}{m-n} H_{ii}$$

where m is the number of residuals and n the number of parameters [75]. Hence a 95% confidence interval for the true solution parameter is approximately

$$X_{i \text{ sol}} \pm 2 \sqrt{2 S H_{ii} / (m - n)}$$

As H is the inverse of G it is given by

$$H = \text{adj}(G) / \det(G),$$

where $\text{adj}(G)$ is the adjoint matrix of G and $\det(G)$ the determinant of G , if $\det(G)$ is small then the components of H can assume very large values. The values of G and S are provided by E04FCF and further analysis could establish estimates of the confidence limits.

A number of the spectral the I/λ curves of which were analysed (and parameter values obtained listed in Table 5) have atomic transitions with common upper energy levels. Ne I 743.8, 724.5 and 703.2 nm have transitions from $3p [^1/2]_1$, 692.9 and 614.3 nm have transitions from $3p [^3/2]_2$, and 659.9 and 588.2 nm transitions from $3p' [^1/2]_1$.

The values of parameter B obtained for spectral lines with common upper energy levels of their transitions differ by factors ~ 2 .

CHAPTER 7 DISCUSSION AND CONCLUSIONS

7/A SELF - REVERSAL OF SPECTRAL LINE PROFILES

The observation of self - reversal and broadening by self - absorption of the profiles of spectral lines with transitions terminating in metastable state $3s [^3/2]_2^o$, was the first direct evidence obtained in the work that the number density of neon atoms in this state was sufficiently high to make two - step excitation of higher energy levels, via this state, probable. The profiles of all spectral lines studied with transitions terminating in $3s [^3/2]_2^o$ exhibited varying degrees of self - reversal, with the exception of 588.2 nm. The lack of self - reversal of the profile 588.2 nm may be explained by the lower transition probability and less favourable ratio of statistical weights for this spectral line than other lines with transitions terminating in the $3s [^3/2]_2^o$ state.

The lack of self - reversal of the profiles of any of the spectral lines with transitions terminating in other state of the 3s, 3s' group, supports the results of direct measurements of excited state densities that the $3s [^3/2]_2^o$ state is the most highly populated of the group.

Changes in spectral profiles caused by differing degrees of self - absorption and reversal, noted in early stages of the work due to contamination of the lamp gas, were an important indication of the contamination and, subsequently, recording of the profiles provided a useful, sensitive check of neon purity.

7/B NUMBER DENSITIES OF EXCITED ATOMS IN 3s, 3s' STATES

7/B.1 General Features of Number Density Results

The absolute number densities of neon atoms in four excited Ne I states $3s [^3/2]_2^o$, $3s [^3/2]_1^o$, $3s' [^1/2]_0^o$ and $3s' [^1/2]_1^o$ and their variation with discharge current, differed considerably for the four states. The pressure of the neon in the H.C.L. also affected the shape of the number density/current curves ($N(i)/i$) and to a lesser extent the absolute number density values - see Figs. 53 to 57 - .

Starting with the 2 torr results - see Figs. 54 (a) and (b) - for which the best low drift results were available and the most extensive analysis carried out, principal features of the number density results obtained, grouped by energy level, were :

- (a) $3s [^3/2]_2^o$ (the lowest energy metastable state)
- highest population of the 3s, 3s' group of states with mean number density $\sim 1.5 \times 10^{17} \text{ m}^{-3}$
 - the number density attained this value at the lowest current for which a discharge current could be maintained ($\sim 0.5 \text{ mA}$) and varied by less than 20% as the discharge current was increased one hundred fold to 50 mA
 - there is a sharp local peak in number density at low current ($\sim 2 \text{ mA}$) falling in value near $\sim 5 \text{ mA}$ and thereafter increasing slowly and approximately linearly with current up to 50 mA.
- (b) $3s [^3/2]_1^o$ (non - metastable state)
- the second most populated state with mean number density $\sim 0.6 \times 10^{17} \text{ m}^{-3}$
 - the number density attained a significant value $\sim 0.2 \times 10^{17} \text{ m}^{-3}$ at lowest possible discharge current but increased by a factor ~ 4 as the current was increased to 50 mA
 - the $N(i)/i$ curve has smooth shape with no local peaks and slowly decreasing gradient with increasing current.
- (c) $3s' [^1/2]_0^o$ (metastable state)
- one of the least populated of 3s, 3s' group with mean number density $\sim 0.3 \times 10^{17} \text{ m}^{-3}$
 - $N(i)/i$ curve has the same shape as that for the other metastable state of group ($3s [^3/2]_2^o$) but with number density scaled down by a factor ~ 5 . Both exhibit similar strong saturation with increasing lamp current.
- (d) $3s' [^1/2]_1^o$ (non - metastable state)
- one of the least populated of 3s, 3s' group with mean number density $\sim 0.3 \times 10^{17} \text{ m}^{-3}$
 - $N(i)/i$ curve does not saturate with increasing discharge current and the number density is approximately proportional to current.

Considering now the effect of changing neon pressure, the most notable difference in the $N(i)/i$ curves at different pressures is in the low current region, where local peaks occur in the curves for the two metastable states $3s [^3/2]_2^o$ and $3s' [^1/2]_0^o$ at 2 torr. The 1 torr $N(i)/i$ curves are almost identical to those for 2 torr above a lamp current of $\sim 15 \text{ mA}$, but do not have local peaks in the curves for the metastable states in the low current region.

At 5 torr the peaks in the low current region of the $N(i)/i$ curves for the two metastable states are more pronounced than at 2 torr and extend to greater values of lamp

current. The overall number densities of all four excited states are slightly higher at 5 torr than at 1 and 2 torr (however the estimated errors and 'scatter' of $3s [^3/2]_1^0$ and $3s' [^1/2]_1^0$ results are poorer).

7/B.2 Comparison with Results of Other Workers

Measurements of the number densities of excited neon atoms in hollow cathode discharges using various methods have been made by workers principally interested in laser applications [5, 25]. These measurements have been made for higher current densities of the order of 10 to 100 mA/cm², with water cooled copper cathodes of different dimensions than those used by the author and have mainly been concerned with the number densities of the two metastable states $3s [^3/2]_2^0$ and $3s' [^1/2]_0^0$.

Measurements carried out by the author were for current densities < 2.12 mA/cm² without water cooling of the mild steel cathode and were made for all four states of the 3s, 3s' group.

Number densities of atoms in metastable states $3s [^3/2]_2^0$ and $3s' [^1/2]_0^0$ obtained by de Hoog, McNeil, Collins and Persson [5] using the method of Ladenburg and Reiche [64], were $\sim 10^{18}$ and $\sim 1.5 \times 10^{17}$ m⁻³ respectively at 10.6 torr neon pressure, compared with number densities of atoms in these states of $\sim 1.5 \times 10^{17}$ and $\sim 2 \times 10^{16}$ m⁻³ respectively, at neon pressures of 1, 2 and 5 torr, obtained by the author. The number densities of atoms in the two metastable states obtained by these workers also exhibit the strong saturation with increasing discharge current observed by the author, and peaks in the number densities at low currents observed by the author at neon pressures of 2 and 5 torr.

Number densities of neon atoms in metastable state $3s [^3/2]_2^0$ obtained by van Veldhuizen and de Hoog [25] using laser absorption, for a different water cooled Cu - Ne H.C.L. system at current densities ~ 10 to 100 mA/cm² were also $\sim 10^{18}$ m⁻³.

Measurements of the number densities of neon atoms in excited states of the 3s, 3s' group of energy levels have been made by Djulgerova, Jechev, Pacheva and Rashev [65] using a modified form of the method of Ladenburg and Reiche for an H.C.L. with an aluminium cathode, without water cooling, at similar current densities to those used by the author. These workers obtained number densities of neon atoms in the four excited states $\sim 10^{17}$ m⁻³, as did the author; however the relative magnitudes of the number densities of atoms in the four states were different to those obtained in the present work. Most notably these workers reported that the $3s [^3/2]_2^0$ metastable state was not the most highly populated of the 3s, 3s' group of states, whereas the author found that this was the most highly populated state of the group, a conclusion supported

by the fact that self-reversal was detected by the author in the profiles of spectral lines with transitions terminating in this state but not those terminating in other states of the group.

7/B.3 Saturation of Metastable Atom Population

Saturation of the neon metastable atom populations with increasing current, observed in the present work and by de Hoog et al [5, 25] in the H.C.D., has also been observed in the helium metastable population in the He - Ne positive column laser discharge by White and Gordon [66].

How may the strong saturation of the number densities of atoms in the two metastable excited states with increasing discharge current be explained? The explanation put forward by Webb [67, 68] for the saturation with increasing electron number density of the population of noble gas metastable states in all types of discharge, is depopulation of these states by electron collision, particularly those collisions causing ionization of the metastable atoms. He argues that, although only a relatively small proportion of the plasma electrons in the discharge have sufficient energy to excite the metastable states from the ground state (~ 16.6 eV for neon) a larger proportion of the electrons have the energy necessary to ionize atoms in the metastable states (~ 5 eV for neon). In addition, the electron collision cross-section for ionization of metastable atoms is greater than the cross-section for excitation of their ground state atoms. Hence, although increasing the electron density increases the rate of creation of metastable atoms, it also increases the rate of their destruction, so that, once the electron density reaches the point where ionization of the metastables dominates over all other forms of their destruction, the population of metastable atoms becomes insensitive to further increases in electron density. Expressing this argument algebraically, if N_e is the electron number density, N_m the metastable number density and i the discharge current, then

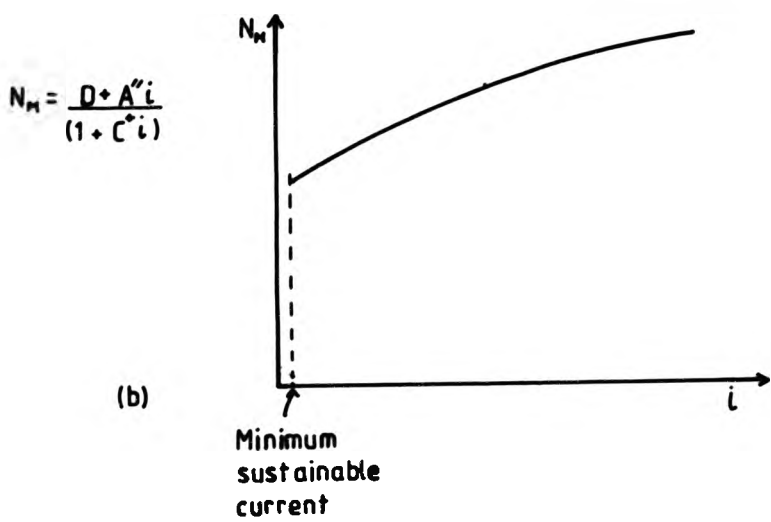
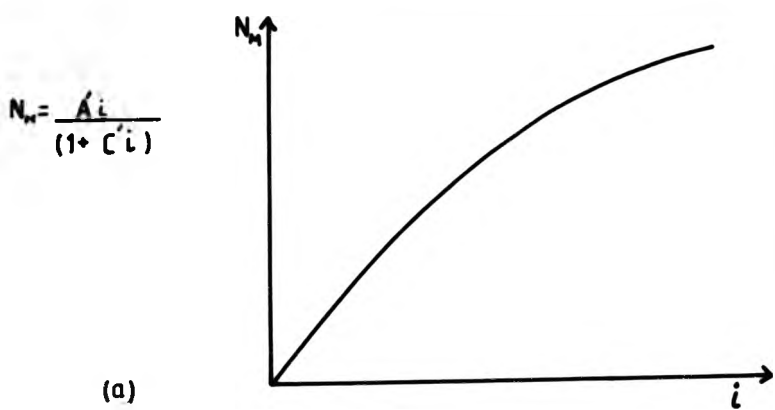
$$N_m = \frac{A_e N_e}{(1 + C_e N_e)} \quad (7.1)$$

where A_e depends on the cross-section for excitation of the metastable state by electron collision and C_e the ratio of the rate of destruction of metastable atoms by electron collision and all other modes of destruction.

If $N_e \propto i$ then this expression becomes

$$N_m = \frac{A_e' i}{(1 + C_e' i)} \quad (7.2)$$

where A_e' and C_e' are related by constant factors to A_e and C_e respectively.



FIGS.67 (a)&(b) SCHEMATIC PLOTS OF META-STABLE ATOM NUMBER DENSITY AGAINST CURRENT

A plot of N_0 against i will then be of the form shown in Fig. 67. If one compares this curve with the observed variation of metastable atom numbers density with current - Figs. 53, 54 and 55 - it can be seen that there are two important differences. Firstly the observed number density 'jumps' very abruptly near the origin so that, at the lowest sustainable current, the number density has a significant value and secondly there are peaks in number density in the low current region at the higher neon pressure of 2 and 5 torr.

Consider first the peaks in metastable atom number density in the low current region at higher neon pressures. These peaks are accompanied by rapid changes in the radial distribution and appearance of the cathode glow observed visually. The number density measurements were made with a wide probe beam so that an average number density across the beam width was measured. A greater proportion of probe beam rays near the centre of the beam finally reached the detector than those near the edge of the beam, because of aperture limitation; hence absorption at the centre of the H.C. glow provided a greater proportion to the measured metastable number density than that near the cathode. Thus, changes in the radial distribution could cause fluctuations in the measured number density not reflecting true variations in the average number density, and produce the local peaks in measured density observed at low currents and higher neon pressure. This effect however cannot explain the sudden jump in measured metastable density from the origin to a significant value at the lowest sustainable discharge current.

This suggests that the assumption of proportionality between electron number density and discharge current breaks down at low currents, with the electron number density increasing abruptly at the lowest sustainable current, so that

$$N_0 = N_0(i \sim 0) + a_0 i \quad (7.3)$$

where $N_0(i \sim 0)$ is the electron number density at the lowest sustainable discharge current and a_0 the increase in electron density per unit current. Equation 7.2 now takes the form

$$N_m = \frac{D_0 + A_0 i}{(1 + C_0 i)} \quad (7.4)$$

and shifts the origin in Fig. 67 (a) to the right so that the plot of N_m against i becomes as shown in Fig. 67 (b), which agrees more closely with the observed variation, ignoring the local peaks in density at low current for 2 and 5 torr discussed above. As discussed further below (see 7/C.2) the I/λ of some spectral lines also indicate that electron number density is not proportional to discharge current at low current. Results by

Borodin and Kagan [19, 20] show an approximate proportionality between electron number density and discharge current, in the current range 15 to 60 mA for similar sized nickel cathodes in a helium H.C. discharge, but they do not give any values for very low currents. Results by van Veldhuizen and de Hoog [25] for neon also show approximate proportionality between electron density and current at higher current density but with slight downward curvature.

At discharge currents greater than ~ 10 mA (~ 0.42 mA/cm²) below which the local peaks in metastable density occur, the main difference between the 1 and 2 torr, and 5 torr measured metastable density versus current curves, is that at 1 and 2 torr the metastable density increases with increasing current whereas at 5 torr the density hardly increases at all. This difference may be associated with the longer diffusion time of metastable atoms at higher neon pressure, so that destruction of the metastable states by electron collision dominates over their destruction at cathode surfaces, at lower current density.

7/B.4 Quasi - metastable Atom Population

The number densities of neon atoms in the two non - metastable states in the 3s, 3s' group might initially be expected to be very small compared to the density of metastables, because of fast radiative de - excitation to the ground state. However the effect of radiation trapping greatly increases the effective lifetime of these two states which may be described as quasi - metastable. Radiation trapping [69] is the strong reabsorption of the ultra - violet emission by ground state atoms, so repopulating the resonance state in question.

Also, another populating mechanism is possible for the two states in addition to excitation from the ground state by electron collision and population by radiative cascade from higher energy excited states. Thermally excited transitions from atoms in the two metastable states $3s [^3/2]_2^o$ and $3s' [^1/2]_0^o$ may also take place [70], as the differences in energy are of the same order of magnitude as that available from thermal collision with atoms, ions or electrons. Clearly the majority of these thermal collisions will be with ground state neon atoms as these particles have the highest number density $\sim 10^{23}$ m⁻³.

The gas temperature of the H.C. discharge estimated from the width of the Ne I 585.2 nm emission spectral line, was ~ 600 K, so that the average thermal kinetic energy $kT \sim 0.052$ eV. This spectral line showed no evidence of broadening by self - absorption and the number density ($\sim 2 \times 10^{16}$ m⁻³) of atoms in the lower state ($3s' [^1/2]_1^o$) of the transition was an order of magnitude less than the number density of $3s [^3/2]_2^o$, for which spectral lines did show evidence of self - absorption. Hence the width of this

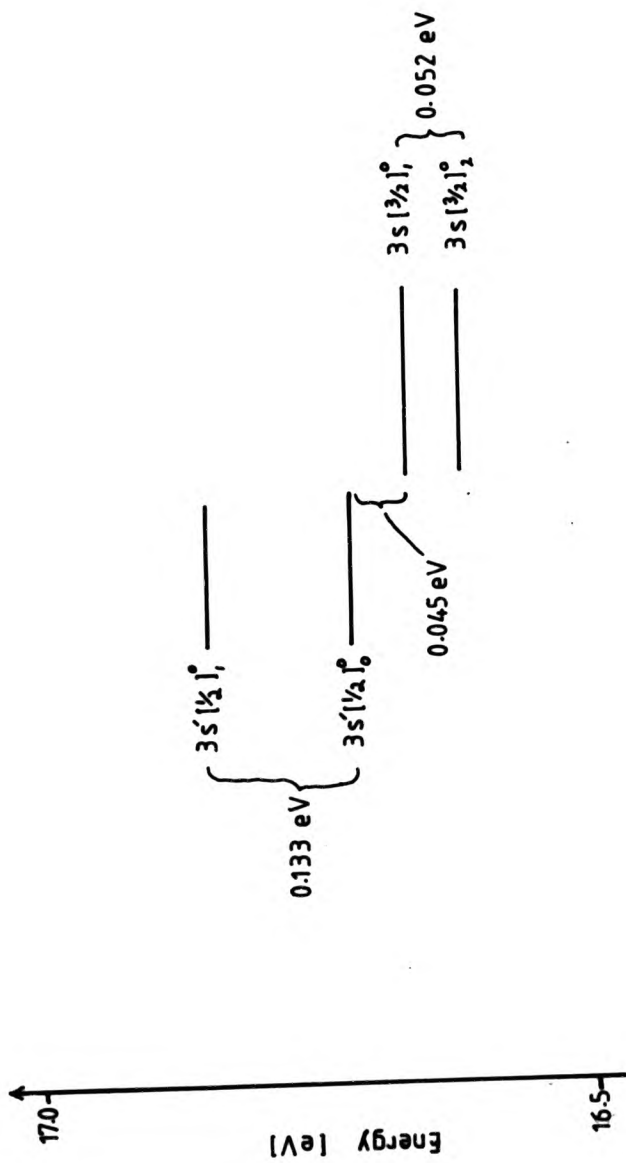


FIG. 68 ENLARGED Ne I ENERGY LEVEL DIAGRAM OF $3s, 3s'$ STATES

spectral line was mainly determined by Doppler broadening. State $3s [^3/2]_1^o$ is roughly halfway between the two metastable states in energy - see Fig. 68 -; $3s [^3/2]_2^o$ is 0.052 eV lower than it in energy and $3s' [^1/2]_0^o$ is 0.045 eV higher in energy. As these differences in energy are approximately equal to the average thermal kinetic energy, the rate of thermally excited transitions between these three states will be very high. State $3s' [^1/2]_1^o$ however, is higher in energy than the two metastable states and the other quasi - metastable states and the differences in energy are significantly greater; $3s' [^1/2]_2^o$ is 0.133 eV higher than $3s' [^1/2]_0^o$ and 0.229 eV higher than $3s [^3/2]_2^o$ in energy. As these differences in energy are several times (~ 2.6 - ~ 4.4) the average thermal kinetic energy, the rate of thermally excited transitions between $3s' [^1/2]_1^o$ and the other states of the 3s, 3s' group will be much lower than for $3s [^3/2]_1^o$ due to the rapid decline of the Boltzmann function with increasing energy difference.

The number density of atoms in the $3s [^3/2]_1^o$ state was found to be intermediate between those of two metastable states and exhibited saturation with increasing discharge current, as did the metastables - see Fig. 54 -. This suggests that populating rate of $3s [^3/2]_1^o$ is dominated by thermally excited transitions from the two metastable states and in particular $3s [^3/2]_2^o$ the most highly populated state. The rate of thermally excited transitions may be expected to change only slowly with increasing discharge current as the gas temperature is relatively insensitive to changes in current.

In contrast the number density of atoms in state $3s' [^1/2]_1^o$ was found to be roughly proportional to discharge current, with no saturation, and exceeded that of metastable state $3s' [^1/2]_0^o$ at currents greater than ~ 30 mA (~ 1.3 mA/cm²) - see Fig. 54 -. This suggests that thermally excited transitions from the other states in the 3s, 3s' group was not the dominant populating mechanism for $3s' [^1/2]_1^o$ but rather excitation from the ground state by electron collision and radiative cascade from higher energy levels. Although excitation by electron collision almost certainly dominates over radiative cascade, both rates may be expected to be approximately proportional to discharge current. As the maintenance voltage of a H.C.L. is essentially independent of discharge current and equal to ~ 200V in the case under discussion, the drift velocity of the electrons is also constant and the electron number density and hence the rate of excitation by electron collisions are proportional to current. The populating rate of a given atomic state by radiative cascade depends on the number densities of the higher energy states from which these transitions take place. In this instance by far the most

intense spectral lines and hence highest rates of transition correspond to transitions from the 3p, 3p' groups of energy levels. As the intensity of these spectral lines was found to be roughly proportional to current - see Figs. 18 to 21 and section 4/A.2 (b) - the rate of population by radiative cascade from them must also be roughly proportional to current.

7/C INTENSITY / CURRENT CURVES

7/C.1 Comparison with Howard's Results

The experimental I/i results obtained by Howard [37, 38] for a limited number of data points and range of currents are in general agreement with those obtained by the author. However the model equation (eq. 1.1) used for fitting Howard's results was based on an assumption of proportionality between the intermediate state number density and discharge current, an assumption shown by the author to be incorrect. A reasonable fit had been obtained for lines originating in high lying levels which correspond to relatively large values of C . The fit had been less satisfactory for I/i curves showing upward curvature. Detailed comparison between the two sets of fitted data will not be carried out.

7/C.2 Summary of I/i Fitting

- (i) 1 and 2 torr I/i curves well represented by equation of the form

$$I = \frac{A i (1 + B \sum N_j(i)) + D}{(1 + C i)} \quad (7.5)$$

where $N_j(i)$, $j = 1, 2, 3, 4$ are the number densities of the four excited states of the 3s, 3s' group of states. An equation of the form

$$I = \frac{A' i (1 + B' i)}{(1 + C i)} \quad (1.1)$$

also represented the I/i curves but fitted less well than 7.5.

- (ii) 5 torr I/i curves could not be fitted to an equation of this form or any other tried.
 (iii) For spectral lines corresponding to transitions between 3s, 3s' and 3p, 3p' groups of states $C = 0$.
 (iv) For spectral lines corresponding to transitions from high energy states $C > 0$.
 (v) B is greater at 2 torr than 1 torr.
 (vi) With the exception of 640.2 nm the I/i curves are not significantly affected by self - absorption.
 (vii) $D > 0$ for spectral lines the I/i curves of which are not asymptotic to the origin at the lowest sustainable discharge current.

Discussion of the above observations will be confined to those for 1 and 2 torr for which a fit could be obtained. The lack of success in fitting the 5 torr results to an

equation of the form of eq. 7.5 or one derived from it was almost certainly because the I/i measurements were made for the centre of the discharge but the measurements of metastable atom number density were average values for a large area of the discharge. At 1 and 2 torr neon pressure the H.C. glow was visibly quite uniform, however at 5 torr it assumed an annular distribution. The work of Kagan et al [19 - 23] Howorka and Pahl [12], and others has shown that the development of an annular glow structure at high pressure is accompanied by radial variations in electron number density and intensity of spectral emission. Van Veldhuizen and de Hoog [25] observed radial variations in metastable atom populations at high pressure. Clearly eq. 7.5 needs to be modified at high pressure to take into account these radial variations.

Equation 7.4 is a balanced rate equation for the variation of the number density of excited atoms in the upper state of the atomic transition corresponding to a spectral line, with the numerator being proportional to the excitation of the state and the denominator the depopulation rate. Equation 1.1 based on the incorrect assumption of proportionality of intermediate state density and discharge current can also be fitted to these results as the intermediate state density increases in an approximately linear manner from an initial high value, so that eq. 7.5 has a similar current dependence as eq. 1.1.

Consider first the excitation of the state in this model, in which single - step and two- step excitation via an intermediate state in the $3s, 3s'$ group, both make significant contribution to the overall excitation; a question that arises is, why they both make contributions of similar orders of magnitude when the number density of neon ground state atoms, from which single step excitation takes place, $\sim 10^{23} \text{ m}^{-3}$, while the number density of excited atoms in states of the $3s, 3s'$ group is only $\sim 10^{17} \text{ m}^{-3}$? Using an argument similar to Webb's [67, 68] explanation of the current saturation of metastable populations, it can be seen that two factors greatly increase the probability of excitation of a state from the metastable and quasi - metastable states of the $3s, 3s'$ group relative to direct excitation. Firstly, the electron collision cross - section for further excitation of atoms in the metastable and quasi - metastable states is much greater than for excitation of atoms in the neon ground state with its compact electronic structure typical of noble gases. Secondly, the proportion of discharge electrons with sufficient energy $\sim 19 \text{ eV}$ needed to directly excite the state from the ground state will be much smaller than proportion of electrons with sufficient energy $\sim 2 \text{ eV}$ to excite the state for a metastable or quasi - metastable state. The larger contribution made by two - step excitation at 2 torr than 1 torr neon pressure, indicated by the larger B at 2 torr, may be explained by changes in the energy distribution of electrons with neon pressure (observed in probe measurements by Borodin and Kagan [20]), so that the proportion of low energy compared to high energy electrons increases with gas pressure.

The need for an excitation contribution, D in equation 7.5, not depending on discharge current, in order to obtain a good fit in the low current region is consistent with the argument put forward to explain the metastable number densities - see 7/B.3 -, that the proportionality between electron number density and discharge current breaks down at low current, with electron density attaining a significant value at the lowest sustainable current, so that

$$N_0 = N_0(i \sim 0) + a_0 i \quad (7.3)$$

The fact that the value of D differs considerably between spectral lines, being negligible for some (eg. 640.2 nm) and of considerable value for others (eg. 585.2 nm), suggests that the energy distribution of electrons arising from the current dependent and current independent terms of eq. 7.3 are different from each other and have different excitation efficiencies for different states because of the variations of excitation cross-section with electron energy [71]. It is known from the measurement by Kagan's group [19 - 23] and others [24, 12] that the electron energy distribution in the H.C.D. is non-Maxwellian and has been described in terms of three groups of electrons of low, intermediate and high energy by Howorka and Pahl [12]. The relative proportions of electrons in three energy groups may be different for the contributions to total electron density made by the two terms in 7.3.

Consider now the depopulation rate term of model equation 7.5, it is apparent that the depopulation rates of states of higher energy are dominated by electron collision but not those of states belonging to the 3p, 3p' group, from which transitions corresponding to the prominent neon spectral lines take place. Clearly the very high probability of radiative transitions from the states of the 3p, 3p' group ensures that radiative de-excitation dominates over de-population by electron collision at the current densities used. In addition, less energy is required to ionize atoms in the higher excited states than in states of the 3p, 3p' group.

The fact that the I/i curve for 640.2 nm was the only one for which inclusion of a self-absorption term provided any improvement in fit, is consistent with the observation that the profile of this spectral line also showed evidence of significant self-absorption.

7/D V/i CHARACTERISTICS AND VISUAL OBSERVATIONS

The recorded V/i characteristics of the H.C.L. and results of visual observation provide additional evidence of changes in electron energy distribution and radial density distribution with increasing discharge current, in the low current regime. At neon pressures of 1 and 2 torr the maintenance voltage only changes significantly with discharge current, at currents below ~ 5 mA (~ 0.21 mA/cm²). Changes in maintenance voltage will cause changes in average electron energy. At these low currents the colour

of the discharge also varies with current, changing from a dull red to an orange colour with increasing current, as well as increasing in overall brightness. At such current densities sputtering of cathode material will be small and these colour changes cannot be explained by emission from sputtered cathode atoms. Rather, they indicate that the relative intensities of neon spectral lines have changed, reflecting changes in electron energy distribution.

The "bumps" in I/i curves and peaks in measured metastable atom density in the low current region, occurring at higher neon pressure, were accompanied by changes in the V/i characteristics and visual appearance of the H.C. discharge. At 5 torr neon pressure these changes extend up to currents of ~ 10 mA (~ 0.5 mA/cm²), above which the properties of the discharge become stable.

7/E EFFECTS OF FILL GAS IMPURITY

The properties of the H.C. discharge in the experimental lamp were found to be very sensitive to the presence of impurities in the neon fill gas, due to contamination. The problem of contamination was overcome and the bulk of the results referred to in the thesis are for conditions of maximum purity with no detectable impurity effects. However these impurity effects are interesting in their own right and warrant separate discussion.

The principal impurity in the carrier gas of the experimental lamp, when contaminated, after initial filling with high purity neon, was identified spectroscopically as CO and to a lesser extent H and OH, outgassing products of the inner surfaces of the UHV lamp system - see 2/B.6 and 4/C -.

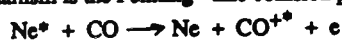
The major effects of the presence of impurities on the observed spectral properties of the H.C. discharge were :

- (i) General reduction of both Ne and Fe spectral intensities, and the almost complete absence of Fe spectral lines in the ultra - violet region of the spectrogram of the contaminated lamp.
- (ii) Reduction in the broadening and self - reversal of Ne I spectral lines corresponding to transitions terminating in metastable state $3s [^3/2]_2^o$. - Eg. see Fig. 17 showing profiles of Ne I 640.2 nm under clean and contaminated conditions - .
- (iii) Alteration of the form of the I/i curve of Ne I spectral lines, see Fig 30.

Changes in the non - spectral properties of the discharge, principally the V/i characteristic, due to the presence of impurities, were also noted but were less pronounced than the changes in spectral properties.

The reduction in broadening and self - reversal of Ne I spectral lines

corresponding to transitions to metastable state $3s [^3/2]_2^o$, indicates that the population of neon atoms in this excited state had been 'quenched' by the presence of the impurity molecules. The spectra of both CO and CO^+ were prominent in the spectrograms recorded of the contaminated lamp emission (see Fig. 31); and potential energy curves of these two molecular species and some excited states are provided in Fig. 69 [72]. The difference in energy between the ground state of CO and the ground state CO^+ is ~ 14 eV and the first excited electronic state ~ 16.5 eV. The difference in energy between the $3s [^3/2]_2^o$ metastable state and the neon ground state is ~ 16.7 eV. The likely quenching mechanism is the Penning - like collision process



where CO^{+*} denotes the first excited electronic state of CO^+ .

This process may be expected to have high relative probability as there is near energy resonance, giving a high matrix element for the reaction, and the three product particles allows a large volume of phase space to be available for the product states.

The reduction of Fe and Ne spectral intensities and the changes in Ne I I/I_0 curves, caused by the presence of impurities may be readily explained in terms of the quenching of the population of metastable excited neon atoms.

Quenching of the population of metastable excited neon atoms will reduce the probability of two - step excitation via the metastable state, so reducing the Ne I spectral intensity and by changing the relative contribution of one - step and two - step excitation, change the form of the I/I_0 curve.

The quenching of the neon metastable population can also be expected to reduce the intensity of Fe spectral lines by reducing the rate of excitation of sputtered cathode atoms in collisions with metastable excited atoms. The marked decrease in Fe spectral intensities when impurities were present, could also be related to a reduction in the population density of sputtered atoms. This could arise if a reduced rate of ionization of neon atoms lead to a reduced number density of neon ions, and hence a reduced rate of sputtering of cathode atoms.

7/F CORRECTION OF SPECTRAL PROFILES FOR INSTRUMENTAL BROADENING

The technique developed in the work for the correction of recorded spectral line profiles for the effect of instrumental broadening, using synthesis of a cubic spline representation of the profile, is applicable to any situation where an approximate solution of a convolution integral equation is required. The main disadvantage of the technique is the occurrence of unwanted oscillations of value. However such oscillations are to a greater or lesser degree unavoidable in approximate solution methods, particularly if a

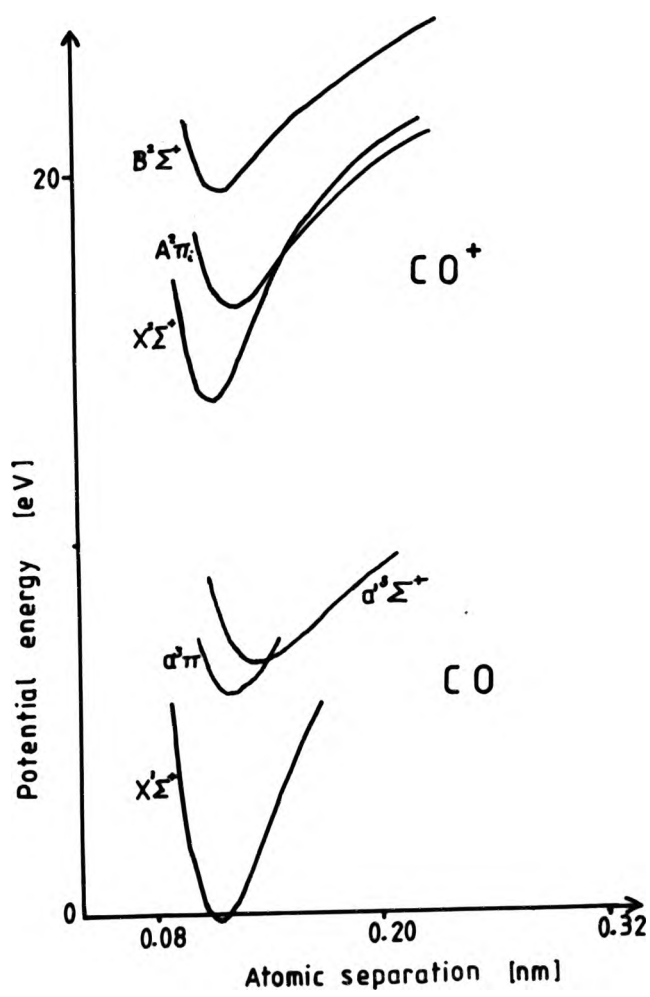


FIG. 69 POTENTIAL ENERGY CURVES
FOR CO & CO⁺

polynomial representation of the solution is used. If the analytic form of the solution is known, the synthesis of a solution of this form may be expected to give better results.

The cubic spline synthesis technique could be developed further, by allowing the spline knot positions to be variable and including them in the set of parameters varied by the minimization algorithm. This would entail use of a constrained least squares minimization algorithm which preserved the order of spline knots.

Another development of the technique could be the use of the set of residual values obtained with a good fit approximate solution, as an indication of the size of value oscillation and then the removal their effect from the approximate solution.

7/G SUMMARY OF CONCLUSIONS

- All states of the 3s, 3s' group of neon levels highly populated with number densities $\sim 0.3 - 2 \times 10^{17} \text{ m}^{-3}$
- Population of metastable state $3s [^3/2]_2^0$ is highest of group with mean density $\sim 1.5 \times 10^{17} \text{ m}^{-3}$
- Populations of the two metastable states $3s [^3/2]_2^0$ and $3s' [^1/2]_0^0$ exhibit strong saturation with the number density attaining significant values at the lowest obtainable current and changing only slowly with increasing current thereafter. Non - metastable state $3s [^3/2]_1^0$ exhibits a weaker saturation effect
- Number density of non - metastable $3s' [^1/2]_1^0$ is approximately proportional to current
- Self - absorption and reversal of most lines with transitions terminating in $3s [^3/2]_2^0$
- Neon pressure in the range 1 - 5 torr has little effect on the average number density of atoms in the 3s, 3s' group of states but does influence the shape of $N(i)/i$ curves.
- The results suggest that the proportionality between electron number density and current breaks down at low current density.
- Electron number density increases approximately linearly with increasing current thereafter
- The energy distribution of electrons changes with increasing discharge current at low current density $\sim 0.1 \text{ mA/cm}^2$
- The form of the I/i curves of Ne I spectral lines can (at least at lower pressure) be explained by a balanced rate model for the population of the upper state of the corresponding transition. There is a small effect by self - absorption for spectral lines such as Ne I 640.2 nm
- In addition to single - step excitation by electron collision of the upper state of the transition, two - step excitation by electron collision is significant.
- De - population of the upper state is both radiative and by electron collision. Radiative

de - population dominates for states of the 3p, 3p' group but de - population by electron collision is important for higher energy states.

- The I/i relationship of most Ne I spectral lines at lower pressure (1 and 2 torr for the size of cathode studied) may be described by an equation of the form

$$I = \frac{A i (1 + B \sum N_j(i)) + D}{(1 + C i)}$$

where A, B, C and D are independent of current and values depend on -

A - the rate of single - step excitation.

B - the relative importance of two- step excitation

C - the relative rates of depopulation by radiation and electron collision

D - the number density and energy distribution of electrons at low current and the energy dependence of the excitation cross - sections.

7/F SUGGESTIONS FOR FURTHER STUDY

The work could be developed further experimentally in two important ways -

- (a) Extension of the measurements to lower currents
- (b) Inclusion of the effect of radial variation within the discharge

The lowest current for which a discharge could be maintained was mainly limited by the stability of the current supply used at low values of current. Increasing the value of load resistance in series with the H.C.L. only slightly improved the low current stability.

Extension of the current range studied below ~ 0.5 mA would require a different electrical supply to be used, which has greater stability at low current. In order to take into account radial variations within the discharge, spatially resolved measurements of absorbance with fixed probe beam and movable cathode could be carried out. These measurements could be related to the I/i relationships of spectral line emission from different regions of the H.C.D.

The model for the population of the upper level of the transitions could be developed theoretically to take into account different cross - sections for excitation from different states of the 3s, 3s' group.

LIST OF REFERENCES

- [1] Paschen, F., 1916, *Ann. Phys.*, **50**, 901
- [2] Scheubel, W.K., 1970, *IEEE J. Quantum Electron.*, **QE - 6**, 654
- [3] Piper, J.A. and Webb, C.E., 1973, *J.Phys. D: App. Phys.*, **6**, 600 - 7
- [4] Csillag, L., Janossy, M., Rosza, K., and Salomom, T., 1974, *Phys. Lett.*, **50B**, 13
- [5] de Hoog, F.J., McNeil, J.R., Collins, G.J., and Persson, K.B., *J.Appl.Phys.*, 1977, **48**, No 9, 3701
- [6] Pillow, M.E., 1981, *Spectrochim. Acta.*, **36B**, No 8, 821
- [7] Caroli, S., 1983, *Prog. Anal. Atom. Spectrosc.*, **6**, 253
- [8] Guntherschulze, A., 1930, *Z. Tech. Phys.*, **11**, 49
- [9] Little, P.F. and Von Engel, A., 1954, *Proc. R. Soc. London*, **A224**, 209
- [10] Ciobotaru, D., 1964, *J. Electron. Control.*, **17**, 529
- [11] Lompe, A., Seeliger, R. and Wolter, E., 1939, *Ann. Phys. (Leipzig)*, **36**, 9
- [12] Howorka, F. and Pahl, M., 1972, *Z. Naturforsch. Teil A.*, **27**, 1425
- [13] Kirichenko, V.I., Tkachenko, V. M. and Tyutyunnik, V. B., 1976, *Sov. Phys. Tech. Phys. (Engl. Transl)*, **21**, 1080
- [14] Dopel, R., 1969, *Wiss. Z. Tech. Hochsch. Ilmenau*, **15**, 55
- [15] Musha, T., 1962, *J. Phys. Soc. Japan*, **17**, 1440
- [16] Musha, T., 1962, *J. Phys. Soc. Japan*, **17**, 1447
- [17] White, A. D., 1959, *J. Appl. Phys.*, **30**, 711
- [18] Warren, R., 1955, *Phys. Rev.*, **98**, 1658
- [19] Borodin, V. S. and Kagan, Yu. M., 1965, *Optics and Spectroscopy (U.S.S.R.) (Engl. Transl.)*, **18**, 546
- [20] Borodin, V. S. and Kagan, Yu. M., 1966, *Sov. Phys. Tech. Phys. (Engl. Transl.)*, **11**, 131
- [21] Borodin, V. S., Gerasimov, G. N. and Kagan, Yu. M., 1967, *Sov. Phys. Tech. Phys. (Engl. Transl.)*, **12**, 283
- [22] Gofmeister, V. P. and Kagan, Yu. M., 1968, *Optics and Spectroscopy (U.S.S.R.) (Engl. Transl.)*, **25**, 185
- [23] Desai, Sh. K. and Kagan, Yu. M., 1970, *Optics and Spectroscopy (U.S.S.R.) (Engl. Transl.)*, **28**, 352
- [24] Okhmatovski, G. V., 1978, *Sov. Phys. Tech. Phys. (Engl. Transl.)*, **23**, 552
- [25] van Veldhuizen, E.M. and de Hoog, F.G., 1984, *J. Phys. D: Appl. Phys.*, **17**, 953
- [26] Pringle, D. H. and Farvis, N. E., 1954, *Phys. Rev.*, **96**, 536

- [27] Chaudhri, R. M. and Oliphant, M. L., 1932, Proc. R. Soc. London., A137, 662
- [28] Bodarenko, A. V., 1975, Sov. Phys. Tech. Phys. (Engl. Transl.), 20, 195
- [29] Bodarenko, A. V., 1976, Sov. Phys. Tech. Phys. (Engl. Transl.), 21, 1497
- [30] Howorka, F., Lindinger, W. and Pahl, M., 1973, Int. J. Mass Spectrom. Ion Phys., 12, 67
- [31] Wehner, G. K., 1956, Phys. Rev., 102, 690
- [32] Langreid, N. and Wehner, G. K., 1961, J. Appl. Phys., 32, 365
- [33] Guntherschulze, A., 1953, Vacuum III, 360
- [34] Weston, G. F., Cold Cathode Discharge Tubes Ch 4, Iliffe (London), 1968
- [35] Stuart, R. V. and Wehner, G. K., 1962, J. Appl. Phys., 33, 2345
- [36] Gill, P. and Webb, C.E., 1978, J. Phys. D, 11, 245
- [37] Howard, C., MPhil Thesis, Council for National Academic Awards, 1983
- [38] Howard, C., Pillow, M. E., Steers, E. B. M. and Ward, D. W., 1983, Analysis, 108, 145
- [39] Pirani, M. and Yarwood, J., Principles of Vacuum Engineering, (Chapman and Hall), 1961
- [40] Edwards Manual 01 - C100 - 00 - 895
- [41] Pearce, R. W. B. and Gaydon, A.G., The Identification of Molecular Spectra, (Chapman and Hall), 1965
- [42] EMI Photomultipliers, 1975, P001/D75, 16
- [43] Reed, A. M., PhD Thesis, Council for National Academic Awards, 1980
- [44] Moore, C. E., 1949, N.B.S. Circular 467, 76
- [45] Amer. Inst. Phys. Handbook Ed 2, 1957, 7 - 47
- [46] Wagenaar, H. C., and De Galan, L., Spectrochim. Acta, Part B, 1975, 30, 361
- [47] Steel, W. H., Interferometry, (Cambridge University Press), 1967
- [48] Jacquinet, P., Rep. Progr. Phys., 1960, 23, 267
- [49] Strauss, J. A., et al, Spectrochim. Acta, 37B, 947 - 954
- [50] Mitchell, A. C. G. and Zemansky, M. W., Resonance Radiation and Excited Atoms, 1971, (Cambridge University Press), 92
- [51] Jarrett, S. M. and Franken, P. A., J. Opt. Soc. Amer., 1965, 35, 1603
- [52] Gibbs, H. M. and Hull, R. J., Phys. Rev., 1967, 153, 132
- [53] Wiese, W. L. et al. Nat. Std. Ref. Data, 1966, NBS4, 126 - 129
- [54] Rollett, J. S. and Higgs, L. A., Proc. Phys. Soc., 1962, 79, 87 - 93
- [55] Bracewell, R. N., The Fourier Transform and its Applications (McGraw Hill) 1965
- [56] Stacey, D. N., 1985, Private Communication

- [57] Cox, M. G. and Hayes, J. G., Report NAC26, Nat. Phys. Lab. Teddington, Middlesex, 1973
- [58] NAGFLIB : 1652/0: Mk 7: Jan 1981
- [59] NAGFLIB : 1354/0: Mk 5: Dec 1978
- [60] NAGFLIB : 1356/0: Mk 5: Dec 1978
- [61] NAGFLIB : 1691/1510: Mk 8: Aug 1980
- [62] Cox, M. G., J. Inst. Maths Applics., 1972, **10**, 134 - 149
- [63] De Boor, C., J. Approx. Theory, 1972, **6**, 50 - 62
- [64] Mitchell, A. C. G. and Zemansky, M. W., Resonance Radiation and Excited Atoms, 1971, (Cambridge University Press), 118
- [65] Djulgerova, R., Jechev, D., Pacheva, Y. and Rashev, S., 1975, Spectrosc. Lett., **8(12)**, 1001
- [66] White, A. D. and Gordon, E. L., 1963, Appl. Phys. Lett., **3**, 197
- [67] Webb, C. E., J. Appl. Phys., 1968, **39**, No 12, 5441
- [68] Webb, C. E., Lasers; Physics Systems and Techniques, Proc. 23rd Scottish Univs. Summer School Phys. Heriot - Watt, Ed. Firth, W. J. and Harrison, G. G., (S.U.S.S.P.), 1982, 175
- [69] Corney, A., Atomic and Laser Spectroscopy (Oxford University Press), 1977, 168
- [70] Mitchell, A. C. G. and Zemansky, M. W., Resonance Radiation and Excited Atoms, 1971, (Cambridge University Press), 240
- [71] Hasted, J. B., Physics of Atomic Collsions (Butterworth) 2nd Ed, 1972, 357
- [72] Pillow, M. E., 1982, Private Communication
- [73] Light, C. E. and Steers, E. B. M., 1985, Analyst, **110**, 439
- [74] Light, C. E. and Steers, E. B. M., Proc. Eight International Conference on Gas Discharges and their Applications (Leeds University Press), 1985, 559
- [75] NAGLIB:1499/1417:Mk6:May 77

APPENDIX A. ABSTRACTS & PAPER

ANALYST, MAY 1983, VOL. 110

439

Observations on Metastable Neon Atoms in Hollow-cathode Discharges

Charles E. Light and Edward B. M. Steers
School of Applied Physics, Polytechnic of North London, Holloway, London N7 8DB, UK

Previous work on the intensity versus current relationship for Ne I spectral lines emitted by iron hollow-cathode lamps with neon as the carrier gas has been extended. Spectral line profiles have been recorded using a pressure scanning Fabry-Pérot interferometer. Lines corresponding to transitions to the metastable state $3s[3/2]_2^o$ exhibit self-reversal and broadening due to self-absorption. This indicates the existence of a high density of neon atoms in this state, which is the likely intermediate level in two-step excitation processes.

Keywords: Hollow-cathode discharges; excitation processes; metastable states; neon; self-reversal

Howard¹ and Howard *et al.*² investigated the variation with lamp current, I , of the intensity, I , of spectral lines emitted by hollow-cathode lamps. For the initial experiments, lamps of standard construction (Cathodeon Ltd.) were used. Subsequently, a demountable lamp attached to a high-vacuum system was developed in which various sizes of cathode could be used and various pressures of filling gas. Howard recorded intensity distributions across the cathode diameter for selected Ne I, Ne II and Fe I lines using a limited number of currents in the range 3–20 mA. Further intensity versus current measurements have now been made, recording only axial intensities for one cathode size (15 mm bore, 30 mm depth) but extending the current range (1–30 mA) and introducing continuous recording of results using an $X-Y$ recorder.

The results for axial intensities of Ne I spectral lines obtained by Howard *et al.*² and in the current work are consistent with an equation of the form

$$I = \frac{A(1+C)}{(1+B)}$$

where A depends on the magnitude of single-step excitation, B on the relative importance of collisional and radiative de-excitation and C on the relative importance of two-step excitation via an intermediate state and single-step excitation. In this model (discussed more fully previously³), the population of the upper level of the transition is determined by the balance between the above excitation and de-excitation processes.

The probability of two step excitation depends on the number density of neon atoms in the intermediate level in the discharge. A high population density of atoms in an excited state is most likely if that state is metastable. Pressure scanning Fabry-Pérot interferometry was used to record the profile of Ne I spectral lines with the aim of observing self-absorption effects caused by a high population of neon atoms in an excited state. Appreciable self-reversal and broadening were observed for Ne I spectral lines originating in the $3s[3/2]_2^o$ metastable state. Results in the literature on self-reversal in hollow-cathode lamps⁴ have applied to the resonance radiation from the cathode material, in contrast to the present results on the carrier gas lines.

Experimental

The same basic optical arrangement (Fig. 1) was used for both intensity versus current (I/I) measurements and Fabry-Pérot interferometer scans, the interferometer and housing being removed for I/I measurements. The spectral lines studied were isolated by an Eagle mounting grating monochromator

(grating blazed for 500 nm, 1 m radius of curvature, 600 grooves mm^{-1} , ruled area 90×52 mm). The amplified photomultiplier output controlled the Y-deflection of an $X-Y$ recorder, the X-deflection being controlled by the lamp

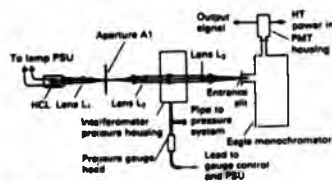


Fig. 1. Optical system layout for Fabry-Pérot scans

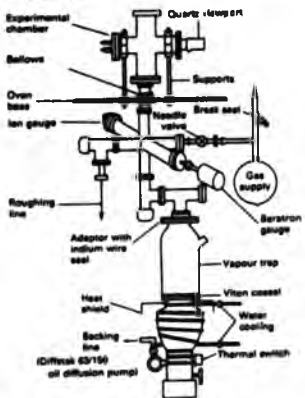


Fig. 2. High-vacuum system for demountable hollow-cathode lamp

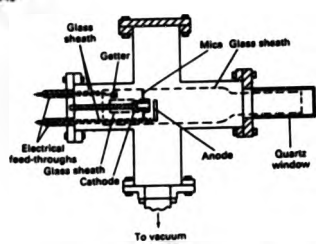


Fig. 3. Experimental chamber showing details of the demountable hollow-cathode lamp

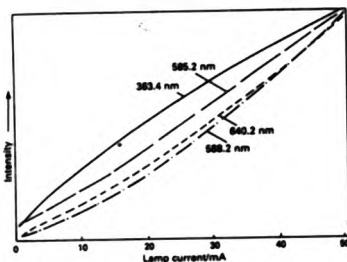


Fig. 4. Graphs of intensity versus current for Ne I spectral lines emitted by the demountable hollow-cathode lamp; neon pressure, 2 Torr. The arbitrary intensity units differ for each line, and are chosen to give approximately full-scale intensity at the maximum current

current when taking I, I measurements. For these, the current was increased smoothly from 1 to 30 mA in about 5 min, using a motor drive on the rheostat controlling the output of the current-stabilized power supply.

The etalon plates of the pressure-scanned interferometer had a reflectivity of 93% in the red spectral region and a 6 mm fused-silica spacer was used. For interferometric scans, the pressure housing was first filled with nitrogen at an excess pressure of about 1 bar, then the gas was allowed to leak to the atmosphere through a needle valve. The pressure within the housing was monitored with a Schaeffler pressure sensor (type P744-002), the output of which controlled the X -deflection of the X - Y recorder via an offset amplifier. The advantage of this method is that direct recording of the pressure removes the requirement for an accurately controlled constant rate of change of pressure.

A diagram of the vacuum system for the demountable lamp is shown in Fig. 2 and a more detailed diagram of the lamp and experimental chamber in Fig. 3. For this work, a mild-steel cathode, bore 15 mm and depth 30 mm, was used with neon as the carrier gas. The experimental chamber could be evacuated and baked, initially achieving a pressure of ca. 10^{-3} Torr, and then filled to the desired pressure of carrier gas. At this stage, progressive contamination of the gas was observed. The impurity was identified spectroscopically as CO, CO and CO $_2$ bands being observed in the photographically recorded

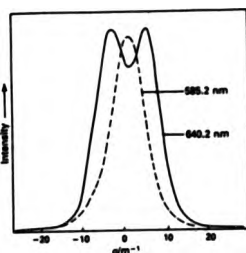


Fig. 5. Fabry-Pérot scans of intensity versus wavenumber (cm^{-1}) for Ne I spectral lines emitted by the demountable hollow-cathode lamp; neon pressure, 1 Torr

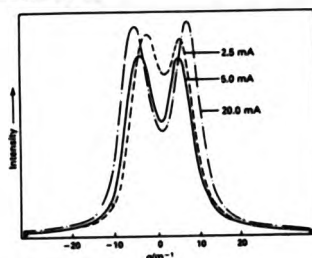


Fig. 6. Variation of line profile with current for Ne I 840.2 nm. emitted by the sealed hollow-cathode lamp

spectrum. Some results obtained while the gas became progressively contaminated are interesting and are discussed below. The replacement of the original needle valve for admitting neon to the experimental chamber by a Vacuum Generators UHV leak valve (Type MD6) and the use of an indium wire seal above the vapour trap allowed the achievement of pressures of ca. 5×10^{-6} Torr after extensive baking of the system, and routine achievement of ca. 10^{-4} Torr before each neon filling; no further problems with contamination were encountered.

Results and Discussion

Measurements of Intensity Versus Current

The I, I curves obtained for four typical Ne I spectral lines are shown in Fig. 4. These curves were consistently recorded for the demountable lamp at 2 Torr pressure. The results are consistent with those of Howard *et al.*¹ and with the predictions of the proposed model. The extended current range enabled the trends to be seen more clearly, and will permit more accurate evaluation of the constants A , B and C . Generally, spectral lines corresponding to transitions from high-lying energy levels (e.g. Ne I 363.4 nm) have I, I curves that turn downwards with increasing current, indicating that de-excitation by electron collision is dominant. Spectral lines corresponding to transitions from the $3p, 3p'$ to the $3s, 3s'$

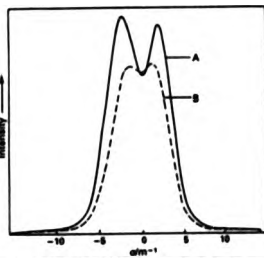


Fig. 7. Line profiles of Ne I 640.2 nm, emitted by the decontaminated hollow-cathode lamp, showing the effect of contamination of neon. A, 5 min after filling with fresh gas; B, 1 h later. Neon pressure, 1 Torr, current, 50 mA.

groups of levels (e.g., Ne I 588.2 nm and 640.2 nm) usually have I, I curves that curve smoothly upwards, indicating that two-step excitation is important. Exceptions are cases where both two-step excitation and de-excitation by electron collisions are important and the curve is displaced from the origin at low current values and exhibits a "knee" (e.g., Ne I 585.2 nm). Continuous recording from the lowest current at which a discharge could be maintained (ca. 1 mA) has permitted the clearer identification of this feature in the current work.

Fabry - Péroit Interferometry

Fig. 5 shows two examples of Fabry - Péroit scans of Ne I spectral lines emitted by the experimental lamp at a pressure of 1 Torr and 50 mA current. Ne I 585.2 nm has the non-metastable state $3d[1/2]$ as the lower level of the transition, and shows no self-reversal. Ne I 640.2 nm has the metastable state $3d[3/2]$ as the lower level of the transition, and is clearly self-reversed and broadened. Most of the spectral lines corresponding to transitions to this metastable state exhibit varying degrees of self-reversal. No spectral lines corresponding to transitions to other levels exhibit self-reversal.

Fig. 6 shows three Fabry - Péroit scans of Ne I 640.2 nm emitted by a sealed hollow-cathode lamp, illustrating the trend of increasing self-reversal and broadening, with increasing current (peak heights have been adjusted for ease of comparison). The degree of self-reversal is greater with this lamp as the current densities are significantly higher than those in the experimental lamp, which had a cathode approximately five

times larger. The self-reversal (as distinct from self-absorption) of spectral lines corresponding to transitions to the $3d[3/2]$ metastable states indicates not only a high population density of neon atoms in that state but also a temperature gradient within the region of high metastable population.

Fig. 7 shows two Fabry - Péroit scans of the spectral line Ne I 640.2 nm emitted by the experimental lamp under conditions of CO contamination (lamp current constant at 50 mA). The self-reversal and broadening were reduced as the neon became progressively contaminated after an initial fill with pure gas. Changes in the form of the I, I curves were also observed. This indicates that the neon metastable atoms had been quenched by the CO impurity. Both CO^+ and CO were noted in the contaminated lamp spectrum. The $3d[3/2]$ neon metastable state has an energy of about 16.7 eV; the difference in energy between the ground states of CO and CO^+ is about 14 eV. The likely quenching mechanism is the Penning-like reaction



Conclusions

The I, I curves of Ne I spectral lines emitted by hollow-cathode lamps under a variety of conditions are consistent with a model balancing single-step excitation, two-step excitation via an intermediate level and de-excitation by electron collision and radiation. The observed self-reversal and self-absorption broadening of Ne I spectral lines corresponding to transitions to the metastable state $3d[3/2]$ give independent evidence of the high population of this state, and confirm that it is the probable intermediate level for two-step excitation. Absorption measurements are currently being carried out in order to determine directly the number density and spatial distribution of neon metastable atoms.

We thank D. W. Ward of Cathodicon Ltd., Cambridge, for discussions and helpful advice, and Cathodicon Ltd. for supplying sealed hollow-cathode lamps.

References

1. Howard, C., *MPhil Thesis*, Council for National Academic Awards, 1963.
2. Howard, C., Piller, M. E., Steers, E. B. M., and Ward, D. W., *Analyst*, 1965, 100, 145.
3. Wiseman, M. C., and De Oelan, L., *Spectrochim. Acta*, Part B, 1973, 28, 361.
4. Reed, A. M., *PhD Thesis*, Council for National Academic Awards, 1963.

Paper A4311
Received September 5th, 1964
Accepted January 15th, 1965

POPULATION OF METASTABLE ATOMS IN A NEON HOLLOW CATHODE DISCHARGE

C E Light and B D N Steers
School of Applied Physics
The Polytechnic of North London
Holloway London N7 8DB
UK

1. INTRODUCTION

Investigation^{1,2} of the variation with lamp current (I) of the intensity (I) of carrier gas spectral lines emitted by neon/iron hollow cathode lamps has indicated that two-step excitation, via an intermediate state, of the upper levels of corresponding atomic transitions is appreciable for many He I spectral lines. Results were obtained for sealed lamps of standard construction (Cathodex Ltd.) and an experimental demountable lamp; in the latter, cathodes of different sizes could be fitted and, after evacuation and degassing, the lamp chamber could be filled with inert gas to the desired pressure.

The rate of two-step excitation will depend on the number density of neon atoms in the intermediate state, a high number density being most likely if the state is metastable. He I has two metastable states, $3s^2[1/2]_1$ and $3s^2[1/2]_2$ at energies of 16.6 and 16.7 eV respectively. Pressure scanning Fabry-Perot interferometry³ was employed in order to detect possible self-absorption effects in spectral lines terminating in these states. Self-reversal and broadening were observed in He I spectral lines with transitions terminating in the metastable state $3s^2[1/2]_1$. No He I spectral lines involving transitions to other levels were observed to exhibit this effect (see Fig. 1).

It was therefore decided that absorption measurements using an exterior primary source should be carried out so that the number density and distribution of metastable excited atoms could be determined directly.

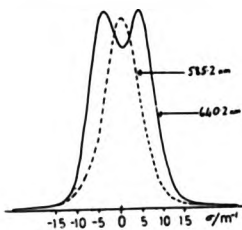


Fig. 1: Fabry-Perot profiles of 1640.2 nm (transition to metastable state) and 1585.2 nm (transition to non-metastable state).

2. EXPERIMENTAL

The demountable lamp was modified to allow a probe beam of light to pass axially through an open-ended, cylindrical, mild steel hollow cathode 50 mm long and of 15 mm bore. Fig. 2 shows a diagram of the UVV part of the lamp vacuum system and Fig. 3 a vertical section through the modified experimental chamber. The cathode was mounted horizontally on three steel rods supported by an annular flange designed also to admit the anneal electrical supply and to support the smaller of the two viewports. The cathode and chamber were earthed, glass and mica shielding

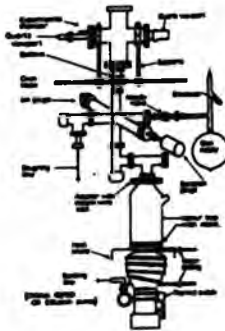


Fig. 2: Schematic diagram of UVV system

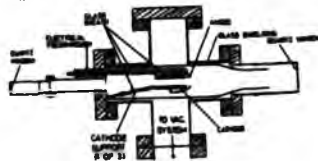


Fig. 3: Section through experimental chamber

were used to eliminate stray discharges. The chamber could be evacuated to $\sim 10^{-6}$ torr and filled with research grade pure neon to the desired pressure.

A neon, microwave excited, electrodeless discharge lamp (EDL) was used as the primary source for the absorption measurements. The probe beam was modulated at 55 Hz by a Chopper which also provided a reference signal for the phase sensitive amplifier used to amplify the photomultiplier tube output. This frequency was chosen to eliminate harmonic interference from the mains. Fig. 4 shows a diagram of the optical arrangement for absorption measurements with Fabry-Perot interferometer and simplified circuitry. No 1 spectral lines emitted by the EDL were isolated by the monochromator and profiles recorded by means of the pressure scanning Fabry-Perot interferometer with the hollow cathode discharge off ($I = 0$) and with it switched on, with the EDL power constant. This was carried out for spectral lines with transitions terminating in $3s^2\ ^3P_2$, e.g. He I 660.1 and 617.3 nm, and in the other three of the $3s^2\ ^3S_1$ group of levels. Measurements were made at three different pressures (1, 2 and 5 torr) and a number of values of discharge current in the range 1 to 50 mA. The instrument function of the interferometer was determined by recording the profile of the He I 633.8 nm line emitted by a mode-stabilized laser. Further details concerning the interferometer have already been given elsewhere.

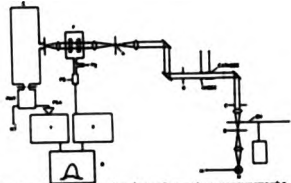


Fig. 4. Arrangement for interferometer measurements. A, B, C, D: Apertures; E: Eagle monochromator; F: Fabry Perot Interferometer and housing; H: Microwave power supply; R: Beam EDL primary source; X, Y: X & Y axis control circuits; R: X-Y recorder; Ch: Chopper; P₁: To gas pressure supply and needle valve; PS: Pressure sensor.

Measurements were also made of the total line absorption, with the interferometer removed. The intensity of the spectral line emitted by the EDL and transmitted by the discharge were continuously recorded with an X-Y recorder, as the discharge current was smoothly increased from 1 to 50 mA. Results were obtained at neon pressures of 1, 2 and 5 torr.

The optical system included four circular apertures labelled A, B, C and D on Fig. 4. Apertures A and D were small (~ 1 mm) and acted as near point sources at lens foci to produce parallel beams. Apertures B and C controlled the width of the beam passing through the hollow cathode which was varied

between the full cathode bore of 15 mm and 3 mm, and could be shifted laterally to isolate different radial positions in the discharge. The loss of intensity encountered when using the Fabry-Perot interferometer and a small beam width caused an unacceptable degrading of signal-to-noise ratio so that these measurements were made with the full beam width of 15 mm.

3. THEORY

Methods usually used^{1,2} to determine number densities of metastable excited atoms are based on one of those described by Mitchell and Zemansky³. All of these methods contain various assumptions as to the form and stability of spectral line profiles and are prone to systematic error. The method used in this work, developed from that employed by Jarrett and Franklin⁴, and Gibbs and Muir⁵ to measure atomic number densities in alkali metal vapours, avoids these uncertainties by determining number densities of absorption line profiles. Absorption line profiles are calculated from Fabry-Perot interferometric measurements of primary source and transmitted line profiles.

The observed primary source and transmitted line profiles ($I_0(\sigma)$ and $I_1(\sigma)$ respectively) are given by:

$$I_0(\sigma) = \int f(\sigma')g(\sigma - \sigma')d\sigma' \quad (1)$$

$$I_1(\sigma) = \int f(\sigma')\exp(-k(\sigma')l)g(\sigma - \sigma')d\sigma' \quad (2)$$

where $k_0(\sigma)$ is the apparent absorption coefficient ($k_0(\sigma)$) by

$$k_0(\sigma) = \sigma^{-1} \ln[I_0(\sigma)/I_1(\sigma)] \quad (3)$$

where $f(\sigma')$ is the primary source line profile
 $g(\sigma')$ the interferometer instrument function
 $k(\sigma')$ the true absorption coefficient
 $k_0(\sigma')$ the apparent absorption coefficient
 l the absorption path length
 and σ wavenumber

Then the number density (N) of absorbing atoms is given by:

$$N = \frac{8\pi g c}{\lambda^3 \sum_j A_{j1}} \int k(\sigma) d\sigma \quad (4)$$

where E_1 is the statistical weight of the upper level
 E_2 the statistical weight of the lower level
 λ the central wavelength of the spectral line
 A_{j1} the probability of the transition
 and c the speed of light

The observed line profiles can be corrected for the effects of the interferometer if the instrument function $g(\sigma)$ is known, and then the true absorption coefficient deduced and used in equation (4) to calculate the number density. Line profile correction must be carried out with care and requires considerable data processing. However, if the instrument function is considerably narrower than the line profiles in question (as is the case in this work) then the apparent absorption coefficient $k_0(\sigma)$ is approximately the same as the true coefficient

$h(\lambda)$ and, if used in equation (4), will give a good first approximation to the number density.

4. RESULTS

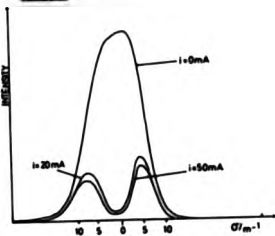


Fig. 5: Fabry Perot profiles of He I 640.2 nm, transmitted through the hollow cathode discharge (neon pressure 2 torr).

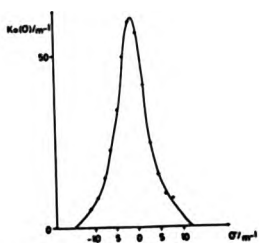


Fig. 6: Plot of apparent absorption coefficient $k(\lambda)$ against wavenumber, for He I 640.2 nm, discharge current 20 mA, pressure 2 torr.

Fig. 5 shows examples of Fabry Perot scans for He I 640.2 nm of the primary source profile, and of the transmitted line profiles for hollow cathode currents (1) of 20 and 50 mA, neon pressure 2 torr. Some preliminary analysis of the experimental data has been carried out neglecting the correction for instrument profile: a plot of apparent absorption coefficient against wavenumber is given in Fig. 6 for He I 640.2 nm, hollow cathode current 20 mA, pressure 2 torr. Number densities for the metastable state $3s[^3P_2]$ have been calculated by graphical integration of the apparent coefficient for He I 640.2 nm, and the use of National Bureau of Standards data on transition probabilities⁸. Fig. 7 shows a plot of number density against discharge current for a pressure of 1 torr, and Table I gives values of the number density for a fixed current of 20 mA at various pressures.

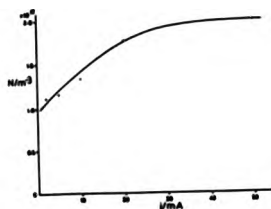


Fig. 7: Plot of number density of metastable state $3s[^3P_2]$, against current, I , for a neon pressure of 1 torr.

Table I: Number density of metastable state $3s[^3P_2]$, for discharge current 20 mA, and various pressures.

Pressure/torr	Number density N/m^3
1	1.7×10^{17}
2	1.6×10^{17}
5	1.65×10^{17}

As can be seen in Fig. 7, the metastable density rises very suddenly from zero with the discharge off to $N = 1 \times 10^{17} m^{-3}$ at a hollow cathode current of 1 mA, and then increases slowly as the current is increased, reaching $N = 2 \times 10^{17} m^{-3}$ at a current of 50 mA. Table I shows that the metastable density varies little with carrier gas pressure.

More detailed analysis of the experimental data is now being carried out, and will be presented at the conference. These direct measurements of metastable number density will be used in an improved model for the variation of intensity with current.

5. REFERENCES

1. Howard C. et al 1983, *Analyst*, **108**, 145-152.
2. Light C.E. and Steers S.S.M. 1983, *Analyst*, **110**, in press.
3. Strauss J.A. et al 1983, *Spectrochim. Acta*, **37B**, 947-954.
4. de Neeg F.J. et al 1977, *J. Appl. Phys.*, **48**, 3701-3704.
5. Mitchell A.C.G. and Zemansky M.M. 1961, *Resonance Radiation and Excited Atoms* (Cambridge University Press).
6. Weiss V.L. et al 1966, *Met. Std. Ref. Data*, **HSB1**, 176-179.
7. Javrett E.W. and Franzen P.A. 1965, *J. Opt. Soc. Amer.*, **55**, 1603-1606.
8. Gibbs H.H. and Hall R.J. 1967, *Phys. Rev.*, **155**, 132-151.

POPULATION OF METASTABLE NEON ATOMS IN HOLLOW CATHODE
AND OTHER LOW PRESSURE DISCHARGES

C.E. Light, H.B.M. Steers and A. Zendejman.

School of Applied Physics, The Polytechnic of North London,
Holloway, London, N7 8DB, U.K.

1. INTRODUCTION

The variation with current, i , of the intensity, I , of neon spectral lines emitted by a demountable neon/iron hollow cathode lamp has been studied as part of an investigation of the excitation processes in hollow cathode discharges. The results indicate that two-step excitation is important for many neon lines, [1], with the metastable state $3s[3/2]_2^o$ as the probable intermediate level [2]. I-I relationships from the positive column of a discharge in low pressure neon have also been investigated for comparison. To assist in interpreting the I-I results, data on the metastable populations in both types of source are required, and high resolution absorption measurements have been made on selected Ne I lines.

Methods usually used to determine number densities of metastable atoms are based on those described by Mitchell and Zemansky [3]; all contain assumptions on the form and constancy of the line profiles. These uncertainties can be avoided by deriving the absorption line profile, $k(\lambda)$, from Fabry-Perot measurements of the primary source and transmitted line profiles [4]. The number density, N , of absorbing atoms is given by

$$N = \frac{S_1 S_2 c}{\lambda_0^2 S_1 A_{12}} \int k(\lambda) d\lambda$$

where S_1 and S_2 are the statistical weights of the upper and lower levels, respectively, A_{12} the Einstein transition probability and λ_0 the central wavelength.

2. EXPERIMENTAL DETAILS

Demountable discharge tubes were used on u.v.v. systems to give high purity conditions; the vacuum system for the positive column tubes was similar to that for the hollow cathode [2]. In both cases, the discharge tubes were filled with research grade

neon to the required pressure, and a getter used to maintain purity.

The hollow cathode assembly was mounted in a 64 mm I.D. 4-way cross (Fig.1); the open-ended cylindrical, mild steel cathode, 50 mm long and 15 mm bore, was held horizontally by three support rods. The cathode and chamber were earthed and glass and mica sheaths used to prevent stray discharges. Pressures to 1 to 5 torr were used, and currents in the range 1-50 mA.

A glass or fused silica discharge tube was used for measurements on the positive column; after preliminary experiments with cold cathodes, hollow cathodes and a heated coated cathode, the last was chosen for most of the measurements. The form of the tube (Fig.2), with alternative anodes (1 and 2) giving different length positive columns, allowed an estimate to be made of the field strength. Neon pressures between 0.1 and 15 torr were used, with currents up to 50 mA.

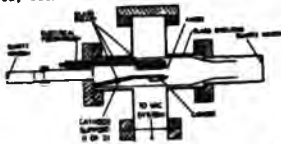


Fig. 1: Section through the hollow cathode chamber

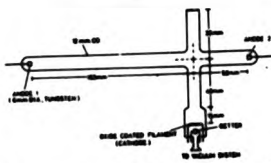


Fig. 2: Positive column discharge tube (mounted with long arm vertical)

A neon, microwave excited, electrodeless discharge lamp (EDL) was used as the primary source for the absorption measurements. No I spectral lines emitted by the EDL were isolated by the monochromator and profiles recorded by means of the pressure scanning Fabry-Perot interferometer [2] with the discharge off ($i = 0$) and with it switched on (Fig. 3). This was carried out for spectral lines with transitions terminating on $3s[3/2]_2^o$ (e.g. Ne I 640.2 and 614.3 nm) and on the other three levels of the $3s, 3s'$ group. Measurements were made at various pressures and discharge currents. The instrument function of the interferometer was determined by recording the profile of the Ne I 632.8 nm line emitted by a mode-stabilized laser.

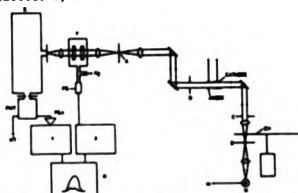


Fig. 3: Arrangement for interferometer measurements for hollow cathode discharge. A, B, C, D: Apertures; E: Eagle monochromator; F: Fabry-Perot Interferometer and housing; G: Microwave power supply; H: Neon EDL primary source; X, Y: X & Y axis control circuits; R: X-Y recorder; CH: Chopper; S: To gas pressure supply and needle valve; PS: Pressure sensor.

For positive column the probe beam was focussed at the centre of the tube.

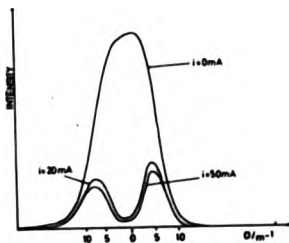


Fig. 4: Fabry-Perot profiles of Ne I 640.2 nm transmitted through the hollow cathode discharge (neon pressure 2 torr).

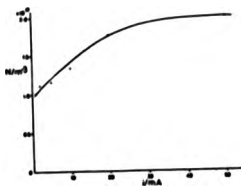


Fig. 5: Plot of number density of metastable state $3s[3/2]_2^o$ against current, I, for a hollow cathode discharge in neon, pressure 1 torr.

3. RESULTS

Fig. 4 shows an example of the Fabry-Perot scans for Ne I 640.2 nm. From such data, the variation of $h(\sigma)$ with wavenumber σ can be derived; a correction for instrument profile must be made, but this is small and has been neglected for preliminary calculation of results. Fig. 5 is a plot of number density of the $3s[3/2]_2^o$ state against current for a hollow cathode discharge at 1 torr. Both sources show the same type of dependence of metastable population on current, with a tendency to saturate with increasing current, in agreement with the results of van Veldhuizen and de Hoog [5]; number densities from both sources are of the same order of magnitude, but those for the hollow cathode discharge showed very little variation with pressure, whilst the positive column results have a marked dependence on pressure. Further experimental work is in progress and more detailed analysis of the results is being carried out, and will be presented.

We wish to thank Coshoden, Ltd., Cambridge for the provision of a range of specially designed discharge tubes for the positive column experiments.

REFERENCES

1. Hayward, C., Pillow, P.E., Steers, E.B.M. and Ward, D.W., *Analyst*, **108**, 145-152 (1983).
2. Light, C.B. and Steers, E.B.M., *Analyst*, **110**, 439-441 (1985).
3. Mitchell, A.C.G. and Zemansky, M.V., *Resonance Radiation and Excited Atoms*, C.U.P. (1981).
4. Light, C.B. and Steers, E.B.M., *Proc. of 8th Int. Conf. on gas Discharges and their Applications*, Oxford (1985), in press.
5. van Veldhuizen, E.M. and de Hoog, F.J., *J. Phys. D.*, **17**, 953-968 (1984).

APPENDIX B. COMPUTER CODE

```

C      PROGRAM CORR1.FOR
REAL A,TYPE,N,XX(500),YY(500),XI(500),YI(500),ANGDEG
REAL XOUT(500),YOUT(500),YSC(500)
CHARACTER*1 DUMP
CHARACTER*10 FILEI,DATEI,CONDS,FILLO,FILES
CHARACTER*10 MAP(30,10)
CHARACTER*80 U
INTEGER I, NPISI, NOUT
NROWS = 20
NCOLS = 5
NR = 30
NC = 10
FILEI='TESTA.D01'
WRITE(5,99999)
READ(5,99990)A
IF (A.EQ.'Y') GOTO 10
WRITE(5,99997)
READ(5,99996) FILLO
IF (FILLO.EQ.'END') GOTO 555
10    CONTINUE
OPEN(UNIT=20,DEVICE='DSK',ACCESS='SEQUIN',FILE=FILEI)
HEAD(20,221) DUMP
FORMAT(A1)
READ(20,99994)A,TYPE,WAVELI,DATEI,NMEASI,CONDS
IF (TYPE.EQ.'1' .AND. WAVELI.NE.632.8) WRITE(5,91)
I=0
30    READ(20,99991,END=40)A,L,XX(I+1),YY(I+1)
IF (A.NE.'*' .AND. A.NE.'M') GOTO 15
I=I+1
15    CONTINUE
GOTO 30
40    CONTINUE
CLOSE(UNIT=20)
CALL POINTC(XX,YY,XI,YI,I,NPISI,ANGDEG)
WRITE(5,99998)ANGDEG
WRITE(5,99989)NPISI
CALL XNOM( XI,YI,NPISI,XOUT,YOUT,IOUT,NDEL )
WRITE(5, 771 ) NDEL, IOUT
FORMAT( ' NUMBER OF NON-DECREASING X POINTS DELETED =',I4,
/, ' NEW NUMBER OF POINTS =',I4)
WRITE(5,991)
READ(5,99990)FILEU
OPEN(UNIT=20, DEVICE='DSK', FILE=FILEU, ACCESS='SEQUIN')
CALL CLEAR2(MAP,NROWS,NCOLS,NR,NC)
MAP(1,1) = FILEU
MAP(2,1) = FILEI
CALL MAPWRT(MAP,NROWS,NCOLS,NR,NC)
WRITE(20,992)TYPE,WAVELI,DATEI,NMEASI,CONDS
WRITE(20, 994)NOUT
DO 100 J = 1, NOUT
WRITE(20,993) XOUT(J), YOUT(J)
100   CONTINUE
CLOSE(UNIT=20)
O = ' DO YOU WANT A SCALED VERSION ?'
CALL DECIDF( O, I, O, IOUT )
IF ( IOUT .EQ. 1 ) THEN
WRITE( 5, 331 )
FORMAT( ' INPUT NAME FILE TO HOLD SCALED VERSION' )
READ( 5, 99990 ) FILEU
CALL SCALE1( YOUT, IOUT, YSC )

CONDS = 'SCALD'
MAP(1,1) = FILEU
MAP(2,1) = FILEU
MAP(3,1) = FILEI
OPEN( UNIT=20, DEVICE='DSK', ACCESS='SEQUIN',FILE=FILEU )
CALL MAPWRT( MAP, NROWS, NCOLS, NR, NC )
WRITE( 20, 992 ) TYPE, WAVELI, DATEI, NMEASI, CONDS
WRITE( 20, 994 ) NOUT
DO 20 J = 1, NOUT
WRITE( 20, 332 ) XOUT(J), YSC(J)
332   FORMAT( F7.3, F6.5 )
20    CONTINUE
CLOSE(UNIT = 20 )
END IF
WRITE(5,99964)
READ(5,99990)A
IF (A.EQ.'Y') GOTO 5

```

```

99999  FORMAT( ' ', 'DO YOU WANT TO USE DEFAULT FILE Y OR N?')
99998  FORMAT(A1)
99997  FORMAT( ' ', 'INPUT NAME FILE CONTAIN PROFILE OR END?')
99996  FORMAT(A10)
99994  FORMAT(A1,1X,A1,F5.1,1X,A10,12,1X,A10)
99991  FORMAT(A1,1X,12,2F6.2)
99990  FORMAT( ' ', 'DIG ANGLE ERROR OF IF FILE="F10.4,"DEGS')
99989  FORMAT( ' ', 'NUM=NUM OF IF DIGITIZATION POINTS=",I7)
99984  FORMAT( ' ', 'DO YOU WANT TO RE-RUN PROG., Y OR N?')
999  FORMAT( ' ', 'INPUT FILENAME TO HOLD CORRECTED POINTS?')
992  FORMAT(A1,F5.1,1X,A10,12,1X,A10)
993  FORMAT(2F7.3)
994  FORMAT( I4 )
91  FORMAT( ' ', 'PROFILE TYPE IF NOT WAVEL. NOT 032.0NM ')
555  STOP
END

SUBROUTINE POINTC(XX,YY,X,Y,LPTS,ANGDEG)
REAL XX(1),YY(1),X(1),Y(1),X1(500),Y1(500)
INTEGER I,NPTS,J,NST
NST = 2
NPTS = 1-NST
ANGLE = ATAN2(YY(2)-YY(1),XX(2)-XX(1))
ANGDEG = 57.3*ANGLE
COSANG = COS(ANGLE)
SINANG = SIN(ANGLE)
DO 10 J = NST+1,I
JNST = J - NST
X1(JNST)=XX(J)-XX(1)
Y1(JNST)=YY(J)-YY(1)
X(JNST)=COSANG*X1(JNST)+SINANG*Y1(JNST)
Y(JNST)=-SINANG*X1(JNST)+COSANG*Y1(JNST)
CONTINUE
RETURN
END

SUBROUTINE AMON( XIN, YIN, NIN, XOUT, YOUT, NOUT, NDEL )
REAL XIN(NIN),YIN(NIN),XOUT(NOUT),YOUT(NOUT)
INTEGER NIN, NOUT, NDEL, J, I
NDEL = 0
I = 1
XOUT(1) = XIN(1)
YOUT(1) = YIN(1)
DO 5 J = 2, NIN
XOUT(J) = 0.0
YOUT(J) = 0.0
CONTINUE
DO 10 J = 2, NIN
IF ( XIN(J).GE.XOUT(I) ) THEN
I = I + 1
XOUT(I) = XIN(J)
YOUT(I) = YIN(J)
ELSE
NDEL = NDEL + 1
WRITE( 5,991) J
FORMAT( ' NUM=DECREASING X, POINT DELETED AT J = ',I4)
END IF
CONTINUE
NOUT = I
IF ( NOUT+NDEL .NE. NIN ) WRITE( 5, 992 )
FORMAT( ' NUMBER OF POINTS AND DELETES DO NOT ADD UP ???' )
RETURN
END

SUBROUTINE SCALC( Y, N, YSC)
REAL Y(N), YSC(N)
INTEGER N, J
C = 1.0
DO 10 J = 1, N
YSC(J) = ALG( C + Y(J) )
CONTINUE
RETURN
END

```

```

C      PROG: FITCS.FOR
CHARACTER*1 L
REAL X(500),Y(500),U(500),V(500),W(500),XS(500),
*Y(500),Z(4,50),C(50),K(50),XCALC(200),YCALC(200),KINT(50),YKNOTS(50)
INTEGER ISCALC(2), IFLAG
CHARACTER*10 FILEC, FILED, CONDS, DATE
CHARACTER*10 U
CHARACTER*10 NAME(J,10),MAPUT(J,10),NROW(10)
NROWS = 20
NCOLS = 5
NK = 30
NC = 10
1      CONTINUE
IFLAG = 0
ISCALE(1) = 0
ISCALE(2) = 0
CALL CLEAR(NROW,NCOLS)
FILEC='XSTB.CM1'
XCALC = 100
WRITE(5,771)
771  FORMAT(' ',*DO YOU WANT TO USE DEFAULT? Y OR N*)
READ(5,995)U
IF (R.EQ.'Y') GOTO 100
WRITE (5, 772)
772  FORMAT(' ',*INPUT FILEC NAME CHOSEN, OR END*)
READ (5,861)FILEC
IF (FILEC.EQ.'END') GOTO 10000
100  CONTINUE
NROWS=50
OPEN(UNIT=20,DEVICE='DISK', FILE=FILEC, ACCESS='SEQIN')
CALL MAPUT(MAPUT,NROWS,NCOLS,NK,NC)
READ(20,9991) TYPE, LABEL, DATE,NFLAG,CONDS
READ(20,9991) NPTS
IF (CONDS.EQ.'SCALED') GOTO 15
DO 2000 J = 1, NPTS
READ(20,333) X(J), YS(J)
333  FORMAT(F7.3,FU.5)
2000 CONTINUE
GOTO 1000
15  DO 1000 J = 1, NPTS
READ(20,9992) X(J), YS(J)
1000 CONTINUE
9991  FORMAT(14)
9992  FORMAT (2F7.3)
9993  FORMAT (A1,F5.1,1X,A10,I2,1X,A10)
CLOSE(UNIT=20)
IF (CONDS.EQ.'SCALED') ISCALF(1)=1
IF (CONDS.EQ.'SCALED') ISCALF(2)=1
IF(NPTS.GT.2) GOTO 600
WRITE(5,999)
GOTO 1
600  CONTINUE
O = 'DO YOU WANT KNOTS FROM FILE?'
CALL DECIDE(O,1,0,IOUT)
IF (IOUT.EQ.1) GOTO 13
WRITE(5,441) X(1), X(NPTS)
441  FORMAT(' ',*KNOTS=(F8.3,4X,'XMAX'=(F8.3)
WRITE(5,998)
READ(5,997)ICAP
NCAP3=NCAP + 3
NCAP7=NCAP + 7
IF(NCAP.LT.1.OR.NCAP.GT.NROWS)WRITE(5,991)
IF(NCAP.LT.1.OR.NCAP.GT.NROWS) GOTO 800
IFAIL=1
IF (NCAP.EQ.1)GOTO 13
DO 13 J = 5, NCAP3
WRITE(5,661)
661  FORMAT(' ',*INPUT POSITION OF KNOT*)
READ(5,662) A(J)
662  FORMAT(F)
13  CONTINUE
IF (IOUT.EQ.1) CALL KNOTS(NCAP,ICAP3,NCAP7,K)
IF (CONDS.EQ.'SCALED') GOTO 11
DO 200 J=1,NPTS
W(J)=1.0
200  CONTINUE
GOTO 12
11  CONTINUE

```

```

DO 12 J = 1, NPTS
*(J) = EXP(YS(J))
CONTINUE
12 CALL LM2BAF(NPTS,NCAP7,X,YS,W,F,WORK1,WORK2,C,SS,IFAIL)
IF(IFAIL,EO,0) GOTO 300
GOTO(10,20,30,40,50),IFAIL
10 WRITE(5,990)
GOTO 2
20 WRITE(5,996)
GOTO 1
30 WRITE(5,995)
GOTO 1
40 WRITE(5,994)
GOTO 1
50 WRITE(5,993)
GOTO 1
300 WRITE(5,989)
WRITE(5,984)
READ(5,985)B
IF (B.EQ.'N') GOTO 500
CALL EVAL1(YS,Y,NPTS,NCAP7,C,I,XCALC,YCALC,NCALC,KINT,YKNOTS,
* ISTOP,TSCALE)
IF (ISTOP,EO,0) GOTO 27
WRITE(5,111)ISTOP
111 F0RMA7(' ',*RETUR: EVAL WITH ISTOP='12,/,*RESTART PROG')
GOTO 1
22 WRITE(5,33331)
33331 F0RMA7(' DO YOU WANT VDU PLOT ? Y OR N' )
READ(5,985)B
IF (B.EQ.'Y') THEN
IPL0T = 1
CALL PLOT3(IPL0T,X,Y,NPTS,XCALC,YCALC,NCALC,KINT,YKNOTS,NCAP,
* FILEC)
FILEC
ENDIF
IF ( IFLAG,EO,0 ) GOTO 515
IPL0T = 2
131 F0RMA7(' ',*DO YOU WANT HP PLOT ? Y OR N' )
READ(5,985)B
IF (B.EQ.'N') GOTO 515
CALL PLOT3(IPL0T,X,Y,NPTS,XCALC,YCALC,NCALC,KINT,YKNOTS,NCAP,
* FILEC)
FILEC

515 CONTINUE
WRITE(5,3031)
3031 F0RMA7(' DO YOU WANT DERSON PLOT ? Y OR N' )
READ(5,985) B
IF (B.EQ.'Y') THEN
IPL0T = 3
CALL PLOT3(IPL0T,X,Y,NPTS,XCALC,YCALC,NCALC,KINT,YKNOTS,NCAP,
* FILEC)
FILEC
ENDIF
WRITE(5,986)
READ(5,985)B
IF(B,EO.'Y') GOTO 800
CONTINUE
WRITE(5,882)
802 F0RMA7(' ',*INPUT NAME FILE TO HOLD SPLINE FIT')
READ(5,881) FILE5
881 F0RMA7(A16)
OPEN (UNIT=20, DEVICE='DSK', FILE=FILE5, ACCFSS='SEQU07')
NEW(1) = FILE5
CALL LOG1(NNR0WS,NC0LS,GR,NC,NAPTR,2,NAP0UT,NEW)
CALL NADWRT(NAP0UT,NNR0WS,NC0LS,NH,L,C)
WRITE(20,9993) TYPE, WAVEI, DATE, NREAS, CONDS
WRITE(20,7772) LCAP7
DO 700 J=1,NCAP7
WRITE(20,7771) F(J)
700 CONTINUE
DO 17 J = 1, LCAP3
WRITE(20,7771)C(J)
17 CONTINUE
CLOSE (UNIT=20)
WRITE(5,33332)
33332 F0RMA7(' DO YOU WANT TO STORE THESE KNOTS ? Y OR N' )
READ(5,985) B
IF (B.EQ.'Y') CALL LOC FILES,K,NCAP7,NCAP3 )
WRITE(5,221)
221 F0RMA7(' ',*DO YOU WANT TO REKUL PROG? Y OR N ' )
READ(5,985)B
IF (B.EQ.'Y') GOTO 1

```

```

7771  FORMAT (E20.7)
7772  FORMAT (I2)
999  FORMAT(' ', 'ERROR IN NUMBER OF POINTS (RESTART)')
998  FORMAT(' ', 'INPUT NCAP IS OF INTERVALS')
997  FORMAT(I2)
996  FORMAT(' ', 'IFAIL=2 NOT ALL POS (RESTART)')
995  FORMAT(' ', 'IFAIL=3 VALUES OF X NOT NON-DECR. (RESTART)')
994  FORMAT(' ', 'IFAIL=4 I RESTART')
993  FORMAT(' ', 'IFAIL=5 TOO MANY KNOTS: RESTART')
991  FORMAT(' ', 'NCAP DEC. OR GY GROWS. //, "TRY AGAIN")
989  FORMAT(' ', 'RETURN FROM E02RDF WITH IFAIL N', //)
986  FORMAT(' ', 'DO YOU WANT TO RE-INPUT NUMBER OF KNOTS? Y OR N')
985  FORMAT(A1)
984  FORMAT(' ', 'DO YOU WANT PLOT OF SPLINE FIT? Y OR N')
980  FORMAT(' ', 'IFAIL=1 KNOT OUTSIDE RANGE OR DECR. REINPUT N')
16000  STOP
      END

```

```

SUBROUTINE EVAL(YB,Y,NPTS,NCAP7,C,K,XCALC,YCALC,NCALC,
* KINT,YKNOTS,ISTOP,ISCALE)
  REAL C(NCAP7),XCALC(NCALC),YCALC(NCALC),
* K(NCAP7),KINT(50),YCALCT(200),Y(NPTS),YB(NPTS),YKNOTS(50),
* YKNOT(50)
  INTEGER ISCALE(2)
  NCAP = NCAP7 - 7
  A = 1.0
  ISTOP = 0
  DO 10 J=1, NPTS
    IF (ISCALE(1),F0.0) Y(J) = YB(J)
    IF (ISCALE(1),N0.0) Y(J) = EXP(YB(J)) * A
10  CONTINUE
  STEP = (K(NCAP7) - 1.0)/FLOAT(NCALC - 1)
  IFAIL = 1
  DO 30 J = 1, NCALC-1
    XCALC(J) = K(1) + STEP*FLOAT(J-1)
    CALL E02RDF (NCAP7, K, C, XCALC(J), YCALCT(J), IFAIL)
    IF (IFAIL.NE.0) GOTO 200
    IF (ISCALE(2),F0.0) YCALC(J) = YCALCT(J)
    IF (ISCALE(2),N0.0) YCALC(J) = LXI(YCALCT(J)) * A
30  CONTINUE
  XCALC(NCALC)=K(NCAP7)
  CALL E02RDF(NCAP7,K,C,XCALC(NCALC),YCALCT(NCALC),IFAIL)
  IF (IFAIL.NE.0) GOTO 200
  IF (ISCALE(2),F0.0)YCALC(NCALC)=YCALCT(NCALC)
  IF (ISCALE(2),N0.0)YCALC(NCALC)=LXI(YCALCT(NCALC))*A
  GOTO 40
200  WRITE (5, 992) IFAIL
992  FORMAT(' ', 'HAG ERROR IN EVAL OF XCALC, IFAIL',I2,/, 'RETURN IST
  OP= 2')
  ISTOP = 2
  GOTO 16000
40  CONTINUE
  IF (NCAP.EQ.1) GOTO 60
  DO 60 J = 1, NCAP - 1
    KINT(J) = K(J+1)
    CALL E02RDF(NCAP7,K,C,KINT(J),YKNOT(J),IFAIL)
    IF (IFAIL.NE.0) THEN
      WRITE (5, 991) IFAIL
991  FORMAT(' RETURN FROM E02RDF WITH IFAIL=',I2, 'RETURN')
      GOTO 16000
    ELSE
      IF (ISCALE(2),F0.0)YKNOTS(J)=YKNOT(J)
      IF (ISCALE(2),N0.0)YKNOTS(J)=EXI(YKNOT(J))*A
60  CONTINUE
  RETURN
16000  END

```

```

SUBROUTINE KNOTS(NCAP,NCAP3,NCAP7,K)
CHARACTER*10 FILEK, NAME
CHARACTER*80 U
REAL K(50)
FILEK = 'KNOTS.DAT'
Q = ' DO YOU WANT KNOTS STORED IN KNOTS.DAT ?'
CALL DECIDE(Q,1,0,IOUT)
IF (IOUT .EQ. 0) THEN
WRITE(5, 881)
801 FORMAT(' INPUT NAME FILE STORING KNOTS TO USE')
802 READ( 5,882 ) FILEK
      FORMAT( A10 )
      ENDDIF
      OPEN(UNIT=20,DEVICE='DISK',ACCESS='SLOIN',FILE=FILEK)
      READ( 20, 771 ) NAME
      771 FORMAT( A14 )
      READ(20,991,ERR=91) NCAP
      991 FORMAT(I2)
      NCAP3 = NCAP+3
      NCAP7 = NCAP+7
      IF (NCAP.LT.2) GOTO 1000
      DO 10 I = 5, NCAP3
      READ(20,992,ERR=91) K(I)
      992 FORMAT(F)
      10 CONTINUE
      GOTO 1000
      91 WRITE(5,993)
      993 FORMAT(' ', 'ERROR IN FILE READ, RETURN NO READ')
      1000 CONTINUE
      CLOSE(UNIT= 20)
      RETURN
      END

```

```

C      PROUSYUCS.F01
CHARACTER*10  FILES(2), FILESY(2), MONIT,CONDS(2),DATEP
CHARACTER*10  MAP1(30,10),MAP2(30,10),MAPOUT(30,10),NEW(10),
*  MAPN(10,10)
CHARACTER*10  FNAME
CHARACTER*1  BU,TYPEI
CHARACTER*80  U
REAL  XPL(2), WAVEI, SEUI(500),
*  SEOP(500), W(27525), G(50), FVEC(500),AP(50),CP(50),
*  FJAC(500,50),A(50),C(50),S(50),V(50,50),CPBYN(50),SEOH(500)
INTEGER  I=(1), ICOND(2)
EXTERNAL  LSFUN, LSONOH
COMMON/A/  SEUI, SEUP
COMMON/B/  NI,N
COMMON/C/  ICOND
COMMON/D/  AP
1      CONTINUE
      NROWS = 20
      NCOLS = 5
      NH = 30
      NC = 10
      CALL START(FILES,IEND,MAPN,NROWS,ICOLS,NH,NC)
      IF (IEND.EQ.1) GOTO 1000
      CALL HEADFL(FILLS,NCAP7,K,C,WAVEI,NCAP7P,KP,CP,CONDS,
*  IERROR,TYPEP,DATEP,HMEASP,MAP1,MAP2,NROWS,NCOLS,NK,NC)
      IF (IERROR.EQ.0) GOTO 100
991     WRITE(5,991)IERROR
      FORMAT(' ',ERROR IN FILES IEND, IERROR='2X,12,/, 'END')
      GOTO 10000
100     CONTINUE
      ICOND(1)=#
      ICOND(2)=#
      IF (CONDS(1).EQ.'SCALD') ICOND(1)= 1
      IF (CONDS(2).EQ.'SCALD') ICOND(2)= 1
      M = 80
      XTOLSF = 20.0
      IPRINT = 1
      U = ' DO YOU WANT TO USE DEFAULT PARAMETER VALUES ?'
      CALL DECIDE(0,1,U,IOUT)
      IF ( IOUT .EQ. 1 ) GOTO 10
3       WRITE(5,992)
992     FORMAT(' ',INPUT NUMBER OF UNPACKED RESIDUALS, RANGE 2-450')
20      READ (5,993)M
993     FORMAT(I3)
      IF (M.GT.2.0M.NE.LT.450) GOTO 10
      WRITE (5, 99)
99      FORMAT(' ',M OUTSIDE RANGE 2-450')
      GOTO 20
110     CONTINUE
      XPE(1) = KP(1)
      XPE(2) = KP(NCAP7P)
      CALL ARMI(NCAP7,K,C,XPE,WAVEI,N,NI,SEUI,ISTOP)
      IF (ISTOP.EQ.0) GOTO 200
994     WRITE(5,994) ISTOP
      FORMAT(' ',RETURN FROM ARMI WITH ISTOP='12,/, 'END')
      GOTO 10000
210     CONTINUE
      NCAP3P = NCAP7P - 4
      N = NCAP3P
      IPAK = 20
      MPAL = M + IPAK + IPAK
      CALL ARMP(NCAP7P, KP,CP, M, SEUP, ISTOP)
      IF (ISTOP.EQ. M ) GOTO 300
      WRITE (5,995) ISTOP
995     FORMAT(' ',RETURN FROM ARMI WITH ISTOP='12,/, 'END')
      GOTO 10000
310     CONTINUE
      CALL PACK(SEOH, M, NPAK, SEUP, ISTOP)
      IF (ISTOP.EQ.M) GOTO 22
      WRITE (5,2229)
2229    FORMAT(' ',RETURN PACK WITH ISTOP=1, END ')
      GOTO 10000
22     CONTINUE
      LJ = 500
      LV = 50
      LI = 1
      LW = 27525

```

```

IF ( IOUT .NE. 1 ) THEN
WRITE (5, 498)
FORMAT(' ', 'INPUT VALUE IPRINT CONTROLLING LSOMON')
REAL(5,993) IPRINT
ENDIF
MAXCAL = 400* N
ETA = 0.5
IF ( IOUT .NE. 1 ) THEN
544 WRITE(5, 544)
FORMAT(' ', 'INPUT XTOL SCALE FACTOR')
545 REAL (5, 545) XTOLR
FORMAT(F)
ENDIF
XTOL = XTOLR* %SORT(XU2AAI(XTOL))
STEPX = 10000.0
DO 500 J=1, NCAPI
CPSYN(J) = CP(J)
500 CONTINUE
600 CONTINUE
111 WRITE(5, 111)
FORMAT(' ', 'INPUT NAME FILE TO HOLD LSOMON OUTPUT')
REAL (5,882) MONIT
IFAIL= 1
OPEN(UNIT=20, DEVICE='DISK', ACCESS='SEQUENT', FILE= MONIT )
* CALL E94FCF(MPAK,N,LSOFUN,LSOMON,IPRINT,MAXCAL,ETA,XTOL,
* STEPMX,CPSYN,FSUMSO,FVEC,FJAC,IJ,S,V,LV,ITER,NF,IM,
* LIM,M,LW,IFAIL)
* CLOSE (UNIT=20)
IF (IFAIL.NE.0) WRITE(5,999)IFAIL
999 FORMAT(' ', 'EXIT E94FCF WITH IAC IFAIL=',I3 )
IF (IFAIL.EQ.1) GOTO 1000
WRITE(5, 331)
331 FORMAT(' ', 'DO YOU WANT PLOT OF SYNTH ? Y OR N')
READ(5, 889) UR
IF (BB.CO.'N') GOTO 112
IF ( COND5(2) .EQ. 'SCALED' ) FNAME = MAP2( 3, 1 )
IF ( COND5(2) .NE. 'SCALFD' ) FNAME = MAP2( 2, 1 )
CALL SYNPLT(NCAP7P, NP, CPSYN, NAFM, NROWS,NCOLS,NR,NC,
* FNAME,FVEC,MPAK,M,IPAK )
WRITE (5, 332)
332 FORMAT(' ', 'DO YOU WANT STORE SYNTH DATA? Y OR N')
READ(5,889)UR
IF (BB.CO.'N') GOTO 33

112 CONTINUE
WRITE(5,861)
861 FORMAT(' ', 'INPUT NAME FILE TO HOLD SYNTH CS PROFILE')
READ(5,882) FILESY(1)
WRITE (5,884)
884 FORMAT(' ', 'INPUT NAME FILE TO HOLD SOLUTION DESCRIPTION')
READ(5,882) FILESY(2)
CALL CLEAR1(NM,N,NCOLS)
NEW(1) = FILESY(1)
NEW(2) = FILESY(2)
NEW(3) = MONIT
CALL LOG2(NROWS,NCOLS,NR,NC,MAP1,4,MAP2,4,MAPOUT,NEW)
OPEN (UNIT= 20,DEVICE='DISK',ACCESS = 'SEQUENT',FILE= FILESY(1))
CALL MAPRT(MAPOUT,NROWS,NCOLS,NR,NC)
TYPEP = 'G'
WRITE(20, 661)TYPEP,MAVIL,DATEP,NI,EASP,COND5(2)
661 FORMAT(A1,F5.1,1X,A10,T2,1X,A10)
WRITE( 20, 5551 ) *
5551 FORMAT( I4 )
WRITE(20, 229) NCAPI
229 FORMAT(I2)
862 FORMAT(A10)
WRITE (20,883) (KP(J),J=1,NCAPI)
WRITE (20, 883) (CPSYN(J), J= 1, I )
863 FORMAT(E20.7)
CLOSE (UNIT=20)
CALL LSUGKO (MPAK,N,FVEC,FJAC,IJ,G)
OPEN (UNIT=20,DEVICE='DISK',ACCESS='SEQUENT',FILE=FILESY(2))
WRITE(20, 885) FSUMSO
865 FORMAT(F12.5)
WRITE(20,551)
551 FORMAT(' ', 'G')
WRITE(20,884) (G(J),J=1, I )
866 FORMAT(F20.5)
WRITE(20,552)
552 FORMAT(' ', 'FVEC')

```

```

WRITE (20,866)(FVEC(J),J=1,IPAK)
CLOSE (UNIT=20)
FORMAT(A1)
869   WRITE(5,771)
33    FORMAT(' ', 'DO YOU WANT TO RE-RUN WITH DIFFERENT M? Y OR N')
771   READ(5,889)M8
      IF (M8.EQ.'Y') GOTO 3
      WRITE(5,772)
772   FORMAT(' ', 'DO YOU WANT TO RE-RUN PLOT ? Y OR N')
      READ (5,889)M9
      IF (M9.EQ.'Y') GOTO 1
10000 STOP
      END

```

```

SUBROUTINE READFL(FILES,NCAP7,K,C,WAVEL,NCAP7P,KP,CP,
* COND5,IERKOR,TYPEP,DATEP,NMEASP,
* MAP1,MAP2,NROWS,NCOLS,NK,NC)
CHARACTER*10 FILES(2), DATE, COND5(2),DATEP
CHARACTER*10 MAP1(NK,NC),MAP2(NK,NC)
REAL WAVEL,K(50),C(50),KP(50),CP(50)
CHARACTER*1 TYPE, TYPEP
IERKOR = 0
OPEN (UNIT=20,DEVICE='DSK',ACCESS='SEQUENTIAL',FILE=FILES(1))
CALL MAPRD(MAP1,NROWS,NCOLS,NK,NC)
READ (20,999,ERR=91) TYPEP,WAVEL, DATE, NMEAS, COND5(1)
999   FORMAT(A1,F5.1,1X,A10,I2,1X,A10)
READ (20,882,ERR=92) NCAP7
882   FORMAT( 2F7.3)
      DO 50 J = 1, NCAP7
      READ ( 20, 883, ERR= 93) I(J)
50    CONTINUE
      DO 10 J = 1, NCAP7 = 4
      READ (20, 883, ERR= 94) C(J)
10    CONTINUE
      CLOSE (UNIT = 20 )
      FORMAT (E20.7)
883   OPEN (UNIT=20, DEVICE='DSK', ACCESS='SEQUENTIAL', FILE=FILES(2))
      CALL MAPRD(MAP2,NROWS,NCOLS,NK,NC)
      READ (20,999,ERR=81) TYPEP, WAVEL, DATEP, NMEASP, COND5(2)
      DO 20 J = 1, NCAP7P
      READ(20, 883, ERR=83 ) KP(J)
20    CONTINUE
      DO 30 J = 1, NCAP7P = 4
      READ (20,883,ERR=84 ) CP(J)
30    CONTINUE
      CLOSE (UNIT = 20)
      GOTO 10000
91    IERKOR = 11
      GOTO 1000
92    IERKOR = 12
      GOTO 1000
93    IERKOR = 13
      GOTO 1000
94    IERKOR = 14
      GOTO 1000
81    IERKOR = 21
      GOTO 1000
82    IERKOR = 22
      GOTO 1000
83    IERKOR = 23
      GOTO 1000
84    IERKOR = 24
10000 CONTINUE
      CLOSE (UNIT= 20)
      RETURN
      END

```

```

SUBROUTINE ARPI(LCAP7,K,C,XPE,NAVEL,H,HI,SEOI,ISTOP)
REAL XPE(2), SEUI(M),XI(500),K(NCAP7),C(NCAP7)
REAL SEOI(500),SEUIB(500)
INTEGER ICOND(2)
COMMON/C/ ICOND
SCA = -0.00161
SUMI = 0.0
CC = 1.0
ISTOP = 0
KFIT1 = KFII + 1
SCALE = 1.0/( 1.0 + SCA*(NAVEL - 032.0) )
D1 = ( K(NCAP7) - K(1) )
DP = ( XPE(2) - XPE(1) )
IF (M.LT.2) GOTO 92
S = (SCALE*DP)/FLOAT(M-1)
DO 10 J=1, 500
XI(J) = K(1)+ FLOAT(J-1)*S
IFAIL = 1
CALL E02BDF(NCAP7,K,C,XI(J),SEUIB(J),IFAIL)
IF (IFAIL.NE.0) GOTO 91
IF (ICOND(1).EQ.1)SEUI(J)=EXP(SEOIB(J)) - CC
IF (ICOND(1).NE.1)SEUI(J)=SEOIB(J)
SUMI = SUMI + SEUI(J)
IF (XI(J)+S.GT.K(NCAP7)) GOTO 100
CONTINUE
CONTINUE
N1 = J
DO 60 J = 1, N1
SEUI(J) = SEUIB(J)/SUMI
60 CONTINUE
GOTO 10000
91 WRITE (5,991) IFAIL
991 FORMAT (' ', 'MAG ERROR, RETURN IFAIL=', I1)
ISTOP = 1
GOTO 10000
92 WRITE(5,992)
992 FORMAT(' ', 'M NOT GT 2, RETURN')
ISTOP = 2
RETURN
END

```

```

SUBROUTINE ARPI(NCAP7P,KP,CP, H, SLOP, ISTOP)
REAL X(500), SEUP(M),SEUPS(500)
REAL KP(NCAP7P), CP(NCAP7P)
INTEGER ICOND(2)
COMMON/C/ ICOND
1 CC = 1.0
IF (M.LT.2) GOTO 92
S = (KP(NCAP7P)-KP(1))/FLOAT(M-1)
IF (ICOND(2).EQ.1) GOTO 30
X(M) = KP(NCAP7P)
DO 10 J=1, M-1
X(J) = KP(1) + FLOAT(J-1)*S
2 IFAIL = 0
CALL E02BDF(NCAP7P,KP,CP, X(J), SEUP(J), IFAIL)
IF (IFAIL.NE.0) GOTO 91
CONTINUE
GOTO 20
30 CONTINUE
X(M) = KP(NCAP7P)
DO 20 J = 1, M-1
X(J) = KP(1) + FLOAT(J-1)*S
IFAIL = 0
CALL E02BDF(NCAP7P,KP,CP,X(J),SLOP(J),IFAIL)
IF (IFAIL.NE.0) GOTO 91
SEUP(J) = EXP(SLOP(J)) - CC
20 CONTINUE
GOTO 10000
91 WRITE (5, 991) IFAIL.
991 FORMAT(' ', 'MAG ERROR RETURN IFAIL=', I1)
ISTOP = 1
GOTO 10000
92 WRITE (5, 992)
992 FORMAT(' ', 'M NOT GT 2, RETURN')
ISTOP = 2
RETURN
END

```

```

SUBROUTINE LSOFUN(FLAG,MPAL,N,CPSYN,FVECC,IM,LIM,M,LW)
REAL FVECC(MPAK),M(LW), SFUC(500), SLPD(1000),KP(50),CPSYN(N)
REAL SLOH(500)
INTEGER IL(LIW)
REAL SEQI(500), SEOP(500)
COMMON/D/ MI, M
COMMON/A/ SEUI, SEOP
COMMON/U/ NP
CONTINUE
331 NCAPT = N + 4
CALL ARKP(NCAP7P, KP,CPSYN, M, SEUH, ISTOP)
IF (ISTOP.NE.M) GOTO 11
CALL PACK(SEQH, M, HPAK, SEUC, ISTOP)
332 IF (ISTOP.NE.0) GOTO 11
333 CALL SP(SEUC, SEUI, SLPD, HPAK, MI)
334 CALL RESUL ( SLPD, SEOP, FVECC, MPAK, NI)
GOTO 10000
11 CONTINUE
IFLAG = -1STOP
10000 RETURN
END

```

```

SUBROUTINE PACK(SEU,M,MPAK,SEOPAK,ISTOP)
REAL SEU(N), SLOPAK(MPAK)
ISTOP = 0
IF (MPAK.LT.M) THEN
ISTOP = 1
ELSE IF (MPAK.LD.M) THEN
DO 10 J = 1, M
SEOPAK(J) = SLO(J)
10 CONTINUE
ELSE IF (MPAK.GT.M) THEN
IF (MOD((MPAK-M)/2),2).EQ.0) K1 = (MPAK-M)/2
IF (MOD((MPAK-M)/2),2).NE.0) K1 = (MPAK-M+1)/2
K2 = K1+M+1
DO 1 J = 1, K1
SEOPAK(J) = M,M
1 CONTINUE
DO 2 J = 1, K1
SEOPAK(K1+J) = SEU(J)
2 CONTINUE
DO 3 J = K2, MPAK
SEOPAK(J) = M,M
3 CONTINUE
END IF
10000 RETURN
END

```

```

SUBROUTINE SP(F, G, H, N, M)
REAL F(N), G(N), H(N+1)
REAL S
INTEGER J, K, M, N
DO 1000 K=1, N+1
S = 0.0
DO 100 J=1, N
IF (J.GE.(K+1).OR.J.LT.(K+1-M)) S=S+0.0
IF (J.LT.(K+1).AND.J.LE.(K+1-N)) S=S+G(J)*F(K-J+1)
1000 CONTINUE
H(K) = S
1000 CONTINUE
RETURN
END

```

```

SUBROUTINE RESUL(SLPD, SPDP, FVECC, M, NI)
REAL SLPD(N+NI-1), SEOP(N), FVECC(N)
IF (MOD(NI,2).EQ.0) N1L = (NI-2)/2
IF (MOD(NI,2).NE.0) N1L = (NI-1)/2
DO 10 J=1, N
FVECC(J) = SLPD(N1L+J) - SEOP(J)
10 CONTINUE
RETURN
END

```

```

SUMEOUTIPL SYPLPLT( ICAP7P, IP, CPSYL, HAPM, HROWS, NCOLS,
* NR, IC, FNAME, FVEC, NPAP, N, IPAL )
REAL KP( ICAP7P ), CPSYN( NCAI7P ), X( 500 ), Y( 500 ), YS( 500 ), XCALC( 200 )
REAL YCALC( 200 ), KINT( 50 ), FVEC( NPAP ), KES( 250 ), XRES( 250 ),
* YKNOTS( 50 )
CHARACTER*10 NAME( NR, IC )
INTEGER ICOND( 2 ), ISCALE( 2 )
CHARACTER*10 FNAME, DATE, CONDS
CHARACTER*1 Z, TYPE
COMMON/ C / ICOND
NCAPP = NCAI7P - 7
NCALC = 100
DATA ISCALE( 1 ), ISCALE( 2 ) / M, V /
CONTINUE
OPEN( UNIT=20, DEVICE='DSK', ACCESS='SEQUEN', FILE=FNAME )
CALL MAPRD( HAPM, NROWS, NCOLS, NR, IC )
993 READ( 20, 993 ) TYPE, WAVEL, DATE, NCFAS, CONDS
FORMAT( A1, F5.1, I1, A10, I2.1, A10 )
994 READ( 20, 994 ) NPTS
FORMAT( I4 )
DO 10 J = 1, NPTS
995 READ( 20, 995 ) X( J ), YS( J )
FORMAT( 2F7.3 )
CONTINUE
11 ISCALE( 1 ) = 0
IF( CONDS.EQ.'SCALED' ) ISCALE( 1 ) = 1
ISCALE( 2 ) = ICOND( 2 )
IF( X( 1 ).EQ.KD( 1 ).AND.X( NPTS ).EQ.KP( NCAI7P ) ) GOTO 20
WRITE( 5, 9951 )
9951 FORMAT( ' ', 'END POINTS MISMATCH -' )
WRITE( 5, 991 )
991 FORMAT( ' ', 'INPUT NAME FILE HOLDING LINE PROFILE' )
992 READ( 5, 992 ) FNAME
FORMAT( A10 )
GOTO 1
20 CONTINUE
STEP = ( X( NPTS ) - X( 1 ) ) / FLOAT( M - 1 )
DO 700 J = 1, M
XRES( J ) = X( 1 ) + STLP * FLOAT( J - 1 )
KES( J ) = FVEC( J + IPAK )
700 CONTINUE
CALL EVAL1( YS, Y, NPTS, ICAP7P, CPSYN, KP, XCALC, YCALC, NCALC,
* KINT, YKNOTS, ISTOP, ISCALE )
IF( ISTOP.EQ.0 ) GOTO 22
996 WRITE( 5, 996 ) ISTOP
FORMAT( ' ', 'RETURN FROM EVAL WITH ISTOP=', I4, '/', 'RETURN MAIN' )
GOTO 10000
22 CONTINUE
WRITE( 5, 997 )
997 FORMAT( ' ', 'DO YOU WANT VDU PLOT ? Y OR N' )
998 READ( 5, 998 ) Z
FORMAT( A1 )
IF( Z.EQ.'N' ) GOTO 30
IPLUT = 1
CALL PLOT4( IPLUT, X, Y, NPTS, XCALC, YCALC, NCALC, KINT, YKNOTS, NCAPP,
* FNAME, XRES, KES, M )
30 CONTINUE
WRITE( 5, 999 )
999 FORMAT( ' ', 'DO YOU WANT HP PLOT ? Y OR N' )
10000 READ( 5, 998 ) Z
IF( Z.EQ.'N' ) GOTO 10001
IPLUT = 2
CALL PLOT4( IPLUT, X, Y, NPTS, XCALC, YCALC, NCALC, KINT, YKNOTS, NCAPP,
* FNAME, XRES, KES, M )
10001 CONTINUE
WRITE( 5, 8881 )
8881 FORMAT( ' DO YOU WANT BENSON PLOT ? Y OR N' )
READ( 5, 998 ) Z
IF( Z.EQ.'Y' ) THEN
IPLUT = 3
CALL PLOT4( IPLUT, X, Y, NPTS, XCALC, YCALC, NCALC, KINT, YKNOTS, NCAPP,
* FNAME, XRES, KES, M )
ENDIF
10000 RETURN
END

```

```

SUBROUTINE PLOT*(IPLT,X,Y,NPTS,XCALC,YCALC,NCALC,KINT,
* YKNOTS,NCAP,FILLC, XRES, RES, NRES )
REAL X(LPIS), Y(NPTS), XCALC(NCALC), YCALC(NCALC)
REAL YFITL(200), YCALCL(200), YKNOT(50), KINT(50)
REAL XRES(NRES), RES(NRES), YKNOTS(50)
REAL A, B, XL, YL
CHARACTER*10 FILEC,FILES
CHARACTER*1 UB
CHARACTER*6 FILEPT
NKNOT = NCAP - 1
ISPACE = 2
SIZLET = 0.3
IFLAG = 0
ISWIT = 0
IF (IPLT.EQ.3) THEN
WRITE(5,993)
993 FORMAT(' INPUT NAME FOR PLOT FILE',/
* , ' UP TO 6 LETTERS, NO EXTENSION')
READ(5,994) FILEPT
994 FORMAT( A6 )
ENDIF
WRITE(5, 991 )
991 FORMAT(' DO YOU WANT KNOT VALUES PRINTED? Y OR N')
READ(5,992) BU
992 FORMAT( A1 )
IF (BU.EQ. 'Y' ) IFLAG = 1
IF (IPLT.EQ. 1 ) THEN
A = 1.5
B = 5.0
XL = 15.0
YL = 8.0
ELSE IF ( IPLT .EQ. 2 ) THEN
A = 1.5
B = 5.0
XL = 15.0
YL = 8.0
ELSE IF (IPLT .EQ. 3) THEN
A = 1.5
B = 5.0
XL = 24.0
YL = 18.0
ENDIF
DO 20 J = 1, NCALC
IF ( YCALC(J).GT.-0.5.AND.YCALC(J).LT.21.0 ) YCALCL(J) = YCALC(J)
IF ( YCALC(J).LT.-0.5 ) YCALCL(J) = -0.5
IF ( YCALC(J).GT.21.0 ) YCALCL(J) = 21.0
20 CONTINUE
CALL GINO
IF (IPLT.EQ.1) CALL T4010
C IF (IPLT.EQ.2) CALL HP
IF (IPLT.EQ.3) THEN
CALL BN1312
CALL STARTP(FILEPT)
ENDIF
CALL UNITS(10.0)
CALL WINDOW(2)
CALL CHASIZ(SIZLET,SIZLET)
CALL AXISCA(1,10,X(1),X(NPTS),1)
CALL AXIPUS(1,A,B,XL,1)
CALL AXIDRA(1,1,1)

CALL AXISCA(1,10,0.0,20.0,2)
CALL AXIPUS(1,A,B,YL,2)
CALL AXIDRA(-1,-1.2)
CALL GNACUR(XCALC,YCALCL,NCALC)
CALL GRASYM( X, Y, NPTS, 3, 0 )
IF ( NCAP.LT.2 ) GOTO 90
IF (IPLT.EQ.3.AND.ISWIT.EQ.0) GOTO 40
DO 40 J=1, NKNOT
CALL GRAMOV( KINT(J), 0.0 )
CALL GRALIN( KINT(J), YKNOTS(J) )
40 CONTINUE
DO 50 J = 1, NKNOT
YKNOT(J) = 0.0
50 CONTINUE
CALL GWASYM(KINT, YKNOT, NKNOT, 7, 0 )
IF ( IFLAG.EQ. 0 ) GOTO 90
YK = 12.0
DO 100 J = 1, NKNOT
CALL MOVTO2(2.5, YK )
CALL CHAIX( KINT(J) , 7, 3 )
YK = YK - 0.5
IF (YK.LT.1.0) YK = 1.0

```

```

100  CONTINUE
90   CONTINUE
      CALL MOVTO2(2.0, 13.2 )
      CALL CHASTR( ILEC )
      CALL AXIPUS(1, A, B=3.0, XI, 1 )
      CALL AXIDRA(1, 0, 1)
      CALL AXISCA(1, 4, -0.2, 0.2, 2 )
      CALL AXIPUS(0, A, U=3.0, 3.0, 2 )
      CALL AXIDRA(-1, -1, 2 )
      CALL GRASYM( XRES, RES, NRES, 3, HSPACE )
      CALL DEVENO
      IF (IPLOT.EQ.3) CALL ENDP
      CALL GTNEID
      RETURN
      END

```

SPLINE DATA FILE

E630.5 (17.08.84) 3 2TOR 0MA
20

```

0.3000000E+01
0.3000000E+01
0.3000000E+01
0.3000000E+01
0.4000000E+01
0.6000000E+01
0.7000000E+01
0.8000000E+01
0.1000000E+02
0.1040000E+02
0.1140000E+02
0.1180000E+02
0.1290000E+02
0.1430000E+02
0.1560000E+02
0.1700000E+02
0.1895000E+02
0.1895000E+02
0.1895000E+02
0.1895000E+02
0.1070968E+00
0.1331844E+00
0.1696811E+00
0.2508675E+00
0.6269897E+00
0.2831079E+01
0.8855422E+01
0.1429090E+02
0.1350510E+02
0.7851004E+01
0.1013342E+01
0.3387222E+00
0.2301675E-01
0.1578004E+00
0.4179825E-01
0.9310230E-01

```

SOLUTION OUTPUT BY LSQMON

ITNS	F EVALS	SUMSQ	GTG	GRADE
3	126	1.87999E-02	4.0E-07	12
	X		G	SINGULAR VALUES
5.06686E-01		7.2E-07		2.5E+00
-3.05005E-02		-8.6E-07		2.3E+00
4.02169E-01		4.3E-06		2.2E+00
5.16065E-02		-2.0E-05		2.0E+00
5.26128E-01		-1.7E-05		1.7E+00
6.29325E-02		-5.2E-04		1.5E+00
1.41007E+00		-1.2E-04		1.3E+00
2.22577E+00		-1.1E-04		1.1E+00
1.20562E+01		7.3E-05		9.3E 01
1.87399E+01		1.3E-05		7.9E-01
7.44687E+00		6.1E-05		6.6E-01
-8.78165E-02		2.7E-04		5.4E-01
9.10010E-01		3.8E-05		4.4E-01
-4.37008E-01		1.5E-04		3.5E-01
5.45776E-01		1.8E-05		2.8E-01
-1.99133E-01		3.0E-06		2.3E-01
3.93612E-01		1.2E-06		2.0E 01
-7.31021E-02		3.0E-07		9.4E-02
1.74040E-01		-4.2E-07		8.8E-02

```

C      PROG: SYMABS.FOR
      CHARACTER*10 FILEN(3),FILESY(2),HUNIT,CONDS(3),DATE,NAME
      CHARACTER*10 MAP1(30,10), MAP2(30,10), MAP3(30,10), NEW(10),
      * MAPOUT(30,10),MAPD(30,10)
      CHARACTER*1  BH,TYPE
      CHARACTER*100  U
      REAL  RE(50),KT(50),CK(50),CT(50),ASYN(10),SEOE(500),SEOT(500),
      * FVEC(500),FJAC(500,10),S(10),V(10,10),M(6105),G(10),
      * SEOI(500),KI(50),CI(50)
      INTEGER  ICONDS(3),IM(1)
      EXTERNAL  USOMON, USOPNA
      COMMON  SEQT,SEOL,SEUT,BASU,IPAK,M,NI
      NROWS = 20
      NCOLS = 5
      NR = 30
      NC = 10
      CONTINUE
      CALL STARTA(FILEN, IEND, NROWS, NCOLS, NR, NC, MAPM )
      IF (IEND.EQ.1) GOTO 10000
      CALL HEADAFILES,NCAP7I,KI,CI,M,NCAP7E,KE,CE,WAVEL,NCAP7T,KT,
      * CT,CONDS,DATE,NREAST,IERKOR,MAP1,MAP2,MAP3,NROWS,NCOLS,NR,NC)
      IF (IERKOR.EQ.0) GOTO 100
      WRITE(5,991) IERKOR
      991  FORMAT(' ',ERROR FILLS READ, IERKOR=' ',I4,3X,'END')
      GOTO 10000
      100  CONTINUE
      ICONDS(1) = M
      ICONDS(2) = 0
      ICONDS(3) = 0
      IF (CONDS(1).EQ.'SCALED') ICONDS(1) = 1
      IF (CONDS(2).EQ.'SCALED') ICONDS(2) = 1
      IF (CONDS(3).EQ.'SCALED') ICONDS(3) = 1
      IF ( M.LT. 2 .OR. M .GT. 450 ) THEN
      5551  WRITE( 5, 5551 ) M
      * 5551  FORMAT(' VALUE OF M TRAIL SEARCHED FROM FILE OUTSIDE RANGE 2-450',/
      * ' M = ',I4)
      3  * WRITE(5,992)
      992  FORMAT(' ',INPUT NUMB, ARRAY CALL, RANGE 2 - 450')
      READ(5, 993) I
      993  FORMAT(I3)
      IF (M.LT.2.OR.M.GT.450) THEN
      994  WRITE(5, 994)
      * 994  FORMAT(' ',M OUTSIDE RANGE 2-450, TRY AGAIN')
      GOTO 3
      END IF
      END IF
      IPAK = 15
      MPAK = M + IPAK + IPAK
      CALL APNS(M,ICONDS,NCAP7I,KI,CI,NCAP7E,KE,CE,NCAP7T,KT,CT,
      * BASE,WAVEL,NI,SLU1,SEUE,SCUT,ISTOP)
      IF (ISTOP.EQ.0) THEN
      995  WRITE(5,995)ISTOP
      * 995  FORMAT(' ',RETURN FROM APNS WITH ERROR=' ',I4,'END')
      GOTO 10000
      END IF
      N = 5
      LJ = 500
      LV = 10
      LIW = 1
      LU = 6105

      IPHINT= 1
      MAXCAL= 40000
      ETA = 0.5
      XTOLSF=2M,M
      XTOL =XTOLSF*SQRT(XOZAAI(XTOL))
      STEPMX= 100000.0
      WRITE(5,1231)
      1231  FORMAT(' DO YOU WANT TO USE DEFAULT STARTING POINT ? Y OR N')
      READ(5,889) BB
      IF (BB.EQ.'Y') THEN
      ASYH(1) = 0.2
      ASYH(2) = 1.0
      ASYH(3) = 0.0
      ASYH(4) = 0.0
      ASYH(5) = 0.0

```

```

ELSE IF (BU.EQ.'Y') THEN
DO 321 J = 1, 5
727 WRITE(5,1232) J
1232 FORMAT(' INPUT VALUE ASYN(J), J = ',I2 )
READ(5,1231,ERR=747) ASYN(J)
1233 FORMAT(I)
321 CONTINUE
GOTO 737
747 WRITE(5,1234)
1234 FORMAT(' ERROR LEADING VALUE, REPEAT INPUT')
GOTO 727
737 CONTINUE
END IF
WRITE(5,996)
996 FORMAT(' ', 'INPUT NAMEFILE TO HOLD LSUMON OUTPUT')
READ(5,997)MONIT
997 FORMAT(A10)
OPEN(UNIT=20,DEVICE='DSK',ACCESS='SEQUENT',FILE=MONIT)
IFAIL = 1
CALL E04FCF(MPAK,N,LSOFNA,LSOHON,IPRINT,MAXCAL,ETA,XTOL,
STEPN,ASYN,FSUMSU,FVLC,FJAC,LJ,S,V,LV,UITER,NP,IN,LIW,
W,LW,IFAIL)
CLOSE(UNIT=20)
998 WRITE(5,998)IFAIL
FORMAT(' ', 'RETURN FROM E04FCF WITH IFAIL=',I4)
IF (IFAIL.EQ.1) GOTO 1000
CALL ANCALC(WAVEL,RABE,ASYN,G1,G2,A12,AN,JFAIL)
WRITE(5,7L71)JFAIL,AN
7L71 FORMAT(' ', 'JFAIL=',I3, 'NUMBER DENSITY*10**17= ',F)
0= ' DO YOU WANT PLOT OF RESIDUALS ?'
CALL DECIDE(0,1,'N,IOUT)
IF (IOUT.EQ.1) THEN
CALL SYN2PT(FVEC,MPAK,N,IPAK,NP(1),RR(MCAPTE),ASYN)
ENDIF
WRITE (5, 332)
332 FORMAT(' ', 'DO YOU WANT STORE SYNTH DATA Y OR N?')
READ(5,889)DR
IF (DR.EQ.'N') GOTO 33
CONTINUE
WRITE (5,884)
884 FORMAT(' ', 'INPUT NAME FILE TO HOLD SOLUTION DESCRIPTION')
READ(5,882) FILESY(2)
CALL LSOGND (MPAK,N,FVEC,FJAC,LJ,G)
OPEN (UNIT=20,DEVICE='DSK',ACCESS='SEQUENT',FILE=FILES(2))
WRITE(20,885) FSUMSU
885 FORMAT(I2.5)
WRITE(20,551)
551 FORMAT(' ', 'G')
WRITE(20,883) (G(J),J=1, G)
886 FORMAT(F20.5)
WRITE(20,552)
552 FORMAT(' ', 'FVLC')
WRITE (20,886)(FVLC(J),J=1,MPAK)
CLOSE (UNIT=20)
WRITE(5,881)
881 FORMAT(' ', 'INPUT NAME FILE TO HOLD SYNTH ABS COEFS')
READ(5,882) FILESY(1)
CALL CLEAR1( NEW, NCOLS )
NEW(1) = FILESY(1)
NEW(2) = FILESY(2)
NEW(3) = MONIT
CALL LOG3(NROWS,NCOLS,NR,LC,MAP1,4,MAP2,10,MAP3,4,MAPOUT,NEW)
OPEN (UNIT= 20,DEVICE='DSK',ACCESS='SEQUENT',FILE= FILESY(1))
TYPE = 'A'
CALL MAPWRT(MAPOUT,NROWS,NCOLS,DR,NC)
WRITE(20, 6b1)TYPE,WAVEL,UATE,UMEAST
6b1 FORMAT(A1,F5.1,1X,A10,I2.1X,A10)
882 FORMAT(A10)
WRITE (20, 883) (ASYN(J), J= 1, N )
883 FORMAT(E20.7)
CLOSE (UNIT=20)
WRITE(5,9991)
9991 FORMAT(' ', 'DO YOU WANT TO STORE THIS AS RESULT?, Y OR N?')
READ(5,889)DR
IF (DR.EQ.'Y')CALL STORE(WAVEL,A,IFAIL,AN,FILES,MONIT,FILESY,
G1,G2,A12)
889 FORMAT(A1)
WRITE(5,771)
33 WRITE(5,771)
771 FORMAT(' ', 'DO YOU WANT TO RE-RUN WITH DIFFERENT NT Y OR N?')
READ(5,889)DR
IF (DR.EQ.'Y') GOTO 3
WRITE(5,772)
772 FORMAT(' ', 'DO YOU WANT TO REKUR: PRNG ? Y OR N?')
READ (5,889)DR
IF (DR.EQ.'Y') GOTO 1
1000 STOP
END

```

```

SUBROUTINE ARIS(M,ICONS,NCAP7,KI,CI,NCAP7E,KE,CE,NCAP7T,
* XT,CT,BASE,MAVEL,NI,SEOI,SEWE,REOT,ISTOP)
REAL K(NCAP7L),K(NCAP7T),CF(NCAP7L),CT(NCAP7T),SEUI(500),
* SLOW(500),SEUL(N),SLOT(N),XL(500),XT(500),*I(NCAP7I),CI(NCAP7I)
INTEGER ICONS(3)
CC = 1.0
ISTOP = 0
BASE = KE(NCAP7E) - KI(1)
KASLT = KT(NCAP7T) - KI(1)
IF (BASE.EQ.0) BASE = BASRT
IF (BASE.LT.0) BASE = BASEL
STEP = BASE/FL0AT(M-1)
XL(M) = KE(1) + BASE
XT(M) = KI(1) + KASLT
DO 10 J = 1, M-1
XINC = STEP*FL0AT(J-1)
XE(J) = KE(1) + XINC
XT(J) = KI(1) + XINC
IFAIL = 0
CALL E02B0F(NCAP7E,KE,CE,XE(J),SEW(J),IFAIL)
IF (IFAIL.NE.0) GOTO 1000
IF (ICONS(2).EQ.0) SEW(J) = SEW(J)
IF (ICONS(2).NE.0) SEW(J) = EXP(SEW(J)) - CC
IFAIL = 0
CALL E02B0F(NCAP7T,KT,CT,XT(J),SEW(J),IFAIL)
IF (IFAIL.NE.0) GOTO 2000
IF (ICONS(3).EQ.0) SLOT(J) = SEW(J)
IF (ICONS(3).NE.0) SLOT(J) = EXP(SEW(J)) - CC
CONTINUE
IFAIL = 0
CALL E02B0F(NCAP7E,KE,CE,XE(M),SEW(M),IFAIL)
IF (IFAIL.NE.0) GOTO 1000
IF (ICONS(2).EQ.0) SEW(M) = SEW(M)
IF (ICONS(2).NE.0) SEW(M) = EXP(SEW(M)) - CC
IFAIL = 0
CALL E02B0F(NCAP7T,KT,CT,XT(M),SEW(M),IFAIL)
IF (IFAIL.NE.0) GOTO 1000
IF (ICONS(3).EQ.0) SLOT(M) = SEW(M)
IF (ICONS(3).NE.0) SLOT(M) = EXP(SEW(M)) - CC
CALL ARRIA(ICONS,NCAP7I,KI,CI,BASE,MAVEL,M,NI,SEUI,ISTOP)
CONTINUE
IF (ISTOP.NE.0) GOTO 3000
GOTO 20
1000 WRITE(5,991) IFAIL
991 FORMAT(' ',*RETURN FROM E02B0F CALC SEW, IFAIL='*,12)
ISTOP = 1
GOTO 10000
2000 WRITE(5,992) IFAIL
992 FORMAT(' ',*RETURN FROM E02B0F CALC SLOT, IFAIL='*,12)
ISTOP = 2
GOTO 10000
3000 WRITE(5,993) ISTOP
993 FORMAT(' ',*RETURN FROM ARRIA WITH ISTOP='*,13)
ISTOP = 3
GOTO 10000
20 CONTINUE
10000 RETURN
END

SUBROUTINE ARRIA(ICONS,NCAP7I,KI,CI,BASE,MAVEL,M,NI,SEUI,ISTOP)
REAL SEUI(500),XI(500),K(NCAP7),C(NCAP7)
REAL SEUI(500),SEUI(500)
INTEGER ICONS(3)
SCA = -0.00181
SUMI = 0.0
CC = 1.0
ISTOP = 0
KFIT1 = KFIT1 + 1
SCALE = 1.0/(1.0 + SCA*(MAVEL - 0.328))
DI = (K(NCAP7) - K(1))
IF (M.LT.7) GOTO 92
S = (SCALE*BASE)/FL0AT(M-1)
DO 10 J = 1, 510
XI(J) = K(1) + FL0AT(J-1)*S
IFAIL = 1
CALL E02B0F(NCAP7I,K,C,XI(J),SEUI(J),IFAIL)
IF (IFAIL.NE.0) GOTO 91
IF (ICONS(1).EQ.1) SEUI(J) = EXP(SLOIUS(J)) - CC
IF (ICONS(1).NE.1) SEUI(J) = SLOIUS(J)
SUMI = SUMI + SEUI(J)
IF (XI(J)+S.GT.K(NCAP7I)) GOTO 100
CONTINUE
CONTINUE

```

```

      P1 = J
      DO 60 J = 1, N1
      SEQ1(J) = SEQ1U(J)/SUM1
60      CONTINUE
      GOTO 10000
91      WRITE (5,991) IFAIL
991     FORMAT (' ', 'HAG LRROR, RETURN IFAIL=', I1)
      ISTOP = 1
      GOTO 10000
92      WRITE(5,992)
992     FORMAT(' ', 'H NOT GT 2, RETURN.')
10000  RETURN
      END

SUBROUTINE ANCALC(WAVEL, BASE, ASYN, G1, G2, A12, AN, JFAIL)
      REAL ASYN(10), G(500)
      REAL WAVEL
      C     *WAVEL IN NM
      CHARACTER*32 DUMF
      NCALC = 200
      JFAIL = 0
      OPEN(UNIT=20, DEVICE='DSK', ACCESS='SEQIN', FILE='GGA.DAT')
      READ(20, 991, ERR=91) JMAX, DUMF
991     FORMAT(12, A32)
      DO 10 J = 1, JMAX
      READ(20, 992, ERR=91) NLINE, WAVELL, IG1, IG2, A12
992     FORMAT(12, 2X, F5.1, 2X, 12, 2X, 12, 2X, F6.4)
      IF (WAVELL.EQ.WAVEL) GOTO 20
10      CONTINUE
20      CONTINUE
      CLOSE(UNIT=20)
      GOTO 100
91      WRITE(5, 9922)
9922     FORMAT(' ', 'ERROR READING FILE GGA.DAT, RETURN')
      CLOSE(UNIT=20)
      JFAIL = 1
      GOTO 10000
100     CONTINUE
      IF (WAVELL.NE.WAVEL) THEN
993     WRITE(5, 993)
          FORMAT(' ', 'WAVLL NOT FOUND IN GGA.DAT, RETURN')
          JFAIL = 2
          GOTO 10000
      END IF
      G1 = FLOAT(IG1)
      G2 = FLOAT(IG2)
      ALPHA = 10.0*75.35*G2/(G1*A12*WAVLL*WAVEL)
      C     *10 POWER 17 OMITTED
      SCALE = 3.2 - 0.00505*(WAVEL - 020.0)
      C     CHECK COEFS
      CALL GCALC(ASYN, NCALC, G)
      SUM = 0.5*(G(1) + G(NCALC))
      DO 200 J = 2, NCALC-1
      SUR = SUM + G(J)
200     CONTINUE
      AN = ALPHA*20.0*SCALE*BASE*SUM/PI*PI*AT(NCALC-1)
      C     *10 POWER 17 OMITTED
10000  RETURN
      END

```

GGA.DAT

#	WAVEL	G1	G2	A12	*10 POWER R
1	640.2	07	05	0.433	
2	614.3	05	05	0.216	
3	580.2	03	05	0.128	
4	630.5	05	03	0.0537	
5	616.4	03	01	0.160	
6	585.2	01	03	0.719	
7	703.2	03	05	0.192	
8	626.0	03	01	0.223	

```

SUBROUTINE LSFAC(LI,LAG,MI,AF,1,ASYN,PVRCC,IV,LIW,M,LW)
REAL FVCCC(MI,AF),ASYN(LI),M(LI)
REAL SEU(500),SEUT(500),SEUAS(500),SEUW(500),SEUFW(500)
SLO(1) = SLO(1)
INTRIGER = IV(LI)
COMMON SEU,SEU,SEUT,BASE,IPAK,M,MI
IF (MPAK.LT.2.OR.M.PAK.GT.500) GOTO 1000
IF (MPAK.NE.(M+IPAK+IPAK)) GOTO 2000
CALL ABS(ASYN(1),ASYN(2),ASYN(3),F,SEUAS)
CONTINUE
DO 10 J = 1, IPAK
SLO(J) = 0.0
CONTINUE
DO 20 J = IPAK+1, IPAK+M
SEU(J) = SEU(J-IPAK)*SEUAS(J-IPAK)
CONTINUE
DO 30 J = IPAK+M+1, MPAK
SEU(J) = 0.0
CONTINUE
CALL SP(SEU,SEU,SLO,MPAK,M,1)
DO 100 J = 1, IPAK
SEUW(J) = 0.0
CONTINUE
DO 200 J = IPAK+1, IPAK+M
SEUW(J) = SEUT(J-IPAK) + ASYN(5)
CONTINUE
DO 300 J = IPAK+M+1, MPAK
SEUW(J) = 0.0
CONTINUE
CALL SHIFTX(SLO,M,SEUW,SEU)
CALL RESOL(SLO,SLO,FVCCC,IPAK,MI)
GOTO 1000
1000 FLAG = -1
GOTO 1000
2000 FLAG = -2
RETURN
END

```

```

SUBROUTINE ABS(PEAK,WIDPAR,XOFF,M,SLO)
REAL SEU(M), X(500)
S = 0.0/FLUAT(M-1)
DO 10 J = 1, M
X(J) = -3.0 + S*FLOAT(J-1) + XOFF
F = X(J)*X(J)*WIDPAR*WIDPAR
IF (F.GT.15.0) F = 15.0
G = PEAK*EXP(-F)
IF (G.GT.15.0) G = 15.0
IF (G.LT.-15.0) G = -15.0
SLO(J) = EXP(-G)
CONTINUE
RETURN
END

```

```

SUBROUTINE SHIFTX(SLO,M,SHX,SEU)
REAL SEU(M),SEU(M),SEU(1000)
ISHX = INT(SHX)
DSHX = SHX-FLUAT(ISHX)
CONTINUE
IF (ISHX.EQ.0) THEN
DO 10 J = 1, M
SEU(J) = SLO(J)
CONTINUE
ELSE IF (ISHX.GT.0) THEN
DO 20 J = 1, ISHX
SEU(J) = M.0
CONTINUE
DO 30 J = ISHX+1, M
SEU(J) = SEU(J-ISHX)
CONTINUE
ELSE IF (ISHX.LT.0) THEN
DO 40 J = 1, M+ISHX
SEU(J) = SEU(J-ISHX)
CONTINUE
DO 50 J = M+ISHX+1, M
SEU(J) = 0.0
CONTINUE
END IF
22 CONTINUE
IF (DSHX.NE.0.0) THEN
A = (1.0 - DSHX)
SLO(1) = A*SEU(1)
DO 100 J = 2, M
SLO(J) = A*SLO(J) + DSHX*SEU(J-1)
CONTINUE
100

```

```

ELSE IF ( DSHX.LT.0.0 ) THEN
  H = (1.0 + DSHX )
DO 200 J = 1, N-1
  SLOP(J)=H*SEU(1)- DSHX*SEU(J+1)
CONTINUE
SEU(N) = H * SLOP(N)
END IF
RETURN
END

SUBROUTINE READA(FILES,NCAP71,K1,CI,H,NCAP7E,KE,CE,NAVEL,
* NCAP7T,KT,CT,CONDS,DATE,NMEAS,IERROR,MAP1,MAP2,MAP3,
* NROWS,NCOLS,NR,NC )
CHARACTER*10 FILES(3), DATE, CONDS(3),DATEP
CHARACTER*10 MAP1(NR,NC),MAP2(NR,NC),MAP3(NR,NC)
REAL NAVEL,K1(50),CI(50),KE(50),CE(50),KT(50),CT(50)
CHARACTER*1 TYPE, TYPEP
IERROR = 0
OPEN( UNIT=20,DEVICE='DSK',ACCESS='SEQIN',FILE=FILES(1))
CALL MAPRD( MAP1,NROWS,NCOLS,NR,NC )
REAL (20,999,ERR=91) TYPE,NAVEL, DATE, NMEAS, CONDS(1)
999 FORMAT(A1,F5.1,1X,A10,I2,1X,A10)
READ (20,802,ERR=92) NCAP71
801 FORMAT( 2I7.3 )
DO 50 J = 1, NCAP71
  READ ( 20, 803, ERR= 93 ) KI(J)
802 FORMAT ( I2 )
50 CONTINUE
DO 10 J = 1, NCAP71 - 4
  READ (20,803,ERR=94) CI(J)
10 CONTINUE
CLOSE (UNIT = 20 )
803 FORMAT (E20.7)
OPEN( UNIT=20, DEVICE='DSK', ACCESS='SEQIN', FILE=FILES(2))
CALL MAPRD( MAP2,NROWS,NCOLS,NR,NC )
REAL (20,999,ERR=91) TYPEP,NAVEL, DATEP, NMEASP, CONDS(2)
551 READ( 20, 551 ) H
FORMAT( I4 )
READ ( 20, 802, ERR=82 ) NCAP7E
DO 20 J = 1, NCAP7E
  READ(20,803,ERR=83) KE(J)
20 CONTINUE
DO 30 J = 1, NCAP7E - 4
  READ (20,803,ERR=84 ) CE(J)
30 CONTINUE
CLOSE (UNIT = 20)
OPEN(UNIT=20,DEVICE='DSK',ACCESS='SEQIN',FILE=FILES(3))
CALL MAPRD( MAP3,NROWS,NCOLS,NR,NC )
READ(20,999,ERR=71)TYPE,NAVEL,DATE,NMEAS,CONDS(3)
READ(20,802,ERR=72)NCAP7T
DO 60 J = 1, NCAP7T
  READ(20,803,ERR=73)KT(J)
60 CONTINUE
DO 70 J = 1, NCAP7T-4
  READ(20,803,ERR=74)CT(J)
70 CONTINUE
GOTO 10000
IERROR = 11
GOTO 1000
IERROR = 12
GOTO 1000
IERROR = 13
GOTO 1000
IERROR = 14
GOTO 1000
81 IERROR = 21
GOTO 1000
82 IERROR = 22
GOTO 1000
83 IERROR = 23
GOTO 1000
84 IERROR = 24
71 IERROR = 31
GOTO 1000
72 IERROR = 32
GOTO 1000
73 IERROR = 33
GOTO 1000
74 IERROR = 34
GOTO 1000
1000 CONTINUE
CLOSE (UNIT= 20)
10000 RETURN
END

```

```

SUBROUTINE GCALC(ASYN,NCALC,G)
REAL ASYN(10), G(500), X(500)
S = 6.0/FL0AT(NCALC-1)
DO 10 J = 1, NCALC
X(J) = -3.0 + S*FL0AT(J-1) + ASYN(3)
F(J) = X(J)*X(J)*ASYN(2)*ASYN(2)
IF (F(J).GT.15.0) F(J) = 15.0
G(J) = ASYN(1)*EXP(-F(J))
IF (G(J).GT.15.0) G(J) = 15.0
IF (G(J).LT.-15.0) G(J) = -15.0
CONTINUE
RETURN
END

SUBROUTINE STORE(WAVEL,N,IFAIL,AN,FILES,MONIT,FILLESY,
G1,G2,A12)
CHARACTER*1 BU
CHARACTER*10 FILEG(3),MONIT,FILLESY(2),NAME
WRITE(5,9992)
9992  F0RMA'T(' ', 'DO YOU WANT TO STORE IN MAIN.DAT? Y OR N')
READ(5,889)BU
IF (BU.EQ.'Y') NAME = 'MAIN.DAT'
889  F0RMA'T(A1)
IF (BU.NE.'Y') T0LN
WRITE(5,9993)
9993  F0RMA'T(' ', 'INPUT NAME OF FILE TO STORE THIS RESULT')
READ(5,9995)NAME
9995  F0RMA'T(A10)
END IF
OPEN(UNIT=20,DEVICE='DISK',ACCESS='APPEND',FILE=NAME)
WRITE(20,9994)WAVEL,G1,G2,A12,N,IFAIL,AN,FILES,MONIT,FILLESY
9994  F0RMA'T(F5.1,F6.1,1X,F7.4,1X,I3,I3,F10.5,1X,3A11,A11,2A11)
CLOSE(UNIT=20)
RETURN
END

SUBROUTINE LSGM0N(M,N,XC,FVECC,IJACC,LJC,S,IGRADE,NITER,NF,IV,
L1,M,L6)
REAL IJACC(LJC,N),FVECC(M),S(M),M(L6),XC(N)
INTEGER I(L1)
REAL G(100)
REAL F0RMLF
DATA HOUT /20/
FSUMS0 = F0RMLF (FVECC,FVECC,M)
CALL LSG0ND (M,N,FVECC,IJACC,LJC,G)
GTC = F0RMLF (G,G,M)
WRITE (HOUT,9999) NITER,NF,FSUMS0,GTC,IGRADE
WRITE (HOUT,9999b)
9999  DO 20 J = 1, N
WRITE (HOUT,99997) XC(J),G(J),S(J)
CONTINUE
RETURN
99999  F0RMA'T(///6H 1TNS,4X,7HF EVALS,10X,5HSUMS0,13X,3HGTG,
0X,5HGRADE/1H ,14, 6X,15,0X,1PF13.5,6X,1PE9.1,6X,I3 )
99998  F0RMA'T(8X,1HX,20X, 1HG,11X,15HSINGULAR VALUES )
99997  F0RMA'T(1H ,1PL13.5,10X,1PE9.1,10X, 1PE9.1 )
END

SUBROUTINE LSG0ND (M, N, FVECC, IJACC, LJC, G)
REAL IJACC(LJC, N), FVECC(M), G(N)
DO 40 J=1, N
SUM = 0.0 E+0
DO 20 I=1, I
SUM = SUM+IJACC(I,J)*FVECC(I)
20  CONTINUE
G(J) = SUM + 500
40  CONTINUE
RETURN
END

```

```

C      PATH SEGMENT: FIT17.FOR
      INTEGER N, N, IPRTY, MAXCAL, LJ, LV, NITER,
      * NF, IN(1), LIW, LW, IFAIL
      INTEGER ICONDS, NCAP7, IPRES, IEXIST
      INTEGER IMOD(2), NCAP74(4), ICOND4(4)

      REAL ETA, XTOL, STEPHX, SYN(10), FSUNSU, FVPC(300),
      * FJAC(300,10), S(10), V(10,10), W(3705), AINT(300),
      * CURR(300), AN(300), AN4(300,4)
      REAL K(50), C(50)
      REAL K4(50,4), C4(50,4)

      EXTERNAL RES12, LSMON
      COMMON IMOD, AINT, CURR, AN, AN4

      CHARACTER*12 EXPT(2)
      CHARACTER*1  BL
      CHARACTER*10 FILES(8)

C      FILES(1)= NAME OF I/I DATA FILE
C      FILES(2)= NAME OF AN/I SPLINE FIT FILE
C      FILES(3)= NAME OF FILE FOR LSMON OUTPUT
C      FITUS(4)= NAME OF SOLUTION OUTPUT FILE

      WRITE( 5, 10606 )
10606  FORMAT(' DO YOU WANT FILE EXISTS PROTECTION ? Y OR N' )
      REAL( 5, 993 ) BR
      IF ( BR.EQ.'N' ) THEN
          ISWIT2 = 0
      ELSE
          ISWIT2 = 1
      ENDIF
1      CONTINUE
      IREM = 0
      ICOUNT = 1
700  CONTINUE

C ISWIT IS MAIN DEFAULT SWITCH
C ISWIT2 IS FILE EXISTS SWITCH
C ISWIT3 IS IFAIL=3 RERUN SWITCH

      ISWIT3 = 0

      ISWIT = 0
      BR = 'Y'
33331  WRITE( 5, 33331 ) ICOUNT
      FORMAT(' MODEL COUNT =', 14 )
      CALL CHOOSE( IMOD )
      CALL PARAM( IMOD, N )
      CALL ARRS12( IMOD, IPRES, N, CURR, AINT, AN, AN4, FILES, EXPT,
      *          ISTOP, NCAP7, K, C, ICONDS,
      *          NCAP74, K4, C4, ICOND4, IREM )
      IF ( ISTOP .NE. 0 ) THEN
          WRITE( 5, 991 ) ISTOP
991  FORMAT( ' RETURN FROM ARRS12 WITH ISTOP=', I3, '/',
      *      ' TERMINATE EXECUTION' )
          GOTO 10000
      ENDIF
      IF ( ISWIT.EQ.0 ) GOTO 1001

      WRITE(5, 992)
992  FORMAT(' DO YOU WANT TO USE DEFAULT STARTING POINT ? Y OR N' )
      REAL(5, 993) BR
993  FORMAT( A1 )
1001  IF ( BR.EQ.'Y' ) THEN
      SYN(1) = 0.5
      DO 500 J = 2, N
          SYN(J) = 0.0
500  CONTINUE

      ELSE IF ( BR .EQ. 'Y' ) THEN
      DO 10 J = 1, N
          WRITE(5,994) J
994  FORMAT(' INPUT VALUE OF STARTING POINT SYN(', I1, ',')' )
          READ( 5, 995 ) SYN(J)
995  FORMAT( F )
10  CONTINUE

```

```

ENDIF
MAXCAL = 40000
RIA = 0.5
XTOLSF = 0.0
2  XINL = XTOLSF*SQRT( XL2AAI( XINL ) )
STEPMX = INUM*RIA
LJ = 300
LV = 10
LIM = 1
LW = 3705
IPRINT = 1
LQU = 0
300 CONTINUE
BU = 'Y'
IF ( ISMTL.EQ.0 ) GOTO 1002
WRITE( 5, 442 )
442 FORMAT(' DO YOU WANT TO USE AUTOMATIC CHOICE OF FILENAME TO HOLD
* USONOH OUTPUT?', /, ' Y OR N' )
READ( 5, 993 ) BR
1002 IF ( BR.EQ.'Y' ) THEN
CALL NAME5( FILES(1), FILES(3), INUM )
FUSL
WRITE ( 5, 9992 )
9992 FORMAT(' INPUT NAME OF FILE TO HOLD USONOH OUTPUT' )
READ( 5, 9993 ) FILES(3)
9993 FORMAT( A10 )
ENDIF
IFAIL = 1
INUM = INUM + 1
IF ( INUM.GT.20 ) THEN
WRITE( 5, 1777 )
1777 FORMAT(' MORE THAN 20 IFAIL=2 LOOPS, ERMON??...TERMINATE' )
GOTO 10000
ENDIF
OPEN( UNIT=20, DEVICE='DRA', ACCESS='SEQU', FILE=FILES(3) )
CALL EM4PCF( N, N, REF12, USONOH, IPRINT, MAXCAL, ETA, XTOL,
* STEPMX, SYN, FSUMJ0, FVEC, FJAC, LJ, S, V, LV, NITR,
* IF, IW, LIL, I, IL, IFAIL )
CLOSE( UNIT=20 )
WRITE( 5, 996 ) IFAIL
996 FORMAT(' EXIT FROM EM4PCF WITH IFAIL =', I3 )
IF ( IFAIL.LT.0 .OR. IFAIL.EQ.1 .OR.
* IFAIL.EQ.4 ) THEN
WRITE( 5, 997 )
997 FORMAT(' TERMINATE EXECUTION' )
GOTO 10000
ELSE IF ( IFAIL.EQ.3 ) THEN
BU = 'N'
IF ( ISMTL.EQ.0 ) GOTO 1067
WRITE ( 5, 998 )
998 FORMAT(' DO YOU WANT TO RERUN WITH LARGER XTOLSF ? Y OR N' )
READ( 5, 993 ) BR
1067 CONTINUE
IF ( BR.EQ.'Y' ) THEN
WRITE( 5, 999 ) XTOLSF
999 FORMAT(' OLD VALUE =', F3.2, /, ' INPUT NEW VALUE XTOLSF' )
READ( 5, 993 ) XTOLSF
801 FORMAT( F )
GOTO 2
ENDIF
ELSE IF ( IFAIL.EQ.2 ) THEN
WRITE( 5, 444 )
444 FORMAT(' VALUES OF SYN ON EXIT FROM EM4PCF ARE 1' )
DO 20 J = 1, N
WRITE( 5, 443 ) J, SYN(J)
443 FORMAT(' SYN(', I1, ') = ', F9.5 )
20 CONTINUE
BU = 'Y'
IF ( ISMTL.EQ.0 ) GOTO 711
WRITE( 5, 445 )
445 FORMAT(' DO YOU WANT TO RESTART MIN. FROM THIS POINT ? Y OR N' )
READ( 5, 993 ) BR
711 CONTINUE
IF ( BR.EQ.'Y' ) GOTO 300
ENDIF
BU = 'Y'
IF ( ISMTL.EQ.0 ) GOTO 1003
WRITE( 5, 4441 )
4441 FORMAT(' DO YOU WANT TO USE AUTOMATIC NAMING OF OUTPUT FILE?',
* /, ' INPUT Y OR N' )
READ( 5, 993 ) BR
1003 IF ( BR.EQ.'Y' ) THEN
CALL NAME5( FILES(1), FILES(4), INUM )

```

```

      PLSL
110  WRITE( 5, 803 )
803  FORMAT(' INPUT DATA FILE TO HOLD SOLUTION' )
      READ( 5, 993 ) FILES(4)
      ENDIF
      IF ( I8=I17.EQ.0 ) GOTO 1066
      CALL EXIST( FILES(4), IEXIST )
      IF ( IEXIST.EQ.1 ) THEN
44441 WRITE( 5, 44441 ) FILES(4)
      FORMAT(' FILE NAMED ', A10, ' EXISTS ALREADY', /,
            ' DO YOU WANT TO OVERWRITE IT?.....INPUT Y OR N' )
      READ( 5, 993 ) BR
            IF ( BR.EQ.'Y' ) GOTO 100
      ENDIF
1000  CONTINUE
      WRITE( 5, 802 )
802  FORMAT(' DO YOU WANT PLOT OF FIT? Y OR N' )
      READ( 5, 993 ) BR
      IF ( BR.EQ.'Y' ) CALL PLOT12( IMOD, FILES, EXPT, N, CURR, AINT,
            N, SYN, FVEC, ISTOP, ICAP7, K, C, ICOUN3,
            ICAP74, K4, L4, ICOUN4, ICOUNT )
      IF ( ISTOP.NE.0 ) GOTO 10000
      WRITE( 5, 11900 )
11900  FORMAT(' COMPONENTS OF SYN ARE :' )
      DO 1800 J = 1, N
      WRITE( 5, 11800 ) SYN(J)
11800  FORMAT(' ', F10.6 )
1800  CONTINUE
      WRITE( 5, 804 )
804  FORMAT(' DO YOU WANT TO STORE SOLUTION? Y OR N' )
      READ( 5, 993 ) BR
      IF ( BR.EQ.'Y' ) THEN
            OPEN( UNIT=20, DEVICE='DISK', ACCESS='SEQUENT', FILE=FILES(4) )
885  WRITE( 20, 885 ) ( FILES(J), J = 1,4 )
            FORMAT( 4( 2X, A10 ) )
            WRITE( 20, 886 ) ( EXPT(J), J = 1,2 )
886  FORMAT( 2( 2X, A10 ) )
            WRITE( 20, 887 ) ( IMOD(J), J = 1, 2 )
887  FORMAT( ' IMOD(1) =', I3, 4X, ' IMOD(2) =', I3 )
            DO 200 J = 1, N
            WRITE( 20, 887 ) SYN(J)
            FORMAT( E20.7 )
200  CONTINUE
            CLOSE( UNIT=20 )
            ENDIF
888  WRITE( 5, 80601 )
80601  FORMAT(' DO YOU WANT TO TRY DIFFERENT MODEL ? Y OR N' )
      READ( 5, 993 ) BR
      IF ( BR.EQ.'Y' ) THEN
            IREM = 1
            ICOUNT = ICOUNT + 1
            GOTO 700
      ENDIF
806  WRITE( 5, 806 )
806  FORMAT(' DO YOU WANT TO RERUN PROC? Y OR N' )
      READ( 5, 993 ) BR
      IF ( BR.EQ.'Y' ) GOTO 1
10000 STOP
      END
      SUBROUTINE PAPAN( IMOD, N )
      INTEGER IMOD(2), N
      IF ( IMOD(1).LE.1 ) THEN
            IF ( IMOD(2).LE.1 ) I = 2
            IF ( IMOD(2).EQ.2 ) I = 3
            IF ( IMOD(2).GE.3 ) I = 4
      ELSE IF ( IMOD(1).EQ.2 ) THEN
            IF ( IMOD(2).LE.1 ) I = 2
            IF ( IMOD(2).EQ.2 ) I = 3
            IF ( IMOD(2).EQ.3 ) I = 3
            IF ( IMOD(2).EQ.4 ) I = 4
            IF ( IMOD(2).EQ.5 ) I = 3
            IF ( IMOD(2).EQ.6 ) I = 3
            IF ( IMOD(2).EQ.7 ) I = 4
            IF ( IMOD(2).EQ.8 ) I = 4
      ELSE IF ( IMOD(1).GE.3 ) THEN
            I = 7
      ENDIF
      RETURN
      END

```

```

SUBROUTINE RES12( IFLAG, N, H, SYN, FVECC, IW, LIW, W, LW )
REAL SYN(N), FVECC(M), W(LW)
REAL AINT(3M), CURR(3M), AL(JM), AN4(3M,4), VALS(3M)
INTEGER IFLAG, N, H, IH(LIW), LIW, IH, IMOD(2)

COMMON IMOD, AINT, CURR, AH, AN4
CONTINUE
CALL VALS( IMOD, N, H, CURR, AH, AN4, SYN, VALS, IFLAG )
CALL DIFF( H, VALS, AINT, FVECC )
RETURN
END

SUBROUTINE VALS( IMOD, N, H, CURR, AH, AN4, SYN, VALS, IFLAG )
REAL CURR(N), SYN(1), VALS(M), AL(M)
REAL AN4(3M,4)
INTEGER IMOD(2)
CONTINUE
DO 100 J = 1, N
  SYN(J) = ABS( SYN(J) )
CONTINUE

IF ( IMOD(1).EQ.1 ) THEN
  CALL MODA( IMOD(2), N, N, CURR, SYN, VALS, IFLAG )
ELSE IF ( IMOD(1).EQ.2 ) THEN
  CALL MODB( IMOD(2), N, N, CURR, AH, SYN, VALS, IFLAG )
ELSE IF ( IMOD(1).EQ.3 ) THEN
  CALL MODC( IMOD(2), N, N, CURR, AN4, SYN, VALS, IFLAG )
ENDIF
RETURN
END

SUBROUTINE MODA( IMOD, N, H, CURR, SYN, VALS, IFLAG )
INTEGER IMOD, N, H, IFLAG, J
REAL CURR(N), VALS(M), SYN(N)

IF ( IMOD.EQ.1 .AND. N.EQ.2 ) THEN
  DO 10 J = 1, N
    VALS(J) = TERM1( CURR(J), SYN(1), SYN(2) )
  CONTINUE
ELSE IF ( IMOD.EQ.2 .AND. N.EQ.3 ) THEN
  DO 20 J = 1, N
    VALS(J) = TERM1( CURR(J), SYN(1), SYN(2) ) *
      TERM2( CURR(J), SYN(3) )
  CONTINUE
ELSE IF ( IMOD.EQ.3 .AND. N.EQ.4 ) THEN
  DO 30 J = 1, N
    VALS(J) = TERM1( CURR(J), SYN(1), SYN(2) ) *
      TERM2( CURR(J), SYN(3) ) *
      TERM3( CURR(J), SYN(4) )
  CONTINUE
ELSE IF ( IMOD.EQ.4 .AND. N.EQ.4 ) THEN
  DO 40 J = 1, N
    VALS(J) = TERM1( CURR(J), SYN(1), SYN(2) ) *
      TERM2( CURR(J), SYN(3) ) *
      TERM3( CURR(J), SYN(4) )
  CONTINUE
ELSE
  IFLAG = -1
ENDIF
RETURN
END

SUBROUTINE DIFF( N, ARK1, ARK2, ARKDIF )
REAL ARK1(N), ARK2(M), ARKDIF(N)
DO 10 J = 1, N
  ARKDIF(J) = ARK1(J) - ARK2(J)
CONTINUE
RETURN
END

```

```

SUBROUTINE MODE( IMOD, M, N, CURR, AN, SYN, VALS, IFLAG )
REAL CURR(M), VALS(M), SYN(N), AN(M)
INTEGER IMOD, M, N, IFLAG, J
IF ( IMOD.EQ.1 .AND. N.EQ.2 ) THEN
  DO 10 J = 1, M
    VALS(J) = TERM4( CURR(J), AN(J), SYN(1), SYN(2) )
10  CONTINUE
ELSE IF ( IMOD.EQ.2 .AND. N.EQ.3 ) THEN
  DO 20 J = 1, M
    VALS(J) = TERM4( CURR(J), AN(J), SYN(1), SYN(2) ) *
    * TERM2( CURR(J), SYN(3) )
20  CONTINUE
ELSE IF ( IMOD.EQ.3 .AND. N.EQ.3 ) THEN
  DO 30 J = 1, M
    VALS(J) = TERM4( CURR(J), AN(J), SYN(1), SYN(2) ) *
    * TERM5( SYN(3), AN(J) )
30  CONTINUE
ELSE IF ( IMOD.EQ.4 .AND. N.EQ.4 ) THEN
  DO 40 J = 1, M
    VALS(J) = TERM4( CURR(J), AN(J), SYN(1), SYN(2) ) *
    * TERM2( CURR(J), SYN(3) ) *
    * TERM5( SYN(4), AN(J) )
40  CONTINUE
ELSE IF ( IMOD.EQ.5 .AND. N.EQ.3 ) THEN
  DO 50 J = 1, M
    VALS(J) = TERM6( CURR(J), AN(J), SYN(1), SYN(2) ) *
    * TERM2( CURR(J), SYN(3) )
50  CONTINUE
ELSE IF ( IMOD.EQ.6 .AND. N.GE. 3 ) THEN
  DO 60 J = 1, M
    VALS(J)=(TERM4( CURR(J), AN(J), SYN(1), SYN(2) )+SYN(3) )
60  CONTINUE
ELSE IF ( IMOD.EQ.7 .AND. N.GE.4 ) THEN
  DO 70 J = 1, M
    VALS(J)=(TERM4( CURR(J), AN(J), SYN(1), SYN(2) ) + SYN(4) ) *
    * TERM2( CURR(J), SYN(3) )
70  CONTINUE
ELSE IF ( IMOD.EQ.8 .AND. N.GE.4 ) THEN
  DO 80 J = 1, M
    VALS(J) =(TERM4( CURR(J), AN(J), SYN(1), SYN(2) )+SYN(3)) *
    * TERM3( CURR(J), SYN(4) )
80  CONTINUE
ELSE
  IFLAG = -2
ENDIF
RETURN
END

FUNCTION TERM1( CURR, A, B )
REAL CURR, A, B
TERM1 = A*CURR*( 1.0 + B*CURR )
RETURN
END

FUNCTION TERM2( CURR, C )
REAL CURR, C
TERM2 = 1.0/( 1.0 + C*CURR )
RETURN
END

FUNCTION TERM3( CURR, GAMMA )
REAL CURR, GAMMA
TERM3 = ( 1.0 - GAMMA*CURR )
RETURN
END

FUNCTION TERM4( CURR, AN, A, B )
REAL CURR, A, B, AN
TERM4 = A*CURR*( 1.0 + B*AN )
RETURN
END

```

```

FUNCTION TERN6( CURR, AN, A, B )
REAL CURR, AN, A, B
TERN6 = CURR*A + CURR*B*AN
RETURN
END

```

```

FUNCTION TERN5( DELTA, AN )
REAL DELTA, AN
TERN5 = ( 1.0 - DELTA*AN )
RETURN
END

```

```

SUBROUTINE CALC2( IMOD, NCALC, I, SYN, XCALC, YCALC, ISTOP,
*          NCAP7, I, C, ICONDS,
*          NCAP74, K4, C4, ICOND4 )
INTEGER NCALC, N, NCAP7, ICONDS
INTEGER IMOD(2), NCAP74(4), ICOND4(4)
REAL SYN(N), XCALC(NCALC), YCALC(NCALC)
REAL K(50), C(50), RANGE, STEP, AN(300)
REAL K4(50,4), C4(50,4), AN4(300,4)

ISTOP = 0
XCALC(1) = 1.0
XCALC(NCALC) = 49.0
RANGE = XCALC( NCALC ) - XCALC(1)

STEP = RANGE/FLOAT( NCALC - 1 )
DO 10 J = 2, NCALC - 1
XCALC(J) = XCALC(1) + STEP*FLOAT(J-1)
CONTINUE
10 IF ( IMOD(1).EQ.2 ) THEN
CALL ARRCAL( NCAP7, K, C, NCALC, XCALC, AN, ICONDS, ISTOP )
IF ( ISTOP.NE.0 ) GOTO 10000
ELSE IF ( IMOD(1).EQ.3 ) THEN
ISTOP = - 100
ENDIF
CALL VALSS( IMOD, NCALC, N, XCALC, AN, AN4, SYN, YCALC, IFLAG )
IF ( IFLAG.LT.0 ) ISTOP = IFLAG
20 CONTINUE
10000 RETURN
END

```

```

SUBROUTINE ARPCAL( NCAP7, I, C, K, CURR, AN, ICONDS, ISTOP )
REAL K(NCAP7), C(NCAP7), CURR(N), AN(N)
REAL A

INTEGER NCAP7, N, ISTOP, IFAIL

ISTOP = 0
A = 1.0

DO 10 J = 1, N

IF ( CURR(J).LT.K(1) .OR. CURR(J).GT.K(NCAP7) ) THEN
991 * WRITE( 5, 991 ) J
FORMAT( ' CURR OUTSIDE KNOT RANGE AT J =', I3,
* AN(J) NOT CALCULATED' )
GOTO 10
ENDIF

IFAIL = 0
CALL EWZBFF( NCAP7, K, C, CURR(J), AN(J), IFAIL )

IF ( IFAIL.NE.0 ) THEN
992 * WRITE( 5, 992 ) IFAIL
FORMAT( ' RETURN FROM EWZBFF WITH IFAIL =', I2, '/',
* RETURN WITH ISTOP = IFAIL' )
ISTOP = IFAIL
GOTO 10000
ENDIF

10 IF ( ICONDS.EQ.1 ) AN(J) = EXP( AN(J) ) - A
CONTINUE
10000 RETURN
END

```

```

SUBROUTINE ALRAN( IPRESS, I, CURF, NAME, AN, ISTOP,
                NCAP7, I, C, ICONDS )

INTEGER IPRESS, I, ISTOP, NCAP7, ICONDS

REAL CURF(I), AN(I)
REAL K(50), C(50)

CHARACTER*10 NAME, CONDS
CHARACTER*12 EXPT(2)
CHARACTER*1  RL

      ISHIT = 0
      CONTINUE
      ISTOP = 0
      IF ( IPRESS.EQ.1 ) NAME = 'AN1.DAT'
      IF ( IPRESS.EQ.2 ) NAME = 'AN2.DAT'
      IF ( IPRESS.EQ.5 ) NAME = 'ANS.DAT'
      RL = 'Y'
      IF ( ISHIT.EQ.0 ) GOTO 1001
      WRITE( 5, 991 )
991  FORMAT(' DO YOU WANT TO AN/I FIT FIXED BY IPRESS ? Y OR N' )
      READ( 5, 992 ) BR
992  FORMAT( A1 )
1001 IF ( BR.EQ.'Y' ) THEN
      WRITE( 5, 993 )
993  FORMAT(' INPUT NAME OF FILE HOLDING AN/I FIT' )
      READ( 5, 994 ) NAME
994  FORMAT( A10 )
      ELSE IF ( BR.EQ.'N' ) THEN
      IF ( IPRESS.NE.1 .AND. IPRESS.NE.2 .AND. IPRESS.NE.5 ) THEN
995  WRITE( 5, 995 ) IPRESS
      FORMAT(' IPRESS =', I2, ' ??', //,
            * ' INPUT NAME FILE HOLDING AN/I FIT OR END' )
      READ( 5, 994 ) NAME
      ISTOP = 21
      GOTO 10000
      ENDIF
      ENDIF
      OPEN( UNIT=20, DEVICE='DSK', ACCESS='SEQIN', FILE=NAME, ERR=9000 )
      READ(20, 801, ERR=9000) IIPRES, TORR, EXPT(1), EXPT(2), CONDS
      ICONDS = 0
      IF ( CONDS.EQ.'SCALD' ) ICONDS = 1
801  FORMAT( I1, A4, 2X, A12, 2X, A12, 2X, A10 )
      IF ( IIPRES.NE.IPRESS ) WRITE( 5, 771 )
771  FORMAT(' IPRES NOT CORRECT' )
      READ( 20, 802, ERR=7000 ) NCAP7
802  FORMAT( I2 )
      DO 10 J = 1, NCAP7
      READ ( 20, 803, ERR = 6000 ) I(J)
803  FORMAT( E20,7 )
10  CONTINUE
      DO 20 J = 1, NCAP7 = 4
      READ( 20, 803, ERR= 5000 ) C(J)
20  CONTINUE
      CLOSE( UNIT = 20 )
      GOTO 100
9000 WRITE(5,804)
804  FORMAT(' ERROR OPENING FILE OF THIS NAME', //,
            * ' DO YOU WANT TO RESTART THIS SUBROUTINE ? Y OR N' )
      READ( 5,992 ) BR
      IF ( BR.EQ.'Y' ) GOTO 1
      ISTOP = 22
      WRITE( 5, 3032 )
3032  FORMAT(' RETURN ISTOP = 22' )
      GOTO 10000
8100  CLOSE( UNIT=20 )
      WRITE( 5, 805 )
805  FORMAT(' ERROR IN READING 1ST LINE OF THIS FILE', //,
            * ' DO YOU WANT TO RESTART SUBROUTINE ? Y OR N' )
      READ( 5, 992 ) BR
      IF ( BR.EQ.'Y' ) GOTO 1
      ISTOP = 23
      WRITE(5, 3033 )
3033  FORMAT(' RETURN ISTOP = 23' )
      GOTO 10000
7000  CLOSE( UNIT=20 )
      WRITE( 5, 3031 )
3031  FORMAT(' ERROR READING NCAP7, RETURN ISTOP = 24' )
      ISTOP = 24
      GOTO 10000

```

```

6100 WRITE( 5, 806 ) J
886 FORMAT(' ERROR READING K(J) AT J =',I2,' RETURN ISTOP = 25' )
      ISTOP = 24
      CLOSE( UNIT=20 )
      GOTO 10000
5100 WRITE( 5, 887 ) J
887 FORMAT(' ERROR READING C(J) AT J =',I2,' RETURN ISTOP = 26' )
      ISTOP = 26
      CLOSE( UNIT=20 )
      GOTO 10000
110 CONTINUE
      CALL ARRCAL( NCAP7, K, C, M, CURR, AN, ICONDS, ISTOP )
11000 RETURN
      END
SUBROUTINE ARRCAL( NAME, N, CURR, AINT, IPRESS, EXPT, ISTOP )
      INTEGER N, IPRESS, ISTOP, J
      REAL CURR(300), AINT(300)
      CHARACTER*1 M
      CHARACTER*10 NAME, CONDS
      CHARACTER*12 EXPT(2)
      CHARACTER*4 TORQ
      CONTINUE
      ISTOP = 0
      OPEN( UNIT=20, DEVICE='DISK', ACCESS='SEQUENTIAL', FILE=NAME,
      * ERR=9000 )
      REAL( 20, 991, ERR=9000 ) IPRESS, TORQ, EXPT(1), EXPT(2), CONDS
991 FORMAT( 11, A4, 2X, A12, 2X, A12, 2X, A10 )
      READ( 20, 771 ) M
771 FORMAT( 14 )
      DO 10 J = 1, M
      READ( 20, 992, ERR=7000 ) CURR(J), AINT(J)
992 FORMAT( 2F7.3 )
10 CONTINUE
      CLOSE( UNIT=20 )
      GOTO 10000
9000 CONTINUE
      WRITE( 5, 993 ) NAME
993 FORMAT(' ERROR OPENING FILE OF NAME =',A12,/,
      * ' DO YOU WANT TO INPUT NEW FILENAME ? Y OR N' )
      READ( 5, 998 ) M
998 FORMAT( A1 )
      IF ( M.EQ.'Y' ) THEN
      WRITE( 5, 994 )
994 FORMAT(' INPUT NEW FILENAME' )
      READ( 5, 995 ) NAME
995 FORMAT( A10 )
      GOTO 1
      ENDIF
      ISTOP = 11
      WRITE( 5, 996 )
996 FORMAT(' RETURN WITH ISTOP = 11' )
      GOTO 10000
8000 CONTINUE
      CLOSE( UNIT=20 )
      WRITE( 5, 997 )
997 FORMAT(' ERROR READING FIRST LINE OF FILE',/,
      * ' DO YOU WANT TO INPUT NEW FILENAME ?, Y OR N' )
      READ( 5, 998 ) M
      IF ( M.EQ.'Y' ) THEN
      WRITE( 5, 999 )
999 FORMAT(' INPUT NEW FILENAME' )
      READ( 5, 995 ) NAME
      GOTO 1
      ENDIF
      ISTOP = 12
      WRITE( 5, 881 )
881 FORMAT(' RETURN WITH ISTOP = 12' )
      GOTO 10000
7000 CONTINUE
      CLOSE( UNIT=20 )
      WRITE( 5, 882 ) J
882 FORMAT(' ERROR READING LINE J =', I4, /,
      * ' DO YOU WANT TO INPUT NEW FILENAME ? Y OR N' )
      READ( 5, 998 ) M
      IF ( M.EQ.'Y' ) THEN
      WRITE( 5, 883 )
883 FORMAT(' INPUT NEW FILENAME' )
      READ( 5, 995 ) NAME
      GOTO 1
      ENDIF
      WRITE( 5, 884 )
884 FORMAT(' RETURN WITH ISTOP = 13' )
      ISTOP = 13
10000 RETURN
      END

```

THE BRITISH LIBRARY DOCUMENT SUPPLY CENTRE

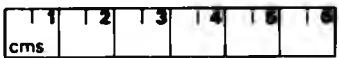
TITLE A study of spectral line intensities
and excited atom populations in a
..... hollow cathode discharge.

AUTHOR C E. Light

INSTITUTION
and DATE North London Polytechnic
..... 1988

Attention is drawn to the fact that the copyright of this thesis rests with its author.

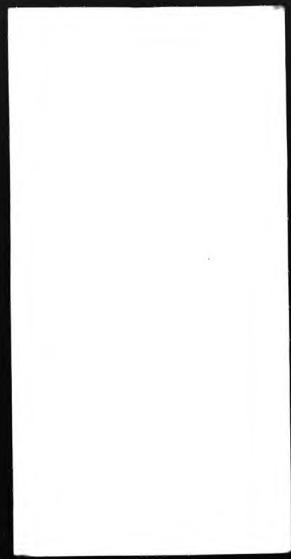
This copy of the thesis has been supplied on condition that anyone who consults it is understood to recognise that its copyright rests with its author and that no information derived from it may be published without the author's prior written consent.



THE BRITISH LIBRARY
DOCUMENT SUPPLY CENTRE
Boston Spa, Wetherby
West Yorkshire
United Kingdom

20

REDUCTION X



DX



85359

